

DETECTION AND IDENTIFICATION OF ENGINEERED SURFACES USING IMAGING SPECTROMETRY

A Thesis Submitted to

Delhi Technological University

For the Award of Degree of

Doctor of Philosophy

In

Electronics and Communication Engineering

By

DWIJENDRA PANDEY

(2K17/PhD/EC/09)

Under the Supervision of

Dr K. C. Tiwari

Professor, Multidisciplinary Centre for Geoinformatics



Department of Electronics & Communication Engineering

Delhi Technological University

(Formerly Delhi college of Engineering)

Delhi-110042, India

SEPTEMBER-2020



©DELHI TECHNOLOGICAL UNIVERSITY-2020
ALL RIGHTS RESERVED

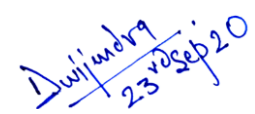
*Dedicated to My Late
Grandparents*

DECLARATION

I declare that the research work reported in the thesis entitled "**Detection and Identification of Engineered Surfaces using Imaging Spectrometry**" for the award of the degree of *Doctor of Philosophy* in the *Department of Electronics and Communication Engineering (ECE)* has been carried out by me under the supervision of *Dr K. C. Tiwari*, Professor in Multidisciplinary Centre for Geoinformatics (MCG), Delhi Technological University (DTU), Delhi, India.

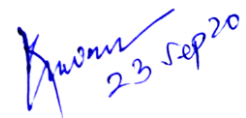
The research work embodied in this thesis, except where otherwise indicated, is my original research. This thesis has not been submitted earlier in part or full to any other University or Institute for the award of any degree or diploma. This thesis does not contain other person's data, graphs or other information, unless specifically acknowledged.

Date: 23rd Sep 2020


(Dwijendra Pandey)
2K17/PhD/EC/09
Department of ECE
Delhi Technological University,
Delhi-110042, India

CERTIFICATE

This is to certify that the thesis entitled "**Detection and Identification of Engineered Surfaces using Imaging Spectrometry**", submitted by **Mr. Dwijendra Pandey** (Reg. No: 2K17/PHD/EC/09) for the award of degree of Doctor of Philosophy, to the Delhi Technological University, is based on the original research work carried out by him. He has worked under my supervision and has fulfilled the requirements, which to my knowledge have reached the requisite standard for the submission of this thesis. It is further certified that the work embodied in this thesis is neither partially nor fully submitted to any other university or institution for the award of any other degree or diploma.



23 Sep 20

Dr K. C. Tiwari

Supervisor and Professor,
Multidisciplinary Centre for Geoinformatics
Delhi Technological University,
Delhi- 110042, India

ACKNOWLEDGMENTS

I would like to express my deepest gratitude to **Prof. K. C. Tiwari**, Multidisciplinary Centre for Geoinformatics, Delhi Technological University (DTU), Delhi for his invaluable guidance, suggestions and endless encouragement. He has always given me the freedom to pursue my interests and provided me with insightful suggestions and support in developing independent thinking and research skills. He has been an exceptional mentor, and I appreciate both our professional and personal conversations over the years. The knowledge and wisdom I have gained from him will forever guide me in education and life.

I would like to extend my sincere gratitude to the DRC chairman Prof. Asok De, my SRC members; Dr R. N. Sahoo, Principal Scientist, IARI, Delhi, Prof. Dharmendra Singh, IIT Roorkee, Prof. S. Indu and Prof. J. Panda, Department of ECE, DTU, and Prof. A. K. Sahoo, Department of CE, DTU for generously sharing their knowledge and time. I would also like to thank Prof. N. S. Raghava, HOD, ECE and Prof. Nirendra Dev, HOD, CE, DTU, Delhi for providing all the essential facilities in the department and the centre.

I wish to express my sincerest thanks and appreciation to Dr L. K. Sinha, Director, DTRL, DRDO, Delhi, for fruitful discussion and his encouragement. I wish to thank Mr T. S. Rawat, Scientist-F, DTRL for his helpful discussions and suggestions during field data collection campaign.

I gratefully acknowledge the financial support received from Department of Science and Technology (DST), Ministry of Science and Technology and Space Application Centre (SAC), Indian Space Research Organisation (ISRO). I am also extremely grateful to the team members of Material and Terrain Theme of NISA

project specifically from DTRL, DRDO for providing their valuable support in field data collection.

I would like to make a special note of thanks to my all the colleagues Mr Anupam Srivastava, Dr Deepti, Dr Rubeena, Ms Shalini, Mr Sanjay Singh, Mr Gopinadh, Ms Amrita and Ms Vaishnavi for their co-operation and making the work environment so positive and vibrant with their presence. Further, I express my sincere thanks to all research scholars of the Department of Electronics & Communication, and Civil Engineering for their valuable support and suggestions.

Words cannot completely express my love and gratitude to my family members who have supported and encouraged me through this journey. I owe a lot to my parents, who encouraged and helped me at every stage of my personal and academic life, and longed to see this achievement come true. I would like to thank my parents, sisters Sadhna, Rashmi, and Priyanka, brothers Gavendra and Shivendra for their life-long support, everlasting love, and sacrifices, which sustained my interest in research and motivated me towards the successful completion of this study.

As I write these pages, I finally remember my late grandparents and dedicate this work in their names.

Lastly, I thank the almighty God for the passion, strength, perseverance, and the resources to complete this study.

Date: 23rd Sep 2020
Place: Delhi

(Dwijendra Pandey)
2K17/PhD/EC/09
Department of ECE
Delhi Technological University,
Delhi-110042, India

ABSTRACT

The urban environment in developing countries is transforming from rural to urban areas at a rapid pace. Urbanization brings economic and social benefits (e.g. economic prosperity and improved quality of life), but it also causes many environmental effects such as it directly impacts surface runoff [1] [2], degradation in water quality, loss of biodiversity and urban heat island effect [3] [4] [5], etc. Due to these major impacts, understanding the behavior of the urban environment and their spatio-temporal analysis, become essential for local and regional planning and environmental management. This demands development of some cost-efficient approaches to get urban sprawl information timely. As an indicator of urbanization, built-up surface mapping has turned out to be an active area of research and various techniques have been developed in the recent past [6] [7] [8] [9]. Therefore, taking advantage of imaging spectrometry, in this research, the detection and identification of engineered or built-up surfaces have been carried out under different objectives:

- i. The first objective deals with the creation of a spectral library of urban built-up surfaces and materials for Indian regions, and analysis of spectral signatures of these surfaces and materials.
- ii. In the second objective, the research has been carried out in four different sub-objectives:
 - a. In the first sub-objective, three new spectral indices i.e. New Impervious Index (NII), Road Detection Index (RDI) and New Roof Extraction Index (NREI) have been proposed for detection of built-up (Level-1), road and roof surfaces (Level-2), respectively.

- b. In second, two new spectral indices have been introduced, in which Condition Index-Road (CI-Road) is utilized for condition analysis of road surfaces while Deterioration Index-Roof (DI-Roof) is used for deterioration analysis of roof surfaces in AVIRIS-NG hyperspectral imagery.
 - c. In third sub-objective, existing multispectral built-up indices formulated for extraction of built-up surfaces, have been used for extraction of urban built-up surfaces along with its sub-categories in hyperspectral imagery.
 - d. Finally, based on existing literature, extraction of impervious or engineered surfaces has been carried out using index based Red-Green-Blue (RGB) and Near Infrared (NIR) band combinations in AVIRIS-NG imagery.
- iii. In the third objective, a new method is proposed, in which different combinations of feature bands have been created for extraction of built-up surfaces, sub-surfaces and materials in different levels (Level-1, 2 and 3) using AVIRIS-NG hyperspectral imagery. The knowledge based features identified in this study are thematic spectral indices, major principal components and fractional abundances.
- iv. In the fourth and final objective of the research, a performance evaluation of Sentinel-2B, Landsat-8 multispectral, and AVIRIS-NG hyperspectral imageries for extraction of road and roof surfaces using proposed spectral index based, and other conventional algorithms has been presented. The New Road Extraction Index (NREI) and New Building Extraction Index (NBEI) are developed for extraction of road and roof surfaces, respectively. Moreover, existing Spectral Angle Mapper (SAM), Spectral Information Divergence

(SID), Matched Filtering (MF), and Support Vector Machine (SVM) are utilized as angle, information, filtering, and machine learning based algorithms, respectively, for detection of both the surfaces.

The entire analysis has been carried out using AVIRIS-NG and ground hyperspectral data of the Udaipur and Jodhpur, Rajasthan region of India. The results of the analysis depict that, indices based approach outperforms other conventional classification / detection algorithms for extraction and estimation of engineered / built-up surfaces, sub-surfaces, and materials in AVIRIS-NG hyperspectral imagery with less time and computational complexity.

LIST OF PUBLICATIONS

International Journal (Published)

- i. Pandey, D. and Tiwari, K.C., 2020. Extraction of Urban Built-up Surfaces and Its Subclasses using Existing Built-up Indices with Separability Analysis of Spectrally Mixed Classes in AVIRIS-NG Imagery. **Advances in Space Research (SCI, IF- 2.177)**
- ii. Pandey, D. and Tiwari, K.C., 2020. Feature Identification and Extraction of Urban Built-up Surfaces and Materials in AVIRIS-NG Hyperspectral Imagery. **Geocarto International**, (just-accepted), pp.1-18 (**SCIE, IF- 3.789**)
- iii. Pandey, D. and Tiwari, K.C., 2020. Performance evaluation and comparative assessment of Sentinel-2B, Landsat-8, and AVIRIS-NG sensor imageries for extraction of road and roof surfaces using different algorithms. **Journal of Applied Remote Sensing**, 14(3), p.034502 (**SCIE, IF- 1.36**)
- iv. Pandey, D. and Tiwari, K.C., 2020. New Spectral Indices for Detection of Urban Built-Up Surfaces and its Subclasses in AVIRIS-NG Hyperspectral Imagery, **Geocarto International (SCIE, IF- 3.789)**

Papers in International Journal (Under Publication/Review)

- i. Pandey, D. and Tiwari, K.C. Spectral Library Creation and Identification of Significant Wavelengths for Urban Built-Up Surfaces and Materials using Field Spectrometry, **Arabian Journal of Geosciences (SCIE, IF- 1.327)**
(Accepted with Revision)

- ii. Pandey, D. and Tiwari, K.C. Development of Spectral Index for Road Condition and Roof Deterioration Analysis using AVIRIS-NG and Field Hyperspectral Data, **PFG – Journal of Photogrammetry, Remote Sensing and Geo-Information Science (SCIE, IF- 1.395) (Under Review)**
- iii. Pandey, D. and Tiwari, K.C. Spectral Index based Extraction of Impervious Surfaces and its Sub-categories in Hyperspectral Imagery, **Journal of the Indian Society of Remote Sensing (SCIE, IF- 0.997) (Under Review)**

Papers in International Conference (Published/Under Review)

- i. Dwijendra Pandey, K. C. Tiwari, 2017. Sensors and Instruments for Spectral data collection in field, **38th Asian Conference on Remote Sensing, New Delhi, India (Published)**
- ii. Dwijendra Pandey, K. C. Tiwari, 2019. Spectral Library Creation and analysis of Urban Built-Up Materials using Hyperspectral Remote Sensing, **4th Indian Society of Systems for Science & Engineering (ISSE) Conference, Ahmedabad, India (Published)**
- iii. Dwijendra Pandey, K. C. Tiwari. Extraction of Impervious surfaces using Index based RGB and NIR band combinations in AVIRIS-NG Hyperspectral imagery, **IEEE IGRSS 2020 (Under Review)**

TABLE OF CONTENTS

<i>ACKNOWLEDGMENTS</i>	<i>i</i>
<i>ABSTRACT</i>	<i>iii</i>
<i>LIST OF PUBLICATIONS</i>	<i>vi</i>
<i>LIST OF FIGURES</i>	<i>xiv</i>
<i>LIST OF TABLES</i>	<i>xviii</i>
CHAPTER 1 INTRODUCTION	1
1.1 Motivation	1
1.2 Imaging Spectrometry	3
1.3 Engineered Surfaces	5
1.4 Significance of the Study	6
1.5 Research Gaps	7
1.6 Research Objectives	9
1.7 Thesis Overview	9
CHAPTER 2 LITERATURE REVIEW	11
2.1 Spectral library creation	11
2.2 Spectral index based algorithms	14
2.3 Significant features in remote sensing imagery	15
2.4 Comparative assessment of different algorithms using multi-sensor imageries	17
CHAPTER 3 SPECTRAL LIBRARY CREATION AND ANALYSIS OF SPECTRAL SIGNATURES	20
3.1 Study area	21
3.2 Instrumentation and software	21
3.3 Urban Engineered or Built-up surfaces	22

3.4	Implementation	25
3.5	Spectral library creation and analysis of signatures of Urban Engineered / Built-up surfaces.....	26
3.5.1	Roof / Building	26
3.5.2	Roads and Pavements.....	28
3.5.3	Railway Track.....	31
3.5.4	Sports Infrastructure.....	32
3.6	Identification of significant wavelengths and regions for extraction of different built-up surfaces and materials.....	34
3.7	Summary.....	44
 CHAPTER 4 DEVELOPMENT OF SPECTRAL INDICES FOR EXTRACTION OF ENGINEERED SURFACES AND ITS SUB-CATEGORIES.....		
4.1	Study area and Data	46
4.2	Data preprocessing	47
4.2.1	Kullback-Leibler (K-L) Divergence and Mutual Information (M-I) algorithms.....	49
4.2.2	Stepwise Discriminant Analysis (SDA).....	50
4.3	New spectral indices for built-up extraction (Level-1 and 2).....	51
4.4	Otsu's thresholding.....	54
4.5	Existing built-up indices.....	55
4.6	Separability analysis of urban land cover classes.....	56
4.7	Implementation.....	56
4.8	Results	58
4.8.1	Identification of significant wavelengths for extraction of built-up surfaces (Level-1 and 2).....	58

4.8.2	Optimal thresholding of built-up indices (Level-1 and 2).....	59
4.8.3	Extraction of built-up surfaces (Level-1).....	60
4.8.4	Extraction of road surfaces (Level-2)	62
4.8.5	Extraction of roof surfaces (Level-2)	64
4.8.6	Accuracy assessment and validation of results.....	66
4.8.7	Inter and intra-class separability analysis of urban built-up surfaces.....	68
4.9	Discussion.....	70
4.10	Summary.....	72
CHAPTER 5 NEW SPECTRAL INDICES FOR CONDITION AND DETERIORATION ANALYSIS OF ROAD AND ROOF SURFACES		74
5.1	AVIRIS-NG hyperspectral data and processing.....	75
5.2	Ground data acquisition and materials.....	75
5.2.1	Spectral characteristics of road surfaces.....	77
5.2.2	Spectral characteristics of roof surfaces	80
5.3	Multiple endmember spectral mixture analysis (MESMA)	81
5.4	Implementation	82
5.5	Spectral index for condition analysis of road surfaces	83
5.6	Spectral index for deterioration analysis of roof surfaces	84
5.7	Results	85
5.7.1	Mapping of road surfaces of different condition	85
5.7.2	Mapping of roof surfaces of different deterioration	88
5.8	Summary	91

CHAPTER 6 EXTRACTION OF BUILT-UP SURFACES AND ITS SUB-CATEGORIES USING EXISTING BUILT-UP INDICES IN AVIRIS-NG	
--	--

IMAGERY	93
6.1 Study area and Data.....	94
6.2 Spectral indices for extraction of urban built-up surfaces	94
6.3 Implementation	97
6.4 Results	98
6.4.1 Identification of significant wavelengths for extraction of built-up surfaces (Level-1 and 2)	99
6.4.2 Extraction of built-up surfaces (Level-1)	102
6.4.3 Extraction of road surfaces (Level-2)	104
6.4.4 Extraction of roof surfaces (Level-2)	106
6.4.5 Accuracy assessment	107
6.4.6 Separability analysis between spectrally mixed urban land cover classes.....	109
6.4.6.1 Separability analysis using histogram representation (Level-1 and 2).....	109
6.4.6.2 Separability analysis using statistical measures (Level-1 and 2).....	112
6.5 Discussion.....	115
6.6 Summary.....	117
 CHAPTER 7 EXTRACTION OF IMPERVIOUS SURFACES USING INDEX BASED RGB AND NIR BAND COMBINATIONS.....	 119
7.1 Study area and Dataset.....	119
7.2 Spectral index based band combinations.....	120
7.3 Results and Discussion.....	120
7.3.1 Separability analysis between various land cover classes.....	120
7.3.2 Extraction of impervious surfaces.....	122
7.3.3 Accuracy assessment.....	122
7.4 Summary.....	124

CHAPTER 8 EXTRACTION AND ESTIMATION OF BUILT-UP SURFACES AND ITS CATEGORIES USING FEATURE COMBINATION BASED APPROACH 125

8.1	Study area and Data	125
8.2	Experimental feature band combination.....	128
8.2.1	Principal Components.....	128
8.2.2	Spectral Indices	129
8.2.3	Fractional Abundances	129
8.3	Support Vector Machine.....	132
8.4	Results and Discussion.....	134
8.4.1	Features identified for extraction of urban built-up surfaces and materials.....	134
8.4.2	Extraction of built-up surfaces, sub-surfaces and materials (Level-1 to 3)	143
8.4.3	Accuracy Assessment	147
8.4.4	Area estimation of built-up surfaces, sub-surfaces and materials (Level-1 to 3)	152
8.5	Summary.....	154

CHAPTER 9 EVALUATION OF SPECTRAL INDICES BASED APPROACH FOR EXTRACTION OF ROAD AND ROOF SURFACES IN DIFFERENT SENSOR IMAGERIES 156

9.1	Study area and Dataset.....	156
9.2	Performance evaluation of different sensor imageries on the basis of spectral profile of road and roof surfaces	159
9.3	Proposed spectral indices	161
9.3.1	New Road Extraction Index (NREI).....	161
9.3.2	New Building Extraction Index (NBEI).....	161
9.4	Existing approaches.....	162
9.4.1	Spectral Angle Mapper (SAM)	162
9.4.2	Spectral Information Divergence (SID).....	163

9.4.3	Matched Filter (MF)	163
9.4.4	Support Vector Machine (SVM).....	164
9.5	Implementation.....	165
9.6	Results and Discussion.....	167
9.6.1	Road Extraction in different sensor imageries.....	167
9.6.1.1	Sentinel-2B.....	167
9.6.1.2	Landsat-8.....	168
9.6.1.3	AVIRIS-NG.....	169
9.6.2	Roof Extraction in different sensor imageries.....	171
9.6.2.1	Sentinel-2B.....	171
9.6.2.2	Landsat-8.....	172
9.6.2.3	AVIRIS-NG.....	173
9.6.3	Accuracy Assessment	175
9.6.3.1	Road surfaces.....	176
9.6.3.2	Roof surfaces.....	180
9.7	Summary	187
CHAPTER 10 CONCLUSIONS AND CONTRIBUTIONS.....		189
10.1	Conclusions.....	190
10.2	Research contributions.....	192
10.3	Limitations	194
CHAPTER 11 FUTURE SCOPE.....		195
11.1	Future Scope of the research	195
REFERENCES.....		196
AUTHOR’S BIOGRAPHY.....		215

LIST OF FIGURES

Figure 1.1 Imaging spectrometry of Earth Surface.....	4
Figure 1.2 Hyperspectral Image Cube.....	5
Figure 1.3 Matrix of image showing various types of Engineered surfaces.....	6
Figure 3.1 (a) The green points on the imagery of Udaipur, Rajasthan, India represent the actual locations of ground spectral data collection (b) Some of the selected photographs of field data collection campaign.....	24
Figure 3.2 (a) Sample spectral signature of a rock with continuum removal curve (b) Spectral analysis in IDL DISPEC 18.03 tool (c) Normalized reflectance of a sample.....	36
Figure 4.1 Hyperspectral data collection campaign at Udaipur, Rajasthan, India (a) AVIRIS-NG data (b) Locations of field data collection (c) Photographs of field data collection.....	48
Figure 4.2 Spectral signatures of different urban land cover classes utilized for extraction of built-up surfaces (Level-1 and 2).....	51
Figure 4.3 Implementation steps of the study	57
Figure 4.4 (a-d) Extraction results of urban built-up surfaces using different built-up indices in which the range of indices is shown along the x-axis of the respective index band (e-h) extraction results of ROI (i-l) histogram representation of different land cover classes in respective built-up indices	62
Figure 4.5 (a-d) Extraction results of road surfaces using different built-up indices in which the range of indices is shown along the x-axis of the respective index image (e-h) extraction results of ROI (i-l) histogram representation of different land cover classes in respective built-up indices.....	64
Figure 4.6 (a-d) Extraction results of roof surfaces using different built-up indices in which the range of indices is shown along the x-axis of the respective index band (e-h) extraction results of ROI (i-l) histogram representation of different land cover classes in respective built-up indices.....	66
Figure 5.1 Images with respective spectral characteristics of bitumen or asphalt road surfaces of different condition (a) Old road damaged condition (b) New road good condition (c) spectral signatures of road surfaces shown in (a) and (b).....	78
Figure 5.2 Images with respective spectral characteristics of concrete roof surfaces of various level of deterioration (a) New or less deterioration (b) Old or more deterioration (c) spectral signatures of roof surfaces shown in (a) and (b).....	81
Figure 5.3 Road condition analysis using hyperspectral imagery (a) original image (b) analysis using index based approach (c) analysis using MESMA unmixing (d) (g)	

(j) three regions of interest of original image (e) (h) (k) analysis of regions of interest using index based approach (f) (i) (l) analysis of regions of interest using MESMA unmixing.....	88
--	----

Figure 5.4 Deterioration analysis of roof using hyperspectral imagery (a) original image (b) analysis using index based approach (c) analysis using MESMA unmixing algorithm (d) (g) (j) three regions of interest of original image (e) (h) (k) analysis of regions of interest using index based approach (f) (i) (l) analysis of regions of interest using MESMA unmixing algorithm.....	90
---	----

Figure 6.1 Implementation steps for extraction of built-up surfaces (Level-1 and 2) using different built-up indices.....	98
---	----

Figure 6.2 Urban built-up extraction using different built-up indices. The range of indices of grayscale image is shown along the <i>x</i> -axis.....	104
---	-----

Figure 6.3 Extraction of road surfaces using various spectral indices. The range of indices of grayscale image is shown along the <i>x</i> -axis.....	105
---	-----

Figure 6.4 Roof extraction using different built-up indices. The range of indices of grayscale image is shown along the <i>x</i> -axis.....	107
---	-----

Figure 6.5 Histogram representation of different urban classes in various built-up indices used for (a-e) built-up extraction (Level-1) (f-h) road extraction (Level-2) (i-k) roof extraction (Level-2).....	110
--	-----

Figure 7.1 Histogram plot of various urban classes and ISIs (a) Red-NIR (b) Green-NIR (c) Blue-NIR.....	121
---	-----

Figure 7.2 Extraction results of impervious surfaces in AVIRIS-NG imagery (a) Original imagery (b) SVM classified results for accuracy assessment, in which red and green pixels are impervious surfaces and black pixels are related to pervious surfaces (c) Red-NIR (d) Green-NIR (e) Blue-NIR.....	123
--	-----

Figure 8.1 (a) Hyperspectral image of study area of size 400 samples x 400 lines (b) Water mask band (c) Field photographs of ground data collection campaign (d) Mean spectral signatures of different built-up and non-built-up classes.....	128
--	-----

Figure 8.2 Major principal components having maximum eigen values and variance (a) PC1 (b) PC2 (c) PC3.....	135
---	-----

Figure 8.3 Thematics spectral index based features (a) IBI (b) REI (c) NBAI (d) SAVI (e) MNDWI.....	136
---	-----

Figure 8.4 Fractional abundances of difference built-up and non-built-up classes (a) Bitumen road (b) Concrete pavement (c) Concrete roof (d) Metallic roof (e) Vegetation (f) Soil.....	137
--	-----

Figure 8.5 Graphical representation of different statistical parameters (a) Correlation between various feature bands (b) Mean, and (c) Standard Deviation of individual	
--	--

feature bands	140
Figure 8.6 Statistical analysis of different urban land cover classes using (a) Mean, and (b) Standard deviation	142
Figure 8.7 Extraction of built-up surfaces (Level-1 to 3) using combination of Spectral Index and Fractional Abundance based features, in which bright pixels are target and darks pixels are background (a) Built-up Surfaces (b) Roofs (c) Concrete Roofs (d) Metallic Roofs (e) Roads (f) Bitumen Roads (g) Concrete Pavements	144
Figure 8.8 Extraction of built-up surfaces (Level-1 to 3) using combination of Spectral Index and Major Principal Component based features, in which bright pixels are target and darks pixels are background (a) Built-up Surfaces (b) Roofs (c) Concrete Roofs (d) Metallic Roofs (e) Roads (f) Bitumen Roads (g) Concrete Pavements	146
Figure 8.9 Extraction of built-up surfaces (Level-1 to 3) using combination of Spectral Index, Fractional Abundance and Major Principal Component based features, in which bright pixels are target and darks pixels are background (a) Built-up Surfaces (b) Roofs (c) Concrete Roofs (d) Metallic Roofs (e) Roads (f) Bitumen Roads (g) Concrete Pavements	146
Figure 8.10 Comparative assessment of different combinations of features on the basis of (a) Overall Accuracy and (b) Kappa Index.....	153
Figure 9.1 Remote sensing images captured from various sensors (a) Sentinel- 2B (b) Landsat-8 (c) AVIRIS-NG (d) Locations of ground data collection (e) Field photographs of data collection campaign.....	158
Figure 9.2 Spectral characteristics of roads and roofs in different sensor imageries (a) Sentinel- 2B (b) Landsat-8 (c) AVIRIS-NG.....	160
Figure 9.3 Flowchart describing implementation steps of the study.....	166
Figure 9.4 Road extraction in Sentinel-2B imagery using various algorithms, in which bright pixels are related to roads while dark pixels to non-road (a) NREI (b) SAM (c) SID (d) MF (e) SVM	168
Figure 9.5 Road extraction in Landsat-8 imagery using various algorithms, in which bright pixels are related to roads while dark pixels to non-road (a) NREI (b) SAM (c) SID (d) MF (e) SVM	169
Figure 9.6 Road extraction in AVIRIS-NG imagery using different algorithms, in which bright pixels are related to roads while dark pixels to non-road (a) NREI (b) SAM (c) SID (d) MF (e) SVM.....	170
Figure 9.7 Roof extraction in Sentinel-2B imagery using various algorithms, in which bright pixels are related to roofs while dark pixels to non-roof (a) NBEI (b) SAM (c) SID (d) MF (e) SVM	172
Figure 9.8 Roof extraction results from Landsat-8 imagery using different algorithms, in which bright pixels are related to roofs while dark pixels to non-roof (a) NBEI (b)	

SAM (c) SID (d) MF (e) SVM.....	173
---------------------------------	-----

Figure 9.9 Roof extraction in AVIRIS-NG imagery using various algorithms, in which bright pixels are related to roofs while dark pixels to non-roof (a) NBEI (b) SAM (c) SID (d) MF (e) SVM.....	174
--	-----

Figure 9.10 Comparison on the basis of sensor performance using (a) Overall Accuracy (b) Kappa Index.....	179
---	-----

Figure 9.11 Comparison on the basis of different algorithms using (a) Overall Accuracy (b) Kappa Index.....	180
---	-----

Figure 9.12 Comparison on the basis of sensor performance using (a) Overall Accuracy (b) Kappa Index.....	183
---	-----

Figure 9.13 Comparison on the basis of different algorithms using (a) Overall Accuracy (b) Kappa Index.....	184
---	-----

LIST OF TABLES

Table 2.1 Existing spectral libraries of urban built-up surfaces and materials.....	13
Table 3.1 Categorization of various engineered surfaces in different levels.....	22
Table 3.2 Division of full spectral range into different wavelength regions.....	25
Table 3.3 Spectral library creation and analysis of roof surfaces.....	26
Table 3.4 Spectral library creation and analysis of roads and pavements.....	29
Table 3.5 Spectral library creation and analysis of railway track.....	31
Table 3.6 Spectral library creation and analysis of sports infrastructure.....	32
Table 3.7 Significant absorption parameters and wavelengths of different built-up surfaces and materials.....	37
Table 3.8 Significant wavelengths and regions for different built-up surfaces and materials (Level-1, 2, 3 and 4)	42
Table 4.1 AVIRIS-NG image data specifications	47
Table 4.2 Existing built-up indices utilized for extraction of built-up surfaces and subclasses.....	55
Table 4.3 Significant wavelengths used to compute built-up indices	59
Table 4.4 Mapping of appropriate wavelength bands, statistical parameters and optimal thresholds for different built-up indices (Level- 1 and 2).....	60
Table 4.5 Accuracy assessment of various built-up indices (Level-1 and 2) based on different parameters.....	68
Table 4.6 Inter and intra-class separability measures of built-up surfaces (Level-1 and 2).....	70
Table 5.1 The range of spectral indices for different road and roof surfaces.....	85
Table 5.2 Quantitative analysis of road surfaces in all regions of interest.....	87
Table 5.3 Quantitative analysis of roof surfaces in all regions of interest.....	91
Table 6.1 Spectral indices utilized for extraction of built-up surfaces (Level-1 and 2).....	96
Table 6.2 Significant wavelengths obtained using stepwise discriminant analysis....	101

Table 6.3 Significant wavelength combination and optimal threshold for different spectral indices.....	101
Table 6.4 Accuracy assessment of built-up indices (Level-1 and 2).....	108
Table 6.5 Separability measures between built-up surfaces and soil, and road and roof surfaces.....	114
Table 7.1 Statistical analysis of various ISIs.....	121
Table 7.2 Accuracy assessment of extraction results of impervious surfaces.....	123
Table 8.1 Number of known samples of different classes.....	127
Table 8.2 Different significant features used for extraction of built-up surfaces, sub-surfaces and materials	131
Table 8.3 Different levels of extraction of built-up surfaces	132
Table 8.4 Parameters of SVM kernel	134
Table 8.5 Eigen values and percentage variance of PCs.....	135
Table 8.6 Appropriate band combinations for different spectral indices	135
Table 8.7 Mean and Standard deviation of different feature bands	139
Table 8.8 Correlation between different feature bands in which major principal components are B1- PC1, B2- PC2 and B3- PC3, spectral indices are B4- IBI, B5- REI, B6- NBAI, B7- SAVI and B8- MNDWI, and fractional abundances of different surfaces B9- Concrete Roof, B10- Metal Roof, B11- Asphalt Road, B12- Concrete Pavement, B13- Vegetation and B14- Soil.....	139
Table 8.9 Accuracy assessment of extraction of built-up surfaces and materials (Level-1 to 3)	148
Table 8.10 Area estimation of built-up surfaces and materials in different levels....	154
Table 9.1 Remote Sensing data specification of different sensors.....	157
Table 9.2 Accuracy assessment of road extraction using various algorithms in Sentinel-2B imagery.....	177
Table 9.3 Accuracy assessment of road extraction using various algorithms in Landsat-8 imagery.....	177
Table 9.4 Accuracy assessment of road extraction using various algorithms in AVIRIS-NG imagery.....	178
Table 9.5 Accuracy assessment of roof extraction using various algorithms in	

Sentinel-2B imagery	181
Table 9.6 Accuracy assessment of roof extraction using various algorithms in Landsat-8 imagery.....	182
Table 9.7 Accuracy assessment of roof extraction using various algorithms in AVIRIS-NG imagery.....	182
Table 9.8 Performance of various algorithms in different sensor imageries on the basis of overall accuracy	186
Table 9.9 Performance of various algorithms in different sensor imageries on the basis of kappa index	186

Chapter 1

Introduction

1.1 Motivation

The urban environment in developing countries is transforming from rural to urban at a rapid pace. According to the report of the United Nations submitted in the year 2018, urbanization has increased all around the world, rising from 30 % in 1950 to 47 % in 2000, and it further increased to 55% in the year 2018. It is also projected that 68 % of the population would survive in the urban areas by 2050. The estimation for the developed countries is significantly higher than the aforementioned figures, with 76 % of their population residing in urban areas in 2018 and estimated to be 90 % by 2050 (<https://www.un.org/development/desa/en/> accessed on 2nd March 2020).

Urbanization leads to several environmental problems such as air pollution, water quality degradation, urban heat island effect and loss of biodiversity etc. [1] [2] [3]. Due to these major environmental impacts, understanding of the urban environment and their spatio-temporal effects is necessary for local and regional planning along with sustainable development. The need of the hour is to develop cost-effective approaches to achieve urban sprawl information temporally.

Remote sensing images have been extensively used for extraction of built-up surfaces (e.g. roads, roofs etc.) due to its suitability in the mapping of built-up surfaces over large areas [4] [5]. Furthermore, the regions which are hard to access using field survey make remote sensing technology the only feasible means of urban land cover mapping. Substantial efforts have been made to enhance the accuracy of urban built-up mapping, but mapping with better accuracy continues to be problematic. This may be due to the large diversity of built-up surface materials such

as asphalt, concrete, cement, plastic, and metal [6] [7]. Their spectral characteristics may be similar to other natural surfaces (e.g. bare soil and sand). Dry soil and bright built-up surfaces are similar in spectral responses while shades originated by trees and tall buildings are easy to be confused with dark built-up surfaces [4]. Hence, discriminating built-up surfaces from non-built-up surfaces is a critical and challenging task.

Further, it is highly desirable to develop reliable methods for mapping of urban land covers. The diversified urban activities and spatio-temporal variations imply a challenge to classify and map land covers in these areas. Over the past few decades, remote sensing data have proved efficient for mapping urban land covers and monitoring multi-temporal changes. Various land cover classification / target detection approaches have been used to map different land covers. However, it is difficult to select the best classifiers because each of the methods has its own strengths and limitations [8] [9].

The applicability of imaging spectrometry / hyperspectral remote sensing has already shown its efficacy for snow and glacier, coastal-ocean chemistry, coral reef and cloud microphysical characterization. In India, the hyperspectral science initiative is also included in the **“Big Data Initiatives”** of Department of Science and Technology (DST), Government of India. Keeping the future applicability potential in tandem with the development of advanced technology, the Space Application Centre (SAC), Indian Space Research Organisation (ISRO) has undertaken the Airborne Visible / Infrared Imaging Spectrometer- Next Generation (AVIRIS-NG) data collection campaign over different cities of India in conjunction with Jet Propulsion Laboratory (JPL), National Aeronautics and Space Administration (NASA) (https://vedas.sac.gov.in/aviris_web/ accessed on 10th January 2018).

The motivation for the work presented in this thesis comes from the points

enumerated above and a desire to contribute, howsoever small, towards understanding and mapping of urban environment using high resolution remote sensing data.

1.2 Imaging Spectrometry

Imaging Spectrometry of Earth's land and ocean environments is based on the principles of spectroscopy, either reflectance or emission spectroscopy over shortwave (300 – 3000 nm) and longwave (5000 – 50000 nm) spectral wavelength range. Interaction of energy with the molecular structure of surface materials results into characteristic or diagnostic absorption or emission features in the reflectance or emittance spectra [10]. These diagnostic features occur due to changes in energy state of the molecules as a function of electronic or vibrational transitions. The electronic transitions occur predominantly at shorter wavelengths due to changes in energy state of electrons bound to atoms or molecules or lattices. Normally, the vibrational transitions occur in longer wavelength due to stretches and bendings where overtones occur at sums or multiples of the fundamental vibration frequencies.

The Hyperspectral Remote Sensing (HSRS) combines imaging and spectroscopy in a single system which includes large data sets and require new processing methods. The HSRS refers to 100 – 500 spectral bands generally in continuum with relatively narrow band interval (5 – 10 nm) in contrast to Multispectral Remote Sensing (MSRS) that refers usually to 5 – 15 discrete wide bands with bandwidths of about 50 – 400 nm. The advantages of HSRS over MSRS are (i) the HSRS can detect more materials or surface types such as minerals, rocks, built-up, vegetation, snow, (ii) relates directly to surface chemistry and (iii) can estimate the abundance of material present. This greater information content enables new methods for detection, characterization and quantification in a broad range of Earth system

environments [11].

The ability to develop HSRS instrument is only recently enabled by technologies of the 21st Century. Further, handheld field spectrometers are generally useful for ground-based survey. However, they provide only point target spectra but not the continuous spatial coverage over large areas required for many local or regional research and applications [12] [13]. Several imaging HSRS instruments such as micro-hyperspec and nano-hyperspec are available for hyperspectral imaging to provide data with centimeter spatial resolution from airborne (e.g. Aeroplane, Robotic UAV, Drones etc.) and ground-based platforms. The satellite-based HSRS mission such as EO-1 Hyperion of NASA provided reasonably good datasets sampled around the globe, including India, but Hyperion suffers from low Signal-to-Noise Ratio (SNR). Figure 1.1 represents process of imaging spectrometry using spaceborne hyperspectral sensor, while Figure 1.2 shows the captured data in the form of hyperspectral image cube, in which x and y dimensions represent spatial domain while z is associated with spectral domain.

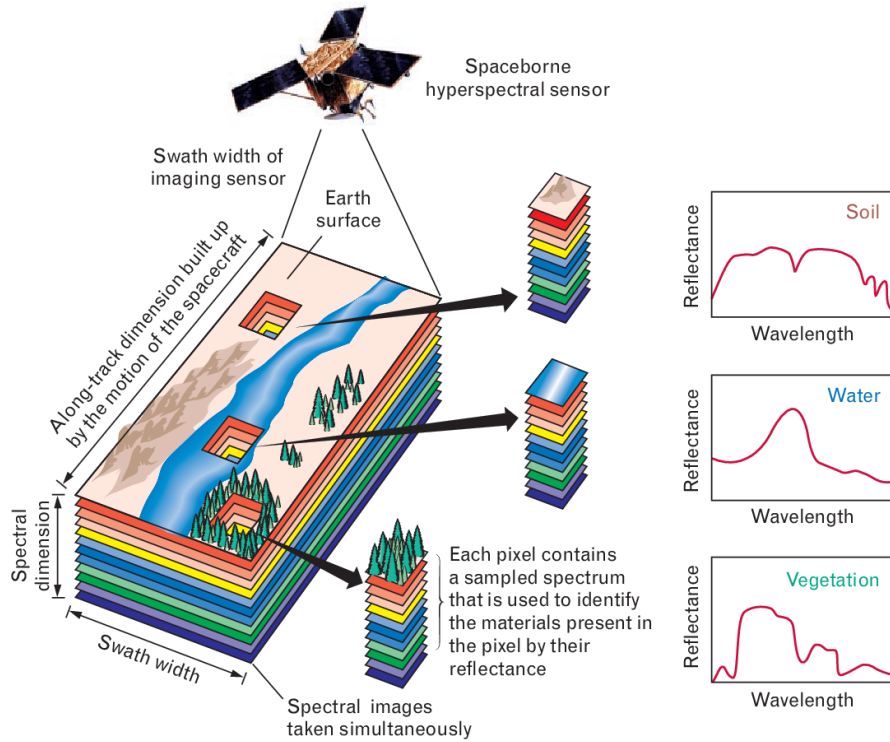


Figure 1.1 Imaging spectrometry of Earth Surface [8]

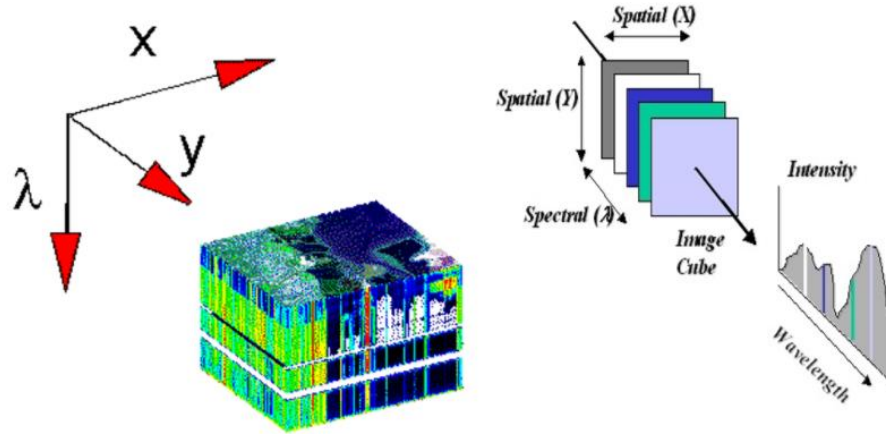


Figure 1.2 Hyperspectral Image Cube [14]

1.3 Engineered Surfaces

Engineered surfaces or built-up surfaces are the anthropogenic features through which water can not infiltrate into the soil, such as roads, driveways, sidewalks, parking lots, rooftops, and so on [15], as shown in Figure 1.3. In recent years, engineered surfaces have emerged not only as an indicator of the degree of urbanization, but also a major indicator of environmental quality [16]. An engineered surface may be defined as a stationary surface bearing the following characteristics:

- A man-made surface created artificially
- Less Depth/Thickness
- Single/mixed composition
- Stationary over a large span of time
- An identifiable collection of matter which is preferably 3-dimensional in nature

Examples: Roads, Roofs, Pavements, Sports infrastructures etc.



Figure 1.3 Matrix of image showing various types of Engineered surfaces

1.4 Significance of the Study

An Engineered or built-up surface is a unifying theme for all the communities including planners, landscape architects, engineers, scientists, social scientists, local officials, and others [17]. The magnitude, location, geometry and spatial pattern of built surfaces, and the built-up and non-built-up ratio in a watershed have hydrological impacts. Also, roof and transport related built-up surfaces could have a greater impact on land use zoning. The increase of built-up cover would lead to the increase in the volume, duration, and intensity of urban runoff [1]. Watersheds with large amounts of built-up cover may experience an overall decrease of groundwater recharge and base flow and an increase of storm flow and flood frequency [18]. Furthermore, increase in built-up cover and runoff directly impact the transport of non-point source pollutants including pathogens, nutrients, toxic contaminants, and sediment [19]. Increases in runoff volume and discharge rates, in conjunction with non-point source pollution, will inevitably alter in-stream and riparian habitats, and the loss of some critical aquatic habits [20]. In addition, the areal extent and spatial

occurrence of engineered surfaces may significantly influence urban climate by altering sensible and latent heat fluxes within the urban canopy and boundary layers [21]. As built-up cover increases within a watershed/administrative unit, vegetation cover would decrease. The percentage of land covered by built-up surfaces varies significantly with land use categories and sub-categories.

Therefore, estimating and mapping engineered surface is significant to a range of issues and themes in environmental science central to global environmental change and human environment interactions. The datasets of engineered surfaces are valuable for urban planning, e.g., building infrastructure and sustainable urban development, environmental management, e.g., water quality assessment and storm water taxation.

1.5 Research Gaps

This study proposes to address different research gaps identified through extensive literature survey. Following point-wise discussion summarizes the research gaps which have been considered for investigation:

- i. In Indian continent, no such spectral library has been explored for urban built-up surfaces and the study of urban surfaces and materials using HSRS is also yet to be explored intensively.
- ii. Various existing built-up indices are effective to some extent when applied to the urban environment but several problems still persist. The first problem is that most of the built-up indices are proposed to extract only single land cover class and confusion among other land cover classes still exists. For example, the confusion between built-up surfaces and bare soil has not been effectively reported in the literature [3] [60] [65] [72] [101] [102]. Furthermore, even though NDBI is projected to highlight built-up surfaces but it was not able to

efficiently differentiate built-up surfaces from bare soil [53]. The second problem of indices is related to limited applicability in remote sensing images at different spectral and spatial resolutions. Except vegetation indices such as NDVI and SAVI, most of the built-up indices are unavailable for high spectral resolution remote sensing images. Another challenge is that, most of the built-up indices have only been utilized to detect built-up surfaces in remote sensing imagery but not used to extract subcategories of these surfaces (e.g. roads and roofs). Even, several vegetation indices have already been reported in the literature to extract subclasses of vegetation (e.g. coniferous and deciduous). The next problem is associated with the identification of the most significant wavelength bands for extraction of built-up surfaces and its subclasses. Most of the built-up indices have not successfully utilized band selection approaches for the identification of suitable bands for development of built-up indices.

- iii. Urban built-up surface extraction using moderate and high resolution remote sensing data is still a challenging task due to significant intra-class heterogeneity, inter-class similarity and spectral confusion with other land cover classes. Further, high dimensionality of hyperspectral data increases the system and time complexity for the image analysis.
- iv. In spite of the rapid development of different built-up spectral indices and supervised classification/detection algorithms, there is still a lack of comprehensive comparison applied to various imageries acquired by different multispectral and hyperspectral sensors, especially from AVIRIS-NG sensor. Further, the performance evaluation of various sensors for extraction of road and roof surfaces has also not been explored.

1.6 Research Objectives

Following objectives have been drawn from the research gaps of existing literature:

- i. Spectral library creation and critical analysis of spectral characteristics of selected engineered surfaces and materials.
- ii. Identification of significant wavelengths and development of new spectral indices for extraction of engineered surfaces and sub-surfaces.
- iii. To address mixed pixel classification problem using combination of significant features such as spectral indices, principal components, and fractional abundances.
- iv. Comparative evaluation of indices based approaches with conventional classification/detection algorithms for extraction of engineered surfaces.

1.7 Thesis Overview

This thesis is organized into **Eleven Chapters**. **Chapter-1** discusses the motivation behind the research followed by introduction to imaging spectrometry / Hyperspectral Remote Sensing and Engineered Surfaces. The last section of this chapter describes the significance of the study. It also identifies the research gaps which lead to the formation of objectives of this research.

Chapter-2 is devoted to literature review on spectral library creation, various spectral index based algorithms, and several significant features in remote sensing imagery followed by a review of comparative assessment of different algorithms used for extraction of engineered surfaces in multi-sensor remote sensing imageries.

Chapter 3 to 9 separately discusses each of the objectives or sub-objectives, study area and dataset, description of tasks carried out on each objective, methodology and its implementation, observations and discussion of results.

Chapter-3 describes the spectral library creation of various engineered surfaces, sub-surfaces and materials for Indian regions followed by a critical analysis of spectral characteristics of these surfaces and materials.

In **Chapter-4** three new Spectral Indices have been proposed for extraction of urban built-up surfaces and its sub-classes in AVIRIS-NG hyperspectral Imagery while in **Chapter-5**, two new built-up indices have been proposed for extraction of road and roof surfaces based on their condition and deterioration. In **Chapter-6**, existing built-up indices developed for multispectral dataset, have been utilized for extraction of built-up surfaces and sub-surfaces in AVIRIS-NG imagery while in **Chapter-7**, extraction of aforesaid surfaces has been carried out using different band combinations of Red-Green-Blue (RGB) and Near Infrared (NIR) in AVIRIS-NG imagery.

Chapter-8 focuses on extraction of built-up surfaces, sub-surfaces, and materials by combination of various knowledge based features such as spectral index, principal component and fractional abundance.

Chapter-9 presents a performance evaluation of Sentinel-2B, Landsat-8 multispectral, and AVIRIS-NG hyperspectral imageries for extraction of road and roof surfaces using proposed spectral index based, and other conventional classification / detection algorithms.

Chapter-10 shows the conclusions of research followed by major research contributions, and limitations. Finally, **Chapter-11** describes the scope of future research.

Chapter 2

Literature Review

This chapter discusses the existing state-of-the-art for creation of spectral library of built-up surfaces and materials followed by spectral index based algorithms for extraction of built-up surfaces in remote sensing imagery. Subsequent sections discuss the literature on significant features for detection of built-up surfaces using high resolution hyperspectral imagery followed by a comparative assessment between various algorithms for extraction of aforesaid surfaces using multi-sensor imageries.

2.1 Spectral library creation

Urban environments characterize only a small percentage of the total land area, but these environments have turned into increasingly populated as larger number of individuals move from rural to urban areas and towns [5] [22] [23]. The term urban environment here refers to urbanization, which brings social and economic benefits (e.g. improved quality of life and economic prosperity), it also results in a number of environmental effects such as, degradation in the water quality [24], urban heat island effect and loss of biodiversity [25] etc. Urban environments basically consist of various built-up surfaces i.e. roads, roofs, pavements, sports infrastructure, railway tracks as well as non-built-up surfaces i.e. vegetation, soil and water. Due to aforesaid major environmental effects, the understanding of urban environment and their spatio-temporal analysis become necessary for urban planning, environmental management, risk assessment and disaster management. The dynamic behavior of urban environments demand technologies that are fast, repeatable and offer large

areal coverage at a reasonable price, makes remote sensing as one of the most feasible technologies [1] [25] [26] [27].

Modern advancement in the technology has witnessed extensive applications of Hyperspectral Remote Sensing (HSRS) in the field of image processing for identification of different urban built-up surfaces and materials on the basis of their unique characteristics [26] [27] [28]. HSRS technology is very useful in the study of urban environments due to its high potential in investigating the spectral properties or characteristics of urban surfaces and materials [29] [30]. The spectral properties of different surfaces and materials are responsible for the identification of various classes and sub-classes using HSRS [6] [31] [32].

Urban environments may be considered as one of the most demanding areas to carry out remote sensing analysis [33] [34] [35] due to high heterogeneity of urban built-up surfaces and materials [36]. Further, difficulty is attributed to the fact that urban area is characterized by typical land cover surface along with existence of various types of materials [29] [37]. Therefore, in remote sensing, it is of primary importance to study the spectral behavior of different built-up surfaces and materials. In view of this, most of the studies on urban built-up surfaces and materials have resulted in creation of a spectral library of these features followed by analysis on the basis of their unique spectral characteristics [6] [30] [33] [38] [39] [40] [41] [42] [43] [44] [45]. List of existing libraries as surveyed from literature is given in Table 1. These libraries include pure spectral signatures of the various built-up surfaces called as end members. Such libraries include wide range of materials over different wavelength in different spectral regions along with other information in the form of metadata and documentation regarding the quality of the spectral signature and surface characteristics [36]. The spectral samples of different surfaces and materials can be derived from the HSRS observations together with laboratory or field spectral

measurement [46] [47].

Table 2.1 Existing spectral libraries of urban built-up surfaces and materials

Study Area	Spectral Range (nm)	No. of Samples	Data Acquisition Platform	Spectral Library Reference
Various locations, USA	2500-14500	74	Laboratory and In- situ	[38]
Dresden and Potsdam, Germany	400-2500	32	Airborne and In- situ	[6] [39]
Santa Barbara, CA, USA	350-2400	26	In-situ	[30]
Tel-Aviv, Israel	400-1100	55	Airborne and In- situ	[33]
Serdang, Malaysia	350-2500	15	In-situ	[40]
London, UK	350-15400	74	Laboratory and In- situ	[41]
Various locations, USA	400-15400	3420	Laboratory	[42]
Various locations, USA	200-200000	2468	Airborne, Laboratory and In- situ	[43]
Madrid, Spain	350-2500 8000-14000	27	Airborne and In- situ	[44]
Karlsruhe, Germany	350-2500	181	In-situ	[45]

2.2 Spectral index based algorithms

Many approaches have been proposed for the extraction of built-up surfaces from remote sensing imageries in recent past, which include artificial neural network (ANN) [48] [49] [50], multiple regression [9] [48] [51], classification trees [5] [48] and spectral unmixing [52] [53] [54]. Nevertheless, the outcomes of these methods, to some extent, are dependent on the characteristics of the selected training samples. The detection results of parametric classifiers are also directly affected by the size, location, and representativeness of the training dataset. Further, it is difficult to identify the pure endmembers or the most representative endmembers from the heterogeneous urban environment to construct a model for subpixel analysis, as the spectral characteristics of built-up surfaces vary geographically [55] [56]. Consequently, the aforementioned classification and detection based approaches are often considered as computationally intensive, complex, and sometimes subjective, particularly when applied to the large geographical areas [57].

When compared with the aforesaid conventional algorithms for extraction and estimation of built-up surfaces, spectral index based approaches illustrate apparent advantages due to their ease of implementation, parameter independence, and convenience in practical applications. Initially, Kawamura *et al.* (1996) [58] observed the spectral behavior of built-up surfaces and developed urban index (UI) for the extraction of urban built-up surfaces. Afterward, extensive efforts have gone into formulating and applying indices to extract built-up surfaces over the preceding years [3] [57] [59] [60] [61] [62] [63] [64] [65] [66] [67] [68] [69] [70] [71] [72] [73]. The indices developed may typically be categorized into three groups, these are i) Band-ratio method using spectral bands as components in the index directly. Zha *et al.* (2003) [59] examined the spectral characteristics of urban built-up surfaces and proposed normalized difference built-up index (NDBI), which utilized a combination

of short-wave infrared (SWIR) and near-infrared (NIR) bands to enhance the contrast of built-up surfaces. After that, a series of specific spectral indices have been formulated and applied on various remote sensing imageries to extract urban built-up surfaces. Few examples of these are, built-up area index (BAI) [74], visible red near-infrared built-up index (VrNIR-BI), visible green near-infrared built-up index (VgNIR-BI) [75] and road extraction index (REI) [67]. Most of these indices are derived from multispectral data set by directly comparing the spectral characteristics of built-up and non-built-up surfaces ii) Through the association of built-up surfaces with other land cover classes, such as soil adjusted vegetation index (SAVI) [76] and modified normalized difference water index (MNDWI) [77]. In these indices, the negative correlation between imperviousness and vegetation indices is monitored, which is useful for the development of spectral indices for built-up extraction iii) By feature extraction methods, such as index based built-up index (IBI) [78] and biophysical composition index (BCI) [57] [79]. It is identical to the approaches that utilize more than one method for improvement of accuracy of detection in support with studies only utilized a single detection method.

2.3 Significant features in remote sensing imagery

Mapping of urban land covers using thematic spectral index based approach has proved to be effective because these indices mainly characterize a particular land cover class and demonstrate the relative abundance value of features of interest. Further, the extensively used approach in remote sensing to extract built-up surfaces in an urban environment is Spectral Mixture Analysis (SMA) based on V-I-S model [22] [80] [81]. The V-I-S model was first proposed by Ridd (1995) [80], which states that any urban landscape can be conceptualized as having three main components,

which are Vegetation (V), Impervious Surfaces (I) and Soil (S), in addition to the water. This model assumes that land cover in the urban environment is a linear mixture of these three components [80], which gives a guideline for decomposing urban environment and a relation for those components to remote sensing spectral characteristics. Prior to further spectral analysis, a method called feature selection is generally applied to determine the bands that are most efficient in discriminating each class from the others [5] [82] [83]. The objective of feature selection is to remove those bands that offer redundant spectral information, as well as to reduce the dimensionality. The widely used approaches in feature selection are Maximum Noise Fraction (MNF) and Principal Component Analysis (PCA). MNF is actually a revised PCA, which is suitable for hyperspectral imagery rather than the multispectral Thematic Mapper (TM) image [84] [85].

PCA is generally used to create new images for transforming high dimensional data from highly correlated bands to an orthogonal subset [85]. In PCA transformation, the rescaling and decorrelation of noise in the image based on an estimated covariance matrix generate different images in which there are no band to band correlations. The noise is separated from useful data, therefore improving spectral processing results. A study in the past has shown that the use of PCA transformation can improve the degree of recognition, then enhancing the accuracy of urban built-up extraction [84] [85]. But still, the ability of PCA is limited for hyperspectral data set as it relies only on the second order statistical information [85].

Normalized indices derived from multispectral bands have been commonly utilized in most of the studies for extraction of a particular land cover class. For example, Soil Adjusted Vegetation Index (SAVI) [76] has been used to estimate

vegetation as well as built-up surfaces in an urban watershed, in Index based Built-up Index (IBI) [86], Normalized Difference Built-up Index (NDBI) [3] has been combined with SAVI and Modified Normalized Difference Water Index (MNDWI) [77] to enhance the built-up estimation. Further, Normalized difference Built-up Area Index (NBAI) [62] and Road Extraction Index (REI) [67] have been utilized to extract built-up areas as well as road surfaces directly by selecting an appropriate threshold. The major problem with all the aforesaid built-up spectral indices is that, these are not capable of effectively separating bare soil from built-up surfaces due to limitations of multispectral dataset [3] [77] [86] [87] [67] [88] [89].

Next, in comparison with traditional pixel based methods, some sub-pixel based algorithms, commonly Linear Spectral Mixture Analysis (LSMA) have shown its effectiveness for abundance estimation and mapping of urban built-up surfaces. LSMA has been extensively applied in coarse to medium and high resolution remote sensing images to quantitatively extract the urban built-up surface fractions in mixed pixels at a sub-pixel scale. However, the LSMA still has some complexity in extracting high-precision urban built-up surfaces and materials because of the similar spectral response among different land cover types [54] [90].

2.4 Comparative assessment of different algorithms using multi-sensor imageries

As for urbanization, it is a primary requirement to derive land use land cover (LULC) maps from remote sensing imageries. In recent years, Landsat, ASTER, Sentinel and Hyperion imageries are frequently utilized for LULC mapping and for now, some researches focused on modeling of urban sprawl and its environmental impact, and simulating the phenomenon of heat island. In general, there are three main indicators

to describe the urban environment including the density of vegetation, biodiversity and built-up surfaces. The increase in the built-up surfaces in urban area has led to the decrement of natural resources and degradation of the environment [25] [67].

A large number of remote sensing satellites provide us with continuous imageries in different wavelength bands for the applications of land use, marine, agriculture, climate, defense and security etc. The new generation of moderate resolution (10–30 m) Earth Observation (EO) satellites have become operational during the last few years. Landsat-8 OLI (Operational Land Imager) / TIRS (Thermal Infrared Sensor) was launched on 11 February 2013. The bands of multispectral OLI sensor have a 30 m spatial resolution and wavelength ranges similar to the prior Landsat TM (Thematic Mapper) and ETM (Enhanced Thematic Mapper) sensors to provide data continuity [91]. The European Sentinel-2 satellite aims at offering multispectral data with a 5 day revisit cycle. The Sentinel-2A and Sentinel-2B satellites became operational on 23rd June 2015 and on 7th March 2017, respectively. The Sentinel-2A and 2B MSI (Multi Spectral Instrument) sensors have 13 spectral bands with a 10–60 m spatial resolution [92] [93]. Further, Jet Propulsion Laboratory's Airborne Visible / Infrared Imaging Spectrometer- Next Generation (AVIRIS-NG) sensor is a hyperspectral sensor, which measures the spectral range over the interval of 376–2500 nm at 5 nm intervals with high SNR (>2000 @ 600 nm and >1000 @ 2200 nm) and an accuracy of 95%. The field-of-view (FOV) is 34° and instantaneous FOV (IFOV) of AVIRIS-NG sensor is 1 milli radian. In the past 30 years, Landsat series data are extensively used in the mapping of LULC. Though, with the development of new sensors, it is essential to use numerous types of remote sensing data, particularly in the monitoring of long term dynamics. During the process, there may be a discrepancy between the dissimilar sensors. When two sensors are utilized, a number of problems may appear due to the differences in solar illumination condition,

viewing angle, spectral band pass and radiometric precision. In the past, the comparisons were conducted based on bands, spectral indices and classification algorithms. In recent years, some researchers have also carried out comparative analysis and integrated application utilizing Sentinel-2A MSI and Landsat-8 data [4] [94] [95]. It is worth stating that Zhang *et al.* (2018) [79] characterized the differences in nadir bidirectional reflectance distribution function (BRDF) adjusted reflectance, top of atmosphere (TOA) and Normalized Difference Vegetation Index (NDVI) between Landsat-8 and Sentinel-2A.

In order to accurately and rapidly map built-up surfaces from satellite imageries, previous studies have put forward various algorithms based on spectral indices and supervised learning. Spectral index based algorithms include Road Extraction Index (REI) [67], Normalized Built-up Area Index (NBEI) [62], Normalized Difference Built-up Index (NDBI) [3], Index-based Built-up Index (IBI) [3], and the Normalized Difference Impervious Surface Index (NDISI) [25] etc. Further, different supervised learning algorithms cover Spectral angle Mapper (SAM) [96], Spectral Information Divergence (SID) [97], Matched Filter (MF) [98], Minimum Distance to mean and Support Vector Machine (SVM) [99] [100] etc. All the aforesaid built-up indices have been proposed for specific sensor imageries. Besides, extraction of road and roof surfaces, using these indices for aforesaid imageries has not been explored.

Finally, in view of the literature review on spectral library creation, spectral index based algorithms, significant features in remote sensing imagery, and comparative assessment of different algorithms used for extraction of engineered surfaces in multi-sensor imageries, various research gaps are identified, which lead to different research objectives. These research gaps and objectives of the research have been discussed in Chapter 1 Section 1.5 and 1.6, respectively.

Chapter 3

Spectral Library Creation and Analysis of Spectral Signatures

Most of the studies on urban built-up surfaces and materials have resulted in a spectral library creation followed by its analysis [39] [40] [41] [42] [43] [44] [45]. Further, in Indian continent, no such spectral library has been explored for these surfaces and materials and the study using HSRS is also yet to be explored intensively. This chapter deals with the creation of a spectral library and critical analysis of spectral characteristics of urban built-up surfaces and materials. Field measurements have been carried out using spectroradiometer over the wavelength range of 350 to 2500 nm. Further, this chapter investigates the unique spectral characteristics and complexity of heterogeneous urban environments using spectral signatures of major urban built-up surfaces and materials in Indian regions.

The tasks under this objective are:

- a) Spectral library creation and critical analysis of spectral signatures of urban engineered / built-up surfaces and materials in Indian continent
- b) Identification of significant wavelengths and regions for extraction of different built-up surfaces and materials

3.1 Study area

The area under examination belongs to the Udaipur, Rajasthan, India, which is a mixture of built-up and non-built-up surfaces. The focus in this study is only on built-up surfaces. Therefore, built-up surfaces are further categorized into different levels upto constituent material, which will be discussed in upcoming section. Spectral signatures of these surfaces and materials are utilized for identification of significant spectral wavelengths and regions for extraction of various classes.

3.2 Instrumentation and software

Ground spectral data in the study region is collected using Spectral Evolution Spectroradiometer. This instrument is having proven effectiveness in the applications in different areas, which require measurement of reflectance, radiance and irradiance. It has 2151 spectral channels over the spectral range of 350 nm to 2500 nm. The whole spectral range is divided into various regions, which are visible, near infra-red (NIR) and short wave infra-red (SWIR), respectively. Further, the data collection has been carried out using gun as well as contact probe, depending on the lighting condition. The field data has been collected between 10 am to 3 pm in cloud free atmospheric condition. The spectral signature has been collected in a set of four for each sample of built-up surfaces. Before recording the spectral signature of target, white reference is recorded using Spectralon plate. Figure 3.1 (a) represents the satellite imagery of Udaipur with some points representing the field sample locations of built-up surfaces and materials. There are various fields of metadata which have been included in the spectral library of built-up surfaces and materials. These fields are Fore Optics (Contact Probe / Gun), Scan ID of Spectra, Latitude, Longitude and

Altitude, Material Composition, Name of class and sub-class, Observation, Temperature, Relative Humidity, Radiometric Calibration and GPS Time.

The spectral analysis of different built-up surfaces have been carried out visually and using continuum removed spectra, which is utilized for identification of significant regions and wavelengths for a particular surface or material. Continuum analysis has been carried out using IDL DISPEC 18.03 tool [47]. The basic software utilized in this study includes Environment for Visualizing Images (ENVI) 5.3 and ArcGIS 10.4. ENVI 5.3 accepts all the spectral data in ASCII format and converts it in the form of spectral library, which can be represented in any of the graphical format for analysis. Further, ArcGIS 10.4 is utilized for mapping of all the point coordinates associated with field data into satellite imagery of the study region. Figure 3.2 (b) represents some of the photographs of ground data collection campaign of different built-up surfaces and materials.

3.3 Urban Engineered or Built-up surfaces

As suggested from the studies in the past [6] [30] [33] [38] [39] [40] [41] [42] [43] [44] [45], in this study, the major urban engineered surfaces exist in the Indian regions, have been categorized into different levels (Level- 1, 2, 3 and 4), which are tabulated in Table 3.1.

Table 3.1 Categorization of various engineered surfaces in different levels

Level - 1	Level - 2	Level - 3	Level-4
Engineered / Built-up Surfaces	Roof / Building	Concrete	
		Asbestos	
		CGI Sheet	New

		Irony
		Cement
		Wood
		DPC Brick
		Sandstone
Roads and Pavements	Bitumen road	New
		Old
		Repaired
	Bitumen Parking Lot	
	Asbestos pavement	
	Concrete Road	
	Concrete Pavement	
	Concrete Bridge	
	Charcoal	
	Brick pavement	
Railway Track	Sleeper	
	Track Iron	
	Ballast boulder	
	RCC	
	Concrete log	
Sports Infrastructure	Basketball court	Concrete
		Blue fabric
		Red fabric
		Bitumen
	Volleyball court	Fabric
		Cement
	Tennis court	Fabric
	Cricket pitch	Cement

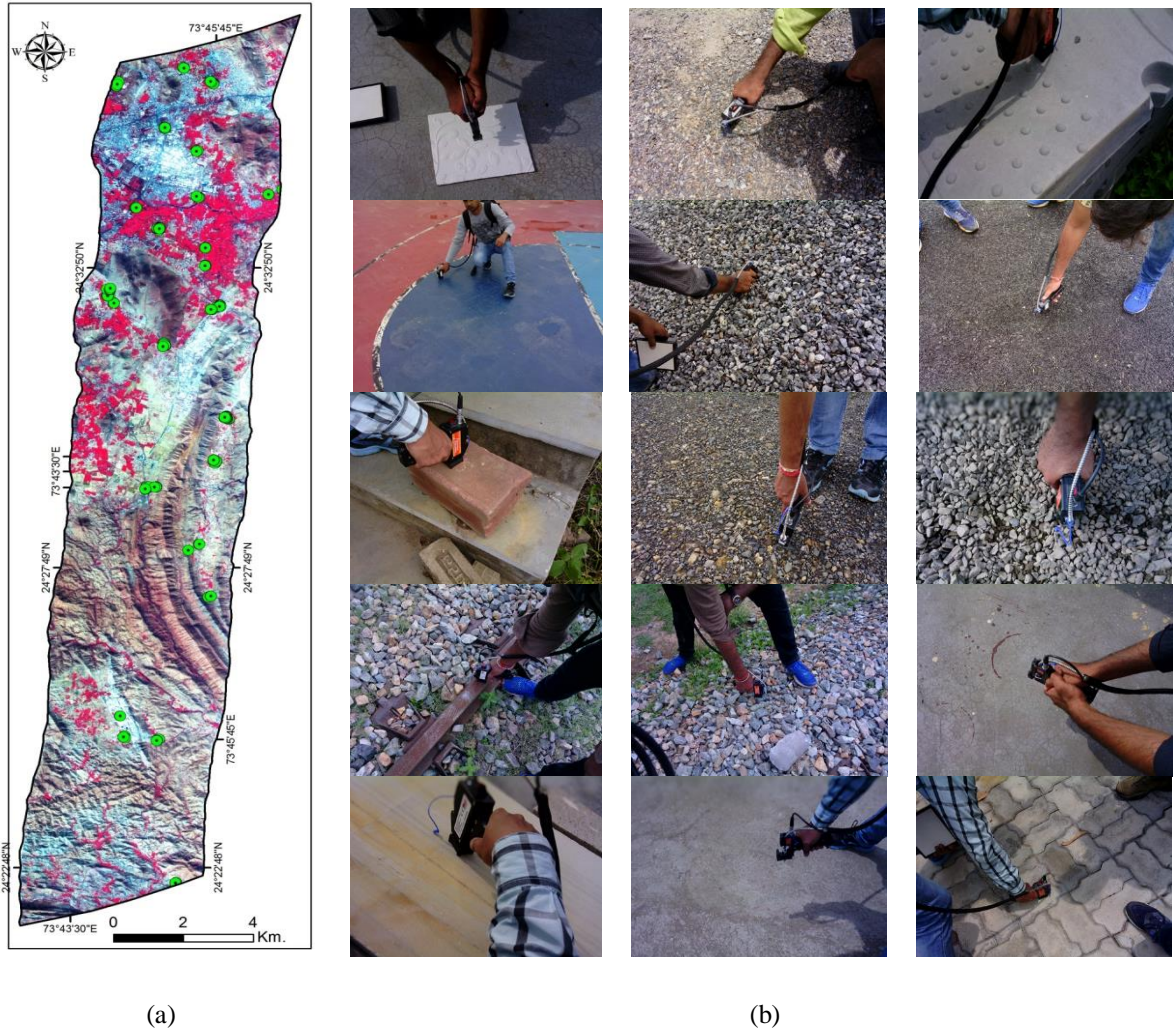


Figure 3.1 (a) The green points on the imagery of Udaipur, Rajasthan, India represent the actual locations of ground spectral data collection (b) Some of the selected photographs of field data collection campaign

As mentioned in the study area, the spectral signatures of built-up surfaces have been captured in the wavelength range of 350 - 2500 nm with 1 nm spectral sampling. These wavelengths are divided into different spectral regions for the analysis of various spectral signatures of engineered surfaces, as shown in Table 3.2.

Table 3.2 Division of full spectral range into different wavelength regions

Region	Wavelength Range
Visible	350 nm – 700 nm
Very Near Infra-Red (VNIR)	700 nm – 1000 nm
Far Near Infra-Red (FNIR)	1000 nm – 1500 nm
Early Short Wave Infra-Red (ESWIR)	1500 nm – 2000 nm
Far Short Wave Infra-Red (FSWIR)	2000 nm – 2500 nm

3.4 Implementation

This research has been carried out in two different stages:

a) Spectral library creation and analysis of spectral signatures of built-up surfaces and materials

- i. Obtaining in-situ spectral signatures of different urban built-up surfaces and materials
- ii. Categorization of urban built-up surfaces (Level-1) into sub-surfaces (Level-2) and then further these sub-surfaces into materials (Level-3 and 4)
- iii. Creation of spectral library of aforesaid surfaces and materials in Level-1, 2, 3 and 4
- iv. Division of full spectral range i.e. 350-2500 nm into different spectral regions, which are visible, VNIR, FNIR, ESWIR and FSWIR
- v. Visual analysis of spectral signatures of built-up surfaces (Level-1, 2, 3 and 4)

b) Identification of different significant wavelengths and regions of built-up surfaces and materials

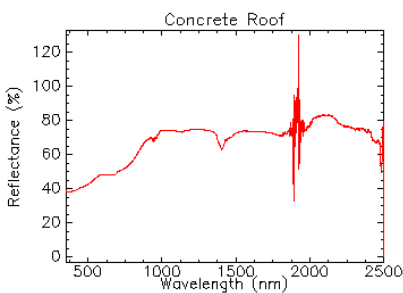
- i. Generation of continuum removed spectra of all the built-up surfaces and materials
- ii. Critical analysis of spectral signatures of built-up surfaces and materials using various statistical parameters
- iii. Finding out the significant wavelengths of absorption in different regions of built-up surfaces and materials

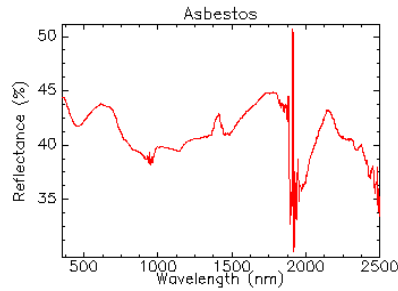
3.5 Spectral library creation and analysis of signatures of Urban Engineered / Built-up surfaces

3.5.1 Roof / Building

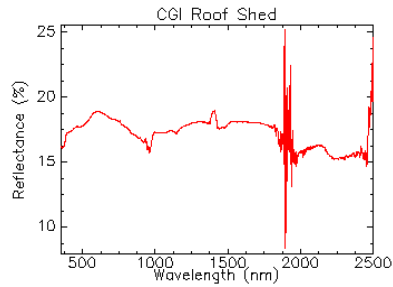
The spectral signatures of different types of roof surfaces and materials along with the observations are tabulated in Table 3.3.

Table 3.3 Spectral library creation and analysis of roof surfaces

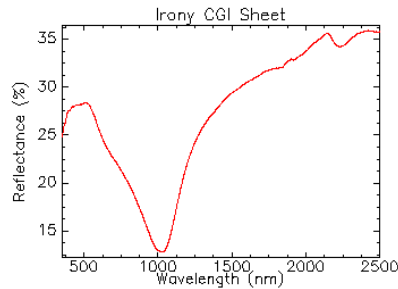
Spectral Signature	Observation
 <p>The graph displays the spectral signature of a concrete roof. The y-axis represents Reflectance (%) from 0 to 120, and the x-axis represents Wavelength (nm) from 500 to 2500. The reflectance is relatively stable around 70-80% in the visible and VNIR regions, with a sharp absorption feature (dip) around 1900 nm in the FSWIR region.</p>	<p>The reflectance is almost constant in all the regions except in visible. Some small absorption features due to metallic component and hydrocarbons, are observed in visible, VNIR, and FSWIR regions, respectively.</p>



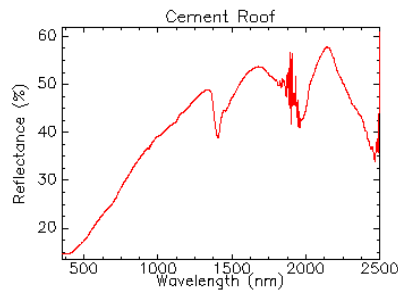
In visible and FSWIR, the response is almost concave with some major peaks. The reflectance decreases from visible to VNIR, while having sinusoidal behavior in FNIR. The response is almost constant in ESWIR. Further, iron oxide and hydrocarbon absorption features dominate in VNIR, FNIR, and FSWIR regions, respectively.



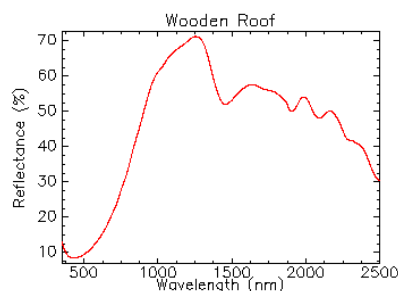
In fresh CGI sheet, response is almost constant in all the regions, which has some absorption features near 1020, 1250 and 2250 nm.



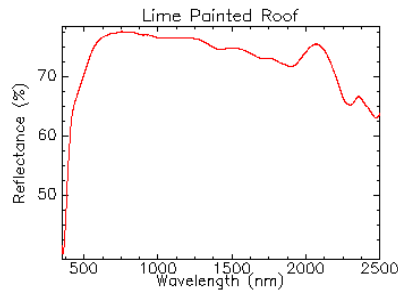
In irony CGI sheet, the reflectance decreases from visible to VNIR while it increases from VNIR to FSWIR with a major absorption near 1050 nm. A minor absorption also appears near 2250 nm.



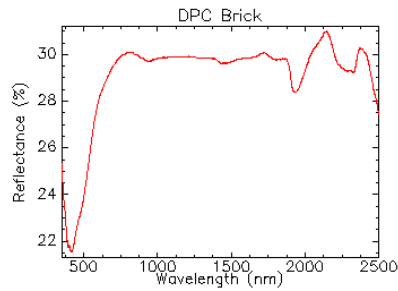
The spectral response of cemented roof surface increases from visible to FNIR while having sinusoidal behavior in ESWIR and FSWIR regions. It has a major peak in FSWIR with some minor absorptions in FNIR.



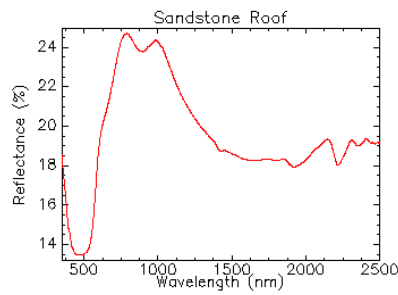
There is a sudden increase in reflectance from visible to VNIR and FNIR while behaves as a decreasing sinusoid in all the other regions with different peaks and absorptions.



The reflectance is high and almost constant in all the regions with different peaks and absorptions in FSWIR. Some minor absorptions also appear in VNIR and FNIR regions.



Spectral signature of DPC brick is almost constant in all the regions with a peak and major absorption in FSWIR. Further, some minor absorptions are observed in visible, FNIR and ESWIR regions.

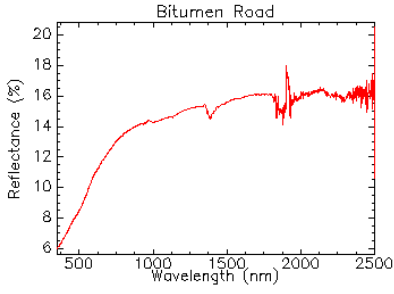
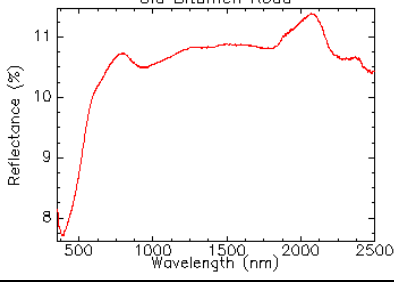
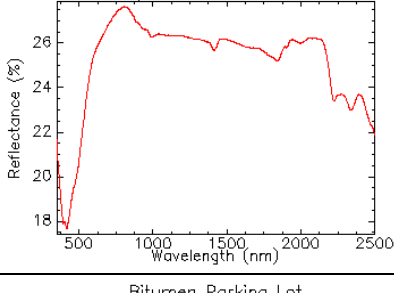
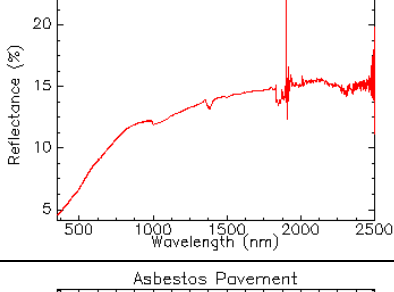
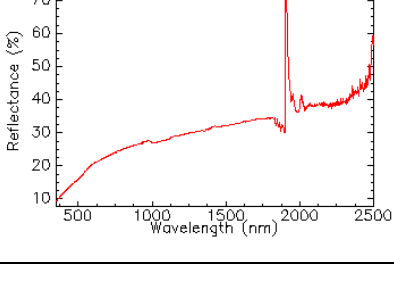


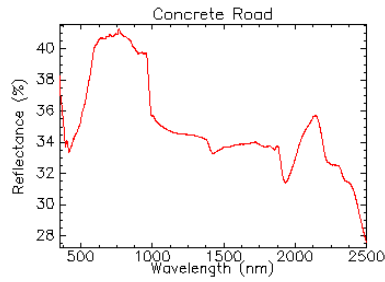
The response of sandstone roof increases from visible to VNIR while decreases from VNIR to ESWIR and almost constant in FSWIR regions. Some absorption features are observed near 890, 2250 and 2390 nm.

3.5.2 Roads and Pavements

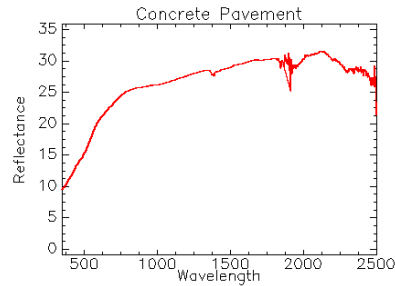
The spectral characteristics of various types of roads and pavements are shown in Table 3.4. The observations drawn from the analysis of signatures are also tabulated in Table 3.4.

Table 3.4 Spectral library creation and analysis of roads and pavements

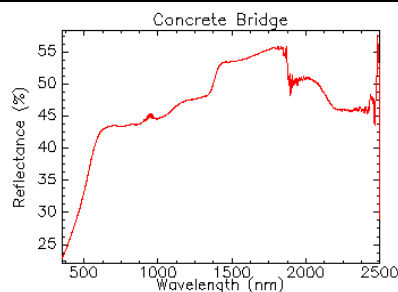
Spectral Signature	Observation
	<p>The spectral response of bitumen roads linearly increases in visible region while almost constant in all the other regions with minor absorptions near 1190 and 2350 nm.</p>
	<p>The spectra of old bitumen road is almost flat in all the regions with major peak in FSWIR region. Iron oxide absorption appears in VNIR.</p>
	<p>The response of repaired bitumen road is almost flat in all the regions with some hydrocarbon absorptions near 2250 and 2400 nm. A minor absorption due to metallic component is observed in VNIR.</p>
	<p>Bitumen Parking lots are having same response as road but more flatter with two absorption bands near 1050 and 2260 nm.</p>
	<p>The spectra of asphalt pavement linearly increases in all the regions with lesser slop. Some small absorptions are observed in VNIR and FNIR regions.</p>



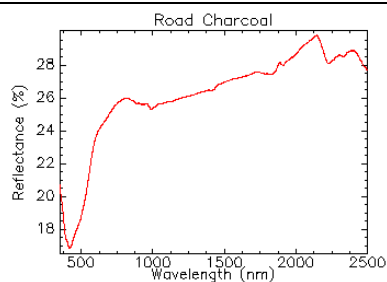
The spectral signature of concrete road appears to have some minor absorptions in VNIR and FSWIR regions.



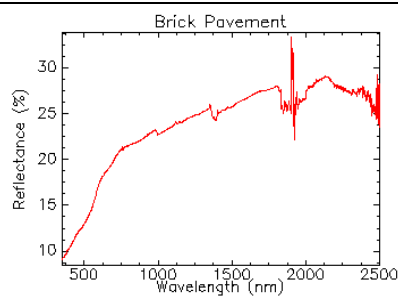
Signature of concrete pavement is almost flat in all the regions except in visible while more concavity with hydrocarbon absorptions is observed near 2290 nm in FSWIR.



The spectral signature of concrete bridge linearly increases in all the regions except FSWIR, while it becomes almost flat in FSWIR region. Some iron oxide and hydrocarbon features highlight in FNIR and FSWIR regions, respectively.



Spectra of road charcoal is almost flat in all the regions with clay absorption near 2350 nm. The iron component appears to dominate in FNIR region near 1020 nm.

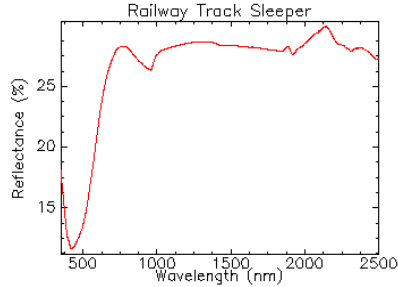
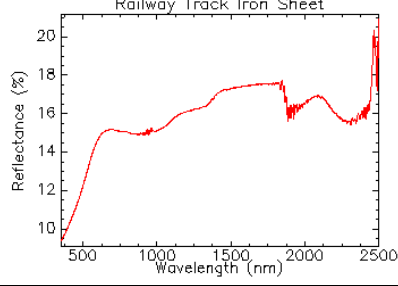
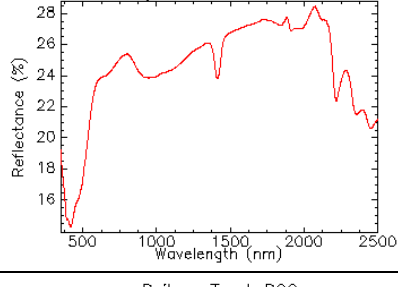
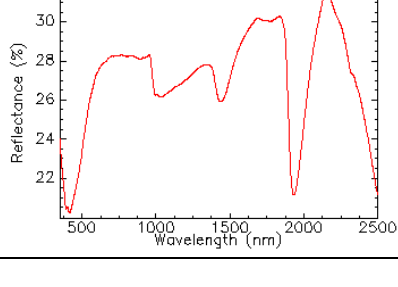


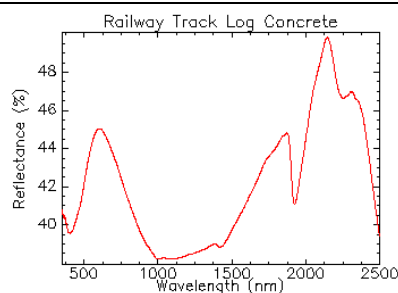
The response of brick pavement gradually increases in all the regions with two minor absorptions near 1050 and 2250 nm.

3.5.3 Railway Track

The spectral responses of various types of surfaces and materials associated with railway track are given in Table 3.5. Several observations have been derived from the analysis of spectral signatures, are also shown in Table 3.5.

Table 3.5 Spectral library creation and analysis of railway track

Spectral Signature	Observation
	<p>The response of railway track sleeper is almost constant in all the regions with some iron oxide and hydrocarbon absorptions in VNIR and FSWIR, and a peak in FSWIR region.</p>
	<p>Here, the iron properties seem to be disappear, as slight absorption is observed in VNIR Also, the hydrocarbon absorption dominates in FSWIR</p>
	<p>Spectra of ballast boulder is almost flat and having different absorptions in FNIR, ESWIR and FSWIR regions. These absorptions may be due to iron oxide and different hydrocarbons.</p>
	<p>Here, the more absorption features appear in FNIR and ESWIR regions. The hydrocarbon absorptions in FSWIR are disappeared.</p>



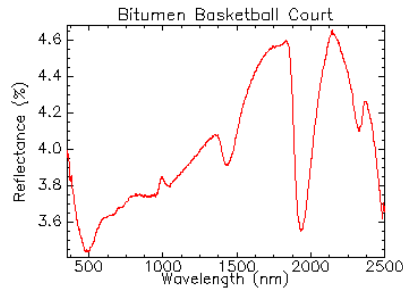
In concrete log, absorption features are observed due to iron oxide and hydrocarbons near 1000 and 2240 nm, respectively.

3.5.4 Sports Infrastructure

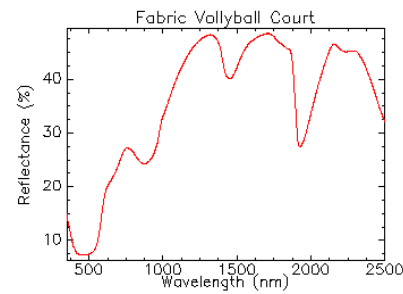
The spectral characteristics and observations of different types of surfaces and materials used in the construction of sports infrastructure are shown in Table 3.6.

Table 3.6 Spectral library creation and analysis of sports infrastructure

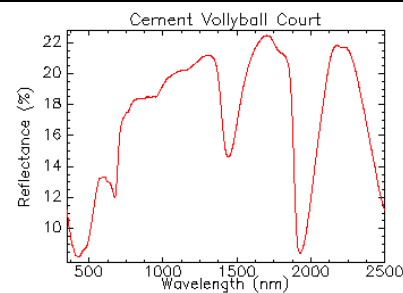
Spectral Signature	Observation
	<p>The signature of concrete surface is almost constant in all the regions except in visible. Further, two minor absorptions due to iron oxide are observed in VNIR with a slight concavity in FSWIR.</p>
	<p>The signature of blue fabric behaves as decreasing sinusoid in FNIR, ESWIR and FSWIR regions with a blue peak in visible region.</p>
	<p>Here, the signature is almost similar to blue fabric but a red peak is observed near 670 nm.</p>



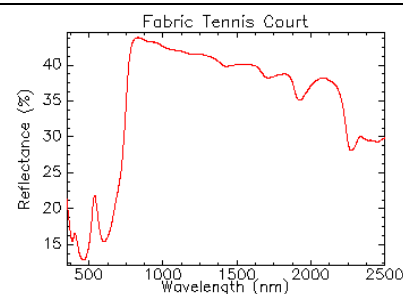
The reflectance of bitumen court appears to have very less reflectance in all the regions with a major peak and concavity in FSWIR. Minor iron oxide and hydrocarbon absorption features appear near 1030 and 2380 nm, respectively.



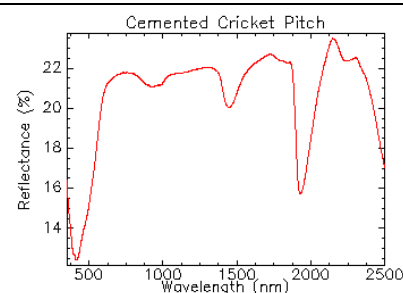
The signature of fabric increases linearly in all the regions with different iron oxide and hydrocarbon absorptions in visible, VNIR and FSWIR regions. Further, due to color of fabric, the red peak is dominating at 665 nm.



The spectral characteristics of cemented volleyball court is almost flat in all the regions with different iron oxide absorptions in visible and VNIR regions.



The signature of tennis court fabric is having a red peak with different hydrocarbon absorptions near 1750 and 2420 nm, while it is almost flat in VNIR, FNIR and ESWIR regions.



In spectral response of cemented cricket pitch, a major peak appears in the FSWIR region with different iron oxide and hydrocarbon absorptions near 890 and 2240 nm, respectively.

3.6 Identification of significant wavelengths and regions for extraction of different built-up surfaces and materials

For quantification of absorption features in spectra, the overall concave shape of a spectrum should be removed. This normalization procedure is referred as continuum removal or convex-hull transform, continuum equation is given as:

$$S_{CR}(\lambda) = \frac{S(\lambda)}{C(\lambda)} \quad (3.1)$$

Where $S_{CR}(\lambda)$ is continuum removed spectra while $S(\lambda)$ is original spectra and $C(\lambda)$ is continuum curve.

The resulting spectrum in Equation 3.1 i.e. $S_{CR}(\lambda)$ is equal to 1.0 where the continuum and the spectra match, and less than 1.0 where absorption features occur. The resulting spectrum has been analyzed for determining the changes in absorption features in different regions of spectra. The continuum removed spectra was further analyzed to calculate the parameters that depict the absorption feature, such as central wavelength position, area of the absorption A , absorption asymmetry and feature depth. The relative depth, D is defined as the difference between the continuum line and minimum value in the continuum removed spectra,

$$D = 1 - \min(S_{CR}(\lambda)) \quad (3.2)$$

The area of absorption feature is defined as the summation of individual areas between continuum line and the channels in the continuum removed feature, it is given as,

$$A = \sum_{i=1}^n (1 - S_{CR}(i)) \quad (3.3)$$

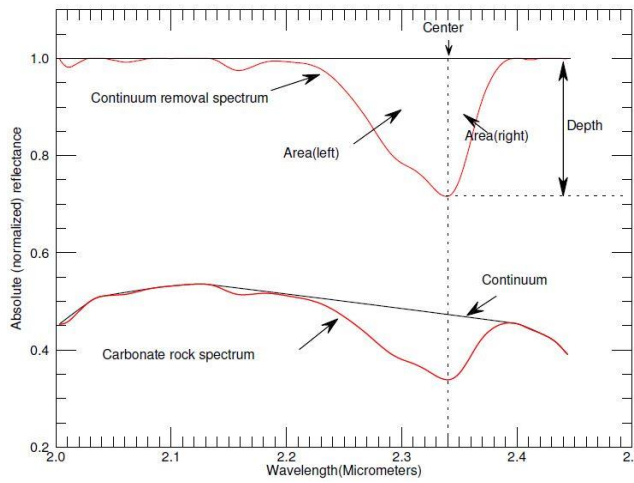
Where i is the number of channels from the starting point to end point. The

asymmetry factor AF of the absorption feature is given as,

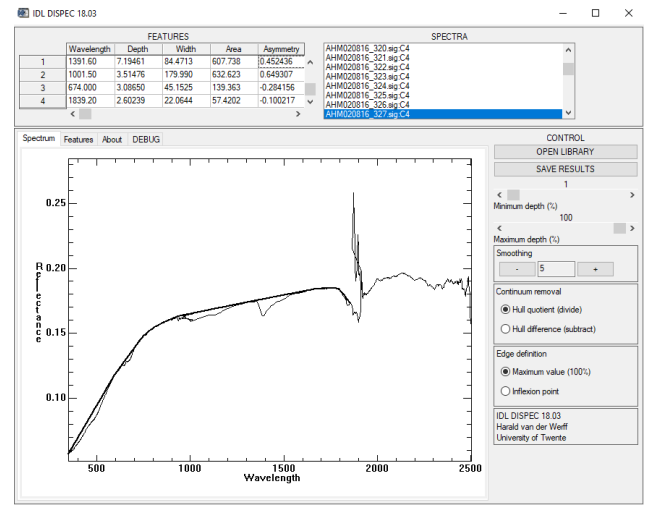
$$AF = \frac{Area_{left}}{Area_{Right}} \quad (3.4)$$

Figure 3.2 represents the analysis of spectral signature of a sample using various statistical parameters i.e. relative depth, area of absorption, and asymmetry factor, using IDL DISPEC 18.03 tool developed by University of Twente, Netherlands [47]. Figure 3.2 (a) shows the spectra of a rock sample along with its continuum removed curve while Figure 3.2 (b) represents the spectral analysis of a particular sample using above mentioned tool and parameters. Further, Figure 3.2 (c) shows the normalized reflectance curve of a sample, which is used for calculating aforesaid statistical parameters associated with spectral signature of a particular class. On the basis of spectrum generated by continuum removal analysis and different statistical parameters, various significant wavelengths in different regions are obtained, which can prove to be effective for extraction of a particular built-up class or material. The significant absorption parameters and central wavelengths of spectral signature of different built-up surfaces and materials are shown in Table 3.7. In this study, these central wavelengths are termed as significant wavelengths. Table 3.8 describes various significant wavelengths and regions for different subcategories of urban built-up surfaces. These significant wavelengths can be utilized for detection and identification of a particular surface or material in hyperspectral imagery. Further, the aforesaid spectral library can be used for extraction and unmixing of different engineered surfaces and materials in hyperspectral imagery. The significant wavelengths and absorption features of the most the surfaces and materials have been validated with the existing literature on spectral library creation and analysis [6] [30]

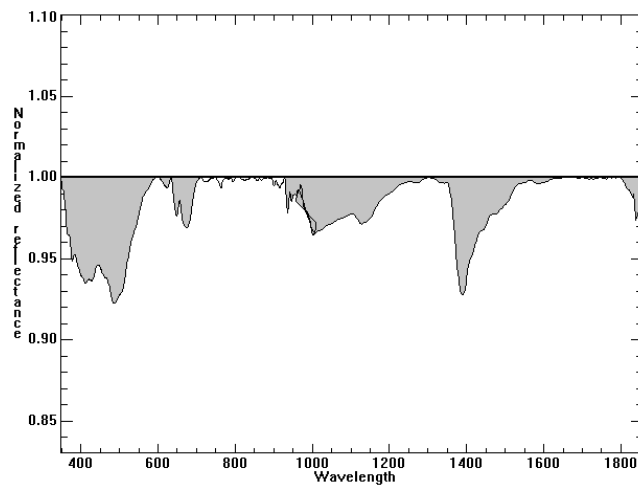
[33] [38] [39] [40] [41] [42] [43] [44] [45].



(a)



(b)



(c)

Figure 3.2 (a) Sample spectral signature of a rock with continuum removal curve (b) Spectral analysis in IDL DISPEC 18.03 tool (c) Normalized reflectance of a sample

Table 3.7 Significant absorption parameters and wavelengths of different built-up surfaces and materials

Built-up Surfaces	Material	Centre wavelength (nm)	Absorption parameters		
			Depth	Area	Asymmetry Factor
Roof / Building	Concrete	576	0.3589	27.8990	0.3426
		733	0.4318	38.3658	0.9486
		2120	0.3687	28.9285	1.1042
		2172	0.4565	40.2638	0.7327
	Asbestos	480	0.2342	20.1669	0.9239
		933	0.2589	21.2892	1.2068
		1119	0.3187	25.5869	0.7139
		1357	0.3713	31.3185	1.8132
		2245	0.2982	28.1563	1.1253
		2290	0.2678	23.7865	1.6747
	New CGI Sheet	985	0.2489	21.0563	2.5136
		1235	0.3256	26.1860	0.6142
		2230	0.2769	24.8906	0.1632
	Irony CGI Sheet	1029	0.1582	16.4378	1.1241
		2250	0.2864	23.5620	0.9285
	Cement	1572	0.4065	35.3217	0.6837
		2120	0.3874	33.1226	3.0921
		2245	0.3689	29.8856	0.5986
	Wood	1632	0.3654	28.3547	1.7143
		1955	0.2986	28.1538	1.1726
		2110	0.2740	23.0542	1.2631
		2230	0.3152	24.6495	1.5204
	Lime painted	834	0.3354	27.1549	1.2683
		2080	0.2786	24.3209	0.3225
		2340	0.2579	22.5438	2.7532

	DPC Brick	980	0.3245	25.9942	1.3129
		2040	0.2465	21.4376	0.2931
		2235	0.2842	25.6203	2.4364
	Sandstone	910	0.2669	24.0962	0.8962
		2240	0.2474	22.1903	0.9626
		2320	0.3128	24.9860	0.7219
Roads and pavements	Bitumen	490	0.4589	35.6032	0.3749
		560	0.4123	32.8937	0.7302
		832	0.3936	29.6039	0.2253
		2115	0.3924	27.1586	1.4542
	Old Bitumen	618	0.4563	31.4679	0.7468
		890	0.3165	27.1834	0.5196
		2142	0.3454	30.3545	2.3184
		2260	0.3786	25.1673	2.0472
	Repaired Bitumen	672	0.4235	31.0589	1.2153
		840	0.3589	29.2130	0.5327
		932	0.3182	31.3902	0.3269
		2258	0.2865	24.5439	2.4326
		2320	0.2674	27.0498	0.9845
	Bitumen Parking Lot	1046	0.2915	25.6548	0.6389
		2065	0.3134	32.5639	1.2545
		2115	0.3060	27.0940	2.2341
	Asbestos Pavement	570	0.3471	28.3871	0.7218
		685	0.4005	35.6232	0.9342
		2352	0.3512	26.7129	0.7894
	Concrete Road	590	0.3265	29.5603	1.3876
		2245	0.2969	24.1689	2.6548
		2310	0.3050	26.8560	0.9030
	Concrete Pavement	2210	0.3267	30.6811	1.4276

		2250	0.2849	26.6232	1.2135
	Concrete Bridge	745	0.3173	28.3019	0.9684
		890	0.3035	23.6833	0.7782
		932	0.3785	24.5627	0.6598
		1366	0.2914	27.1131	0.4973
		2032	0.4189	34.5139	0.3259
		2195	0.3485	27.8523	0.9438
	Road Charcoal	1012	0.2876	25.3910	0.5489
		1265	0.3348	23.6504	0.6578
		2045	0.3187	26.3219	0.5764
		2256	0.2965	31.5921	1.2867
	Brick Pavement	1032	0.3090	26.6125	0.5364
		1380	0.3365	29.1927	0.6485
		2172	0.3498	24.3195	0.4358
		2355	0.3649	21.3295	2.1043
Railway track	Sleeper	1024	0.2819	23.4675	2.1546
		2210	0.3117	28.5198	0.5467
		2235	0.3276	29.0341	0.8965
	Track Iron	932	0.3456	25.9315	0.9327
		2118	0.4678	37.3776	0.7689
		2350	0.3129	26.1732	1.6785
	Ballast boulder	985	0.2854	29.1654	0.4528
		1352	0.3817	31.4187	0.5674
		2250	0.2654	22.3549	2.3583
		2325	0.2918	27.0183	2.1739
	RCC	1013	0.2478	20.6798	0.6549
		2235	0.3587	29.1169	1.5127
		2352	0.3159	26.9932	2.1589
	Concrete log	2240	0.2878	23.8232	2.8631

		2375	0.3295	28.1428	1.7647
Sports infrastructure	Basketball Court :				
	Concrete	1052	0.2967	24.1832	0.6538
		1132	0.2789	28.4259	1.3672
		2140	0.3456	29.3274	1.3281
		2235	0.3080	26.5798	1.6782
	Blue Fabric	670	0.2134	19.3459	0.9658
		1085	0.2767	24.9512	0.8359
		1133	0.3585	30.2649	0.7527
		1365	0.2786	21.6341	1.1324
		1750	0.2675	25.5875	0.8376
		2275	0.3298	30.7023	1.2673
		2340	0.3050	24.9456	2.1273
	Red Fabric	550	0.2334	20.2192	1.2468
		1052	0.2754	23.4236	1.1835
		1136	0.4030	35.7529	0.8694
		1754	0.3125	27.8031	1.3259
		1815	0.3876	29.2643	0.9854
		2245	0.3126	22.8249	1.5284
		2320	0.3656	28.6324	2.2543
	Bitumen	490	0.2345	19.7248	2.3459
		985	0.2786	23.1952	1.7538
		2210	0.2643	24.9562	0.8954
		2355	0.3564	29.0913	1.2143
	Volleyball Court :				
	Fabric	972	0.2605	22.7620	0.3427
		2080	0.3320	27.3546	0.9236
		2135	0.3420	25.9126	0.7395
		2260	0.4007	31.1852	0.9638

Cement	692	0.2730	22.3482	0.7659
	832	0.3023	26.5127	1.3946
	2245	0.3546	30.2454	0.8638
Tennis Court:				
Fabric	425	0.2693	25.1165	0.6392
	635	0.2809	23.8327	0.2955
	1750	0.2846	21.8205	0.9243
	2355	0.3107	27.5720	1.2967
Cricket Ground:				
Cement Pitch	885	0.2871	27.2293	1.7649
	962	0.3628	30.3629	0.6548
	2162	0.3912	32.4105	0.9352
	2332	0.2915	23.0058	1.4283

Table 3.8 Significant wavelengths and regions for different built-up surfaces and materials (Level-1, 2, 3 and 4)

Roof / Building Surfaces										
	Concrete	Asbestos	New CGI	Irony	Cement	Wood	Lime	DPC Brick	Sandstone	
			Sheet	CGI			Pained			
				Sheet						
Significant regions and wavelengths (nm)	VIS (576, 733), FSWIR (2120, 2172)	VIS (480), VNIR (933), FNIR (1119, 1375), FSWIR (2245, 2290)	VNIR (985), FNIR (1235), FSWIR (2230)	FNIR (1029), FSWIR (2250)	ESWIR (1572), FSWIR (2120, 2245)	ESWIR (1632, 1955), FSWIR (2110, 2230)	VNIR (834), FSWIR (2080, 2340)	VNIR (980), FSWIR (2040, 2235)	VNIR (910), FSWIR (2240, 2320)	
Road and Pavement Surfaces										
	Bitumen	Old Bitumen	Repaired	Bitumen	Asbestos	Concrete	Concrete	Concrete	Road Charcoal	Brick Pavement
			Bitumen	Parking	Pavement	Road	Pavement	Bridge		
				Lot						
Significant regions and wavelengths (nm)	VIS (490, 560), VNIR (832), FSWIR (2115)	VIS (618), VNIR (890), FSWIR (2142, 2260)	VIS (672), VNIR (840, 932), FSWIR (2258, 2320)	FNIR (1046), FSWIR (2065, 2115)	VIS (570, 685), FSWIR (2352)	VIS (590), FSWIR (2245, 2310)	FSWIR (2210, 2250)	VNIR (745, 890, 932), FNIR (1366), FSWIR (2032, 2195)	FNIR (1012, 1265), FSWIR (2045, 2256)	FNIR (1032,1380), FSWIR (2172, 2355)

Railway Track								
	Sleeper	Track Iron		Ballast Boulder		RCC	Concrete log	
Significant regions and wavelengths (nm)	FNIR (1024), FSWIR (2210, 2235)	VNIR (932), FSWIR (2118, 2350)		VNIR (985), FNIR (1352), FSWIR (2250, 2325)		FNIR (1013), FSWIR (2235, 2352)		FSWIR (2240, 2375)
Sports Infrastructure								
	Concrete Basketball Court	Blue Fabric Basketball Court	Red Fabric Basketball Court	Bitumen Basketball Court	Fabric Volleyball Court	Cement Volleyball Court	Fabric Tennis Court	Cemented Cricket Pitch
Significant regions and wavelengths (nm)	FNIR (1052, 1132), FSWIR (2140, 2235)	VIS (670), FNIR (1085, 1133, 1365), ESWIR (1750), FSWIR (2275, 2340)	VIS (550), FNIR (1052, 1136), ESWIR (1754, 1815), FSWIR (2245, 2320)	VIS (490), VNIR (985), FSWIR (2210, 2355)	VNIR (972), FSWIR (2080, 2135, 2260)	VIS (692), VNIR (832), FSWIR (2245)	VIS (425, 635), ESWIR (1750), FSWIR (2355)	VNIR (885, 962), FSWIR (2162, 2332)

3.7 Summary

In this study, a comprehensive collection of spectral signatures of various urban built-up surfaces and materials have been obtained in the field using spectral evolution spectroradiometer over the range of 350 to 2500 nm. Further, these built-up or engineered surfaces (Level-1) have been divided into roofs/buildings, roads and pavements, railway track and sports infrastructure in second level while different sub-classes and materials related to these surfaces into third and fourth level. The aforesaid signatures were captured in the urban environment of Udaipur, Rajasthan, India. Further, a spectral library of built-up surfaces and materials is created with a critical analysis of spectral signatures of these surfaces and materials in different spectral regions, which are visible, VNIR, FNIR, ESWIR and FSWIR, respectively. The results of the analysis suggested that, various engineered surfaces can be differentiated on the basis of different significant absorption features at different wavelengths. These features may be due to iron oxide, silicates, organic components, hydrocarbons and clay etc. These significant wavelengths in different spectral regions may be effective for extraction of different built-up surfaces and materials in hyperspectral imagery. These wavelengths may also be useful for determining the age, condition and deterioration status of various engineered surfaces.

Chapter 4

Development of Spectral Indices for extraction of Engineered surfaces and its Sub-categories

In comparison to traditional algorithms for extraction and estimation of engineered / built-up surfaces, spectral index based approaches show distinct advantages due to their ease of implementation and parameter independence. In the past, several indices have been reported in the literature to extract only built-up or impervious surfaces, and confusion among spectrally similar classes still exists. Also, these indices have not been used for hyperspectral imageries [3] [60] [65] [72] [101] [102]. In this chapter, development of three new spectral indices i.e. New Impervious Index (NII), Road Detection Index (RDI) and New Roof Extraction Index (NREI) have been proposed for detection of built-up (Level-1), road and roof surfaces (Level-2), respectively, followed by a separability analysis between spectrally confused urban land cover classes. The whole analysis has been carried out using AVIRIS-NG image and in-situ hyperspectral data of Udaipur, Rajasthan region of India.

The tasks in this study are to develop new built-up indices using a hyperspectral dataset with a view to:

- a) Extract built-up surfaces in the first level followed by its subclasses i.e. roads and roofs in second level by proper identification of significant wavelengths.
- b) Carry out a comparative analysis of proposed indices with the existing built-up indices.
- c) Analyze the separability between most spectrally confused urban land cover classes to further validate the detection results of proposed built-up indices.

4.1 Study area and Data

The remote sensing image used in this study is atmospherically corrected AVIRIS-NG hyperspectral imagery acquired on 2nd February 2016. The AVIRIS-NG sensor measures the reflectance/radiance in the wavelength over the spectral range of 376 – 2500 nm with 5 nm sampling. The area under examination belongs to a region of Udaipur, Rajasthan, India, which is a combination of built-up and non-built-up surfaces as shown in Figure 4.1 (a). In this region, the majority of built-up surfaces were present in the form of bitumen road, concrete pavement as well as concrete and metallic roofs. The salient details of hyperspectral imagery are given in Table 4.1. Ground spectral signatures of the same region were collected using Spectral Evolution Spectroradiometer, with 2151 channels over a spectral range of 350 – 2500 nm. The results of the study are validated using a high-resolution satellite base map of ArcGIS 10.4 in addition to 2297 known ground sample locations, out of which 1032 belong to built-up and 1265 to non-built-up surfaces. The actual locations of field data collection along with some of the selected photographs are shown in Figure 4.1 (b) and (c), respectively. The signatures of built-up surfaces are further divided into 500 road and 532 roof surfaces (uploaded in nisa.geos.iitb.ac.in). For brief visual and quantitative analysis of the extraction results of built-up surfaces, two geographical regions of interest are selected, which are shown under red rectangles in Figure 4.1 (a). The bottom rectangle comprises of 62 truth pixels of roads and 68 of roofs while the rectangle on the top consists of 78 pixels of roof surfaces. Further, the ward map of the study area has been used for validating the results of area estimation of different built-up surfaces using different built-up indices.

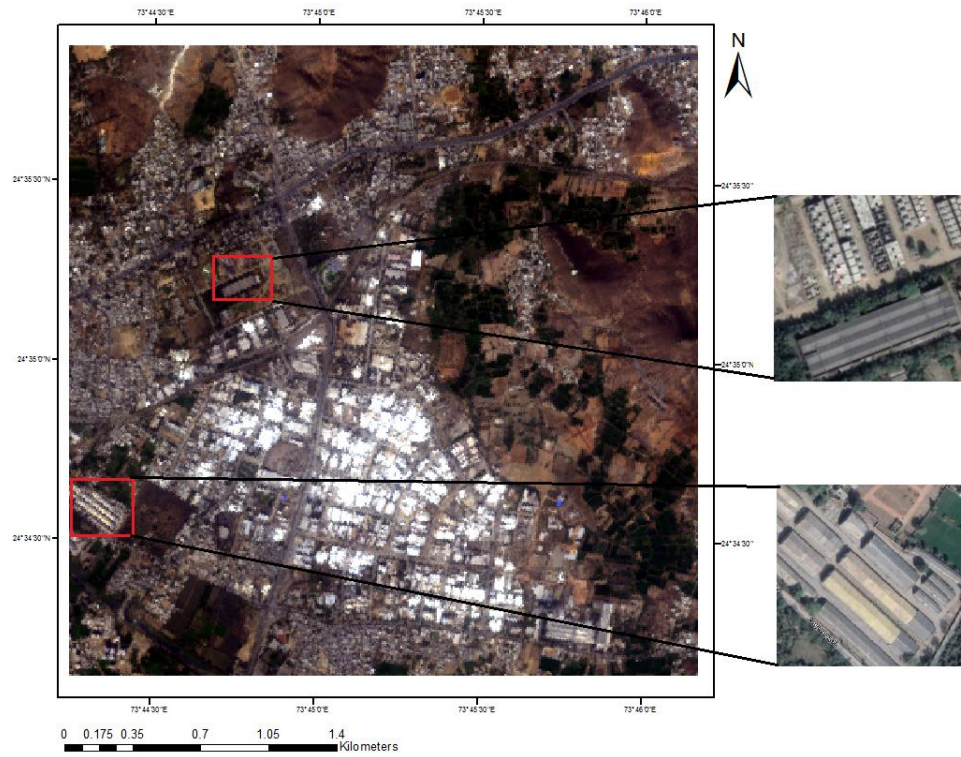
Table 4.1 AVIRIS-NG image data specifications

SN	Parameters	Description
1	Location	Udaipur, Rajasthan, India
2	Airborne Sensor	AVIRIS-NG
3	Date and Time of Data acquisition	02/02/2016, 08:14:45 Am
4	Spatial and Spectral resolution	8.1 meter, 5 nm
5	Number of samples, lines, and bands	400, 400, 425

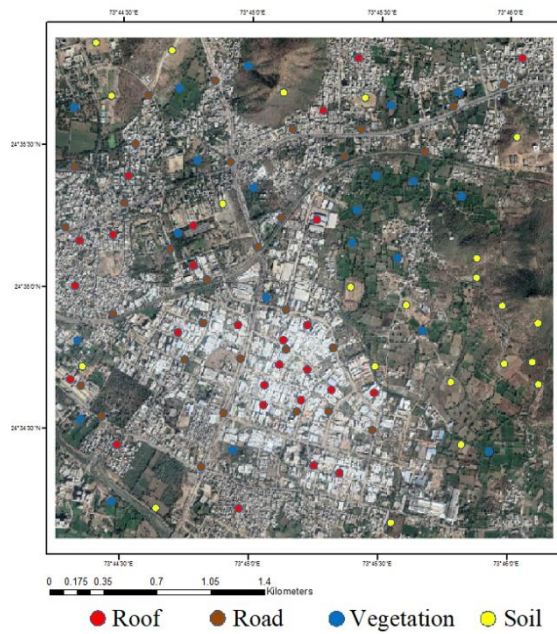
4.2 Data preprocessing

In the preprocessing stage, the spectral bands of AVIRIS-NG imagery which are severely affected by atmospheric gases and particles with visible, NIR, and SWIR detector overlap, with a high frequency of band noise and poor data quality have been removed, which results in 380 bands. Since the reduced data redundancy between original bands, significantly avoided the confusion between built-up surfaces and bare soil as well as between roads and roofs, and therefore enhances the accuracy of extraction of built-up surfaces along with its subcategories. Hence, dimensionality reduction of the remote sensing imagery is carried out using divergence and mutual information based algorithms. Next, the resampling of ground spectral data is carried out with respect to image bands using the nearest neighbor resampling technique. In the next stage of preprocessing, water pixels are masked out using the ISODATA unsupervised classification algorithm [70] [103]. Therefore, the three urban land cover classes that are vegetation, impervious/built-up surfaces, and soil (V-I-S) [80] [104] are considered for further analysis. In the next stage, the stepwise discriminant analysis is utilized for identification and selection of significant wavelengths for extraction of built-up surfaces using ground and image data simultaneously. This algorithm is executed on the SPSS tool [105] [106], which

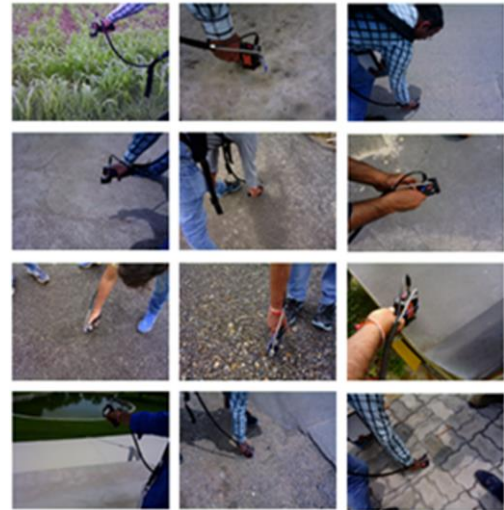
identifies suitable wavelengths for detection of built-up surfaces and its subclasses based on two parameters i.e. tolerance and Wilks's Lambda.



(a)



(b)



(c)

Figure 4.1 Hyperspectral data collection campaign at Udaipur, Rajasthan, India (a) AVIRIS-NG image data (b) Locations of field data collection (c) Photographs of field data collection

4.2.1 Kullback-Leibler (K-L) Divergence and Mutual Information (M-I) algorithms

To overcome the demerits of reduced image quality and information contents of Principle Component Analysis (PCA) and Minimum Noise Fraction (MNF) based dimensionality reduction approaches [107] [108] [109] [110], this study utilizes two widely used algorithms for dimensionality reduction and band selection in hyperspectral imagery, which are Kullback-Leibler (K-L) divergence and Mutual Information (M-I) [111] [112] [113]. K-L divergence approach is utilized for dissimilarity measurement between two bands of the remote sensing imagery by using their respective probability distributions. Let us consider X_a and X_b be two random variables representing the a^{th} and b^{th} bands of hyperspectral imagery. Assuming $P_a(x)$ and $P_b(x)$ as the probability distribution of these random variables, the divergence can be represented in terms of distance or dissimilarity measure as,

$$D_{KL}(X_a, X_b) = \sum_{x \in \Omega} P_a(x) \log \frac{P_a(x)}{P_b(x)} + \sum_{x \in \Omega} P_b(x) \log \frac{P_b(x)}{P_a(x)} \quad (4.1)$$

M-I based algorithm is employed to quantify the degree of independence between random variables. Let us assume a set of K random variables that represent their corresponding bands X_1, \dots, X_K in hyperspectral imagery. If X_a and X_b be two random variables representing a^{th} and b^{th} bands of hyperspectral imagery. Then, mutual information $I(X_a, X_b)$ is given as,

$$I(X_a, X_b) = \sum_{x_a \in \Omega} \sum_{x_b \in \Omega} P(X_a, X_b) \log \frac{P(X_a, X_b)}{P(X_a)P(X_b)} \quad (4.2)$$

Mutual information can be represented in terms of entropy measures as,

$$I(X_a, X_b) = H(X_a) + H(X_b) - H(X_a, X_b) \quad (4.3)$$

Where entropy and joint entropy of a random variable is given as,

$$\begin{aligned}
H(X_a) &= -\sum_{x_a \in \Omega} P(X_a) \log P(X_a) \\
H(X_b) &= -\sum_{x_b \in \Omega} P(X_b) \log P(X_b) \\
H(X_a, X_b) &= -\sum_{x_a \in \Omega} \sum_{x_b \in \Omega} P(X_a, X_b) \log P(X_a, X_b)
\end{aligned} \tag{4.4}$$

The following measure is used to calculate the similarity between two random variables,

$$NI(X_a, X_b) = \frac{2 * I(X_a, X_b)}{H(X_a) + H(X_b)} \tag{4.5}$$

Which is the normalized form of information measure I . Furthermore, this normalized M-I is used as a distance or dissimilarity measure as,

$$D_{NI}(X_a, X_b) = \left(1 - \sqrt{NI(X_a, X_b)}\right)^2 \tag{4.6}$$

4.2.2 Stepwise Discriminant Analysis (SDA)

The Stepwise Discriminant Analysis (SDA) is used for the identification of significant wavelengths in remote sensing imagery. In SDA, the standard for eliminating or introducing the random variable is measured using two parameters i.e. Wilk's Lambda and tolerance [114] [115] [116].

Wilk's Lambda is a combination of statistics of each variable that contributes to the discrimination function and it has values in the range of 0 and 1. The values of this parameter indicate the discriminatory power or separability of spectral bands. A smaller value of this variable specifies that it will provide a greater contribution to the discriminant model.

Tolerance is another parameter that is used for the identification of significant bands in remote sensing imagery. It is the proportion of the variance of a random variable that is not considered by other independent random variables in the equation. A random variable with very low tolerance provides less information and

causes computational difficulties.

The SPSS (IBM Corporation) tool is used for the execution of stepwise discriminant analysis. Further, 40 pure pixels of each category of urban surfaces i.e. road, roof, vegetation, and soil are identified in AVIRIS-NG imagery. The spectral signatures of these pure pixels and ground spectral signatures of the respective urban land cover classes are utilized for the identification of significant wavelengths in hyperspectral imagery.

4.3 New spectral indices for built-up extraction (Level-1 and 2)

In this study, road and roof surfaces have been considered under built-up surfaces while vegetation and soil under non-built-up surfaces. Further, concrete and metallic roofs are associated with roof surfaces, while bitumen roads and concrete pavements to road surfaces. The resampled ground spectral signatures of built-up and non-built-up surfaces are shown in Figure 4.2.

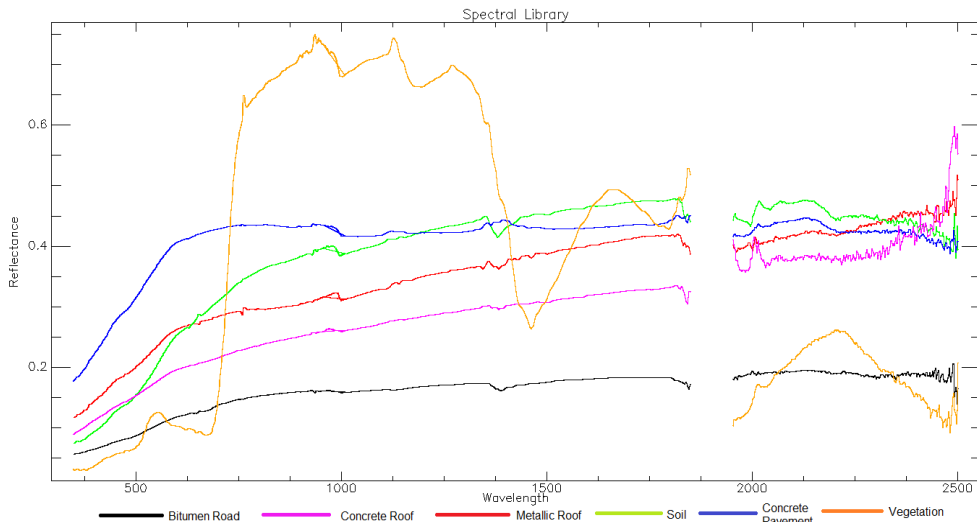


Figure 4.2 Spectral signatures of different urban land cover classes utilized for extraction of built-up surfaces (Level-1 and 2)

Further, due to too much noise, the wavelength bands in the interval of 1850-1950 nm have been removed and hence not considered for the analysis. Following is observed from Figure 4.2:

- The spectral response of bitumen road gradually increases in the visible region between 400-700 nm while it is almost constant in NIR and SWIR regions.
- In the spectra of concrete pavement, there appears a sudden increase in the visible region between 405-555 nm while it is almost constant in NIR and SWIR regions. Also, some iron oxide and clay absorption features are observed near 490 and 2250 nm, respectively.
- The spectral characteristics of concrete and metallic roof surfaces gradually increase in all the regions from visible to SWIR. The difference between the two signatures is that, the concrete roof shows some hydrocarbon absorptions near 2100 nm, while the metallic roof shows some iron oxide absorption features near 490, 620, and 860 nm.
- The spectra of vegetation depicts a red edge near 665 nm with a sudden increase from visible to NIR region. Furthermore, a concavity is observed in the SWIR region between 2100 to 2300 nm.
- The spectra of soil is almost similar to all the man-made surfaces in the NIR region but, in visible it differs from all the built-up surfaces except concrete pavement. Moreover, in the SWIR region, absorptions due to various C-H components are observed between 2050 to 2300 nm.
- In the NIR region, maximum correlation is observed between soil, concrete roof, and metallic roof surfaces, while in SWIR, high overlapping is observed

between spectral signatures of soil and concrete pavement.

- In the visible region, built-up surfaces and their subcategories can easily be separated from non-built-up surfaces.

Therefore, based on aforesaid analysis and taking advantage of various absorption features, it is observed that, bands in visible and NIR regions can prove to be effective for the extraction of built-up surfaces (Level-1) and roads (Level-2), while a combination of visible and SWIR bands may be effective for extraction of roof surfaces in AVIRIS-NG hyperspectral imagery. Vegetation can be easily separated from the rest of the classes in all the regions, while soil may create some problem of overlapping with built-up surfaces to some extent. This overlapping can be reduced by the proper selection of significant wavelengths in the respective regions.

New Impervious Index (NII) and Road Detection Index (RDI) are developed for the extraction of urban built-up surfaces and roads, respectively, in AVIRIS-NG hyperspectral imagery. It is observed that built-up surfaces and roads can be perfectly extracted using appropriate combinations of NIR and visible bands in AVIRIS-NG imagery.

$$NII = \left(\frac{B_{VIS} - B_{NIR1}}{B_{VIS} + B_{NIR1}} \right) \quad (4.7)$$

$$RDI = \left(\frac{B_{VIS1} - B_{NIR1}}{B_{VIS1} + B_{NIR1}} \right) \quad (4.8)$$

Where VIS is the wavelength band in the range of 450 – 690 nm, while $VIS1$ in the interval of 405 – 555 nm. Further, $NIR1$ is the wavelength band over the range of 730 – 1340 nm and B represents reflectance at a particular wavelength.

New Roof Extraction Index (NREI) is proposed for the detection of roof surfaces in AVIRIS-NG imagery. It is examined that roof surfaces can easily be extracted

using proper combinations of SWIR and visible bands in hyperspectral imagery.

$$NREI = \left(\frac{B_{SWIR2} - \frac{B_{SWIR1}}{B_{VIS}}}{B_{SWIR2} - \frac{B_{SWIR1}}{B_{VIS}}} \right) \quad (4.9)$$

$$B_{SWIR2} > B_{SWIR1}$$

Where *SWIR1* is the wavelength band over the interval of 1500 – 1790 nm and *SWIR2* in the range of 1960 – 2490 nm followed by *VIS* over the interval of 450 – 690 nm.

All the proposed indices have been used visible bands of hyperspectral data, it may be due to the large tonal variation of major urban built-up surfaces. For example, roof surfaces are having more reflectance and brightness in comparison to road surfaces, which are characterized by low reflectance or dark surfaces.

4.4 Otsu's thresholding

For the detection of built-up surfaces using spectral index based approach, thresholding plays an important role. Recent studies have revealed that Otsu's method [117] of optimization may be utilized for extraction of built-up surfaces from the index map generated from satellite images [75] [118] [119] [120]. Therefore, this study makes use of Otsu's optimization approach for separating urban built-up targets from the background.

Otsu's method was formulated to discriminate between target and background in an image by generating two classes with minimum intra-class and maximum inter-class variance to produce optimal threshold [121]. In this method, pixels may be labeled into two classes, that are the target (*T*) ranging from [*a*, ..., *t*] and background (*B*) ranging from [*t*, ..., *b*], where *t* is the threshold value. The optimal threshold T_H

can be generated by determining the between-class variance of B and T .

$$\sigma^2 = P_B \times (M_B - M)^2 + P_T \times (M_T - M)^2 \quad (4.10)$$

$$M = P_B \times M_B + P_T \times M_T \quad (4.11)$$

$$P_B + P_T = 1 \quad (4.12)$$

Where σ^2 is the between-class variance of B and T ; M is the mean of the index image; P_B and P_T are the probabilities of the pixel being present in B and T . M_B and M_T are the mean of pixel values in B and T , respectively. The optimal threshold is given as,

$$T_H = \text{Argmax}_{a \leq t \leq b} (\sigma^2) \quad (4.13)$$

4.5 Existing built-up indices

The proposed built-up indices are compared with existing indices for the extraction of urban built-up surfaces in AVIRIS-NG imagery. These existing indices are visible red NIR built-up Index (VrNIR-BI), visible green NIR built-up Index (VgNIR-BI), Road Extraction Index (REI), Built-up Areas Index (BAI), Urban Index (UI) and Normalized Difference Built-up Index (NDBI). Table 4.2 provides a brief overview of these existing built-up indices.

Table 4.2 Existing built-up indices utilized for extraction of built-up surfaces and subclasses

SN	Spectral Index	Expression	Dataset
1	VrNIR-BI, VgNIR-BI	$VrNIR - BI = \frac{B_{RED} - B_{NIR}}{B_{RED} + B_{NIR}}$	Landsat-8 Operational Land
	[75]		Imager/Thermal Infrared
		$VgNIR - BI = \frac{B_{GREEN} - B_{NIR}}{B_{GREEN} + B_{NIR}}$	Sensor (OLI/TIRS) and
			Landsat-7 Enhanced
			Thematic Mapper Plus

2	REI [67]	$REI = \frac{B_{NIR} - B_{BLUE}}{B_{NIR} + B_{BLUE} * B_{NIR}}$	Worldview (WV) – 2 imagery
3	BAI [74]	$BAI = \frac{(B_{BLUE} - B_{NIR})}{(B_{BLUE} + B_{NIR})}$	High resolution multispectral aerial imagery
4	UI [58]	$UI = \frac{B_{SWIR} - B_{NIR}}{B_{SWIR} + B_{NIR}}$	Landsat Thematic Mapper (TM) imagery
5	NDBI [59]	$NDBI = \frac{(B_{SWIR} - B_{NIR})}{(B_{SWIR} + B_{NIR})}$	Landsat TM imagery

4.6 Separability analysis of urban land cover classes

Inter-class separability between built-up surfaces and bare soil, and between two types of built-up surfaces i.e. roads and roofs have been carried out using following statistical measures:

- Spectral Discrimination Index (SDI) [122]
- Jeffries-Matusita (J-M) distance [124]
- Transformed-Divergence (T-D) [125]

4.7 Implementation

In this study, the whole analysis has been carried out using image processing and statistical tools available with MATLAB 2018B, ArcGIS 10.4, ENVI 5.3, and SPSS. The implementation steps of the study are represented by a flow chart shown in Figure 4.3.

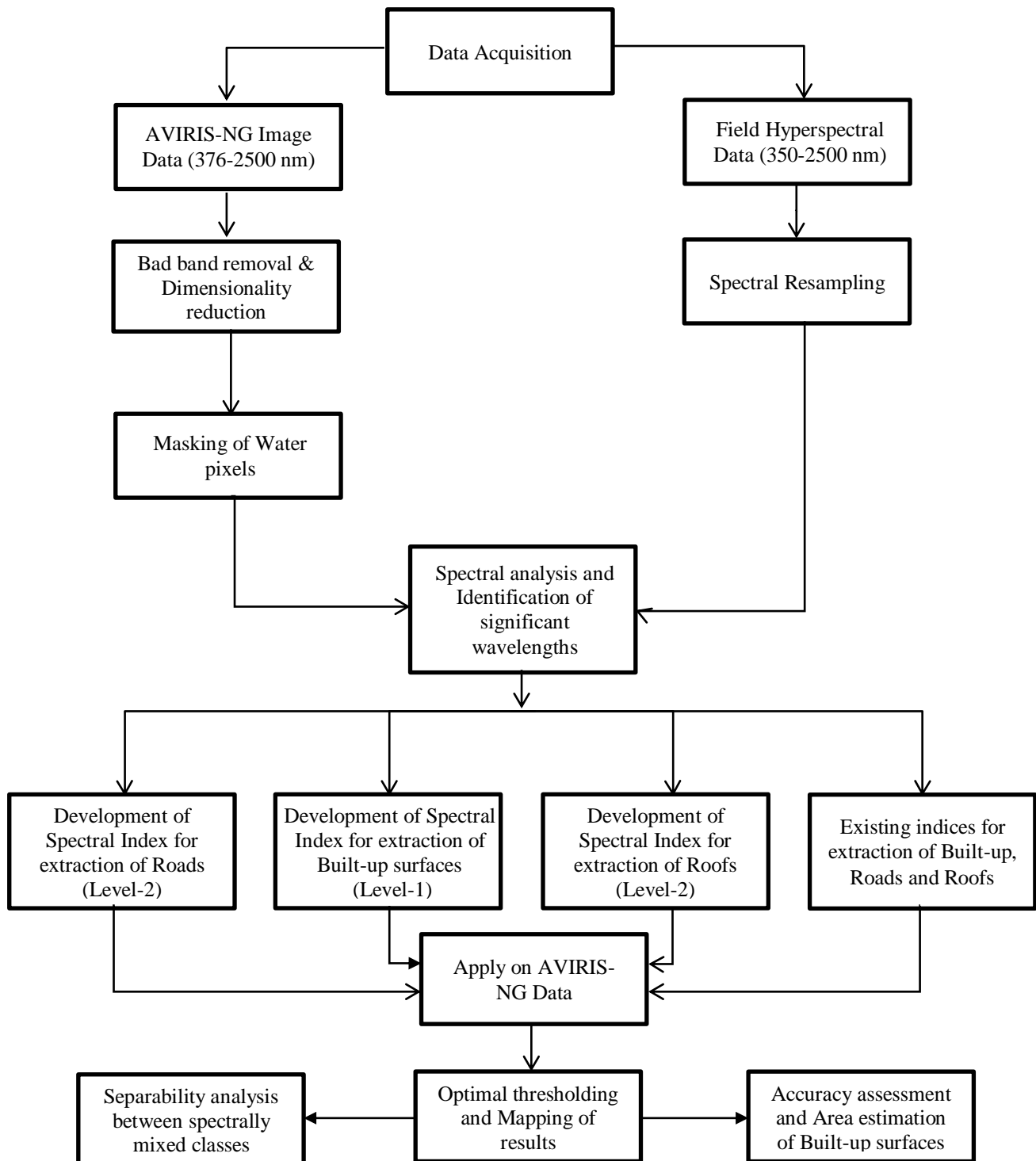


Figure 4.3 Implementation steps of the study

4.8 Results

4.8.1 Identification of significant wavelengths for extraction of built-up surfaces (Level-1 and 2)

The dissimilarity measures based on divergence and mutual information algorithms are utilized to reduce the data dimensionality and non-useful information amongst hyperspectral bands. These approaches are based on a hierarchical clustering structure to group clusters or bands of the hyperspectral image to maximize the inter-cluster and minimize the intra-cluster variance. The final selected bands will be the best representative of each cluster. A band selection tool for dimensionality reduction of image bands based on these two criteria is utilized in this study [111]. In this tool 380 bands of remote sensing imagery are selected as input cluster. On setting the number of output clusters as 150 and after execution of both of the algorithms, 70 common bands have been identified. Next, ground spectral data of 1032 built-up and 1265 non-built-up surfaces along with the aforementioned 70 bands of hyperspectral imagery have been utilized to obtain significant wavelengths using SDA. The SDA is executed on SPSS (IBM Corporation) tool. Using SDA, suitable wavelengths have been identified for the detection of built-up surfaces and its subclasses using two parameters i.e. tolerance and Wilks's Lambda.

Based on tolerance and Wilks's Lambda parameters, different significant wavelengths in visible, NIR, and SWIR regions are obtained, which are listed in Table 4.3. Using these wavelengths, various combinations have been generated for each of the proposed and existing built-up indices. Table 4.4 depicts the appropriate mapping of wavelengths in proposed and existing built-up indices, which have been generated based on the histogram plot of various land cover classes mentioned in the study area. Further, to validate the applicability of the developed approach, two most

suitable combinations are selected for each of the proposed built-up indices (Level-1 and 2).

Table 4.3 Significant wavelengths used to compute built-up indices

Visible region							
Wavelength (nm)	416	466	481	486	560	631	656
Tolerance	0.985	0.978	0.965	0.989	0.980	0.991	0.976
Wilks's Lambda	0.342	0.352	0.401	0.258	0.286	0.265	0.389
NIR							
Wavelength (nm)	842	862	867	982	1042	1232	
Tolerance	0.975	0.968	0.902	0.915	0.982	0.960	
Wilks's Lambda	0.079	0.124	0.156	0.109	0.095	0.085	
SWIR							
Wavelength (nm)	1548	1613	1628	2149	2199		
Tolerance	0.995	0.972	0.980	0.984	0.945		
Wilks's Lambda	0.039	0.089	0.057	0.073	0.154		

4.8.2 Optimal thresholding of built-up indices (Level-1 and 2)

The optimization of index images is carried out using Otsu's thresholding approach. Using histogram representation of respective indices and various statistical parameters of target and background such as mean and standard deviation, a threshold is assigned to each index band, which is considered as optimal. Table 4.4 shows the optimal thresholds along with statistical parameters of different indices, utilized for extraction of built-up surfaces (Level-1) and its subclasses (Level-2). These thresholds are also validated using histogram representation of different land cover classes in respective built-up indices shown in Figure 4.4, 4.5, and 4.6. Since NII, RDI, and NREI have been used two different combinations of wavelengths, and

hence having two different threshold values.

Table 4.4 Mapping of appropriate wavelength bands, statistical parameters and optimal thresholds for different built-up indices (Level- 1 and 2)

Spectral Index	Wavelength Combinations (nm)	Mean	Standard Deviation	Optimal Threshold
Built-up Surfaces (Level-1)				
NII1	631 (VIS), 842 (NIR)	-0.241	0.145	-0.155
NII2	631 (VIS), 1042 (NIR)	-0.282	0.147	-0.175
VrNIR-BI	656 (RED), 862 (NIR)	-0.238	0.155	-0.150
VgNIR-BI	560 (GREEN), 862 (NIR)	-0.281	0.125	-0.220
Road (Level-2)				
RDI1	416 (VIS1), 1232 (NIR)	-0.421	0.118	-0.295
RDI2	416 (VIS1), 842 (NIR)	-0.381	0.118	-0.247
REI	466 (BLUE), 982 (NIR)	-0.321	0.115	-0.162
BAI	481 (BLUE), 867 (NIR)	-0.369	0.121	-0.206
Roof (Level-2)				
NREI1	486 (VIS), 1548 (SWIR1), 1628 (SWIR2)	-0.796	0.046	-0.710
NREI2	631 (VIS), 1628 (SWIR1), 2149 (SWIR2)	-0.799	0.085	-0.662
UI	867 (SWIR), 2199 (NIR)	-0.161	0.073	-0.087
NDBI	867 (NIR), 1613 (SWIR)	-0.095	0.160	0.025

4.8.3 Extraction of built-up surfaces (Level-1)

The optimal results of built-up extraction in hyperspectral imagery using NII along with existing VgNIR-BI and VrNIR-BI are shown in Figure 4.4 (a) to (d). Figure 4.4 (e) to (h) represents the extraction results of a region of interest (ROI) inside the red

rectangle shown in Figure 4.4 (a) to (d). This ROI corresponds to various roof surfaces, which are used for a brief quantitative analysis of the results. Now, by superimposing output images onto a high-resolution satellite base map of ArcGIS 10.4, it is observed that NII can extract most of the built-up surfaces while the detection rate appears to be slightly less in the case of VgNIR-BI and VrNIR-BI. The quantitative analysis of the roofs inside ROI suggests that out of 78 truth pixels, 70 and 73 pixels are detected in NII1 and NII2 while VgNIR-BI and VrNIR-BI are capable of extracting 58 and 61 pixels of those rooftops, respectively. Therefore, NII may outperform VgNIR-BI and VrNIR-BI in AVIRIS-NG imagery. Although VgNIR-BI, VrNIR-BI, and NII utilize similar bands of remote sensing imagery for the development of built-up index but there is still a slight variation in the results, it may be due to the limitation of selection of significant wavelengths in discrete band multispectral imagery.

Figure 4.4 (i) to (l) describes the histogram representation of various urban land cover classes in different built-up indices (Level-1). These land cover classes are road, roof, vegetation, and soil. Histogram plot inside the black circle corresponds to the target class while other plots belong to the background. Road and roof surfaces are considered under built-up surfaces while rest of the classes is associated with non-built-up surfaces. It is observed from Figure 4.4 (i) to (l) that histogram of road and roof surfaces are almost same, it may be due to the similarity in spectral characteristics of the materials used for the construction of these two surfaces. For example, bituminous roof and asphalt road have similar spectral responses. These surfaces have almost similar composition of carbon, hydrogen, sulfur, nitrogen, and oxygen. It is also investigated that built-up surfaces are well separated from soil and vegetation in all the aforementioned indices used for the extraction of built-up

surfaces.

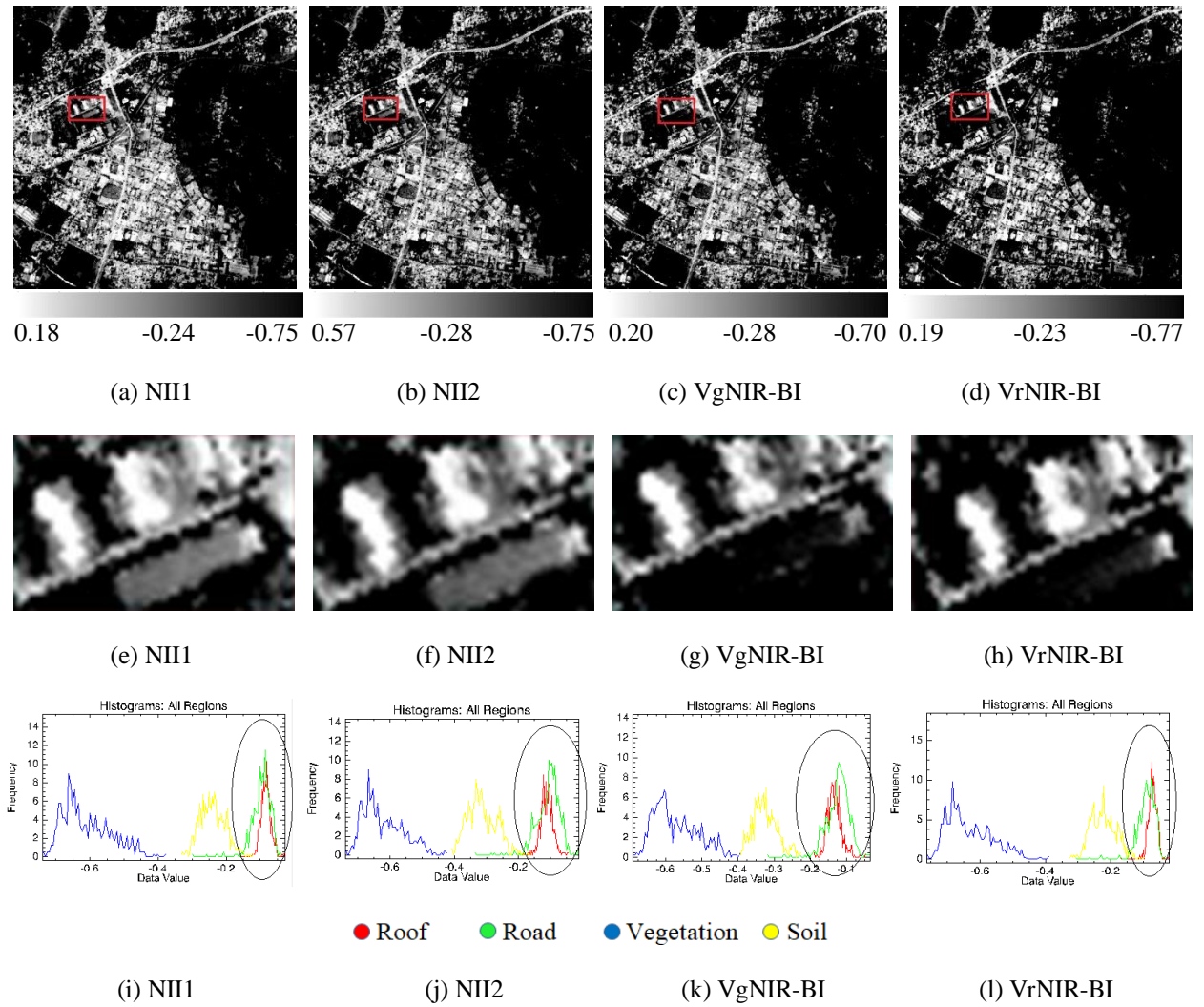


Figure 4.4 (a-d) Extraction results of urban built-up surfaces using different built-up indices in which the range of indices is shown along the x -axis of the respective index band (e-h) extraction results of ROI (i-l) histogram representation of different land cover classes in respective built-up indices

4.8.4 Extraction of road surfaces (Level-2)

Figure 4.5 (a) to (d) depicts the outcomes of road extraction in RDI followed by REI and BAI after the application of optimal threshold. Figure 4.5 (e) to (h) describes the extraction results of ROI inside the red rectangle shown in Figure 4.5 (a) to (d). This ROI consists of five parallel road surfaces, which are utilized for a quantitative analysis of the road detection results. It is observed by overlaying output images into

a high-resolution imagery that, RDI detects most of the road pixels correctly while REI and BAI label these target pixels into background with more false alarms. Further, the quantitative analysis of the 62 truth pixels of roads inside ROI suggests that 56 and 54 pixels of those roads are highlighted in RDI1 and RDI2, while REI and BAI are capable of detecting only 37 and 41 target pixels, respectively. Thus, it appears that RDI can prove to be effective for the extraction of road surfaces in hyperspectral imagery in comparison to REI and BAI.

The histogram representation of various urban land cover classes, which are associated with different indices used for extraction of roads, is shown in Figure 4.5 (i) to (l). The histogram plot inside the black circle corresponds to the roads while remaining plots is associated with non-road background. Water pixels have already been masked in the preprocessing stage, accordingly, the rest of the urban land cover classes such as road, roof, vegetation, and soil are used for the analysis. It is observed from Figure 4.5 (i) to (l) that, vegetation and soil can be easily discriminated from roads and roofs but some part of the road surfaces is still overlapping with roofs. Therefore, the separability of spectrally similar road and roof surfaces is still a challenging task. This problem may be further worsened by the issues connected with the occlusion of road surfaces by trees, shadow, and the presence of vehicles. It also appears that, the overlapping behavior of road and roof surfaces is more in REI and BAI while moderate in case of RDI. Therefore, the selection of significant bands and optimal thresholds play a major role in the extraction of road surfaces. It is also investigated that, indices used for extraction of roads may also be utilized for the detection of built-up surfaces by changing in the threshold.

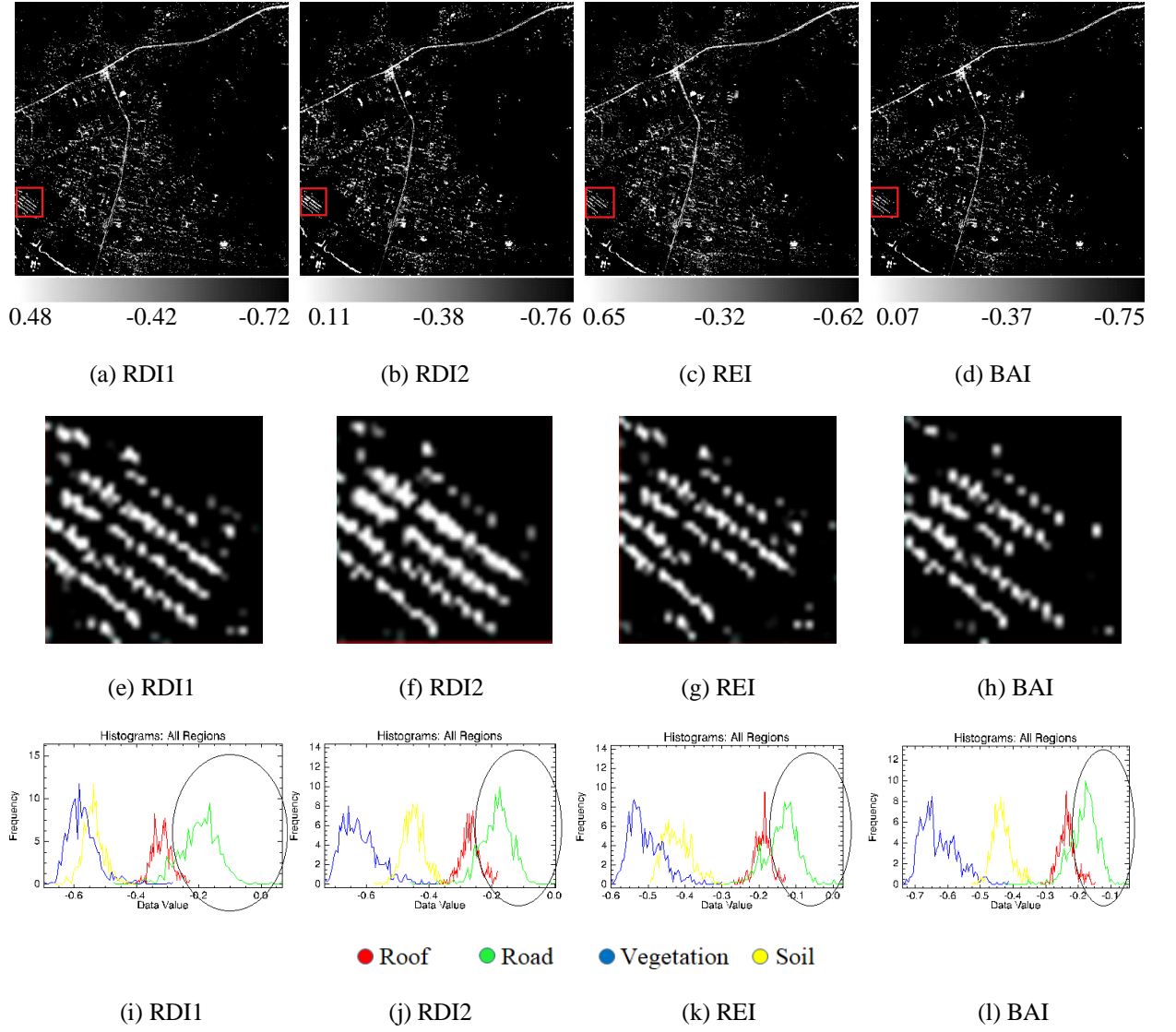


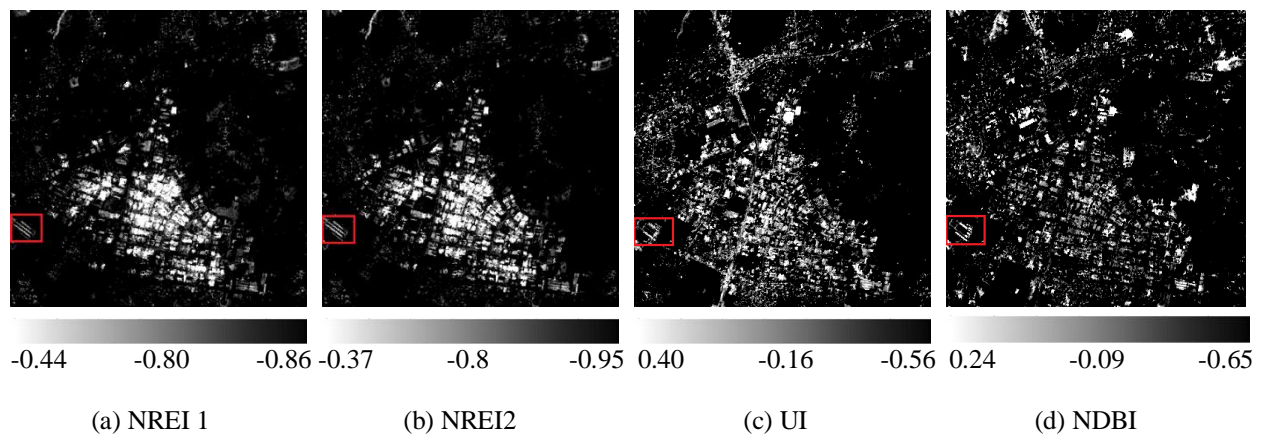
Figure 4.5 (a-d) Extraction results of road surfaces using different built-up indices in which the range of indices is shown along the x -axis of the respective index image (e-h) extraction results of ROI (i-l) histogram representation of different land cover classes in respective built-up indices

4.8.5 Extraction of roof surfaces (Level-2)

The roof extraction results in AVIRIS-NG imagery using NREI and existing UI and NDBI are shown in Figure 4.6 (a) to (d). Figure 4.6 (e) to (h) represents the extraction results of ROI inside the red rectangle shown in Figure 4.6 (a) to (d). This ROI belongs to some specific roof surfaces, which are used for a brief quantitative analysis of the results. It is observed by a comparison of results with reference

imagery that, most of the roof pixels are detected in NREI while only a few pixels are highlighted in the case of UI and NDBI with more false alarms. Further, when the quantitative analysis of 68 true pixels of rooftops inside ROI is carried out, then it appears that 61 and 64 pixels are detected in the case of NREI1 and NREI2, while only 47 and 52 roof pixels are highlighted in UI and NDBI, respectively. Therefore, NREI may perform better in comparison UI and NDBI for the extraction of rooftops in AVIRIS-NG imagery.

Histogram representation of different urban land cover classes in roof extraction indices is shown in Figure 4.6 (i) to (l). It appears from Figure 4.6 (i) to (l) that non-built-up surfaces such as vegetation and soil can easily be discriminated from roof surfaces in NREI while some portion of soil is overlapped with roof surfaces in case of UI and NDBI. Further, if the analysis is carried out for roads and roofs, then it is observed that, roof surfaces can easily be separated from road surfaces in case of NREI while overlapping between roofs and roads is more in case of UI and NDBI. It also appears that UI has most of the false alarms in the form of road surfaces while in NDBI, it is in the form of soil. Therefore, the whole analysis suggests that, NREI may perform better separation of roof surfaces from other non-roof classes in comparison to UI and NDBI.



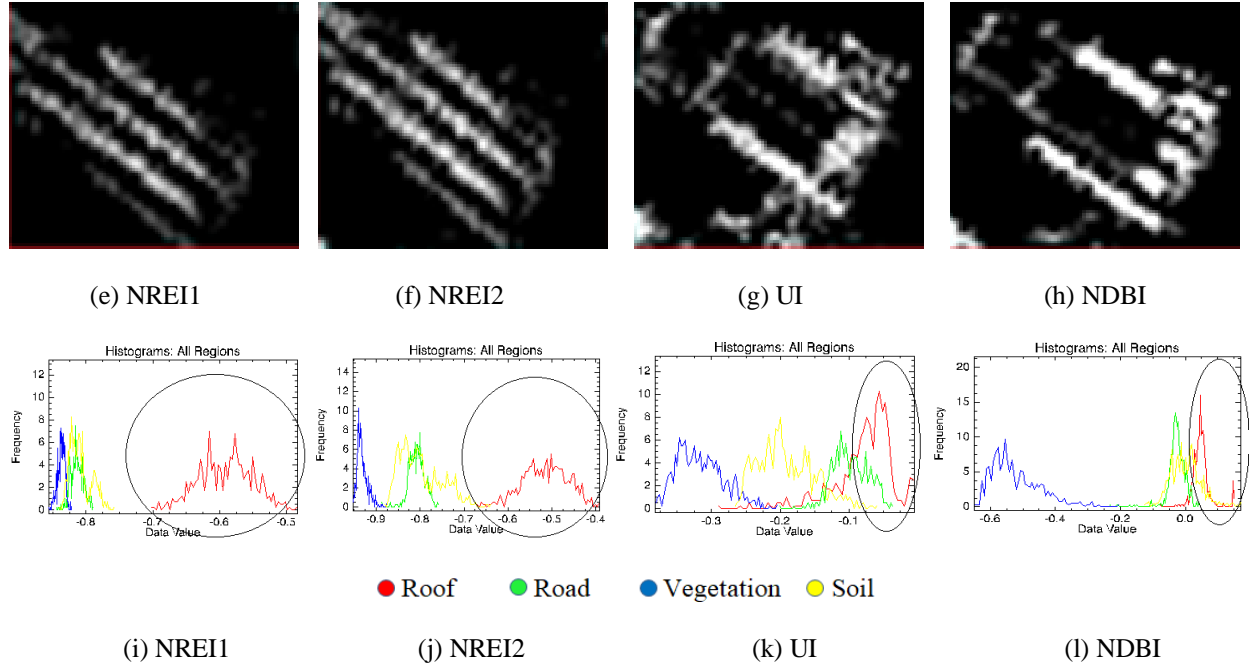


Figure 4.6 (a-d) Extraction results of roof surfaces using different built-up indices in which the range of indices is shown along the x -axis of the respective index band (e-h) extraction results of ROI (i-l) histogram representation of different land cover classes in respective built-up indices

4.8.6 Accuracy assessment and validation of results

The detection results of built-up surfaces and its subclasses, shown in Figure 4.4, 4.5, and 4.6, are validated using a high-resolution satellite base map in addition to 2297 field location information of different urban samples, out of which 1032 belong to built-up surfaces and 1265 to non-built-up surfaces. 1032 samples of built-up surfaces are further categorized into 500 roads and 532 roofs, respectively. The overall accuracy and kappa index of different built-up indices are tabulated in Table 4.5. The overall accuracy is calculated by considering built-up surfaces (Level-1 and 2) as target while other non-target classes as background. It is observed that proposed indices i.e. NII, RDI, and NREI outperform other existing built-up indices i.e. VrNIR-BI, VgNIR-BI, REI, BAI, UI, and NDBI for extraction of built-up surfaces (Level-1 and 2). It appears that the accuracies of NII, VrNIR-BI, and VgNIR-BI are

comparable. It may be due to utilization of similar spectral regions of different datasets for development of these built-up indices. Also, the overall accuracy of RDI and REI is comparable, as NIR and visible bands have been used by both of these indices for their formulation. Further, NREI utilizes a combination of SWIR and visible while UI and NDBI make use of SWIR and NIR regions. It has been previously discussed that due to the brighter tone of most of the roof surfaces, visible region may be a better choice for detection of roof surfaces. Therefore, the accuracy of roof extraction enhances in NREI while it gets worse in the case of UI and NDBI.

Table 4.5 also describes the quantification of built-up surfaces and its subcategories using proposed and existing built-up indices. In the study region, the actual percentage of built-up area is about 22.45%, out of which roads are 11.45% and roof surfaces of approximately 11% of the total area. The actual percentages and geographic locations of all these classes are verified from the ward map of Udaipur Municipal Corporation, Rajasthan, India (<http://www.udaipurmc.org/HomePage.aspx> accessed on 22nd August 2019) along with high-resolution satellite imagery. It appears from Table 4.5 that the NII approaches towards an actual percentage of built-up surfaces, while VrNIR-BI and VgNIR-BI are included some false alarms in the form of non-built-up surfaces. Similarly, RDI appears to have better extraction of road surfaces with slight confusion with roof surfaces. Also, it seems that the effect of false alarms in the form of roofs and soil is more in REI and BAI. In case of roof extraction indices, it is observed that NREI approaches perfectly towards the actual percentage of roof surfaces while UI and NDBI are over determined with more false alarms in the form of soil and roads.

Table 4.5 Accuracy assessment of various built-up indices (Level-1 and 2) based on different parameters

	Spectral	Overall	Kappa	Target	Background	Area (%)	Actual
	Index	Accuracy	Index	pixels	pixels		Area (%)
		(%)	(%)				
Built-up	NII1	95.83	87.27	35432	124568	22.15	22.45
surfaces	NII2	96.41	86.53	35580	124420	22.23	
(Level-1)	VrNIR-BI	86.32	78.07	41559	118441	25.97	
	VgNIR-BI	83.53	76.24	38370	121630	23.98	
Road	RDI1	92.60	83.25	19056	140944	11.91	11.45
(Level-2)	RDI2	91.89	81.89	19560	140440	12.22	
	REI	85.65	76.96	21248	138752	13.28	
	BAI	78.25	71.20	19981	140019	12.48	
Roof	NREI1	96.24	88.25	17696	142304	11.06	11%
(Level-2)	NREI2	93.30	84.63	17760	142240	11.10	
	UI	76.89	68.64	18619	141381	11.63	
	NDBI	81.14	72.18	18990	141010	11.86	

4.8.7 Inter and intra-class separability analysis of urban built-up surfaces

Built-up surfaces and soil tend to share almost similar spectral characteristics, so the separability between built-up surfaces and soil is a major concern, as reported in most of the literature. Therefore, in this study, various statistical measures such as SDI, J-M distance, and T-D are utilized for the analysis of separability between built-up surfaces and soil. If we assume SDI value to be greater than 3 for best separability, between 2 to 3 for moderate and less than 2 for worst separability, then from Table 4.6, it appears that NII can provide best separability between built-up

surfaces and soil and moderate separability is attained in case of VrNIR-BI and VgNIR-BI. Further, RDI, REI, and BAI are perfectly separated built-up surfaces from the soil. The NREI provides best separation, while the worst separation is obtained in case of UI and NDBI. Similarly, if we consider J-M distance to be greater than 1.6 for best separability, between 1.4 and 1.6 for moderate and less than 1.4 for worst separability, then it is observed from Table 4.6 that, NII can offer the best separability between built-up surfaces and soil while moderate separability is obtained in VrNIR-BI and VgNIR-BI. Also, all the road detection indices can provide the best separability. In case of roof extraction indices, NREI provides the best separability between built-up surfaces and soil while worst is obtained in case of UI and NDBI. Moreover, if the analysis is carried out using T-D approach by assuming T-D values to be greater than 1900 for best separability, between 1800 to 1900 for moderate and less than 1800 for worst separability, then it is examined that NII is capable of providing best separability between built-up surfaces and soil while moderate is obtained in VrNIR-BI followed by worst in VgNIR-BI. Further, in road detection indices, best separability is achieved in RDI whereas moderate in case of REI and BAI. Finally, NREI generates the best separability between built-up surfaces and soil while worst in case of UI and NDBI.

Similar spectral characteristics of different types of road and roof surfaces such as concrete roofs and pavements, bitumen roads and roofs also affect the extraction results of built-up surfaces (Level-2). Therefore, in this study, separability analysis between road and roof surfaces has also been carried out as an accuracy measure for extraction of road and roof surfaces. The aforesaid statistical measures have been used for the analysis of separability, as shown in Table 4.6. The SDI analysis suggests that RDI can provide better separability while REI and BAI are worst in

terms of separability between road and roof surfaces. Finally, NREI appears to have the best separability whereas worst in case of UI and NDBI. When the separability analysis is performed using J-M distance and T-D based criteria then similar results are obtained as in SDI.

Table 4.6 Inter and intra-class separability measures of built-up surfaces (Level-1 and 2)

Separability between →		Built-up and Soil			Road and Roof		
	Spectral	SDI	J-M	T-D	SDI	J-M	T-D
	Index	distance			distance		
Built-up surfaces (Level- 1)	NII1	2.95	1.65	1865	-----		
	NII2	3.48	1.82	1902	-----		
	VrNIR-BI	2.61	1.53	1825	-----		
	VgNIR-BI	2.29	1.41	1790	-----		
Road (Level- 2)	RDI1	3.86	1.89	1918	1.36	1.49	1793
	RDI2	3.48	1.84	1905	1.25	1.41	1769
	REI	3.08	1.72	1875	0.471	0.83	1422
	BAI	3.47	1.80	1895	0.670	0.92	1453
Roof (Level- 2)	NREI1	3.12	1.85	1910	4.17	1.91	1931
	NREI2	2.82	1.61	1845	4.14	1.85	1941
	UI	0.45	0.85	1425	1.29	1.52	1632
	NDBI	0.42	0.70	1403	1.13	1.21	1524

4.9 Discussion

The major aim of developing NII, RDI, and NREI, is to derive a simple and convenient spectral index based approach which can highlight the urban built-up surfaces along with its subcategories in AVIRIS-NG hyperspectral imagery. Due to high dimensionality of hyperspectral data, widely used mutual information and

divergence based approaches [111] have been used for dimensionality reduction followed by stepwise discriminant analysis for selection of most significant wavelengths. The analysis of the results suggests that, NII and RDI can prove to be effective for extraction of built-up and road surfaces, respectively. These indices are developed using visible and NIR bands of hyperspectral imagery. More importantly, NII and RDI showed their effectiveness in discriminating soil from built-up surfaces, which has proven to be a difficult problem [54] [126]. Also, RDI has shown its efficacy in intra-class separability of built-up surfaces i.e. between roads and roofs. Another advantage of NII and RDI is that, it may be applied to different narrow band imageries of small spectral range, as these are independent of SWIR bands. Further, NREI has also shown its effectiveness for the extraction of roof surfaces in hyperspectral imagery, which employs a combination of visible and SWIR bands for its development. The major advantage of NREI is that, it can perfectly separate roof surfaces from bare soil and roads. The utilization of narrower band spectrally rich hyperspectral imagery may be a reason for the better performance of all the proposed indices. Moreover, NII, RDI, and NREI may have the potential to assist in a large number of applications associated with urban remote sensing, which includes urban growth analysis, land use classification, urban target detection, urban heat island analysis, and image endmember extraction etc. Furthermore, NII performs slightly better when compared to the similar indices i.e. VgNIR-BI and VrNIR-BI [75], while RDI proves to be efficient when compared with REI [67] and BAI [74] and in case of roof extraction, NREI shows to be effective in comparison to UI [58] and NDBI [59]. Therefore, NII, RDI, and NREI may serve as a convenient spectral index based method, rather than an approach for extraction and estimation of built-up, road, and roof surfaces, respectively. The development of proposed indices is mainly

dependent on the spectral signatures of various urban land cover classes, which are vegetation, soil, road, and roof surfaces, as suggested by V-I-S model [80]. Therefore, the limitation of these indices is that they have not considered the effect of water as it has already been masked in the preprocessing stage of the study using unsupervised classification based approach [70].

4.10 Summary

In this study, three new built-up indices i.e. NII, RDI, and NREI have been proposed for the extraction of built-up surfaces along with its subcategories i.e. roads and roofs by proper identification of significant wavelength bands. The divergence and mutual information based algorithms were utilized to reduce data redundancy between original bands of remote sensing imagery. Further, stepwise discriminant analysis was used to identify the most significant wavelengths, which resulted in improved built-up surface mapping. The NII has been utilized for extraction of built-up surfaces followed by RDI for detection of road and NREI for roof surfaces. The NII and RDI employed a combination of NIR and visible bands while NREI utilized a combination of SWIR and visible bands. These indices have been applied in AVIRIS-NG hyperspectral imagery of Udaipur, Rajasthan, India. Further, separability analysis between spectrally confused urban land cover classes such as between built-up surfaces and soil as well as between road and roof surfaces, has been performed using various statistical measures i.e. SDI, J-M distance, and T-D. The results of the proposed indices have been compared with mapping results obtained by other existing indices. The NII, RDI, and NREI showed an overall average accuracy of 96.12 %, 92.24 %, and 94.77 %, respectively, which is higher than all the other existing built-up indices. Therefore, the proposed indices found to

be effective for extraction of built-up surfaces (Level-1 and 2) in comparison to existing indices. The quantification of built-up surfaces and its subclasses using aforesaid indices has also been carried out. The quantification results suggested that the proposed indices can prove to be effective for estimation of built-up surfaces of different levels. Similarly, these indices have shown their effectiveness for separating built-up surfaces from soil as well as roads from roofs, when compared with other existing indices.

Chapter 5

New Spectral Indices for Condition and Deterioration analysis of Road and Roof surfaces

Comprehensive and precise information about the condition of road and deterioration of roof surfaces is required for effective planning and management of urban infrastructure. Some of the major problems associated with road condition are traffic congestion and reconstruction. Further, the weathered roof surfaces that emit various harmful toxins need to be monitored regularly [7] [30] [135] [136]. Therefore, in this study, condition analysis of road surfaces and deterioration analysis of roof surfaces are carried out using AVIRIS-NG image and field hyperspectral data of Udaipur, Rajasthan, India. Various significant bands are identified using spectral characteristics of roads and roofs of different condition and deterioration, respectively.

The tasks in this study are subdivided into:

- a) Develop a new spectral index for determining the condition of road surfaces using hyperspectral image and field spectrometry.
- b) Introduce a new spectral index for determining the deterioration status of roof surfaces using hyperspectral image and field data.
- c) Compare the results of spectral unmixing of road and roof surfaces on the basis of their condition and deterioration with proposed spectral indices.

5.1 AVIRIS-NG hyperspectral data and processing

The original hyperspectral imagery of Udaipur, Rajasthan region of India with different regions of interest, is utilized for the study. The AVIRIS-NG sensor is equipped with multiple bands in ultra violet (UV), visible, NIR and SWIR regions, respectively. A total number of bands present in this imagery are 425, which have been reduced to 380 after removal of bad bands that are affected by water vapor, carbon dioxide, and detectors overlap.

Further, it is required to apply the mask to the natural land cover classes such as vegetation and water bodies. Therefore, this study uses green and red band along with NIR to apply the mask on vegetation and water, respectively. The NDVI [127] is used to extract vegetation in the image. NDVI identifies vegetation based on the positive values instead of the remaining pixels. These values are used to apply a mask by setting a proper threshold value.

$$NDVI = \frac{(B_{NIR} - B_{RED})}{(B_{NIR} + B_{RED})} \quad (5.1)$$

To apply the mask to water bodies in hyperspectral imagery, the Normalized Difference Water Index (NDWI) [134] is used.

$$NDWI = \frac{(B_{GREEN} - B_{NIR})}{(B_{GREEN} + B_{NIR})} \quad (5.2)$$

The elimination of water bodies is required because they may influence the detection of bitumen surfaces because both water bodies and road surfaces may tend to share similar spectral properties.

5.2 Ground data acquisition and materials

This study utilizes field spectroscopy data along with AVIRIS-NG hyperspectral

imagery. Field spectroscopy data has been collected using Spectral Evolution spectroradiometer with wavelengths in the interval of 350 – 2500 nm. Spectral measurements were conducted at Udaipur, Rajasthan, India in the year 2016. The reflectance measurements have been obtained from 10 am to 3 pm in ambience lighting conditions. The spectroradiometer utilized in this research was equipped with the detectors that covered the visible to short wave infrared spectra, with a spectral resolution of 1.5 nm at 350 – 1000 nm, 3.0 nm at 1500 nm and 3.8 nm at 2100 nm, respectively. Apart from field spectral data, AVIRIS-NG hyperspectral imagery is also utilized in this study for the development of a spectral index for condition analysis of road surfaces followed by deterioration analysis of roof surfaces.

Ground spectral signatures have been collected for asphalt or bitumen road surfaces under new or good conditions and old or damaged conditions. These two classes of road surfaces have been considered for condition analysis. A total of 4 spectral signatures have been collected per sample, and accordingly, 2000 spectral signatures of 500 samples have been obtained based on the aforementioned conditions of road surfaces. Further, out of these 500 samples, 378 samples are associated with new or good condition road surfaces while 122 are related to old or damaged condition road surfaces. Next, mean spectral signatures are extracted from 378 and 122 samples of road surfaces, respectively, which are shown in Figure 5.1 (c). Further, these spectral signatures are selected for condition analysis of road surfaces. Ground inspection has also been carried out across the study area to examine the condition of road surfaces based on the physical appearance. Accuracy assessment and validation of the mapping results are performed with the help of ground truth information of above mentioned 500 samples of road surfaces.

In a similar way, ground spectral signatures have been collected for concrete roof surfaces under new or less deteriorated roofs and old or more deteriorated roofs. These two classes have been considered for deterioration analysis of roof surfaces. A total of 4 spectral signatures have been collected per sample of roof surface and accordingly, 2128 spectral signatures of 532 samples have been obtained based on the aforementioned deterioration status of concrete roof surfaces. Further, out of these 532 samples, 312 samples are associated with new or less deteriorated roof surfaces while 220 samples are related to old or more deteriorated roof surfaces. Next, mean spectral signatures are extracted from 312 and 220 samples of roof surfaces, respectively, as shown in Figure 5.2 (c). These spectral signatures are utilized for deterioration analysis of roof surfaces. Field inspection has also been carried out across the study area to observe the deterioration status of roof surfaces based on the physical appearance. Accuracy assessment and validation of the mapping results are carried out with the help of ground truth information of aforesaid 532 samples of roof surfaces.

5.2.1 Spectral characteristics of road surfaces

Field spectral signatures captured in this research covered the spectral range over the interval of 350 – 2500 nm with 2151 channels. However, the preprocessing of these signatures is required to eliminate the noise caused by atmospheric absorption and detectors overlap. The ranges that are affected by water absorption and noise components include 1343 – 1418 nm (76 channels) and 1793 – 1954 nm (162 channels), respectively. Hence, the remaining 1913 channels (2151 channels - (76+162) channels) are utilized in this study for condition analysis of road surfaces. Figure 5.1 (a) and (b) represent the images of road surfaces of different condition

along with their respective spectral signatures in Figure 5.1 (c). On the basis of these spectral signatures of road surfaces, condition analysis has been carried out in two different classes i.e. new or good condition and old or damaged condition.

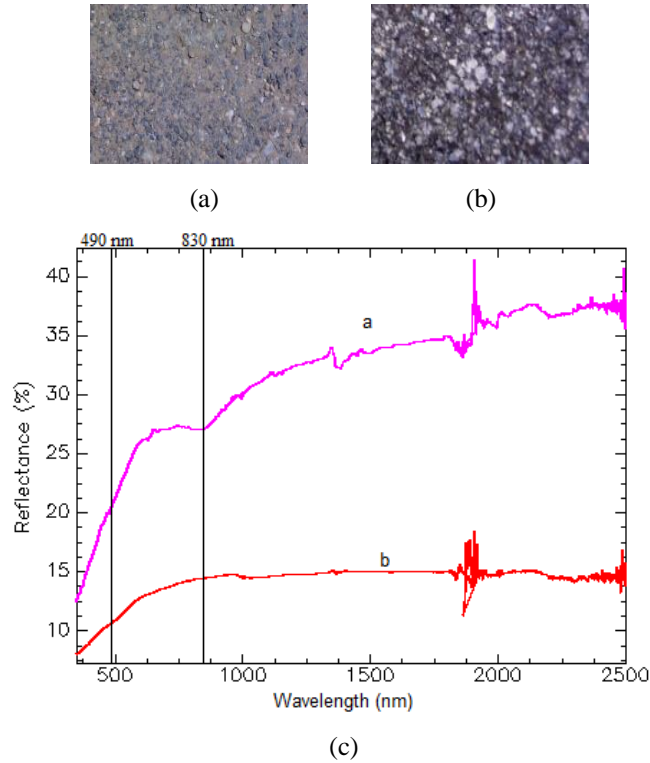


Figure 5.1 Images with respective spectral characteristics of bitumen or asphalt road surfaces of different condition (a) Old road damaged condition (b) New road good condition (c) spectral signatures of road surfaces shown in (a) and (b)

In the recent past, research has been carried out to determine the spectral characteristics of asphalt pavements using field spectroscopy, and it has been observed that deformed surfaces of asphalt reflect high degree of spectral values of NIR and SWIR bands in comparison to un-weathered or new asphalt surfaces [30]. The natural aging of bitumen or asphalt surfaces is caused by photochemical reactions with solar radiations and reaction with atmospheric oxygen followed by the influence of heat. It results in three major processes a) changes of the composition by oxidation b) loss of oily component by absorption and c) molecular structuring that influences the viscosity of bitumen mix [7]. Generally, the loss of oily component is

a short term process while the other two processes are long term [7] [30]. It is observed from the spectral characteristics shown in Figure 5.1 (c) that new bitumen or asphalt surfaces have the lowest reflectance with a linear increase in reflectance towards 2100 nm. Further, the hydrocarbon absorptions are generally evident at 1750 nm and above 2100 nm with a significant absorption at 2310 and 2350 nm, respectively [135] [136]. As the condition of the road surfaces gets worse, the reflectance increases in all regions of the spectrum. The spectral characteristics of bitumen surface in NIR and SWIR region changes from a little concave or nearly flat for new bitumen surfaces to more concave for older bitumen surfaces as shown in Figure 5.1 (c). Exposing of the rocky component and the oxidation process in the road surfaces is generally due to the presence of iron oxide absorption features in the visible region at 520, 670 and 870 nm, respectively [7]. It also appears in Figure 5.1 (c) that the hydrocarbon features are distinct for new bitumen surfaces and enhanced with age and damaged or poorer surfaces conditions. Further, if the analysis is carried out in SWIR region then it appears that for older road surfaces slope of spectral response increases between 2100 and 2200 nm while it decreases between 2250 and 2300 nm, respectively [30].

Spectral analysis of the road surfaces suggests various features in the form of iron oxide and hydrocarbon absorption for the analysis of bitumen or asphalt road condition. On the basis of these features, a spectral index is developed for road condition analysis in hyperspectral imagery. Herold *et al.* (2005) [135], suggests two different indices i.e. VIS2 ratio (the difference between reflectance at wavelengths 830 and 490 nm) and SWIR ratio (the difference between reflectance at wavelengths 2120 and 2340 nm), to analyze the spectral characteristics of bitumen or asphalt road surfaces in visible and SWIR regions.

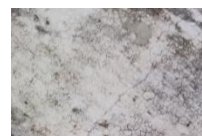
5.2.2 Spectral characteristics of roof surfaces

In a similar way, as in the case of road surfaces, 1913 out of 2151 channels are utilized for the deterioration analysis of roof surfaces. Figure 5.2 (a) and (b) represent the images of roof surfaces with different levels of deterioration along with their respective spectral signatures in Figure 5.2 (c). On the basis of these spectral characteristics of roof surfaces, deterioration analysis can be performed in two different ways i.e. new or less deteriorated surfaces and old or more deteriorated surfaces.

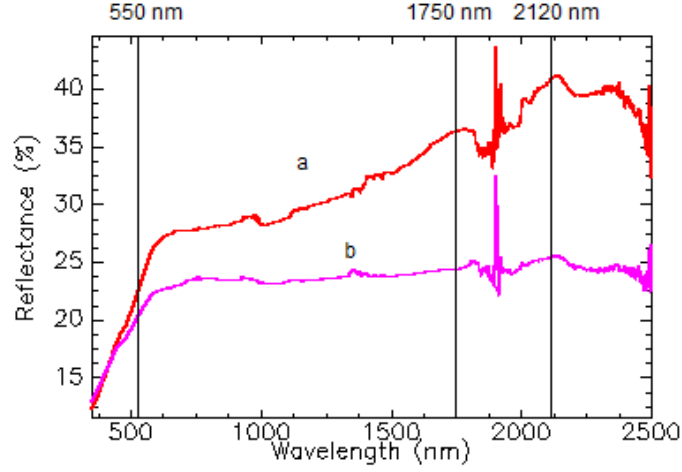
Variation in the spectral characteristics of concrete roof surfaces is shown in Figure 5.2 (c). It is observed from the spectral characteristics of concrete surfaces that, new concrete surfaces have the highest reflectance while degradation and material aging result in a decrease in reflectance in all the regions of spectra. The change in reflectance of concrete surfaces may be due to the continuous oxidation of these surfaces caused by the accumulation of dust and dirt followed by absorption of iron oxide components [135]. Therefore, the brightness of the concrete surfaces also decreases. If the analysis of spectral signatures of concrete roof surfaces is carried out in the SWIR region, then it shows minor change with clay absorption near 2200 nm for older surfaces. Further, the hydrocarbon absorptions are also observed at 1750 nm and above 2100 nm, specifically at 2310 and 2350 nm, respectively. If we consider the spectral response in visible region, then it appears that iron oxide absorption occurs between 520 and 670 nm, particularly at 550 nm [135].



(a)



(b)



(c)

Figure 5.2 Images with respective spectral characteristics of concrete roof surfaces of different level of deterioration (a) New or less deterioration (b) Old or more deterioration (c) spectral signatures of roof surfaces shown in (a) and (b)

5.3 Multiple endmember spectral mixture analysis (MESMA)

Spectral Mixture Analysis (SMA) is based on the assumption that reflectance f measured at pixel i can be represented as a linear summation of M endmembers (spectrally pure materials) weighted by the fraction a_{ki} of each endmember within the pixel i [137] [138]. For a given wavelength λ , it is computed as:

$$f_{i\lambda} = \sum_{k=1}^M a_{ki} \times f_{k\lambda} + e_{i\lambda} \quad (5.3)$$

Where $e_{i\lambda}$ is the residual component that explains the unmodeled portion of radiance/reflectance. It also specifies the difference between the measured and modeled spectral signature. Modeled fractions are usually constrained by the following:

$$\sum_{k=1}^M a_{ki} = 1 \quad (5.4)$$

Model fit is assessed by calculating the root mean squared error (RMSE) of residuals for every pixel across all the bands i.e. between 1 to N [54].

$$RMSE_i = \left(\sum_{\lambda=1}^N \frac{(e_{i\lambda})^2}{N} \right)^{1/2} \quad (5.5)$$

Endmember can be collected in the lab or field or may be extracted from the image itself. Constraints for selecting appropriate models for each pixel can be specified in terms of RMSE, the residuals for each wavelength and range of end member fractions [139].

In standard SMA, a fixed number of endmembers, usually between two to five are used to model the entire image in terms of those spectrally pure components [137]. However, this method is limited because the selected endmember may not efficiently model all the elements in the image. These limitations of SMA are basically challenging in an urban environment. An algorithm that addresses all these limitations is Multiple Endmember Spectral Mixture Analysis (MESMA), which allows the type as well as number of endmembers to differ on per pixel basis [54].

In this study, MESMA is utilized for condition analysis of bitumen or asphalt road surfaces followed by deterioration analysis of concrete roof surfaces. Various aforementioned mean spectral signatures of road and roof surfaces of different condition and deterioration are utilized as endmembers for the unmixing analysis using MESMA approach. Further, a comparative analysis is also carried out between proposed index based approach and existing MESMA unmixing results.

5.4 Implementation

Following steps are used for condition analysis of road surfaces and deterioration

analysis of roof surfaces:

- AVIRIS-NG hyperspectral data acquisition and selection of a spatial subset of image data, which is dominated by urban built-up surfaces
- Removal of the bad band from hyperspectral imagery followed by masking of vegetation and water classes using index based approach
- Field hyperspectral data acquisition for road surfaces of different condition and roof surfaces of different deterioration subsequently removal of bad bands
- Analysis of ground spectral signatures of various road surfaces of different condition, and identification of significant wavelengths followed by formulation of a spectral index for condition analysis of road surfaces
- Analysis of ground spectral signatures of various roof surfaces based on their deterioration, and identification of significant wavelengths subsequently formulation of a spectral index for deterioration analysis of roof surfaces
- Mapping of spectral indices based on road condition and roof deterioration using density slicing approach
- Spectral unmixing of road and roof surfaces on the basis of their condition and deterioration using MESMA approach
- Comparative assessment of the results obtained by proposed index based approach with existing MESMA unmixing

5.5 Spectral index for condition analysis of road surfaces

Statistical analysis of spectral signatures shown in Figure 5.1 (c) suggests that the band at 830 nm reflects the spectral peak between the two iron absorption bands while 490 nm is positioned in the middle of the iron absorption bands [7] [28]. There are some natural reasons that may significantly affect the spectral reflectance of road

surfaces. The effect of heat and reactions with solar radiation along with atmospheric oxygen are the main natural processes. In view of all the aforementioned facts, a spectral index is developed by considering the two wavelengths, which are 490 nm in the visible, and 830 nm in NIR region. Further, this newly introduced spectral index, named as Condition Index- Road (CI- Road) for the condition analysis of road surfaces, is given in Equation 5.6. This index may be more helpful to determine the condition of road surfaces in a more efficient manner.

$$\text{Condition Index} - \text{Road } (CI - \text{Road}) = \frac{(B_{830} - B_{490})}{(B_{830} + B_{490})} \quad (5.6)$$

Where B_{830} and B_{490} are the reflectances of bitumen road at 830 nm and 490 nm, respectively. Otsu's thresholding [117] has been utilized to find out the range of spectral indices, which depicts the condition of road surfaces, as shown in Table 5.1. It appears from the range of spectral indices shown in Table 5.1 that the CI-Road will be low for new or good condition road while high for old or damaged condition road surfaces.

5.6 Spectral index for deterioration analysis of roof surfaces

Using the spectral characteristics of roof surfaces shown in Figure 5.2 (c), a spectral index is introduced for deterioration analysis of concrete roof surfaces, as given in Equation 5.7. When this index is applied on AVIRIS-NG imagery, then it results in a single band image which may be capable of differentiating deteriorated roof surfaces based on the various range of index values. The spectral index is expressed in terms of normalized difference index ratio, which is generated on the basis of most informative band combinations utilized for detecting concrete roof deterioration.

This index utilizes the advantage of hydrocarbon and iron oxide absorption in SWIR and visible regions of Electromagnetic (EM) spectrum for determining the deterioration of concrete roof surfaces.

$$Deterioration\ Index - Roof\ (DI - Roof) = \frac{\left(B_{2120} - \frac{B_{1750}}{B_{550}} \right)}{\left(B_{2120} + \frac{B_{1750}}{B_{550}} \right)} \quad (5.7)$$

Where B_{2120} , B_{1750} and B_{550} are the reflectances of concrete roof surfaces at 2120 nm, 1750 nm, and 550 nm, respectively. Otsu's thresholding has been utilized to find out the range of spectral indices, which depicts the deterioration status of roof surfaces as shown in Table 5.1. DI-Roof will be low for old or more deteriorated roof surfaces while it will be high for new or less deteriorated roof surfaces.

Table 5.1 The range of spectral indices for different road and roof surfaces

Category	Range
CI-Road	
New or good condition	-0.0346 to 0.1245
Old or damaged condition	0.1245 to 0.1882
DI-Roof	
Old or more deteriorated	-0.7282 to -0.6864
New or less deteriorated	-0.6864 to -0.4357

5.7 Results

5.7.1 Mapping of road surfaces of different condition

Mapping of road surfaces of different condition is carried out using two approaches which are proposed index based approach and existing MESMA unmixing algorithm.

The analysis has been performed on original image along with three ROIs, as shown in Figure 5.3 (a), (d), (g) and (j). The results of the analysis are shown in Figure 5.3 (b), (c), (e), (f), (h), (i), (k) and (l). The hyperspectral image is classified into two categories i.e. new or good condition, and old or damaged condition depending upon the condition of road surfaces. Further, for labeling the results of index based approach, density slicing strategy is utilized. In Figure 5.3 (b), (c), (e), (f), (h), (i), (k) and (l), pixels with magenta color represents new road surfaces with good condition while pixels with cyan color depicts old road with damaged or bad condition. As previously discussed, a sum of 500 samples or pixels of road surfaces have been used for accuracy assessment and validation of results. Further, out of these 500 pixels, 378 pixels belong to new or good condition road surfaces and remaining 122 to old or damaged condition road surfaces. The quantitative analysis of the results is carried out for all three sites without considering the false alarms, as shown in Table 5.2.

It is observed that out of 378 pixels of new road surfaces with good condition, 88.88 % of pixels are clearly detected in the outcomes of spectral index while MESMA unmixing is capable of detecting only 79.89 % of those pixels. Further, it is also investigated that out of 122 pixels of old road surfaces with the damaged condition, 83.60 % pixels are clearly highlighted in case of spectral index while 76.22 % of those pixels are detected by MESMA approach. Geographical variability of endmembers of similar material may be one of the reason of degradation of MESMA results. Therefore, index based approach can prove to be effective for condition analysis of road surfaces in comparison to MESMA unmixing.

Table 5.2 Quantitative analysis of road surfaces in all regions of interest

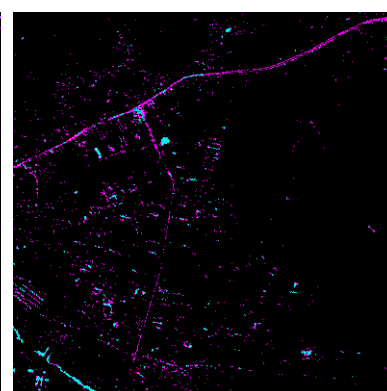
Category	Actual Pixels	Detected Pixels	Detection Percentage
CI-Road			
New or good condition	378	336	88.88
Old or damaged condition	122	102	83.60
MESMA			
New or good condition	378	302	79.89
Old or damaged condition	122	93	76.22



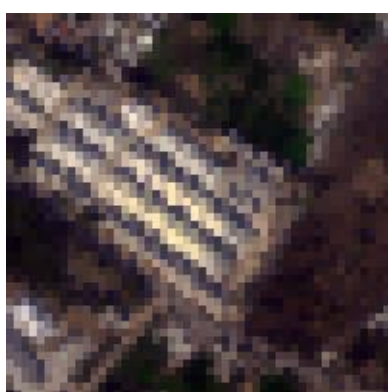
(a)



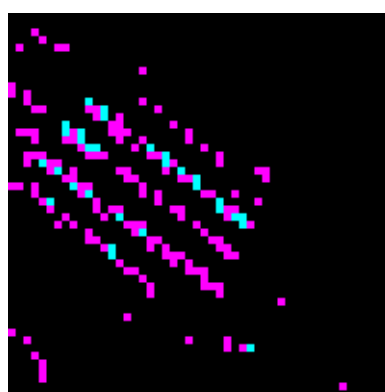
(b)



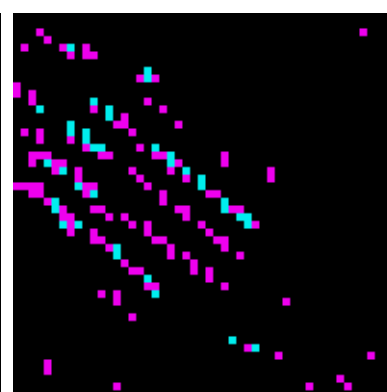
(c)



(d)



(e)



(f)

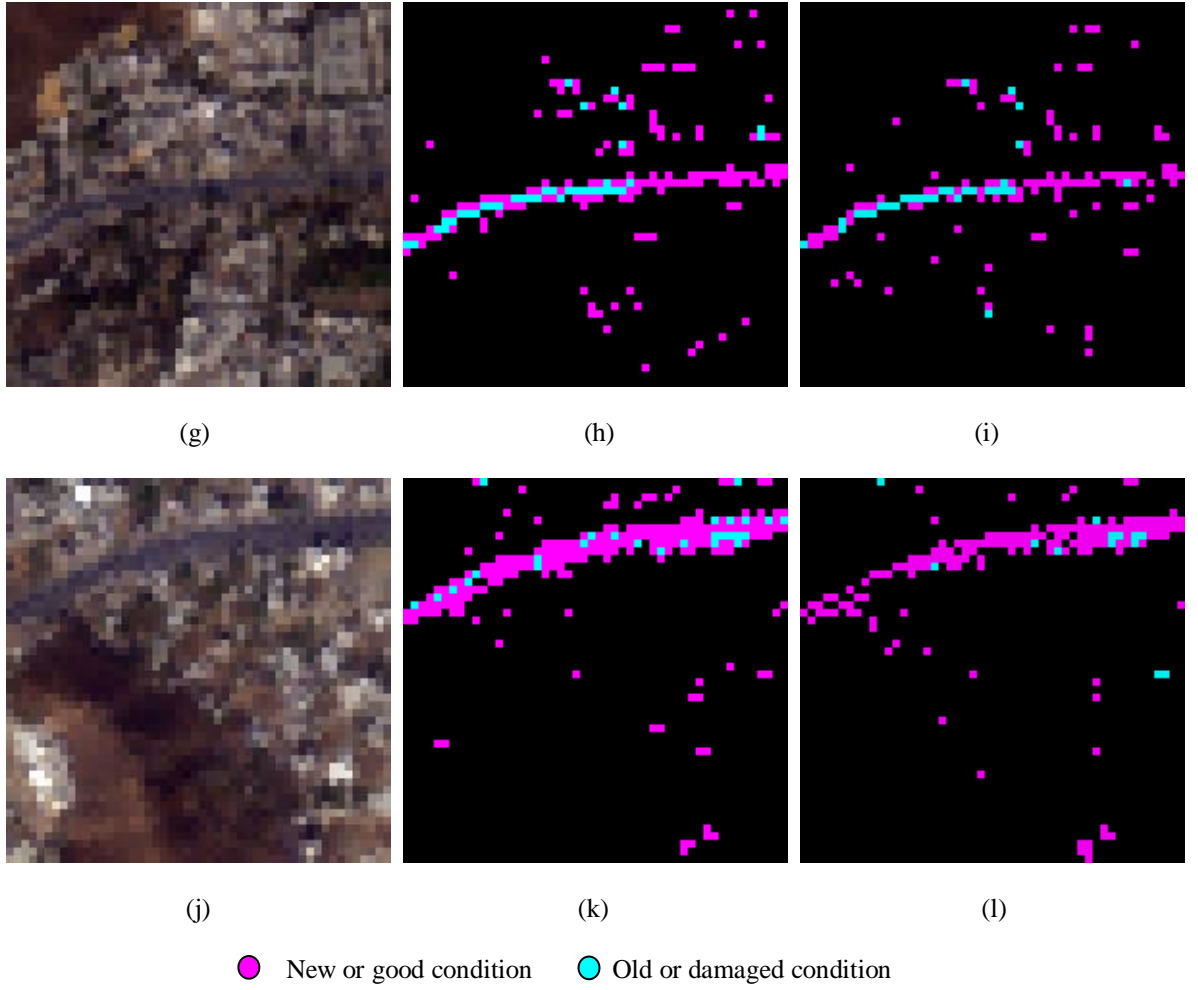
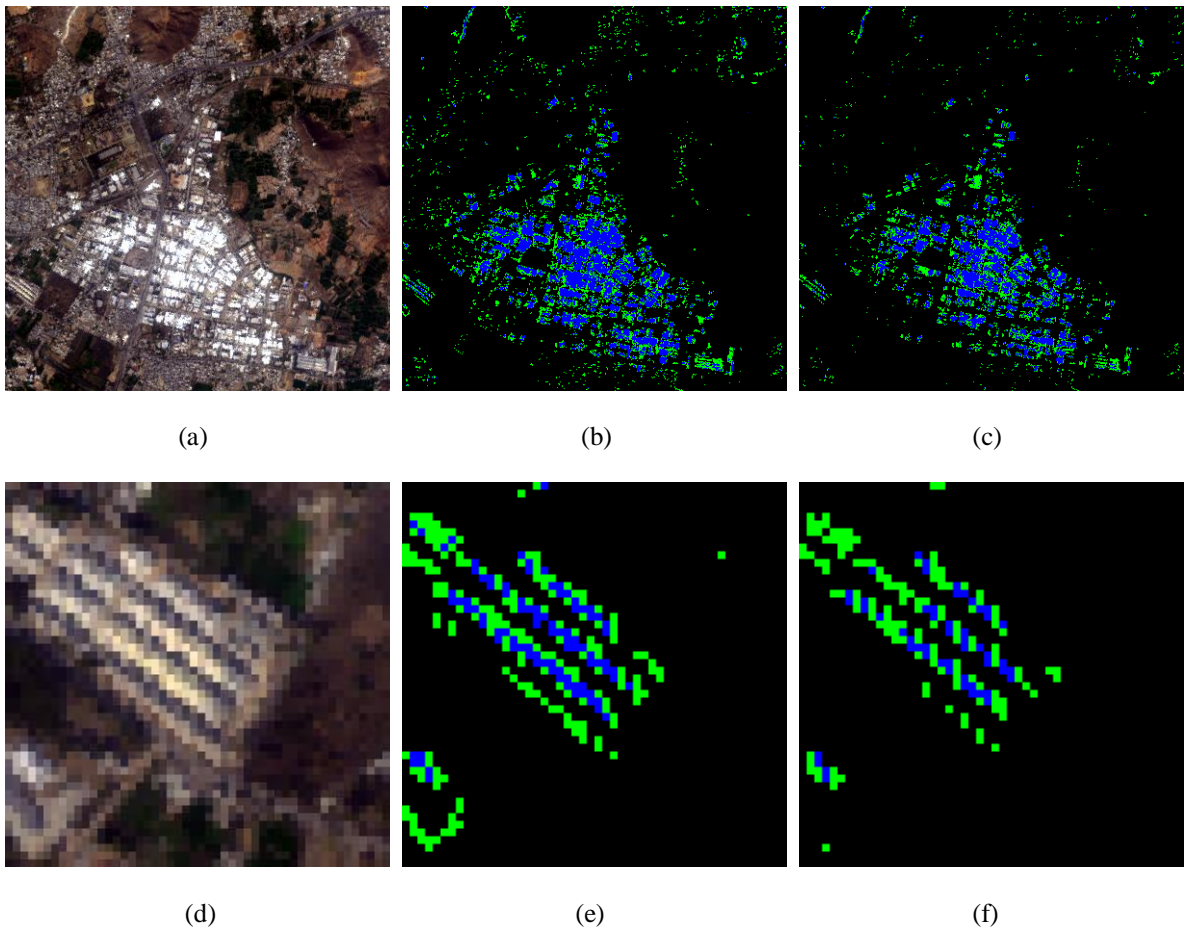


Figure 5.3 Road condition analysis using hyperspectral imagery (a) original image (b) analysis using index based approach (c) analysis using MESMA unmixing (d) (g) (j) three regions of interest of original image (e) (h) (k) analysis of regions of interest using index based approach (f) (i) (l) analysis of regions of interest using MESMA unmixing

5.7.2 Mapping of roof surfaces of different deterioration

Mapping of deteriorated roof surfaces is performed using two different approaches, which are proposed index based approach and MESMA unmixing algorithm. The roof deterioration analysis has been carried out on original image along with three regions of interest, as shown in Figure 5.4 (a), (d), (g) and (j). The results of the analysis are shown in Figure 5.4 (b), (c), (e), (f), (h), (i), (k) and (l). The AVIRIS-NG imagery is classified into two categories i.e. new or less deteriorated and old or more

deteriorated roof surfaces. The labeling of index results has been carried out using density slicing approach. In Figure 5.4 (b), (c), (e), (f), (h), (i), (k) and (l), pixels with blue color represent the new and less deteriorated roof surfaces while green color pixels are associated with old roof surfaces with more deterioration. For accuracy assessment and validation of mapping results of roofs, 532 samples or pixels are used, out of which 312 pixels belong to new roof surfaces with less deterioration while 220 pixels to old roof surfaces with more deterioration. The quantitative analysis on the basis of deterioration of roof surfaces is performed for all the three regions of interest shown in Figure 5.4 (d), (g) and (j).



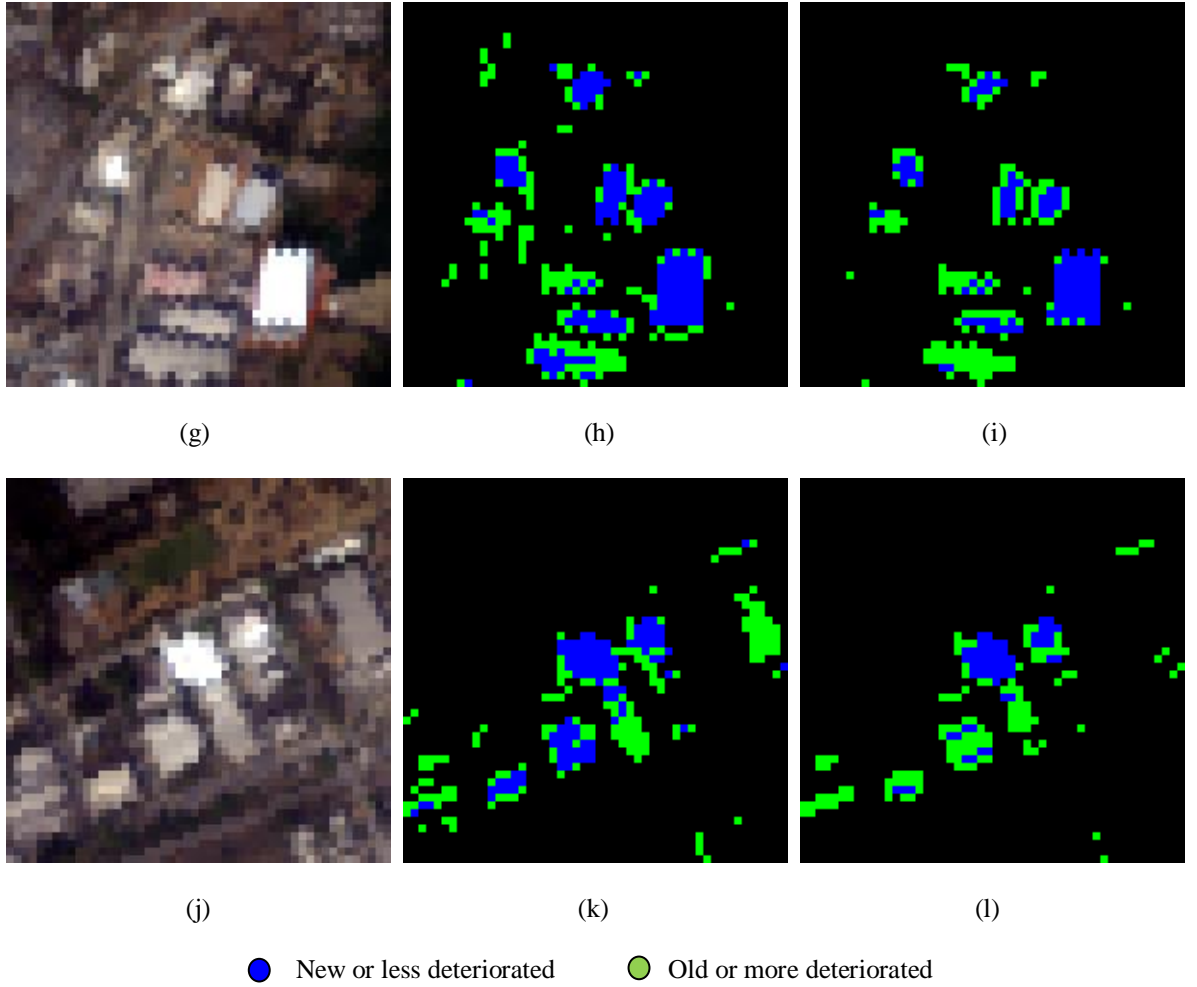


Figure 5.4 Deterioration analysis of roof using hyperspectral imagery (a) original image (b) analysis using index based approach (c) analysis using MESMA unmixing algorithm (d) (g) (j) three regions of interest of original image (e) (h) (k) analysis of regions of interest using index based approach (f) (i) (l) analysis of regions of interest using MESMA unmixing algorithm

It is observed that out of 312 pixels of new or less deteriorated roof surfaces, 90.38 % of pixels are clearly detected in outcome of index while 84.29 % of those truth pixels are highlighted in MESMA, as shown in Table 5.3. Further, if the analysis is carried out for old or more deteriorated roof pixels, then out of 220 pixels, 85.90 % of those pixels are clearly extracted in the index results while only 75.45 % of those pixels are detected in MESMA outcomes. Hence, index based approach has proved its efficacy for deterioration analysis of roof surfaces.

Table 5.3 Quantitative analysis of roof surfaces in all regions of interest

Category	Actual Pixels	Detected Pixels	Detection Percentage
DI-Roof			
New or less deteriorated	312	282	90.38
Old or more deteriorated	220	189	85.90
MESMA			
New or less deteriorated	312	263	84.29
Old or more deteriorated	220	166	75.45

5.8 Summary

In this study, the condition analysis of road surfaces and deterioration analysis of roof surfaces were carried out by utilizing AVIRIS-NG image along with field hyperspectral data. Further, using various significant wavelength bands, two spectral indices i.e. CI-Road and DI-Roof were formulated for condition analysis of road surfaces, and deterioration analysis of roof surfaces, respectively. The aforementioned analysis with respect to road and roof surfaces was also carried out using MESMA unmixing algorithm followed by a comparison with index based approach. The area under investigation belongs to the urban area of Udaipur, Rajasthan, India. The results of the analysis suggest that, as the condition of the road surfaces gets poor, the reflectance in all the regions of EM spectrum increases that may also depict that CI-Road will be larger for old or damaged condition road surfaces while less for new or good condition road surfaces. Further, as the deterioration increases for the roof surfaces, the reflectance of these surfaces

decreases, which depicts that DI-Roof will be larger for new or less deteriorated roof surfaces while less for old or more deteriorated roof surfaces. The comparison of indices results with MESMA unmixing suggests that, indices results may outperform MESMA, which may be due to more geographical variability of endmembers and model complexity of MESMA algorithm.

Chapter 6

Extraction of Built-up surfaces and its Sub-categories using existing Built-up Indices in AVIRIS-NG Imagery

In remote sensing, almost all the built-up indices have been developed for the multispectral dataset [3] [57] [59] [60] [61] [62] [63] [64] [65] [66] [67] [68] [69] [70] [71] [72] [73] and there still exist immense scope to overcome aforesaid limitations using hyperspectral data by way of selection of most significant bands for detection of built-up surfaces and its subcategories. This research explores the most significant spectral bands in AVIRIS-NG hyperspectral imagery for detection of built-up surfaces and its subclasses i.e. roads and roofs. Further, this study utilizes existing built-up indices for detection of urban built-up surfaces in the first level followed by its subcategories in the second level. Finally, a separability analysis between spectrally mixed urban land cover classes using various measures is also addressed. As in previous case, this study has also been carried out using AVIRIS-NG image and field hyperspectral data of Udaipur, Rajasthan region of India.

The main task progressed in this research is to explore most of the existing built-up indices reported in the literature for multispectral dataset, and apply them on AVIRIS-NG hyperspectral dataset with a view to:

- a) Identify the most significant spectral bands for the detection of built-up surfaces and its subclasses i.e. roads and roofs.
- b) Extract built-up surfaces in the first level of detection followed by roads and roofs in its second level.
- c) Carry out a separability analysis of spectrally mixed urban land cover classes

i.e. between built-up surfaces and soil in Level-1 followed by roads and roofs in Level-2 to further validate the result of built-up extraction.

6.1 Study area and Data

The remote sensing data used in this study is AVIRIS-NG image, and field hyperspectral data. The area under investigation belongs to the Udaipur, Rajasthan region of India, which is an amalgamation of artificial i.e. roads and roofs, and natural surfaces i.e. vegetation and soil. The results of the study are validated using a high-resolution satellite base map of ArcGIS 10.4 in addition to 2297 known ground sample locations, out of which 1032 belong to built-up and 1265 to non-built-up surfaces. These built-up surfaces are further divided into 500 road and 532 roof surfaces. The complete description of study area and dataset is given in Chapter 4 Section 4.1.

6.2 Spectral indices for extraction of urban built-up surfaces

The index-based classification and detection algorithms are designed based on the lowest and highest reflectance values in spectral bands, distinguishing the target present in remote sensing data. Therefore, the aim is to calculate the normalized difference between such bands to enhance the intensity contrast between a particular target and the background. If B_i and B_j are the reflectance corresponding to i^{th} and j^{th} bands of hyperspectral imagery, then the Normalized Difference Spectral Index (NDSI) can be represented as:

$$NDSI = \frac{(B_i - B_j)}{(B_i + B_j)} \quad (6.1)$$

Blue, Green, Red, near-infrared (NIR) and short-wavelength infrared (SWIR) regions of remote sensing imagery are generally used for the calculation of spectral indices. Some of the well-known built-up spectral indices are listed in Table 6.1.

The spectral indices reported in the literature for extraction of built-up surfaces can be classified into three different categories:

- i) Band-ratio or normalized difference band-ratio approach using spectral bands as an element in the image directly [59] [62] [69]
- ii) Indices based on the correlation between the built-up index with other land cover indices [60] [63]
- iii) Indices using feature extraction approach [86]

Since the reflectance of built-up areas is higher in SWIR and NIR regions in contrast to other spectral regions, therefore a multitude of spectral indices have been proposed in the literature using these spectral regions. Based on the above three approaches and urban built-up surface reflectance, various spectral indices have been developed for multispectral imagery to extract different built-up surfaces, as listed in Table 6.1.

In this study, different existing built-up indices i.e. BSI, NBI, BAEI, BRBA, VIBI, REI, BUI, NDBI, NBAI, MBI, and IBI have been utilized for the extraction of built-up surfaces in AVIRIS-NG hyperspectral imagery using identification of most significant wavelengths. In the first level of detection, urban surfaces have been divided into built-up and non-built-up surfaces. The built-up surfaces are further categorized into road and non-road surfaces, and roof and non-roof surfaces in the second level of detection. Further, based on a statistical analysis of the mean spectral

signatures of 500 known samples of roads, 532 of roofs, 652 truth samples of vegetation and 613 of soil, in the respective spectral regions of different built-up indices, BSI, NBI, BAEI, BRBA, and VIBI are selected for extraction of urban built-up surfaces (Level-1) while REI, BUI, and NDBI are identified for detection of roads (Level-2) followed by NBAI, MBI, and IBI for extraction of roofs (Level-2) in AVIRIS-NG imagery. Since, VIBI, BUI, and IBI make use of various non-built-up indices such as NDVI, SAVI, and MNDWI, therefore these have also been included in Table 6.1.

Table 6.1 Spectral indices utilized for extraction of built-up surfaces (Level-1 and 2)

SN	Details	Expression	Reference
Indices for extraction of Non-built-up surfaces			
1	Normalized Difference Vegetation Index (NDVI)	$NDVI = \frac{(B_{NIR} - B_{RED})}{(B_{NIR} + B_{RED})}$	[127]
2	Soil Adjusted Vegetation Index (SAVI)	$SAVI = \frac{(B_{NIR} - B_{RED})(1 + L)}{(B_{NIR} + B_{RED} + L)}$ $L = \text{Background adjustment factor}$	[76]
3	Modified Normalized Difference Water Index (MNDWI)	$MNDWI = \frac{(B_{GREEN} - B_{SWIR})}{(B_{GREEN} + B_{SWIR})}$	[77]
Indices for extraction of Built-up surfaces (Level-1)			
4	Built-up Surface Index (BSI)	$BSI = \frac{(B_{YELLOW} - 2 * B_{NIR})}{(B_{YELLOW} + 2 * B_{NIR})}$	[69]
5	New Built-up Index (NBI)	$NBI = \frac{B_{RED} * B_{SWIR}}{B_{NIR}}$	[61]
6	Built-up Area Extraction Index (BAEI)	$BAEI = \frac{B_{RED} + L}{B_{GREEN} + B_{SWIR}}$ $L = \text{Arithmetic constant depends on the}$	[66]

percentage of vegetation cover

7	Band Ratio for Built-up Area (BRBA)	$BRBA = \frac{B_{RED}}{B_{SWIR}}$	[62]
---	-------------------------------------	-----------------------------------	------

8	Vegetation Index Built-up Index (VIBI)	$VIBI = \frac{(NDVI)}{(NDVI + NDBI)}$	[63]
---	--	---------------------------------------	------

Indices for extraction of Roads (Level-2)

9	Road Extraction Index (REI)	$REI = \frac{B_{NIR} - B_{BLUE}}{B_{NIR} + B_{BLUE} * B_{NIR}}$	[67]
---	-----------------------------	---	------

10	Built-up Index (BUI)	$BUI = (NDBI - NDVI)$	[60]
----	----------------------	-----------------------	------

11	Normalized Difference Built-up Index (NDBI)	$NDBI = \frac{(B_{SWIR} - B_{NIR})}{(B_{SWIR} + B_{NIR})}$	[59]
----	---	--	------

Indices for extraction of Roofs (Level-2)

12	Normalized Built-up Area Index (NBAI)	$NBAI = \frac{B_{SWIR2} - \left(\frac{B_{SWIR1}}{B_{GREEN}} \right)}{B_{SWIR2} + \left(\frac{B_{SWIR1}}{B_{GREEN}} \right)}, B_{SWIR1} < B_{SWIR2}$	[62]
----	---------------------------------------	---	------

13	Modified Built-up Index (MBI)	$MBI = \frac{B_{SWIR} * B_{RED} - B_{NIR}^2}{B_{RED} + B_{NIR} + B_{SWIR}}$	[65]
----	-------------------------------	---	------

14	Index-based Built-up Index (IBI)	$IBI = \frac{(NDBI - (SAVI + MNDWI) / 2)}{(NDBI + (SAVI + MNDWI) / 2)}$	[86]
----	----------------------------------	---	------

6.3 Implementation

In this study, different existing built-up indices have been utilized for the detection of built-up surfaces in the first level followed by road and roof surfaces in the second level using AVIRIS-NG and field hyperspectral data. The whole analysis has been carried out using ENVI 5.3, ArcGIS 10.4, MATLAB 2018B, SPSS, and a command prompt based band selection tool. A flow chart describing all the stages of implementation is represented in Figure 6.1.

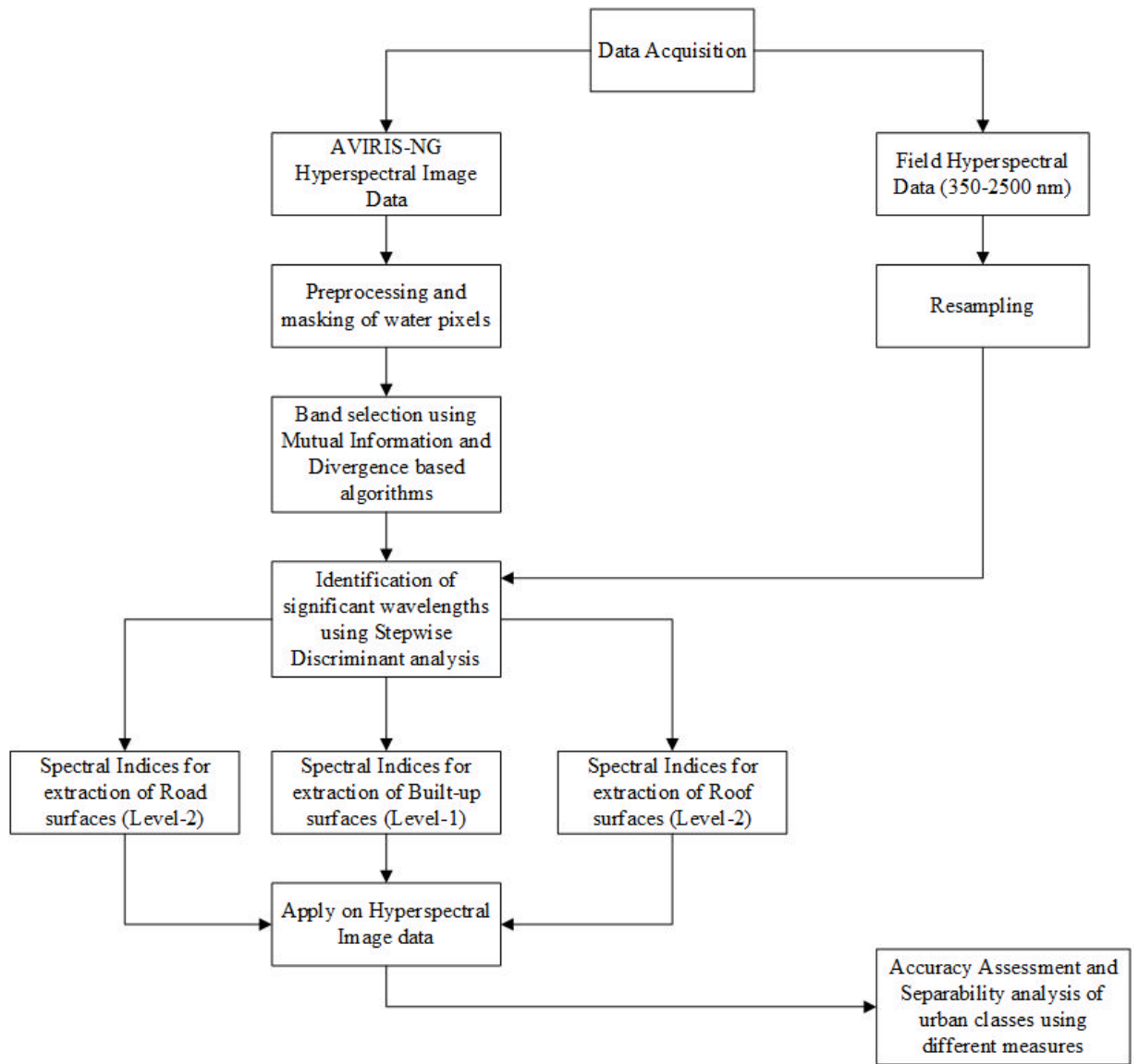


Figure 6.1 Implementation steps for extraction of built-up surfaces (Level-1 and 2) using different built-up indices

6.4 Results

This section starts with the identification of most significant wavelengths for extraction of built-up surfaces and its subclasses in hyperspectral imagery followed by optimal thresholding of different built-up indices (Level-1 and 2). Accordingly, the optimal extraction of built-up surfaces using different built-up indices is carried out in first level subsequently road and roof surfaces in the second level. Further, the

accuracy assessment of built-up extraction results in different levels is performed. Finally, Section 6.4.6 discusses the separability analysis between spectrally mixed urban land cover classes i.e. between built-up surfaces and soil as well as between roads and roofs to further validate the results of detection. This is accomplished using histogram and statistical analysis.

6.4.1 Identification of significant wavelengths for extraction of built-up surfaces (Level-1 and 2)

The mutual information and divergence based algorithms have been used to reduce data redundancy amongst hyperspectral image bands. These approaches are based on a hierarchical clustering to group bands of hyperspectral imagery to minimize the intra-cluster and maximize the inter-cluster variance. The final selected bands will be the best representative from each cluster. In this study, a band selection tool that reduces the number of bands using information and divergence based algorithms [128] [129] [130] has been used. In this command prompt based tool, 380 bands of hyperspectral imagery have been reduced using both of these criteria. On setting the number of output clusters as 100, and after execution using both the criteria, 40 common bands have been identified.

During the ground data collection, 2297 spectral signatures of different urban surfaces and sub-surfaces have been collected. These urban samples consisted of 1032 built-up and 1265 non-built-up surfaces. Next, resampled ground spectral data of 1032 built-up and 1265 non-built-up surfaces along with aforesaid 40 bands of AVIRIS-NG imagery have been utilized to obtain significant wavelengths using stepwise discriminant analysis.

The stepwise discriminant analysis [131] [132] is performed on the SPSS tool

(IBM Corporation) that identifies significant wavelengths based on Wilks's Lambda parameter (Refer Chapter 4 Section 4.2.2). This parameter is a combination of the statistics of each variable that contributes to the discrimination function and it has a value range of 0-1. A smaller value of this variable indicates that it makes a greater contribution to the discriminant model. So, based on Wilks's Lambda values, 4 significant wavelengths of minimum Lambda values are selected from each region of hyperspectral data i.e. Visible, NIR, and SWIR. These wavelengths with respective regions are listed in Table 6.2.

Various indices utilize a combination of two to three spectral wavelengths to increase the contrast between target and background and for enhancing the accuracy of detection. Therefore, different wavelength combinations have been generated using Table 6.2 for each index mentioned in Table 6.1. Further, using histogram analysis of various urban land cover classes (mentioned in section 6.1) in each of the generated index band, the wavelength combination of maximum inter and intra-class separability is selected. The suitable wavelength combination of different built-up indices is tabulated in Table 6.3. Since, some of the built-up indices such as VIBI, BUI, and IBI make use of vegetation and water indices i.e. NDVI, SAVI, and MNDWI for their formulation, so suitable wavelength combinations for these non-built-up indices along with built-up indices have also been mapped as shown in Table 6.3. These vegetation and water indices have been generated before the implementation of built-up indices (Level-1 and 2).

Further, using histogram representation of different built-up indices and various statistical parameters associated with targets and backgrounds, an optimal threshold is obtained for extraction of urban built-up surfaces (Level-1 and 2). Table 6.3 also depicts the optimal threshold values obtained as a result of Otsu's optimization

approach (Refer Chapter 4 Section 4.4).

Table 6.2 Significant wavelengths obtained using stepwise discriminant analysis

Wavelength Region	Wavelength (nm)	Wilks's Lambda
Visible	466	0.405
	561	0.359
	606	0.155
	666	0.116
NIR	737	0.059
	837	0.028
	867	0.032
	982	0.069
SWIR	1548	0.321
	1608	0.219
	1999	0.185
	2189	0.205

Table 6.3 Significant wavelength combination and optimal threshold for different spectral indices

Spectral Index	Wavelength combinations (nm)	Mean	Standard Deviation	Threshold
Non-built-up extraction indices				
NDVI	867 (NIR), 666 (RED)	-----		
SAVI	867 (NIR), 666 (RED)	-----		
MNDWI	1608 (SWIR), 561 (GREEN)	-----		
Built-up extraction indices (Level-1)				
BSI	837 (NIR), 606 (YELLOW)	-0.535	0.101	-0.475
NBI	1999 (SWIR), 867 (NIR), 666 (RED)	-0.251	0.139	-0.150
BAEI	2189 (SWIR), 666 (RED), 561 (GREEN)	-0.281	0.125	-0.220

BRBA	1608 (SWIR), 666 (RED)	0.636	0.126	0.650
VIBI	1608 (SWIR), 867 (NIR), 666 (RED)	0.509	0.139	0.525
Road extraction indices (Level-2)				
REI	867 (NIR), 466 (BLUE)	0.493	0.124	0.375
BUI	1548 (SWIR), 867 (NIR), 466 (BLUE)	0.369	0.121	0.254
NDBI	1548 (SWIR), 737 (NIR)	0.259	0.124	0.138
Roof extraction indices (Level-2)				
NBAI	1999 (SWIR2), 1548 (SWIR1), 561 (GREEN)	-0.819	0.074	-0.720
MBI	1548 (SWIR), 867 (NIR), 666 (RED)	-0.040	0.048	-0.009
IBI	2189 (SWIR), 867 (NIR), 666 (RED), 561 (GREEN)	0.114	0.071	0.250

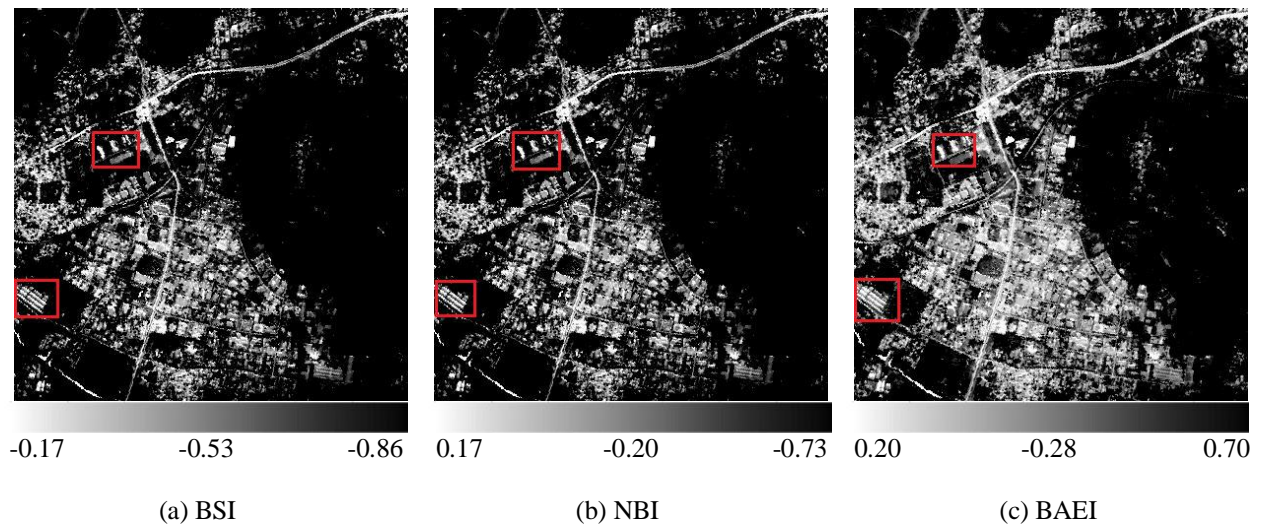
6.4.2 Extraction of built-up surfaces (Level-1)

The built-up extraction results of hyperspectral imagery using various spectral indices such as BSI, NBI, BAEI, BRBA, and VIBI are shown in Figure 6.2 (a) to (e), which demonstrate that the bright pixels are target pixels i.e. urban built-up surfaces while dark pixels are related to background. Two ROIs containing road and roof surfaces are considered for a brief assessment of the results. These surfaces are highlighted inside the two red rectangles in all the images. The following can be observed from built-up extraction results shown in Figure 6.2 (a) to (e):

- Visually, using a high-resolution base map, it is observed that, inside the two red rectangles in each of the images, most of the roads and roofs are fully detected in the outcome of BSI, NBI, and BAEI while partially visible in BRBA and VIBI.
- The quantitative analysis of the built-up surfaces inside these rectangles indicates that out of total 208 known pixels of built-up surfaces, BSI, NBI, and BAEI can detect 193, 181 and 169 pixels correctly while BRBA and VIBI are

detecting only 147 and 141 pixels of those known samples, respectively. This study assumes an index to be efficient if it detects more than 80 % of target pixels correctly. Therefore, this hypothesis makes BSI, NBI, and BAEI to be suitable for the extraction of built-up surfaces in comparison to BRBA and VIBI.

- Further, VIBI appears to enhance the road surfaces by suppressing other urban land cover classes, therefore it may be used for extraction of the roads as well.
- BSI utilizes NIR (730-1340 nm) and visible (450-690 nm), NBI uses SWIR2 (1960-2490 nm), NIR, and visible while BAEI makes use of SWIR2 and visible bands of hyperspectral imagery for their formulation. Further, BRBA utilizes SWIR1 (1500-1790 nm) and visible while VIBI uses SWIR1, NIR, and visible wavelength bands for the detection of built-up surfaces. Therefore, it may be deduced that SWIR2, NIR, and visible bands can prove to be the most suitable for detection of built-up surfaces in AVIRIS-NG imagery.



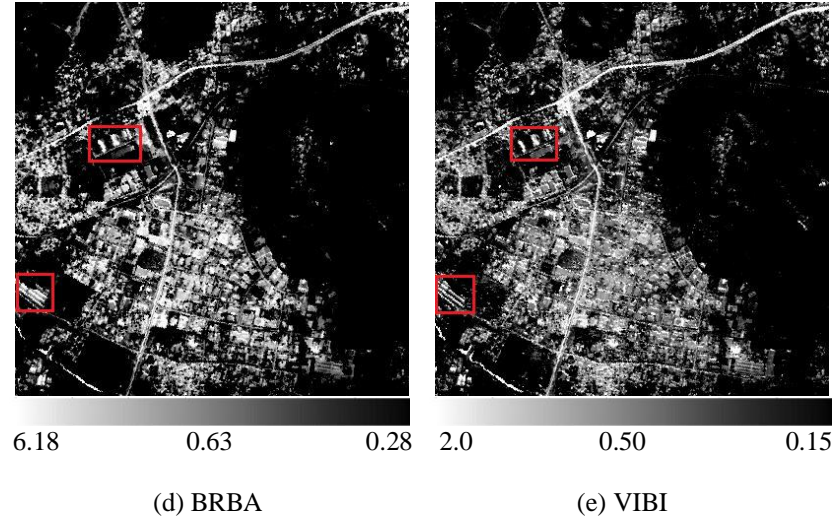


Figure 6.2 Urban built-up extraction using different built-up indices. The range of indices of grayscale image is shown along the x -axis

6.4.3 Extraction of road surfaces (Level-2)

The road extraction results in hyperspectral imagery using various built-up indices such as REI, BUI, and NDBI are shown in Figure 6.3. In Figure 6.3 (a) to (c), dark pixels are associated with road surfaces while bright pixels consist of background. A ROI from the study area consisting of five parallel road surfaces has been considered for a brief analysis of the results. This region is indicated with a red rectangle inside all the images. Following is observed from road extraction results shown in Figure 6.3 (a) to (c):

- It appears from the visual analysis using a high-resolution imagery that, inside the red rectangle in each of the images, five parallel road surfaces are present, these are perfectly detected in case of REI, and few surfaces are visible in BUI while NDBI can detect only very few pixels of these roads.
- The quantitative analysis of the aforesaid road surfaces shows that, out of a total of 62 known pixels of roads, REI detects 57 pixels correctly while BUI and

NDBI detect only 46 and 36 pixels of those road surfaces, respectively. Therefore, REI can provide better detection results in comparison to BUI and NDBI.

- It is also observed that in all the indices, specifically NDBI, along with highways, some walkway, and street roads are also detected with some false alarms. These false alarms may be due to the presence of bituminous roofs, as these roofs and asphalt roads tend to share similar spectral properties. This problem appears to have further worsened due to the occlusion of road surfaces by shadow, trees, and the presence of vehicles.
- Since REI utilizes NIR (730-1340 nm) and visible (450-690 nm) bands of hyperspectral data for its formulation, therefore these bands can prove to be the most suitable for detection of road surfaces in AVIRIS-NG imagery.
- The NDBI makes use of SWIR1 (1500-1790 nm) and NIR (730-1340 nm) bands for its formulation, which implies that the SWIR1 band may not be appropriate for the detection of the road surfaces. As BUI is based on NDBI, and NDBI results in greater false alarms, therefore, BUI also appears to worsen the detection results.

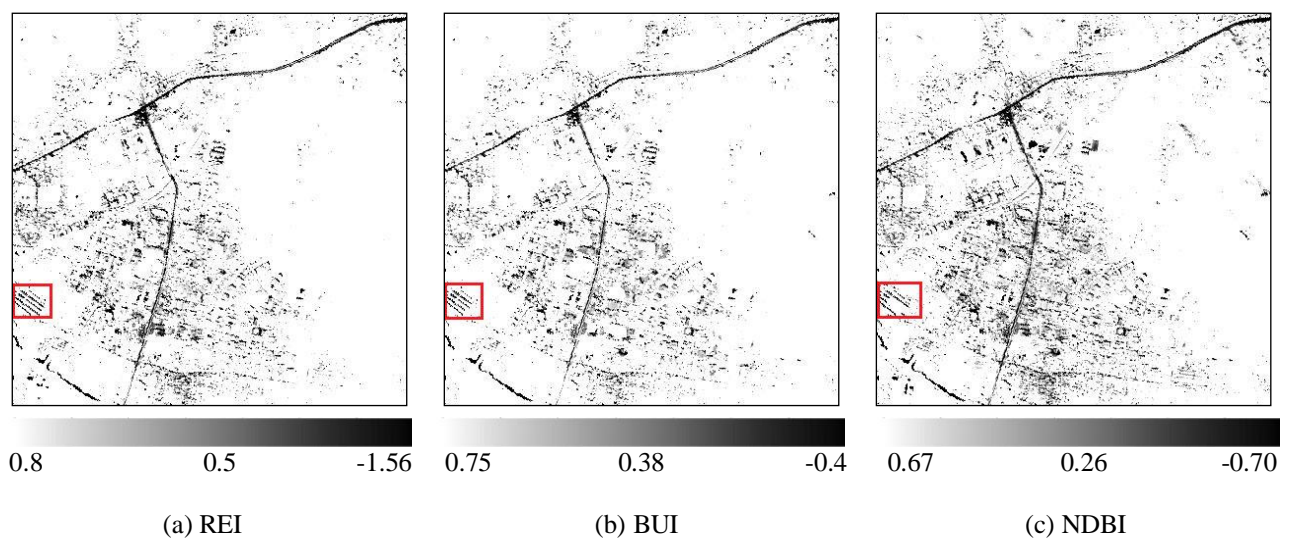


Figure 6.3 Extraction of road surfaces using various spectral indices. The range of indices of grayscale image is shown along the x -axis

6.4.4 Extraction of roof surfaces (Level-2)

The roof extraction results of various indices such as NBAI, IBI, and MBI are shown in Figure 6.4. In Figure 6.4 (a) to (c), bright pixels are associated with roof surfaces while dark pixels are related to background. A ROI containing different rooftops is considered for a brief evaluation of these results. These roofs are highlighted inside a red rectangle in all the images. The following can be observed from roof extraction results shown in Figure 6.4 (a) to (c):

- Visually, using a high-resolution satellite base map, it is investigated in each of the images that, inside red rectangle a metal roof is present, which is detected in NBAI and MBI while partially rather not visible in case of IBI.
- The quantitative analysis of different rooftops inside ROI depicts that, out of a total of 78 truth pixels of roofs, NBAI and MBI detect 71 and 59 pixels correctly while IBI is able to detect only 45 pixels of those roof surfaces, respectively. Therefore, NBAI appears to have better detection result in comparison to MBI and IBI.
- The roof surfaces contain the maximum probability of detection with a very small amount of false alarms in comparison to the extraction of road surfaces. It may be due to more contrast of roof surfaces in comparison to other urban land cover classes. Further, road surfaces may have maximum chances of mixing with non-road surfaces but this problem may lessen in case of roof surfaces, as most of the roof surfaces show clustered behavior.
- The whole analysis of roof extraction results in hyperspectral imagery found NBAI to be suitable for the extraction of roof surfaces. Since, NBAI utilizes SWIR2 (1600-2490 nm), SWIR1 (1500-1790 nm) and visible (450-690 nm) bands

for its formulation, therefore, these bands can prove to be effective for detection of roof surfaces in AVIRIS-NG imagery.

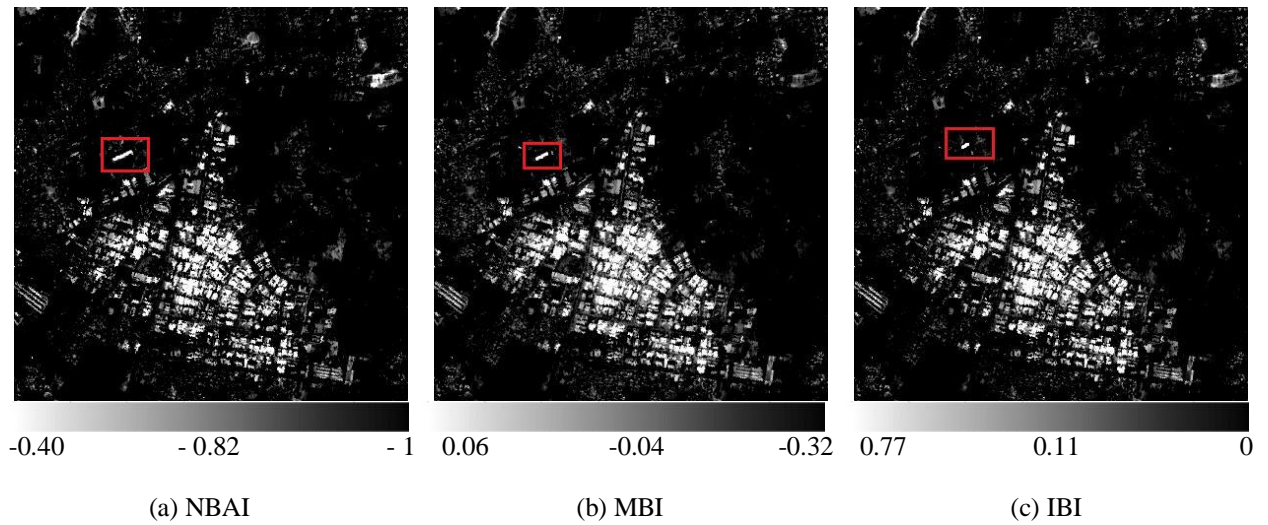


Figure 6.4 Roof extraction using different built-up indices. The range of indices of grayscale image is shown along the x -axis

6.4.5 Accuracy assessment

This study has been considered an overall accuracy of more than 80% and kappa index (normalized between 0 to 100 %) greater than 70% for the spectral index to be efficient in the extraction of built-up surfaces (Level-1 and 2). The built-up extraction results of various indices shown in Figure 6.2, 6.3, and 6.4, are validated using a high-resolution satellite imagery base map of ArcGIS 10.4 along with 2297 known ground locations of different urban samples, out of which 1032 belong to built-up surfaces and 1265 to non-built-up surfaces. Further, out of 1032 samples of built-up surfaces, 500 are associated with roads while the remaining 532 are related to roofs. The overall accuracy and kappa index have been calculated by considering the built-up surfaces (Level-1 and 2) as target and rest of the non-target classes as background. The accuracy measures of various built-up indices used for detection of built-up surfaces at first level followed by roads and roofs in the second level are

given in Table 6.4.

Table 6.4 Accuracy assessment of built-up indices (Level-1 and 2)

Spectral Index	Overall Accuracy	Kappa Index
	(%)	(%)
Built-up extraction indices (Level-1)		
BSI	93.89	87.66
NBI	90.11	82.14
BAEI	85.15	76.44
BRBA	75.24	66.65
VIBI	69.40	60.35
Road extraction indices (Level-2)		
REI	94.40	83.59
BUI	76.20	65.25
NDBI	65.40	56.29
Roof extraction indices (Level-2)		
NBAI	95.00	89.32
MBI	75.74	64.25
IBI	56.34	46.39

The following can be observed from Table 6.4:

- The BSI, NBI, and BAEI give an overall accuracy of 93.89 %, 90.11 %, and 85.15 % with a kappa index of 87.66 %, 82.14 %, and 76.44 %, respectively. Further, BRBA and VIBI provide an overall accuracy of 75.24 % and 69.40 % with a kappa index of 66.65 % and 60.35 %. Therefore, BSI, NBI, and BAEI appear to be the suitable indices for the extraction of built-up surfaces in hyperspectral imagery.

- The REI, BUI, and NDBI provide an overall accuracy of 94.40 %, 76.20 %, and 65.40 % with a kappa index of 83.59 %, 65.25 %, and 56.29 %, respectively. Thus, REI can be suitable for the detection of road surfaces in AVIRIS-NG imagery.
- The roof extraction indices i.e. NBAI, MBI, and IBI offer an overall accuracy of 95.00 %, 75.74 %, and 56.34 % with a kappa index of 89.32 %, 64.25 %, and 46.39 %, respectively. Hence, NBAI appears to provide better roof extraction result in comparison to other indices.

6.4.6 Separability analysis between spectrally mixed urban land cover classes

The bare soil is the major background factor that may affect the performance of built-up indices due to spectral similarity with built-up surfaces [3] [59] [67] [133]. Therefore, in this study, the assessment of the separability between bare soil and built-up surfaces (Level-1 and 2) is performed using the histogram representation of different land cover classes followed by various statistical measures. Since road and roof surfaces also show poor separability due to similarity in the materials used in the construction of these surfaces, thus, in Level-2 the separability analysis is also carried out between these two classes.

6.4.6.1 Separability analysis using histogram representation (Level-1 and 2)

Figure 6.5 (a) to (e) depict the histogram representation of different urban land cover classes such as road, roof, vegetation, and soil in built-up extraction indices i.e. BSI, BAEI, BRBA, NBI, and VIBI. These histograms have been generated using 500,

532, 652, and 613 known samples of roads, roofs, vegetation, and soil, respectively.

Further, in these histograms, the plot inside the circle represents the histogram of the desired target i.e. built-up surface while other plots are associated with background.

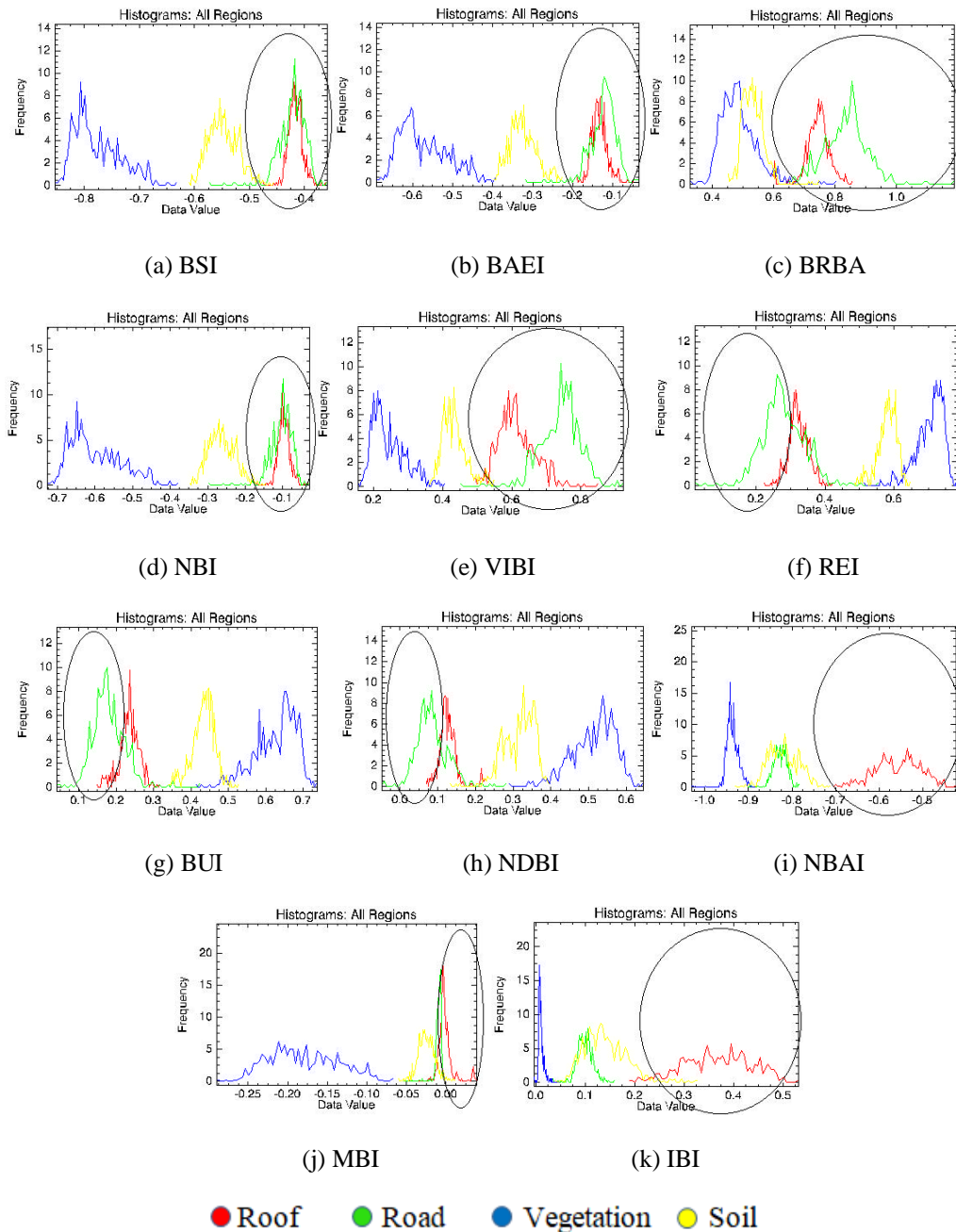


Figure 6.5 Histogram representation of different urban classes in various built-up indices used for (a-e) built-up extraction (Level-1) (f-h) road extraction (Level-2) (i-k) roof extraction (Level-2)

The following can be observed from histogram plots shown in Figure 6.5 (a) to (e).

- The vegetation and soil can easily be separated from urban built-up surfaces in all the aforesaid indices for built-up extraction while a slight overlap is observed between built-up and non-built-up surfaces.
- The BRBA and VIBI may also be used for the extraction of road surfaces along with built-up surfaces by proper selection of threshold while there appears no scope of separation of road and roof surfaces in BSI, NBI, and BAEI due to large overlap.
- It is further observed that, roof surfaces can also be extracted in BRBA and VIBI by using a multi-thresholding approach.

Figure 6.5 (f) to (h) describe the histogram plot of different urban land cover classes in road extraction indices i.e. REI, BUI, and NDBI. As mentioned earlier, these histograms have been produced using various known samples of different urban surfaces. In such histograms, the plot inside the circle corresponds to the histogram of road surfaces while other plots are associated with background i.e. roof, vegetation, and soil. The following observations are derived from Figure 6.5 (f) to (h):

- The non-built-up surfaces such as vegetation and soil can easily be separated from roads in all the road extraction indices with some overlapping between road and roof surfaces. This overlapping may be due to the similarity in the materials used for the construction of these man-made surfaces.
- All the aforementioned indices for road detection may also be utilized for the extraction of built-up surfaces (Level-1) by selection of a suitable threshold.

Figure 6.5 (i) to (k) show the histogram representation of different urban land cover classes in roof extraction indices i.e. NBAI, MBI, and IBI. In these histograms,

the plot inside the circle represents the histogram of roof surfaces while other plots are related to non-roof background. The following can be investigated from Figure 6.5 (i) to (k):

- The background classes i.e. road, vegetation, and soil can easily be separated from the roof in all the indices while NBAI appears to be the best in terms of separation with other urban land cover classes.
- In the case of MBI, roof surfaces are confused with road and soil both while in IBI, roofs are confused with soil. Therefore, MBI and IBI may worsen the detection by including more false alarms.

6.4.6.2 Separability analysis using statistical measures (Level-1 and 2)

Table 6.5 depicts the statistics of separability measures between urban built-up surfaces (Level-1 and 2) and bare soil. Since SDI values of all the built-up indices are larger than one, hence, it is difficult to ascertain the better of indices in case of AVIRIS-NG imagery. Therefore, two other approaches i.e. J-M distance and T-D along with SDI [122] [124] [125], are used for separability analysis between spectrally mixed urban land cover classes. The statistical results of these three approaches for different built-up indices (Level-1 and 2) are tabulated in Table 6.5. The following can be observed from these results:

- The examination of separability of soil with built-up surfaces using the T-D approach investigates that BSI, BAEI, NBAI, and MBI have a high degree of separation with T-D values greater than 1900. Further, NBI, BRBA, VIBI, REI, BUI, NDBI, and IBI depict moderate separability with T-D values between 1700 to 1900.

- The J-M distance criteria suggests that in all the built-up indices, built-up surfaces are separated very well from the soil. Therefore, based on J-M distance results, if we assume J-M distance to be greater than 1.7 for best separation while 1.4 to 1.7 for moderate and less than 1.4 for poor separation with more overlap, then it is observed that BSI, BAEI, REI, NBAI, and MBI are suitable in terms of separation between built-up surfaces and soil while rest of the indices in Level-1 and 2 depict moderate separation.
- The assessment of separability using SDI describes that in all the indices, built-up surfaces are effectively separated from the bare soil. So, if we assume SDI to be greater than 2.0 for best separation while 1.0 to 2.0 for moderate separation with a slight overlap followed by less than 1.0 for worst separation with more overlap. Then, it is observed that BSI, NBI, BAEI, BRBA, NBAI, MBI and IBI can prove to be effective to separate built-up surfaces from the bare soil while rest of the indices in Level-1 and 2 i.e. VIBI, REI, BUI, and NDBI represent moderate separation with a slight overlap between built-up surfaces and bare soil.
- All the indices used for roof extraction differentiate built-up surfaces and soil very effectively. It may be due to the high contrast of roof surfaces in comparison to other urban land cover classes. Also, the chances of spatial mixing of roofs with other backgrounds may be less due to their clustered behavior.

Further, Table 6.5 also represents the outcome of separability analysis between road and roof surfaces (Level-2) using similar statistical measures. The following can be observed:

- Since, the T-D values of BUI, NBAI, and MBI are higher than 1900, thus these indices result in the best separation between road and roof surfaces while

rest of the indices in Level-2 depict moderate separation with T-D values between 1700 to 1900.

- If the analysis is carried out using J-M distance criteria with the previously mentioned range, then NBAI, MBI, and IBI show the better separation between road and roof surfaces with values greater than 1.7 while the rest of the indices depict moderate separation with values in the range between 1.4 to 1.7.
- When the separability analysis is performed using SDI with the same range of values mentioned above, then it is observed that indices used for roof extraction i.e. NBAI, MBI and IBI represent a better separation of road and roof surfaces with values greater than 2.0 while road detection indices such as REI, BUI, and NDBI denote moderate separation with SDI values between 1.0 and 2.0.
- The lower separability of road extraction indices may be due to the similarity in the materials such as bitumen, asphalt, and concrete, which have been used for the construction of road and roof surfaces both.

Table 6.5 Separability measures between built-up surfaces and soil, and road and roof surfaces

Separability between Spectral Index	Built-up surfaces and soil → distance			Road and roof surfaces distance		
	SDI	J-M	T-D	SDI	J-M	T-D
Built-up extraction indices (Level-1)						
BSI	6.161	1.880	1920	-----		
NBI	3.095	1.680	1833	-----		
BAEI	4.881	1.780	1905	-----		
BRBA	2.644	1.605	1855	-----		
VIBI	1.119	1.402	1782	-----		
Road extraction indices (Level-2)						

REI	1.769	1.928	1805	1.605	1.560	1873
BUI	1.990	1.521	1852	1.823	1.652	1908
NDBI	1.451	1.435	1813	1.516	1.425	1682
Roof extraction indices (Level-2)						
NBAI	5.794	1.943	1925	3.568	1.835	1935
MBI	5.566	1.889	1902	2.951	1.752	1912
IBI	3.198	1.689	1890	2.365	1.725	1886

6.5 Discussion

This study extends the applicability of different existing built-up indices, which have been utilized for the detection of built-up surfaces in multispectral imagery, to the narrow band AVIRIS-NG hyperspectral imagery. Further, as part of the image data collection campaign, field data of different built-up and non-built-up surfaces have also been simultaneously collected. In field data collection, the main focus was on the collection of spectral signatures of different types of roads, roofs, pavements, parking lots, vegetation, and soil. These samples of different land cover classes have been utilized for validation of extraction results of built-up surfaces (Level-1 and 2) along with high-resolution imagery. The most of the major and minor roads, pavements and parking lots in the study region were made up of bitumen and concrete while major and minor roof surfaces used concrete and bitumen as construction materials. In this study, highways, walkways, street roads, parking lots, and pavements have been considered under road surfaces (Level-2) while metallic and non-metallic roofs have been considered under roof surfaces (Level-2). Accordingly, the combination of road and roof surfaces have been taken under built-up surfaces (Level-1). Further, due to the heterogeneity of urban built-up and non-

built-up surfaces, this study has been considered mean spectral signatures of different urban land cover classes with some standard deviation for the analysis. Next, using ground and image data, extraction of built-up surfaces has been carried out in Level-1 while road and roof surfaces have been extracted in Level-2. It is observed that most of the built-up indices used for the multispectral dataset can also prove to be effective for hyperspectral data. In AVIRIS-NG imagery, these indices not only effectively extracted built-up surfaces but many of them are well suited for the extraction of road and roof surfaces by proper selection of significant bands and suitable thresholds. Various techniques for dimensionality reduction and significant band selection have been used, which include mutual information and divergence based approaches for dimensionality reduction while stepwise discriminant analysis for selection of significant bands. Next, Otsu's thresholding approach has been utilized for the optimization of various built-up indices. It has been found that visible (450-690 nm), NIR (730-1340 nm) and SWIR2 (1960-2490 nm) regions are most suitable for detection of built-up surfaces while visible (450-690 nm) and NIR (730-1340 nm) regions found to be most appropriate for extraction of road surfaces subsequently visible (450-690 nm), SWIR1 (1500-1790 nm) and SWIR2 (1960-2490 nm) for detection of roofs. The major problem of separation between built-up surfaces and bare soil can be eliminated by using hyperspectral imagery followed by a proper selection of significant wavelengths. The NBAI provides the best separability amongst bare soil and built-up surfaces in terms of T-D and J-M distance measures while BSI produces the best separation in terms of SDI. The fully separation of road and roof surfaces is still a challenge, it may be due to the within-class similarity in the built-up surfaces e.g. bitumen and concrete are the commonly used materials for construction of roads and roofs both in Indian regions. In all the

aforesaid separability measures, NBAI produces the best separation between roads and roofs. Further, all the indices used for road detection may also be used for extraction of built-up surfaces by using multi-thresholding approach but all the roof extraction indices may not be utilized for extraction of other urban built-up classes. Moreover, some of the indices used for extraction of built-up surfaces may be used for the extraction of road and roof surfaces as well by proper selection of thresholds.

6.6 Summary

In this study, different multispectral built-up indices were taken from previous studies and utilized them for detection of built-up surfaces in first level followed by road and roof surfaces in the second level by identification of most significant wavelength bands in AVIRIS-NG hyperspectral imagery. Further, separability analysis between spectrally mixed urban land cover classes (Level-1 and 2) was performed using various plots and statistical measures. The AVIRIS-NG imagery and ground spectral data of Udaipur, Rajasthan, India, were used for the precise detection of urban built-up surfaces (Level-1) and its subclasses (Level-2). As part of preprocessing, different bad bands were removed from the imagery followed by masking of water pixels using unsupervised classification, and finally, dimensionality reduction using mutual information and divergence based algorithms. Further, the stepwise discriminant analysis was utilized for the identification of significant wavelengths using image and ground data. The BSI, NBI, BAEI, BRBA, and VIBI were used for the extraction of urban built-up surfaces while REI, BUI, and NDBI were implemented for the detection of road surfaces followed by NBAI, MBI, and IBI for extraction of roof surfaces. The validation of extraction results was carried out using a high-resolution satellite imagery base map and 2297 ground

samples collected from different locations, out of which 1032 belong to built-up surfaces and 1265 to non-built-up surfaces. Further, the separability analysis between built-up surfaces and bare soil, and roads and roofs was performed using histogram representation and multiple statistical measures, which are SDI, J-M distance, and T-D. The overall results of the study illustrate that BSI, NBI, and BAEI can prove to be the most suitable indices for extraction of urban built-up surfaces. Further, REI can be appropriate for detection of the roads followed by NBAI for the roofs. It can also be concluded that hyperspectral data is a rich source of spectral information, which is capable of reducing data redundancy between original bands, thereby enhancing the inter-class separability of built-up surfaces and soil subsequently intra-class separability between road and roof surfaces.

Chapter 7

Extraction of Impervious Surfaces using Index based RGB and NIR Band Combinations

The recently developed high spatial and spectral resolution hyperspectral sensors are capable of extracting impervious or engineered surfaces with very high accuracy in comparison to coarse resolution sensors. Therefore, this study utilizes AVIRIS-NG hyperspectral data of Jodhpur, Rajasthan region of India for the analysis. Further, based on existing literature, various spectral bands such as Red-Green-Blue (RGB) and NIR are selected for generation of Normalized Difference Spectral Indices, which have been used for extraction of impervious or engineered surfaces.

The tasks of this study are:

- a) To create different index based combinations of RGB and NIR bands for extraction of impervious surfaces in AVIRIS-NG hyperspectral imagery.
- b) To analyze the separability between different land cover classes to further validate the extraction results of impervious surfaces.

7.1 Study area and dataset

The Jodhpur city in Rajasthan, India is selected as study area for the analysis. This city was selected for AVIRIS-NG data collection, jointly organized by SAC-ISRO and JPL-NASA in the second phase of the campaign. This study utilizes a spatial subset of AVIRIS-NG data with pixel dimension, spatial, and spectral resolution of (410 sample x 1732 lines), 3 m, and 5 nm, respectively, as shown in Figure 7.2 (a).

Further, taking advantage of Support Vector Machine (SVM) algorithm, SVM classified result has been used for accuracy assessment, in which total 1482 pixels were randomly selected from the image, wherein 864 belong to impervious / engineered while 618 to pervious / natural surfaces.

7.2 Spectral index based band combinations

The major objective of this study is to investigate the behavior of RGB and NIR bands for mapping of impervious surfaces in AVIRIS-NG imagery. As suggested from the existing spectral indices, already developed using visible and NIR bands of multispectral imageries for extraction of impervious or engineered surfaces, this study generates three spectral indices named as Impervious Surface Index (ISI). ISI is formulated using three combinations of RGB and NIR bands of AVIRIS-NG imagery, as shown in Equation 7.1, 7.2, and 7.3.

$$\text{Impervious Surface Index}_1 = \frac{(\text{Red} - \text{NIR})}{(\text{Red} + \text{NIR})} \quad (7.1)$$

$$\text{Impervious Surface Index}_2 = \frac{(\text{Green} - \text{NIR})}{(\text{Green} + \text{NIR})} \quad (7.2)$$

$$\text{Impervious Surface Index}_3 = \frac{(\text{Blue} - \text{NIR})}{(\text{Blue} + \text{NIR})} \quad (7.3)$$

7.3 Results and Discussion

7.3.1 Separability analysis between various land cover classes

Histogram representation of various major urban land cover classes such as vegetation, soil, road and roof along with plot of different impervious indices, are

shown in Figure 7.1, in which Figure 7.1 (a), (b), and (c) represent the plots associated with Red-NIR, Green-NIR and Blue-NIR band combinations, respectively. It is observed that the vegetation can be very easily segregated from all the classes in all the combinations, while only few samples of soil are overlapped with road and roof surfaces in Green-NIR and moderate in Blue-NIR. Further, more overlapping between impervious surfaces and soil is observed in Red-NIR. Thresholding has been carried out using Otsu's thresholding approach and the results of the thresholding are shown in the bottom part of Figure 7.1 (a), (b), and (c). In bimodal histogram plots, Otsu's approach work well, therefore Green-NIR and Blue-NIR appear to be perfect in terms of separation of different land cover classes. Table 7.1 depicts the statistical analysis of aforesaid band combinations. It is observed that on moving from Red-NIR to Blue-NIR, mean shifts towards negative value and therefore threshold is more negative for Blue-NIR and less for Red-NIR.

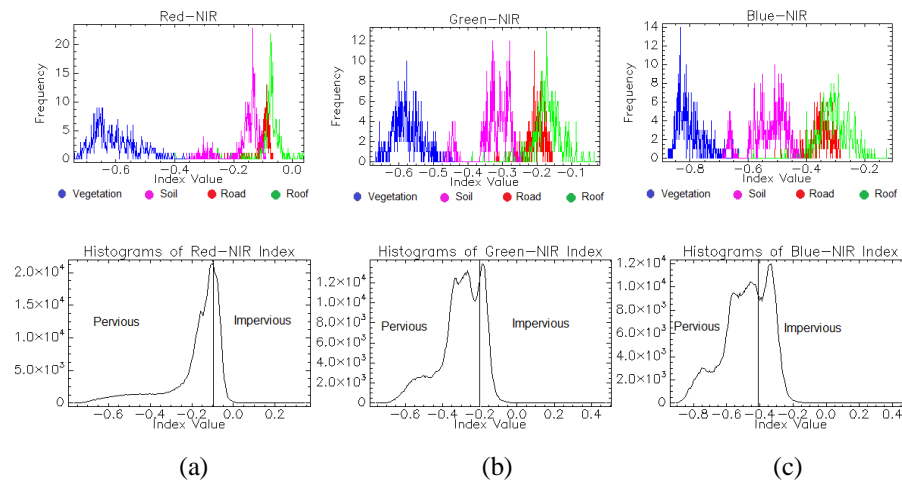


Figure 7.1 Histogram plot of various urban classes and ISIs (a) Red-NIR (b) Green-NIR (c) Blue-NIR

Table 7.1 Statistical analysis of various ISIs

Band	Min	Max	Mean	Standard	Threshold
Combination	Deviation				
Red-NIR	-0.764349	0.342346	-0.179779	0.138265	-0.09

Green-NIR	-0.758927	0.475223	-0.298476	0.116040	-0.24
Blue-NIR	-0.905113	0.483855	-0.474860	0.138700	-0.41

7.3.2 Extraction of impervious surfaces

Figure 7.2 represents the extraction results of impervious surfaces in AVIRIS-NG hyperspectral imagery, wherein Figure 7.2 (a) depicts 380 bands original AVIRIS-NG imagery while Figure 7.2 (b) is the classified results of SVM classifier, which has been used for the accuracy assessment and validation of the extraction results. Figure 7.2 (c), (d) and (e) are the extraction results of index based Red-NIR, Green-NIR and Blue-NIR band combinations, respectively. It appears that, there is a maximum correlation between SVM and Green-NIR with moderate in Blue-NIR and least correlation is observed between SVM and Red-NIR band combinations. Further, the detection rate of impervious surfaces is larger in case of Green-NIR while it is least for Red-NIR. Therefore, spectral index based on Green-NIR band combination appears to be suitable for extraction of impervious surfaces in AVIRIS-NG imagery.

7.3.3 Accuracy assessment

Table 7.2 represents the accuracy assessment of the extraction results of impervious surfaces in hyperspectral imagery. As discussed earlier, random pixel locations of 864 impervious and 618 pervious surfaces are used for the accuracy assessment and validation. It is observed that maximum Overall Accuracy (OA) of 95.20 % is obtained in case of Green-NIR while moderate as 90.28 % for Blue-NIR. Further, due to confusion with soil samples, least accuracy is obtained in case of Red-NIR.

Therefore, Green-NIR band combination outperforms the other two.

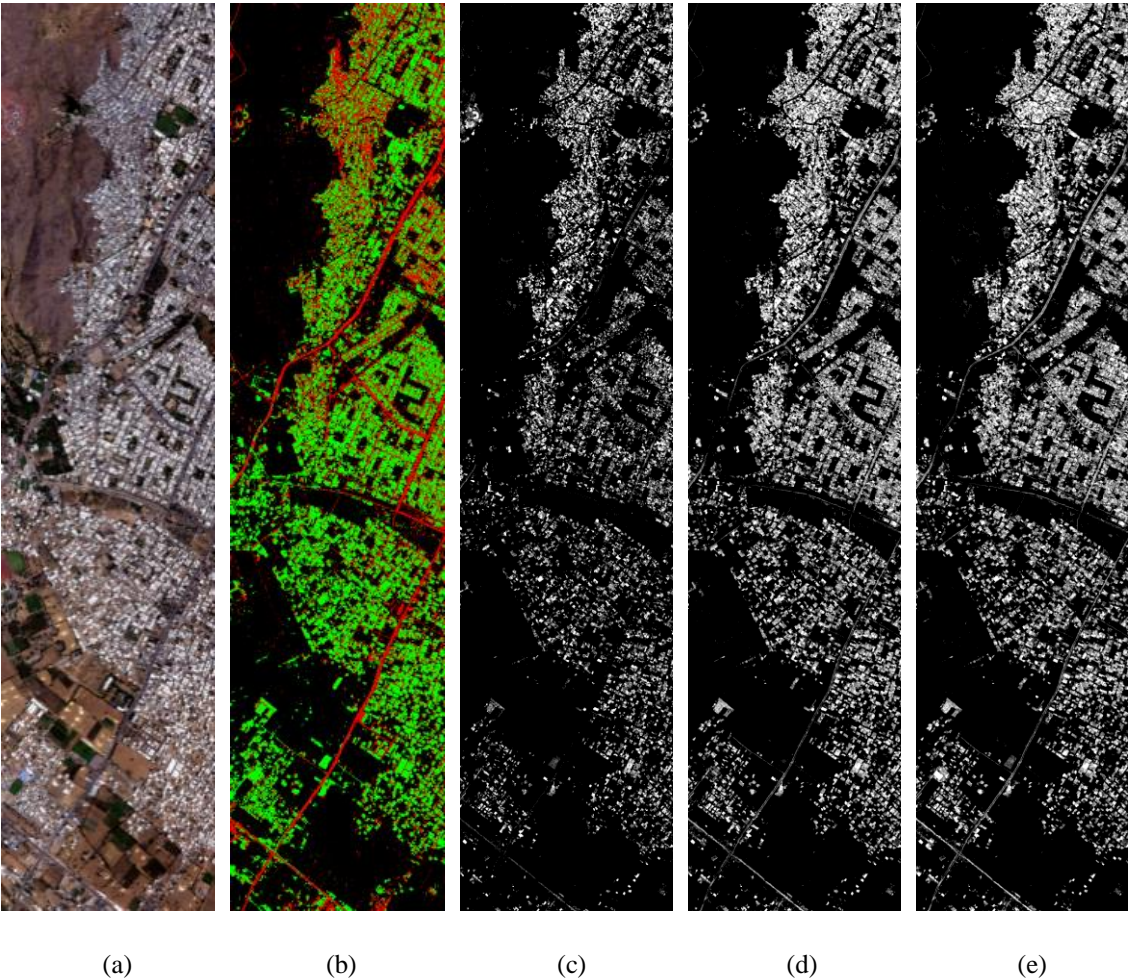


Figure 7.2 Extraction results of impervious surfaces in AVIRIS-NG imagery (a) Original imagery (b) SVM classified results for accuracy assessment, in which red and green pixels are impervious surfaces and black pixels are related to pervious surfaces (c) Red-NIR (d) Green-NIR (e) Blue-NIR

Table 7.2 Accuracy assessment of extraction results of impervious surfaces

Band	Class	Impervious	Pervious	Producer	OA (%)	Kappa
Combination				Accuracy (%)		Index (%)
Red-NIR	Impervious	708	62	91.94	85.29	70.40
	Pervious	156	556	78.09		
	User Accuracy	81.94	89.96			
	(%)					
Green-NIR		Impervious	Pervious			

	Impervious	826	33	96.15	95.20	90.20
	Pervious	38	585	93.90		
	User Accuracy	95.60	94.60			
	(%)					
Blue-NIR	Impervious		Pervious			
	Impervious	776	56	93.26	90.28	80.20
	Pervious	88	562	86.46		
	User Accuracy	89.81	90.93			
	(%)					

7.4 Summary

This study formulated three spectral indices based on existing approaches using RGB and NIR band combinations in AVIRIS-NG hyperspectral imagery. The three indices named as ISI_1 , ISI_2 , ISI_3 , have been applied in AVIRIS-NG hyperspectral imagery for extraction of impervious surfaces. Further, random 1482 labeled pixels selected from SVM classified image, is used for accuracy assessment and validation of the extraction results. A separability analysis between major urban land cover classes has been carried out to further validate the results of impervious extraction. It is observed that, index based Green-NIR band combination generates better inter-class separability with an OA of 95.20 %, Blue-NIR produces moderate OA as 90.28 % while least OA as 85.29 % is obtained for Red-NIR.

Chapter 8

Extraction and Estimation of Built-up surfaces and Its Categories using Feature Combination based Approach

The high dimensionality of hyperspectral data increases the system and time complexity for the image analysis [5] [22] [82] [83]. In this chapter, a new method is proposed, in which different combinations of feature bands have been utilized for extraction of built-up surfaces, sub-surfaces and materials in different levels (Level-1, 2 and 3) using high resolution AVIRIS-NG hyperspectral imagery of Jodhpur, Rajasthan region of India. The features identified in this study are based on spectral indices, major principal components, and fractional abundances, in which the first combination is developed using spectral indices and fractional abundances while second is made using spectral indices and major principal components and finally third using combination of all the aforesaid features.

The tasks of this study are:

- a) To identify different significant features for extraction of built-up surfaces, sub-surfaces, and materials.
- b) To extract built-up surfaces (Level-1), sub-surfaces (Level-2), and materials (Level-3) using combination of different features in AVIRIS-NG imagery.

8.1 Study area and Data

Jodhpur city is the second largest city in the Rajasthan state of India, and officially

the second largest metropolitan city of the state. It is located at latitude of 26.28° North and longitude of 73.02° East and is located in the mid of the Thar Desert of western Rajasthan, which is about 250 km from the Pakistan border. Its general geography is characterized by the hills located in the North and North-west region. The mid of the city is covered with different types and patterns of urban built-up surfaces and materials.

AVIRIS-NG Level-2 (atmospherically corrected reflectance) hyperspectral data captured on 31st March 2018, consisting of 425 bands of aforesaid region (UTM zone 43N) is used to extract different urban built-up surfaces and to estimate the proportion of those surfaces. Further, in the preprocessing stage, bands affected by atmospheric gases, water vapor, detectors overlap and poor data quality have been removed. A total of 14 wavelength bands (1343-1418 nm) in NIR region as well as 31 bands (1793-1954 nm) in the SWIR region are investigated as bad bands, which after removal results in 380 bands hyperspectral imagery. The spatial and spectral resolution of image data is 3 m and 5 nm, respectively. In this study an image subset of size 400 samples x 400 lines is used for the analysis, which is shown in Figure 8.1 (a). The ground data of different built-up and non-built-up surfaces have been simultaneously collected during the AVIRIS-NG phase-2 data collection campaign, using Spectral Evolution spectroradiometer over the wavelength range of 350 to 2500 nm. Spectroradiometer is having spectral resolution of 1 nm with 2151 channels. Ground spectral signatures of 518 samples of different built-up and non-built-up surfaces have been collected using both contact probe and gun in cloud free atmospheric condition between 11 am to 3 pm. Also, the white reference is recorded after capturing of each 4 to 5 spectral signatures. Some of the field photographs of data collection campaign are shown in Figure 8.1 (c) as well as mean spectral

signatures of various land cover classes mentioned in Table 8.1, are shown in Figure 8.1 (d). In the field spectra, bands in the wavelength range 1846 to 1956 nm affected by noise have been removed. The field spectral signatures of different land cover classes have been utilized for extraction of spectral index and fractional abundance based features from the imagery. Further, the re-sampling of ground spectra has been carried out with respect to 380 bands image using nearest neighbor algorithm. Next, as suggested by V-I-S model, water has been masked from the imagery using Normalized Difference Water Index (NDWI) approach [140] based on spectral index. The water mask band is shown in Figure 8.1 (b). The accuracy assessment and validation of results has been carried out using known location of 518 samples as well as high resolution satellite imagery base map of ArcGIS 10.4 along with ward map of the study region. Table 8.1 depicts the total number of samples taken in each category of built-up and non-built-up surfaces for accuracy assessment and validation of the results.

Table 8.1 Number of known samples of different classes

Class	Concrete Roof	Metallic Roof	Bitumen Road	Concrete Pavement	Vegetation	Soil
No. of known Samples	118	67	76	71	61	125



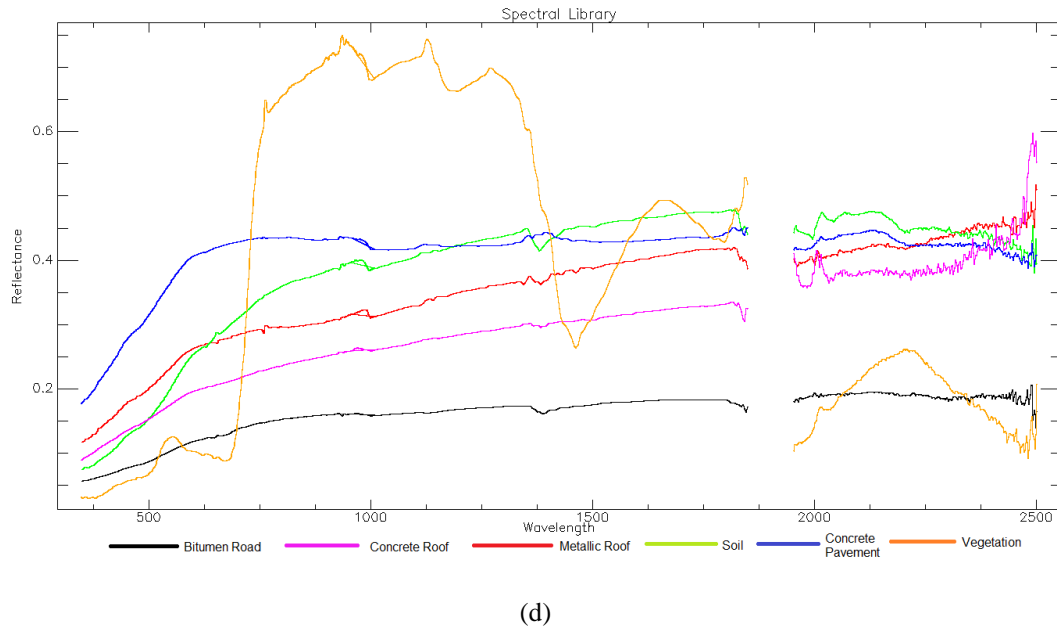


Figure 8.1 (a) Hyperspectral image of the study area of size 400 samples x 400 lines (b) Water mask band (c) Field photographs of ground data collection campaign (d) Mean spectral signatures of different built-up and non-built-up classes

8.2 Experimental feature band combination

8.2.1 Principal Components

Principal Component (PC) transformation is found to be an efficient tool in feature extraction and dimensionality reduction as the number of features are drastically reduced when compared with the original bands [84] [85]. This method is able to predict whether the target land cover class is characterized by bright or dark pixels in the relevant PC image according to the magnitude and sign of the eigenvectors. As an approach that transforms the original high dimensional remotely sensed imagery into a substantially smaller and easier to interpret data set with un-correlated variables, PCA can prove to be an effective technique for reducing the dimensionality of hyperspectral data sets having so many spectral bands. In most of the literature, major principal components have been selected as features for

extraction of various land cover classes [141] [142] [143] [144].

8.2.2 Spectral Indices

To map built-up surfaces, some spectral indices have been developed in recent past and applied in different remote sensing imageries [62] [64] [75] [86] [145] [146]. The IBI is proposed for fast extraction of built-up surfaces in satellite imagery, which has been formulated using three thematic index derived bands i.e. SAVI, MNDWI and NDBI [86]. NBAI is developed for mapping built-up surfaces in urban areas through identifying the significantly different spectral profiles between built-up and other background classes [62]. This index utilized Landsat-TM imagery for mapping of built-up surfaces. Further, REI was proposed to automatically extract asphalt road surfaces using World View (WV)-2 imagery, which has high spatial resolution [67]. To determine the significant bands for WV-2, in-situ spectral data collected using a field spectroradiometer were also used. SAVI was developed to generate a global model for monitoring soil and vegetation from remote sensing imagery [76]. Further, MNDWI has been proposed to extract water bodies from satellite imageries, which utilized Green and NIR band of multispectral imagery [77]. In some of the studies MNDWI has also been used for extraction of built-up surfaces. Since, all the aforesaid indices are specifically designed for extraction of a particular land cover class with low separability between target and background. Therefore, these indices may be utilized as features for extraction of various built-up surfaces and its sub-categories in AVIRIS-NG imagery.

8.2.3 Fractional Abundances

The linear spectral unmixing has proved to be a standard algorithm for Spectral

Mixture Analysis (SMA) [104] [147] [148] [149], that infers a set of pure spectral signatures, called as endmembers, and the fractions of these endmembers, called as fractional abundances, in each pixel of the scene. The SMA model assumes that the spectral signature of a particular pixel can be expressed in the form of a linear combination of endmembers, weighted by their respective abundances [150] [151]. It is because each observed spectral signal is the result of an actual mixing process, which assumes that the fractional abundances satisfy two constraints i.e. they should be non-negative as well as the sum of abundances for a given pixel should be unity. Although the linear SMA model has practical advantages like ease of implementation and flexibility in various applications but the non-linear mixture always creates problem [152] [153]. Therefore, the fractional abundances of different urban land cover classes and materials may be selected as features for the analysis.

Finally, different images have been created using various combinations of aforesaid features, as suggested from the previous literature [72] [85] [145] [149] [154] [155] [156] [157] [158] [159] [160] [161]. The first image combines spectral indices with fractional abundances while second image contains spectral indices along with PCs, and the last image combines all the features i.e. spectral indices, fractional abundances and PCs. The brief detail of all the aforesaid features is given in Table 8.2, while Table 8.3 depicts about different levels of urban targets such as built-up surfaces (Level-1), sub-surfaces (Level-2) and materials (Level-3), which have been extracted from AVIRIS-NG hyperspectral imagery. Further, rest of the non-target classes have been considered as background.

Table 8.2 Different significant features used for extraction of built-up surfaces, sub-surfaces and materials

Feature Class	Details	Expression / Remark
Spectral Indices	Index Based built-up Index (IBI) [86]	$IBI = \left[\frac{NDBI - (SAVI + MNDWI) / 2}{NDBI + (SAVI + MNDWI) / 2} \right]$
	Road Extraction Index (REI) [67]	$REI = \left[\frac{B_{NIR} - B_{BLUE}}{B_{NIR} + B_{BLUE} * B_{NIR}} \right]$
	Normalized Built-up Area Index (NBAI) [62]	$NBAI = \left[\frac{B_{SWIR1} - \left(\frac{B_{SWIR2}}{B_{GREEN}} \right)}{B_{SWIR1} + \left(\frac{B_{SWIR2}}{B_{GREEN}} \right)} \right], B_{SWIR2} < B_{SWIR1}$
	Soil Adjusted Vegetation Index (SAVI) [76]	$SAVI = \left[\frac{(B_{NIR} - B_{RED})(1 + L)}{(B_{NIR} + B_{RED} + L)} \right]$
	Modified Normalized Difference Water Index (MNDWI) [77]	$MNDWI = \left[\frac{(B_{GREEN} - B_{SWIR})}{(B_{GREEN} + B_{SWIR})} \right]$
Principal Components		Bright built-up surfaces have a high albedo in
	PC-1	PC-1 while PC-2 is negatively correlated with
	PC-2	PC-1. PC-3 is the intermediate stage of PC-1 and PC-2.
Fractional Abundances	Abundance estimation has been carried out for following classes and sub-classes:	According to LSMA: Reflectance R measured at pixel i can be represented as a linear summation of K endmembers weighted by the fraction a_{ni} of each endmember within the pixel i . For a wavelength λ , it is given as,
	• Bitumen road	
	• Concrete pavement	
	• Concrete roof	
	• Metallic roof	
	• Vegetation	
	• Soil	
		Where $e_{i\lambda}$ is the residual, which describes the unmodeled portion of reflectance R . Modeled fractions are usually constrained by the

following equations,

$$\sum_{n=1}^K a_{ni} = 1 \quad \text{and} \quad a_{ni} > 0$$

Table 8.3 Different levels of extraction of built-up surfaces

Level -1	Level -2	Level -3
	Road Surfaces	Bitumen
Built-up Surfaces		Concrete Pavement
	Roof Surfaces	Concrete
		Metallic Roof

8.3 Support Vector Machine

In recent years, kernel based methods, such as Support Vector Machine (SVM) particularly, has become more and more popular for target detection and classification in remotely sensed imagery [162] [163] [164] [165] [166] [167]. SVM is an advanced and extensively used target detection as well as a regression approach proposed by Vapnik and his group at Bell Laboratories in 1990s. As a representative kernel based approach, SVM relies on the definition of a distance measure between data points in a proper sample space. Further, SVM does not only minimize the cost function but also controls the intricacy of the target detection function. This property improves the SVM's strength to noises in training samples, thus, target detection based on SVM could be more precise than the other commonly used methods such as maximum likelihood, decision tree and neural network-based algorithms. SVM is a nonlinear model and the nonlinear mapping of SVM is achieved by different kernel

functions. As explained in Table 8.1, a total of 518 samples or pixels of different built up and non-built-up surfaces have been used as truth pixels, these pixels are divided into the ratio of 65:35 for training and testing of SVM model to avoid overfitting. So, total 337 pixels are used for training and remaining 181 pixels have been utilized for testing. Next, each pixel is characterized by 11 element feature vector for combination of spectral indices and fractional abundances, 8 element feature vector for PCs and spectral indices as well as 14 element feature vector for combination of all the features. It is evident from the literature that SVM technique is a two class problem, thus, this study has been utilized SVM approach as target detection instead of classification. Further, as this study deals with 7 different classes (Level- 1 to 3), as tabulated in Table 8.3, therefore, each SVM consist of 7 two-class classifier. The SVM models have been created by selecting various kernels such as Linear, Polynomial, Gaussian Radial Basis Function (GRBF) and Sigmoid [168] [169]. The parameters for these models have been selected on the basis of existing literature based on SVM target detection and classification [162] [163] [170] [171] [172] [173] [174], these parameters are listed in Table 8.4. Further, after execution of each model in each of the 7 two-class classifier for all the aforesaid feature band combinations, the maximum average training accuracy of built-up target detection is obtained in case GRBF, as shown in Table 8.4. Therefore, in view of aforesaid analysis, the extraction of target in this study has been carried out using SVM by selecting GRBF as kernel function with different parameters listed in Table 8.4.

Table 8.4 Parameters of SVM kernel

Kernel	Parameter	Value	Average Training Accuracy
Linear	Penalty	100	78.69
Polynomial	Degree of Kernel	2	80.52
	Bias in Kernel	1.0	
	Gamma in Kernel	0.03	
	Penalty parameter	100	
GRBF	Gamma in Kernel	0.03	86.75
	Penalty parameter	100	
Sigmoid	Bias in Kernel	1.0	82.36
	Gamma in Kernel	0.03	
	Penalty parameter	100	

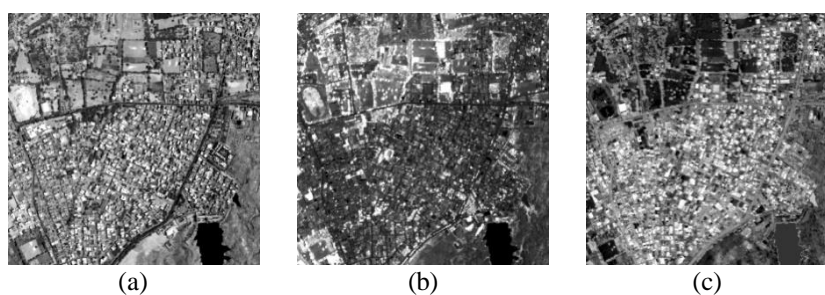
8.4 Results and Discussion

8.4.1 Features identified for extraction of urban built-up surfaces and materials

Table 8.5 depicts the Eigen values along with percentage variance of different principal components i.e. from PC1 to PC5, out of which three major components with maximum Eigen values are selected for the analysis, as these three PCs also accounted for 99.42 % of total variance. The rest of the PCs have been discarded. Further, Figure 8.2 shows that, the PC1 can be used as a feature band for high-albedo materials while PC2 can be utilized for low-albedo materials and the properties of PC3 lie between PC1 and PC2. Moreover, the correlation between PC1, PC2 and PC3 is also less. Therefore, these three components are found to be suitable to use as feature bands for extraction of built-up surfaces and materials.

Table 8.5 Eigen values and percentage variance of PCs

Principal Components	PC1	PC2	PC3	PC4	PC5
Eigen Values	2.2185	0.3584	0.0587	0.0180	0.0032
Percentage Variance	89.76	6.68	2.98	0.34	0.18

**Figure 8.2** Major principal components having maximum eigen values and variance (a) PC1 (b) PC2 (c) PC3

Further, in this study IBI, REI, NBAI, SAVI and MNDWI have been utilized with most appropriate band combination in AVIRIS-NG hyperspectral imagery. The most significant bands in respective regions have been identified using histogram plot of different land cover classes mentioned in Table 8.1 along with stepwise discriminant analysis using mean spectral signatures of those land covers [175] [176] [177]. These band combinations with respective wavelengths are given in Table 8.6, while the outcomes of respective indices are shown in Figure 8.3.

Table 8.6 Appropriate band combinations for different spectral indices

Spectral Index	IBI	REI	NBAI	SAVI	MNDWI
Band Combinations	862 (NIR), 663 (Red), 1613 (SWIR), 556 (Green)	987 (NIR), 461 (Blue)	1999 (SWIR1), 1543 (SWIR2), 556 (Green)	862 (NIR), 663 (Red)	1613 (SWIR), 556 (Green)

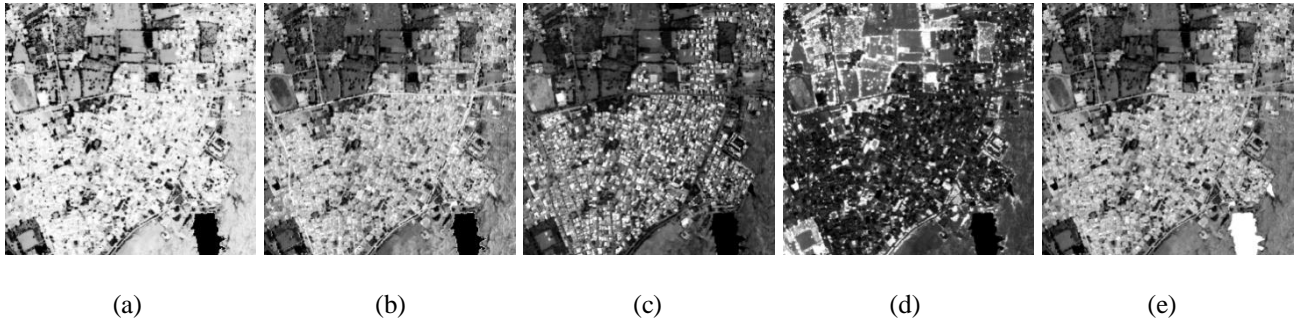
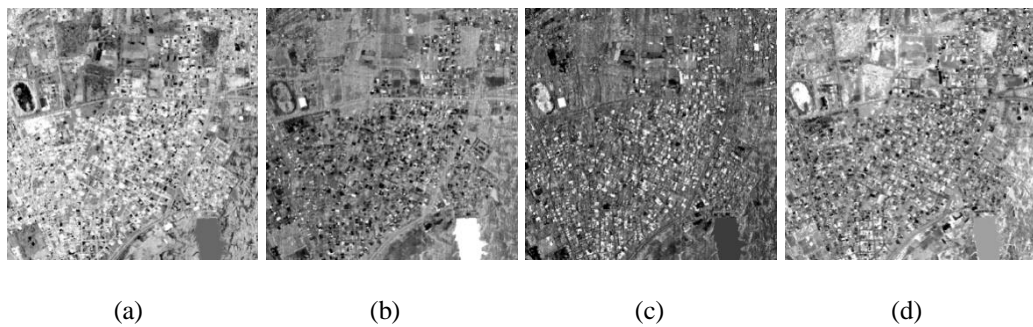


Figure 8.3 Thematic spectral index based features (a) IBI (b) REI (c) NBAI (d) SAVI (e) MNDWI

The study area is an amalgamation of different built-up and non-built-up classes with majority of bitumen road, concrete pavement, concrete roof and metallic roof as built-up surfaces while vegetation and soil as non-built-up classes. Therefore, endmembers of these built-up and non-built-up classes have been selected for spectral mixture analysis. Further, due to having heterogeneity of different urban land cover classes specifically for different built-up surfaces, mean spectral signatures of all the classes mentioned in Table 8.1, are used for extraction of fractional abundance based features. Figure 8.4 shows unmixing results of fractional abundances of different urban land cover classes and sub-classes.



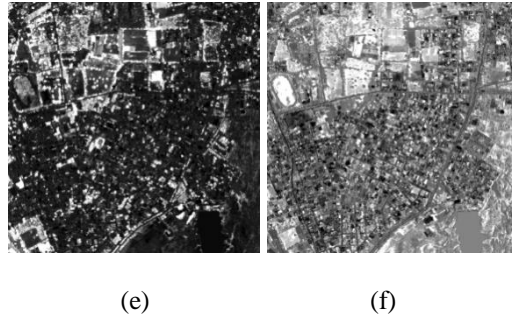


Figure 8.4 Fractional abundances of difference built-up and non-built-up classes (a) Bitumen road (b) Concrete pavement (c) Concrete roof (d) Metallic roof (e) Vegetation (f) Soil

The standard deviation of the all the previously discussed individual feature bands are used to assess the amount of information contained in each band. The higher standard deviation indicates higher information content within the band [178] [179] [180]. Table 8.7, and Figure 8.5 (b) and (c) depict the mean and standard deviation of different individual feature bands extracted from hyperspectral imagery. The statistical analysis has been carried out after scaling all the feature band values between 0 to 255. It is observed that spectral index based features provide maximum standard deviation due to belonging to a particular theme. Principal component based features generate moderate values of standard deviation while lesser is obtained in case of fractional abundance features. Standard deviation of SAVI and MNDWI are comparable with abundance maps of vegetation and soil, respectively.

The correlation coefficient is calculated to examine the correlations between various feature bands. A higher correlation coefficient depicts a higher overlapping of the values of two different feature bands and therefore greater similarity between the feature information in those two bands. To get more feature information, band combinations with smaller correlation coefficients must be selected. The correlation analysis between various feature bands shown in Table 8.8, and Figure 8.5 (a) suggests that, PC1 is least correlated with SAVI and fractional abundance map of

vegetation while maximum correlation is obtained in case of NBAI and abundance map of concrete roof. PC2 is having least correlation with MNDWI and REI while high correlation is obtained for SAVI and fractional abundance map of vegetation. Next, PC3 is less correlated with SAVI and fractional abundance of soil while highly correlated with REI, NBAI and fractional map of asphalt road. Further, IBI depicts less correlation with SAVI, PC2 and vegetation abundance map while highly correlated with REI and MNDWI. Further, REI shows least correlation with PC2, SAVI and vegetation abundance while high correlation is achieved in case of IBI and MNDWI. Similarly, NBAI shows least correlation with PC2, SAVI and abundance map of vegetation while maximum is obtained in case of PC1, MNDWI and IBI. SAVI is least correlated with all the features except PC2. Finally, MNDWI is having high correlation with PC3, IBI, REI, NBAI and abundance map of asphalt road. Moreover, fractional abundance of concrete roof is moderately correlated with all the other bands while less correlation is obtained with asphalt road. Abundance map of metal roof is moderately correlated with spectral index based features while more correlation is obtained with PCs and abundance based features. Further, asphalt road is less correlated with PC2, SAVI, fractional abundances of vegetation and soil while high with IBI and REI. Fractional abundance of concrete pavement is less correlated with PC1 and NBAI while highly correlated with abundances of concrete roof, metal roof and soil. Vegetation abundance is highly correlated with PC2 and SAVI while least with IBI, REI, NBAI and MNDWI. Further, abundance map of soil is least correlated with index based features whereas moderately correlated with rest of the feature bands.

Table 8.7 Mean and Standard deviation of different feature bands

	Principal Components					Spectral Indices		
	PC1	PC2	PC3	IBI	REI	NBAI	SAVI	MNDWI
Mean	120.61	95.15	110.18	179.67	134.88	92.60	85.91	126.75
Standard	58.68	57.63	58.24	69.61	64.48	60.06	65.30	61.14
Deviation								
	Fractional Abundances							
	Bitumen	Concrete	Concrete	Metallic	Vegetation	Soil		
	Road	Pavement	Roof	Roof				
Mean	159.51	124.46	104.93	149.91	68.43	117.40		
Standard	52.31	45.10	48.04	48.34	62.71	62.59		
Deviation								

Table 8.8 Correlation between different feature bands in which major principal components are B1- PC1, B2- PC2 and B3- PC3, spectral indices are B4- IBI, B5- REI, B6- NBAI, B7- SAVI and B8- MNDWI, and fractional abundances of different surfaces are B9- Concrete Roof, B10- Metal Roof, B11- Asphalt Road, B12- Concrete Pavement, B13- Vegetation and B14- Soil

Feature Bands	B1	B2	B3	B4	B5	B6	B7	B8	B9	B10	B11	B12	B13	B14
B1	1	0.58	0.62	0.83	0.70	0.89	0.39	0.70	0.81	0.70	0.76	0.57	0.49	0.76
B2	0.58	1	0.58	0.40	0.32	0.39	0.93	0.29	0.68	0.80	0.54	0.67	0.96	0.75
B3	0.62	0.58	1	0.75	0.81	0.78	0.41	0.81	0.71	0.73	0.77	0.64	0.56	0.47
B4	0.83	0.40	0.75	1	0.96	0.86	0.25	0.92	0.74	0.73	0.87	0.69	0.38	0.67
B5	0.70	0.32	0.81	0.96	1	0.81	0.20	0.94	0.67	0.66	0.86	0.65	0.32	0.51
B6	0.89	0.39	0.78	0.86	0.81	1	0.15	0.83	0.76	0.60	0.74	0.48	0.30	0.52
B7	0.39	0.93	0.41	0.25	0.20	0.15	1	0.14	0.53	0.67	0.48	0.64	0.93	0.66
B8	0.70	0.29	0.81	0.92	0.94	0.83	0.14	1	0.68	0.67	0.83	0.69	0.31	0.53
B9	0.81	0.68	0.71	0.74	0.67	0.76	0.53	0.68	1	0.80	0.61	0.83	0.70	0.82
B10	0.70	0.80	0.73	0.73	0.66	0.60	0.67	0.67	0.80	1	0.67	0.86	0.83	0.90
B11	0.76	0.54	0.77	0.87	0.86	0.74	0.48	0.83	0.61	0.67	1	0.64	0.49	0.56

B12	0.57	0.67	0.64	0.69	0.65	0.48	0.64	0.69	0.83	0.86	0.64	1	0.78	0.85
B13	0.49	0.96	0.56	0.38	0.32	0.30	0.93	0.31	0.70	0.83	0.49	0.78	1	0.79
B14	0.76	0.75	0.47	0.67	0.51	0.52	0.66	0.53	0.82	0.90	0.56	0.85	0.79	1

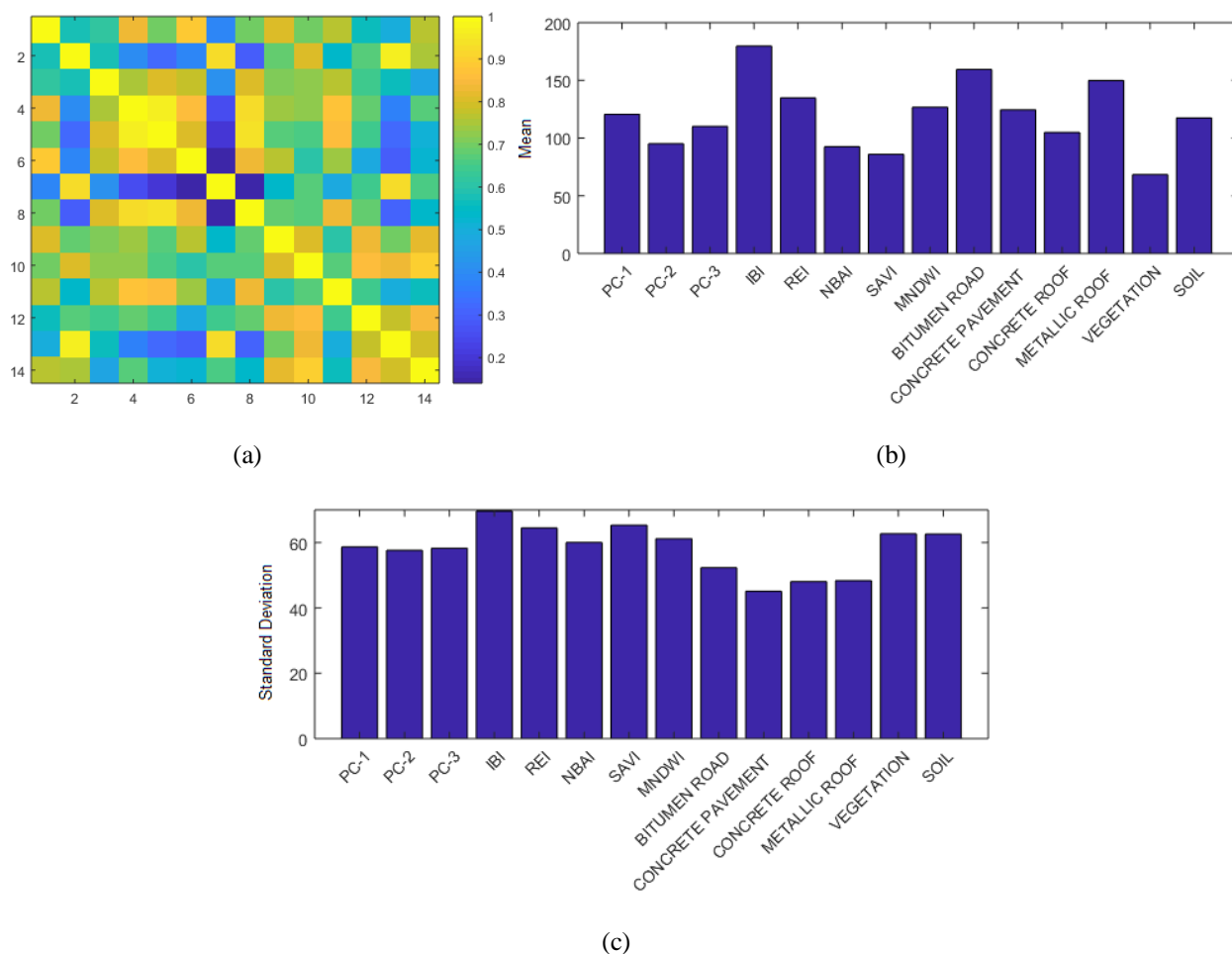


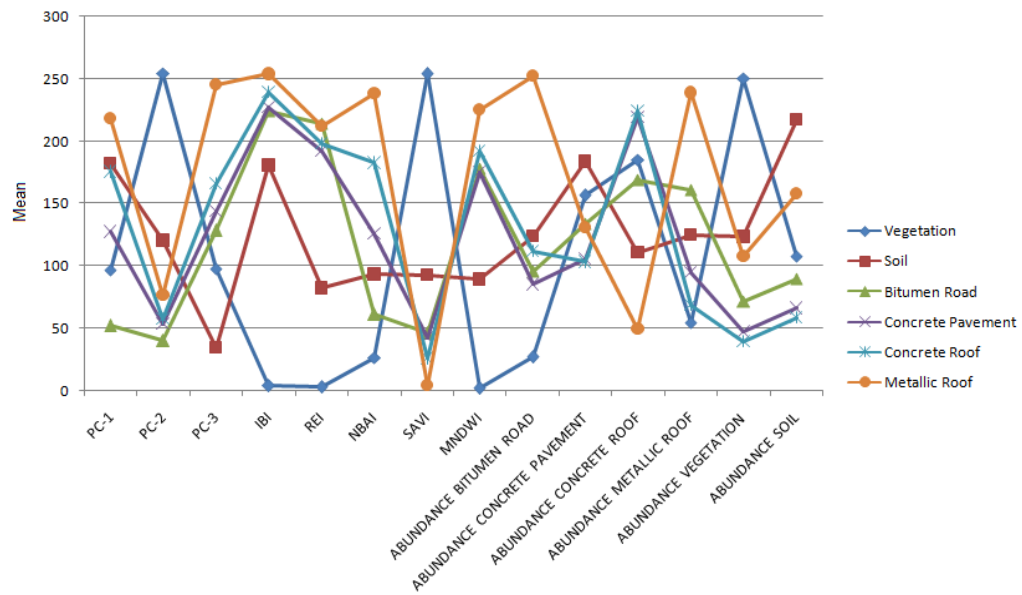
Figure 8.5 Graphical representation of different statistical parameters (a) Correlation between various feature bands (b) Mean, and (c) Standard Deviation of individual feature bands

Figure 8.6 (a) and (b) describe the mean and standard deviation of various artificial and natural land cover classes mentioned in Table 8.1, in each of the feature bands. It is observed from the mean plot shown in Figure 8.6 (a) that, bitumen road can easily be separated from rest of the classes in PC1 while vegetation is more highlighted in case of PC2. Further, in PC3, soil can be easily extracted, as mean value of soil in PC3 is lowest amongst other classes. IBI perfectly separates built-up

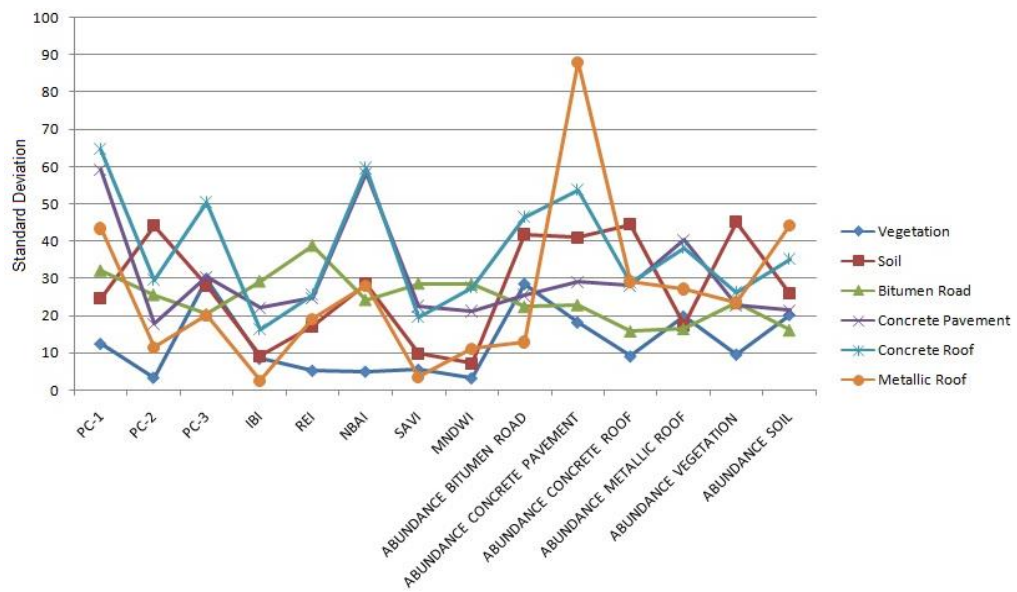
surfaces from vegetation while some overlap is observed with soil. REI seems to be a better approach for separating built-up surfaces from vegetation and soil, as less mean values can be observed for natural surfaces while high values for built-up surfaces. The NBAI may be observed as best approach for extraction of different roofing surfaces, which are concrete and metallic roofs. Further, SAVI can prove to be an effective index for extraction of low and high density vegetation cover of urban area with very high mean values. MNDWI can easily separate built-up surfaces from non-built-up surfaces i.e. vegetation and soil. Further, in abundance map of bitumen road, vegetation and metallic roof can easily be separated from rest of the classes. Next, fractional map of concrete pavement seems to be highly complex with large overlap between all the classes. Finally, in abundance map of metallic roof, vegetation, and soil, the target classes can easily be separated from the respective backgrounds.

Figure 8.6 (b) depicts about standard deviation of various land cover classes in different feature bands. It is observed that PC1 shows maximum information about two land cover classes, which are concrete roof and pavements. Similarly, PC2 and PC3 provide maximum information about vegetation and concrete roof, respectively. The IBI gives almost similar standard deviation for all the classes while for bitumen road and concrete pavement, it provide slightly more information. Similarly, REI offers more information content of bitumen road while NBAI and abundance map of metallic roof have highest information about concrete roof and pavement. Further, SAVI and MNDWI provide almost same information about all the land cover classes while slightly more is observed for bitumen road, concrete pavement and vegetation. Abundance map of bitumen road shows high information about concrete roof and soil while fractional maps of concrete pavement and soil have highest information

about metallic roof surfaces. Finally, fractional maps of concrete roof and vegetation provide highest information about soil.



(a)



(b)

Figure 8.6 Statistical analysis of different urban land cover classes using (a) Mean, and (b) Standard deviation

8.4.2 Extraction of built-up surfaces, sub-surfaces and materials (Level-1 to 3)

The extraction analysis has been carried out using histogram representation of various land cover classes mentioned in Table 8.1, in different resulting images. Further, for brief analysis of the results, all the georeferenced output images with shape files of all the classes mentioned in Table 8.1, are overlapped in high resolution satellite imagery base map of ArcGIS 10.4 by assuming there is no temporal change between AVIRIS-NG and high resolution imagery. The extraction results have also been verified with the ward map of Jodhpur, Rajasthan, India (<http://jodhpurmc.org/HomePage.aspx> accessed on 10th December 2019).

Figure 8.7 (a) to (g) depict the extraction results of built-up surfaces (Level-1 to 3) using combination of spectral index and fractional abundance based features. It is observed from the aforesaid analysis that, in case of built-up surfaces (Level-1), roofs are perfectly extracted while detection rate of road surfaces is not up to the mark. In level-2, roof surfaces are better detected with more overlap with soil pixels. Further, in level-3, concrete roofs are extracted with some overlap with concrete pavements and false alarms due to soil appear to be less in this case. Moreover, metallic roofs in level-3 are detected well with some confusion in the form of soil and bitumen roads. Road surfaces in level-2 are detected perfectly while some part of bituminous roofs are still confused with roads. In level-3, the detection and false alarm rate of bitumen road is less as minor roads and pavements are not perfectly extracted. Also, the same is happened in extraction of concrete pavements.

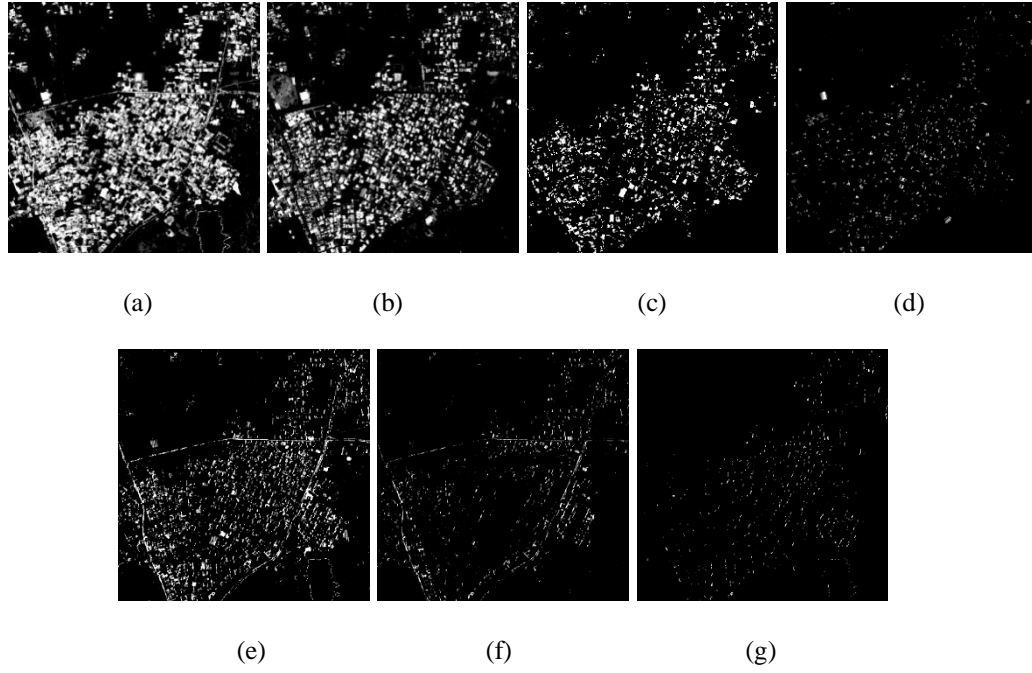


Figure 8.7 Extraction of built-up surfaces (Level-1 to 3) using combination of Spectral Index and Fractional Abundance based features, in which bright pixels are target and darks pixels are background (a) Built-up Surfaces (b) Roofs (c) Concrete Roofs (d) Metallic Roofs (e) Roads (f) Bitumen Roads (g) Concrete Pavements

Figure 8.8 (a) to (g) describe the detection results of built-up surfaces (Level-1 to 3) using combination of spectral index and major principal component based features. On the basis of aforementioned analysis, it is investigated that, in extraction of built-up surfaces (Level-1), rate of detection of roof surfaces is fine but some part of soil is also included in those roofs. In this case major road surfaces are not perfectly extracted but some pavements are highlighted in the extraction results as shown in Figure 8.8 (a). Further, in level-2, roof surfaces are extracted with less significance, as detection rate seems to be slightly less than the previous case of combination of spectral index and fractional abundance. In level-3, concrete roofs are extracted with less detection rate and some overlap with concrete pavement, false alarms due to soil and other backgrounds are least in this case. Further, most of the metallic roofs are extracted well but more overlapping is observed with soil and mixed bitumen surfaces. Road surfaces in level-2 are detected with more confusion

with bitumenous roofs, and some pixels of wet soil are also included and detected as road in this case. It may be due to low albedo of road and wet soil. In level-3, the detection rate of bitumen roads is satisfactory as highway and pavements made-up of bitumen are perfectly extracted. Moreover, in case of concrete pavements, detection and false alarm rates both are high. The false alarms may be due to presence of two classes, which are concrete roof and soil.

Figure 8.9 (a) to (g) represent the extraction results of built-up surfaces (Level-1 to 3) using combination of all the features, which are spectral index, fractional abundance and major principal component. The aforesaid analysis has been carried out for this combination as well. It is examined that, built-up surfaces (Level-1) are extracted perfectly as roofs, and along with that roads are highlighted more in comparison to previous two cases. Also, a very few pixels of soil are included in the built-up surfaces. In level-2, roof surfaces are perfectly extracted with more detection rate and less false alarm. The major problem of separability of soil with roof surfaces has been resolved for this feature combination. In the level-3, concrete and metallic roofs are perfectly detected with better separability from respective backgrounds. Further, concrete and metallic roofs are slightly confused with concrete pavements and bitumen roads, respectively. Road surfaces in level-2 are extracted perfectly with better detection rate and less confusion with other background classes. It appears that all the highways, street roads and small pavements are perfectly highlighted in this case. In level-3, the detection rate of bitumen roads is very high but very few pixels of these roads are still confused with bitumenous roofs. Further, in case of concrete pavements, the target detection rate is better with less false alarms. These false alarms may be due to confusion of concrete pavement with concrete roof surfaces.

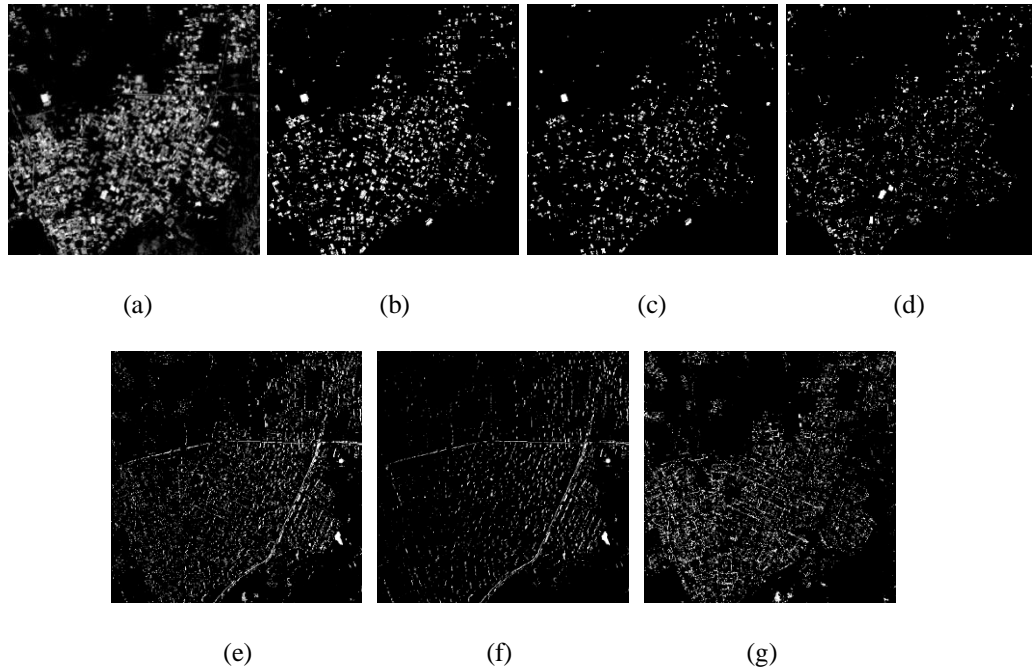


Figure 8.8 Extraction of built-up surfaces (Level-1 to 3) using combination of Spectral Index and Major Principal Component based features, in which bright pixels are target and darks pixels are background (a) Built-up Surfaces (b) Roofs (c) Concrete Roofs (d) Metallic Roofs (e) Roads (f) Bitumen Roads (g) Concrete Pavements

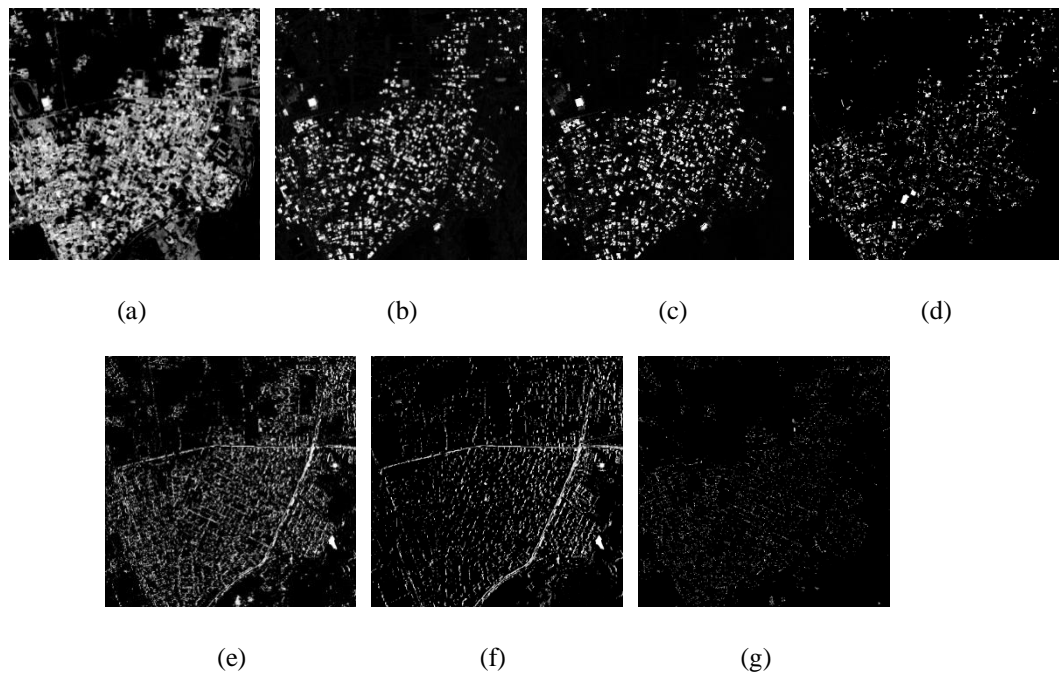


Figure 8.9 Extraction of built-up surfaces (Level-1 to 3) using combination of Spectral Index, Fractional Abundance and Major Principal Component based features, in which bright pixels are target and darks pixels are background (a) Built-up Surfaces (b) Roofs (c) Concrete Roofs (d) Metallic Roofs (e) Roads (f) Bitumen Roads (g) Concrete Pavements

The analysis of results (shown in Figure 8.7 to 8.9) on the basis of histogram representation of various urban land cover classes as well as comparison with high resolution imagery base map of ArcGIS 10.4, and ward map of study region suggest that, combination of spectral index, fractional abundance and major principal component may be more useful for precise extraction of urban built-up surfaces, sub-surfaces, and materials. It is also deduced that feature combination of spectral index and fractional abundance may be a better choice for extraction of aforesaid classes in comparison to combined form of spectral index and major principal component.

8.4.3 Accuracy Assessment

Accuracy assessment of the built-up extraction results shown in Figure 8.7 to 8.9 has been carried out using field information of 518 samples out of which 332 samples are associated with built-up surfaces while remaining 186 with natural surfaces such as vegetation and soil. High resolution satellite imagery base map of ArcGIS 10.4 has also been utilized for validating the extraction results by considering an assumption that there is no temporal change between high resolution base map and AVIRIS-NG imagery. The Overall Accuracy (OA) and Kappa Index (KI) (normalized between 0-100 %) are the two accuracy measures, which have been used for accuracy assessment. Table 8.9 describes the accuracy assessment of different target classes, which are built-up surface in level-1, road (bitumen and concrete pavement) and roof surfaces (concrete and metallic) in level-2, concrete roof, metallic roof, bitumen road and concrete pavement in level-3 while rest of the non-target classes have been considered as background. It is observed from Table 8.9 that, for extraction of built-up surfaces highest OA i.e. 94.59 % is obtained in case of combination of all the features, which are spectral index, fractional abundance and

major principal component. Similarly, for extraction of road and roof surfaces, highest OA i.e. 89.76 %, 91.12 % is achieved for combined form of all the features. Finally, sub-classes of roof surfaces i.e. concrete and metallic roofs produce maximum OA as 89 % and 92.27 %, respectively, which is also for the combination of all the aforesaid features while sub-classes of road surfaces, which are bitumen road and concrete pavement, give highest OA as 91.12 %, 93.24 %, respectively for same set of features. Further, all the aforesaid results have also been verified using KI. Figure 8.10 illustrates about a comparative assessment between various feature combinations, which have been used for extraction of built-up surfaces, sub-surfaces and materials. It is observed from Figure 8.10 (a) and (b) that combined form of spectral index, fractional abundance and major principal component may be more useful for extraction of built-up surfaces (Level-1 to 3), while spectral index with fractional abundance may generate better results in comparison to combined form of spectral index and major principal component.

Table 8.9 Accuracy assessment of extraction of built-up surfaces and materials (Level-1 to 3)

Feature		Level-1				
Combination	Class	Built-up	Background	Producer	OA (%)	Kappa
		Surfaces		Accuracy (%)		Index (%)
Spectral Index +	Built-up Surfaces	298	27	91.69	88.24	74.60
Fractional	Background	34	159	82.38		
Abundance	User Accuracy (%)	89.75	85.48			
		Level-2				
		Roof	Background			
	Roof	162	47	77.51	86.48	71.40
	Background	23	286	92.55		
	User Accuracy (%)	87.56	85.88			

	Road	126	82	60.57	80.11	56.50
	Background	21	289	93.22		
	User Accuracy (%)	85.71	77.90			
	Level-3					
	Concrete Roof	96	57	62.74	84.75	60.80
	Background	22	343	93.97		
	User Accuracy (%)	81.35	85.75			
	Metallic Roof	52	61	46.01	85.32	49.60
	Background	15	390	96.30		
	User Accuracy (%)	77.61	86.47			
	Bitumen Road	63	56	52.94	86.68	56.90
	Background	13	386	96.74		
	User Accuracy (%)	82.89	87.33			
	Concrete Pavement	61	39	61.00	90.54	65.90
	Background	10	408	97.60		
	User Accuracy (%)	85.91	91.27			
Level-1						
Spectral Index + Major Principal Component	Built-up Surfaces	279	33	89.42	83.40	64.80

	Background	53	153	74.27		
	User Accuracy (%)	84.03	82.25			
	Level-2					
		Roof	Background			
	Roof	153	64	70.50	81.70	61.10
	Background	32	269	89.37		
	User Accuracy (%)	82.70	80.78			
		Road	Background			
	Road	119	63	65.38	82.43	59.70
	Background	28	308	91.66		
	User Accuracy (%)	80.95	83.02			
	Level-3					
		Concrete	Background			
		Roof				
	Concrete Roof	92	81	53.17	79.34	49.60
	Background	26	319	92.46		
	User Accuracy (%)	77.96	79.75			
		Metallic	Background			
		Roof				
	Metallic Roof	48	79	37.79	81.08	39.02
	Background	19	372	95.14		
	User Accuracy (%)	71.64	82.48			
		Bitumen	Background			
		Road				
	Bitumen Road	59	62	48.76	84.75	51.10
	Background	17	380	95.71		
	User Accuracy (%)	77.63	85.97			
		Concrete	Background			
		Pavement				

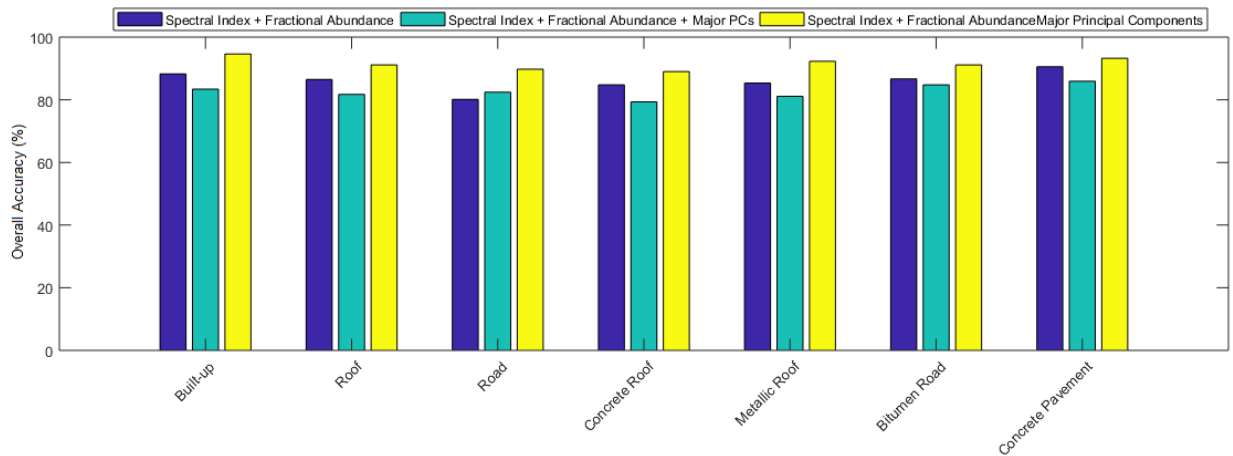
	Concrete Pavement	56	58	49.12	85.90	52.50
	Background	15	389	96.28		
	User Accuracy (%)	78.87	87.02			
Spectral Index +	Level-1					
Fractional		Built-up	Background			
Abundance +		Surfaces				
Major Principal	Built-up Surfaces	315	11	96.62	94.59	88.30
Component	Background	17	175	91.14		
	User Accuracy (%)	94.88	94.08			
	Level-2					
		Roof	Background			
	Roof	173	34	83.57	91.12	81.20
	Background	12	299	96.14		
	User Accuracy (%)	93.51	89.79			
		Road	Background			
	Road	131	39	77.06	89.76	75.90
	Background	14	334	95.98		
	User Accuracy (%)	90.34	89.54			
	Level-3					
		Concrete	Background			
		Roof				
	Concrete Roof	103	42	71.03	89.00	71.10
	Background	15	358	95.97		
	User Accuracy (%)	87.28	89.50			
		Metallic	Background			
		Roof				
	Metallic Roof	61	34	64.21	92.27	70.90
	Background	6	417	98.58		
	User Accuracy (%)	91.04	92.46			

	Bitumen	Background			
	Road				
Bitumen Road	66	36	64.70	91.12	68.90
Background	10	406	97.60		
User Accuracy (%)	86.84	91.85			
	Concrete	Background			
	Pavement				
Concrete Pavement	65	29	69.15	93.24	74.90
Background	6	418	98.58		
User Accuracy (%)	91.55	93.51			

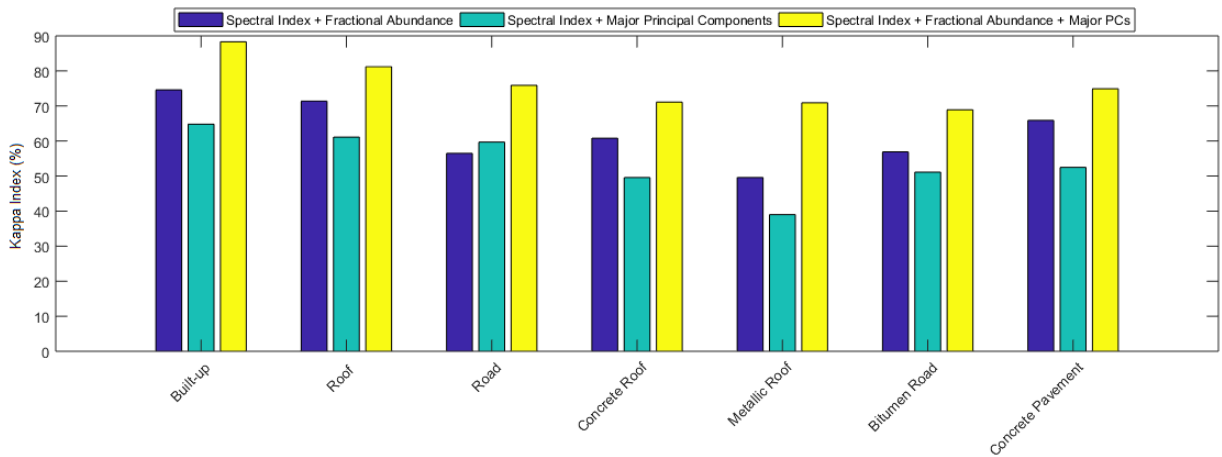
8.4.4 Area estimation of built-up surfaces, sub-surfaces and materials (Level-1 to 3)

Table 8.10 explains about the area estimation of built-up surfaces (Level-1 to 3) for different feature combinations. The actual area of various built-up surfaces and materials in the image has been calculated collectively using high resolution satellite imagery base map of ArcGIS 10.4, ground sample information and ward map of municipal corporation of Jodhpur, Rajasthan, India (<http://jodhpurmc.org/HomePage.aspx> accessed on 10th December 2019), which results in 1.32 km² area of built-up surfaces while roof and road surfaces have area as 1.05 and 0.27 km², respectively. Further, the actual area of sub-classes of roof surfaces i.e. concrete and metallic is 0.96 and 0.12 km², respectively while sub-categories of road surfaces i.e. bitumen road and concrete pavement are having actual area as 0.17 and 0.06 km², respectively. This information has been utilized to further validate the extraction results. It is observed from Table 8.10 that, combination of spectral index, fractional abundance and major principal component

may be more useful for estimation or quantification of built-up surfaces (Level-1 to 3), as area calculated for this combination tends nearly equal to the actual value of built-up surfaces and materials while spectral index with fractional abundance generates better results in comparison to combined form of spectral index and major principal components.



(a)



(b)

Figure 8.10 Comparative assessment of different combinations of features on the basis of (a) Overall Accuracy and (b) Kappa Index

Table 8.10 Area estimation of built-up surfaces and materials in different levels

	Area (m ²)	Area (m ²)		Area (m ²)			
	Level-1	Level-2		Level-3			
Feature Combination	Built-up	Roof	Road	Concrete	Metallic	Bitumen	Concrete
	Surface			Roof	Roof	Road	Pavement
Spectral Index + Fractional Abundance	1219158	1012203	238671	940095	125820	160389	49185
Spectral Index + Major Principal Component	1165077	911538	236565	801000	100800	157455	59868
Spectral Index + Fractional Abundance + Major Principal Component	1350144	1077228	253998	999000	132300	164439	53775

8.5 Summary

Timely and accurate information about urban environment is very important for diverse applications. Due to significant spectral heterogeneity and spectral confusion of urban built-up surfaces with other land cover classes and high dimensionality of hyperspectral data, the urban built-up extraction is become a challenging task. This study indentified different significant features and proposed a method that combines these features based on thematic spectral index, fractional abundance and major principal component. Three combinations have been created for extraction of built-up surfaces, sub-surfaces and materials, which are spectral index and fractional abundance, spectral index and major principal component as well as combination of all aforesaid features. Further, using all these combinations, and training and testing samples extracted from ground, SVM binary classifier has been used for detection of

built-up surfaces in level-1, road and roof surfaces in level-2, sub-categories of roofs i.e. concrete and metallic roofs as well as sub-classes of roads i.e. bitumen road and concrete pavement in level-3. The urban built-up extraction has been carried out using AVIRIS-NG hyperpsectral data of Jodhpur, Rajasthan region of India. It is observed that in all the three aforesaid combinations, the combined form of thematic spectral index, fractional abundance and major principal component generate better extraction and estimation results for built-up surfaces, sub-surfaces and materials. It has also been examined using high resolution base map of ArcGIS 10.4 and ward map of study region that, in case of combined form of all the features, detection rate is high with less false alarm for most of the built-up classes. Further, combination of spectral index and fractional abundance can prove to be effective in comparison to spectral index and major principal component.

Chapter 9

Evaluation of Spectral Indices based Approach for Extraction of Road and Roof Surfaces in different Sensor Imageries

This chapter presents a performance evaluation of Sentinel-2B, Landsat-8 multispectral, and AVIRIS-NG hyperspectral imagery for extraction of road and roof surfaces using proposed spectral index based, and various other conventional algorithms. The New Road Extraction Index (NREI) and New Building Extraction Index (NBEI) have been proposed for extraction of road and roof surfaces, respectively. Moreover, existing Spectral Angle Mapper (SAM), Spectral Information Divergence (SID), Matched Filtering (MF), and Support Vector Machine (SVM) are utilized as angle, information, filtering, and machine learning based algorithms, respectively, for detection of both the surfaces.

The tasks performed under this objective are:

- a) To carry out a performance evaluation of Sentinel-2B, Landsat-8 and AVIRIS-NG sensor imageries for extraction of road and roof surfaces on the basis of proposed and existing approaches.
- b) To perform a comparative analysis between proposed indices and existing conventional SAM, SID, MF, and SVM algorithms for extraction of road and roof surfaces in different sensor imageries.

9.1 Study area and Dataset

The study area belongs to the Udaipur, Rajasthan region of India, which is an

amalgamation of artificial and natural surfaces. The remote sensing imagery used in this study was captured from space-borne Sentinel-2B and Landsat-8 multispectral sensors, and AVIRIS-NG hyperspectral sensor. This image data is shown in Figure 9.1 (a) to (c) while the complete description of data is tabulated in Table 9.1. The ground data of the similar geographical area has been collected using Spectral Evolution spectroradiometer over the wavelength range of 350 nm to 2500 nm. The locations of field data collection of different urban land cover classes are shown in Figure 9.1 (d). The field data collection has been carried out using gun and contact probe in cloud free atmospheric condition between 1000 hrs to 1500 hrs (10 am to 03 pm). Some of the field photographs of field data collection are shown in Figure 9.1 (e). The results of the study have been validated using ground location information of 2297 samples out of which 1032 are associated with built-up surfaces while 1265 to non-built-up surfaces. Built-up surfaces are further categorized into 500 road and 532 roof surfaces. Further, high resolution satellite imagery base map of ArcGIS 10.4 has also been utilized for the assessment of accuracy and validation of results along with shape files of different target and background classes.

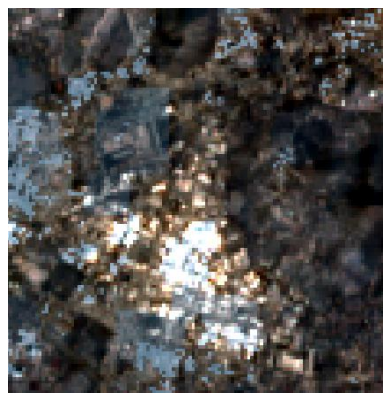
Table 9.1 Remote Sensing data specification of different sensors

SN	Parameters	Description		
1	Image Location	Udaipur, Rajasthan, India	Udaipur, Rajasthan, India	Udaipur, Rajasthan, India
2	Name of Sensor	Sentinel-2B	Landsat-8	AVIRIS-NG
3	Date of Data acquisition	02/06/2018	30/11/2017	02/02/2016
4	Spatial Resolution	60, 10, 20 meter	30 meter	8.1 meter
5	Wavelength Range	443 nm – 2190 nm	430 nm – 2290 nm	376 nm – 2500

				nm
6	Number of Samples, Lines and Bands	400, 400 ,13	400, 400, 7	400, 400, 380
7	Level of data	Level 2	Level 2	Level 1 and Level 2
8	Coordinate system	WGS-84 / UTM Zone 43N	WGS-84 / UTM Zone 43N	WGS-84 / UTM Zone 43N



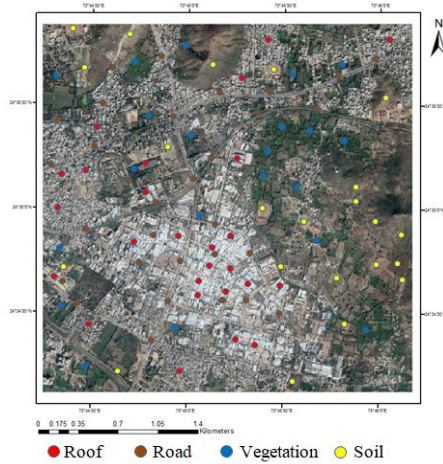
(a)



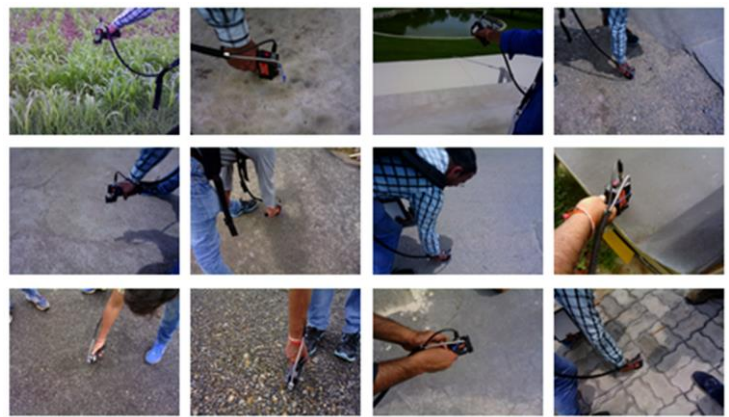
(b)



(c)



(d)



(e)

Figure 9.1 Remote sensing images captured from various sensors (a) Sentinel- 2B (b) Landsat-8 (c) AVIRIS-NG (d) Locations of ground data collection (e) Field photographs of data collection campaign

9.2 Performance evaluation of different sensor imageries on the basis of spectral profile of road and roof surfaces

It is observed from the spectral characteristics of road and roof surfaces in different sensor imageries, shown in Figure 9.2 (a) to (c) that, the intensity of roof surfaces in all the wavelength bands is more in comparison to roads. It may be due to more brightness and fine composition of aggregates of concrete roof surfaces in comparison to asphalt or bituminous roads [46] [135]. Following is observed from Figure 9.2 (a) to (c):

- It appears from the spectral signatures of roads and roofs in Sentinel- 2B imagery, shown in Figure 9.2 (a) that, these surfaces can be differentiated in the visible and NIR regions, as roof surfaces have increasing reflectance while a concavity is observed in the spectra of road surfaces in those regions. Further, a major water absorption band is also observed near 1400 nm.
- It is depicted from the spectral characteristics of roads and roofs in Landsat-8 imagery, shown in Figure 9.2 (b) that, NIR and SWIR regions can prove to be effective for separating road and roof surfaces, as the signature of road surfaces is almost constant in both the regions while for roofs, it gradually increases and decreases in these two regions, respectively.
- The spectral signatures shown in Figure 9.2 (c) are related to road and roof surfaces derived from AVIRIS-NG hyperspectral imagery. There are different absorptions and peaks are present in various narrow bands of hyperspectral imagery. Reflectance of road surfaces is very low and almost constant in all the regions while it is high for roof surfaces. Spectra of roof surfaces increases in visible and NIR regions while it appears to be almost constant in SWIR. Also, different iron oxide absorption features can be observed in the

visible and NIR regions near 490 and 830 nm while some hydrocarbon absorption bands exist near 1700 nm and between 2200 to 2400 nm. These absorption features dominate in roof surfaces while in case of roads, a slight absorption due to iron oxide and clay can be seen near 690 and 2050 nm, respectively. Therefore, visible and SWIR regions can prove to be the more suitable for extraction of roofs followed by visible and NIR for detection of roads in AVIRIS-NG imagery.

It is further observed that, Sentinel-2B and Landsat-8 may be capable of extracting sub-categories of built-up surfaces i.e. roads and roofs with less significance while these can easily separate built-up from non-built-up surfaces by proper selection of wavelength bands with some better accuracy. The AVIRIS-NG is an advanced hyperspectral sensor, which can easily detect built-up surfaces and its sub-categories by proper selection of significant bands. Also, due to large number of narrow bands, sub-categories of road and roof surfaces can also be extracted.

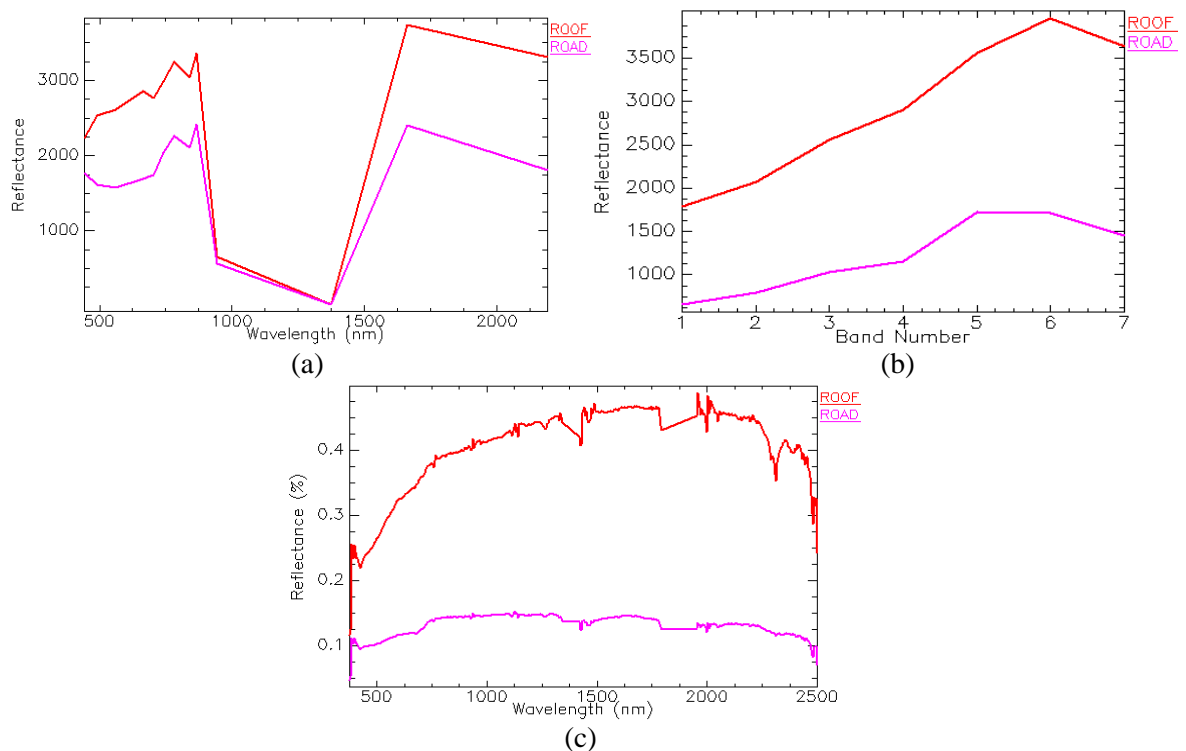


Figure 9.2 Spectral characteristics of roads and roofs in different sensor imagery (a) Sentinel- 2B (b) Landsat-8 (c) AVIRIS-NG

9.3 Proposed spectral indices

9.3.1 New Road Extraction Index (NREI)

NREI is proposed to automatically extract bitumen and asphalt road networks in different remote sensing imageries. This index is tested on low to high spatial resolution multispectral and hyperspectral imageries such as Landsat-8, Sentinel-2B and AVIRIS-NG. To determine the significant bands in all the imageries, image data along with field spectral data have been used. Among the various bands, the best results have been obtained with the NIR and Green bands. Therefore, NREI is developed using the band combination of NIR and Green bands, as given in Equation 9.1. In a similar study an index named as REI has been proposed, but that index was suitable for extraction of road surfaces only in high spatial resolution WV- 2 multispectral imagery [67].

$$NREI = \frac{NIR - Green}{NIR + NIR \times Green} \quad (9.1)$$

9.3.2 New Building Extraction Index (NBEI)

NBEI is developed for extraction of roof surfaces in different remote sensing images. This index extracts roof surfaces over a small range of reflectance values, but after applying contrast stretch, this small range can be stretched to available dynamical range. Such contrast stretch enhances the roof surfaces clearly and suppresses the other background. The NBEI has been utilized a combination of SWIR2, SWIR1 and Green bands for extraction of roof surfaces, as given in Equation in 9.2. In this research, NBEI has been tested on Sentinel-2B, Landsat-8 and AVIRIS-NG imagery for extraction of roof surfaces using appropriate wavelength band combination. A

similar study has been carried out in recent past for extraction of built-up surfaces using NBAI, but it was only applicable for Landsat-7 multispectral imagery [62].

$$NBEI = \frac{SWIR2 - \frac{SWIR1}{Green}}{SWIR2 - \frac{SWIR1}{Green}} \quad (9.2)$$

Where $SWIR2$ is greater than $SWIR1$.

9.4 Existing approaches

9.4.1 Spectral Angle Mapper (SAM)

SAM is a physically-based spectral classification approach that utilizes an n-dimensional angle to match target pixels with the reference spectra. SAM compares the angle between the endmember vector of target and each reference pixel vector in n-D space. Smaller angles represent closer matches to the target spectrum. Pixels farther away than the specified maximum angle threshold are not classified [181] [182] [183]. If K is the number of spectral bands, t is the target pixel, and r is the reference pixel, then spectral angle between target and reference pixel is given as,

$$\theta = \cos^{-1} \left[\frac{\sum_{i=1}^K t_i r_i}{\left(\sum_{i=1}^K t_i^2 \right)^{1/2} \left(\sum_{i=1}^K r_i^2 \right)^{1/2}} \right] \quad (9.3)$$

In this study K varies from 13 for Sentinel-2B to 7 and 380 for Landsat-8 and AVIRIS-NG, respectively.

9.4.2 Spectral Information Divergence (SID)

SID is a spectral classification approach that utilizes a divergence measure to match the target pixel with reference spectra. The smaller the divergence, the more likely the pixels are similar. Pixels with a measurement greater than the specified maximum divergence threshold are not classified [184] [185] [186]. If we consider spectral vector of target as $T = (T_1, T_2, T_3, \dots, T_N)$ and reference as $R = (R_1, R_2, R_3, \dots, R_N)$ with K number of bands, then SID can be given as,

$$SID(T, R) = D(T, R) + D(R, T) \quad (9.4)$$

Where,

$$D(T, R) = \sum_{i=1}^K p_i \log \left(\frac{p_i}{q_i} \right), \quad D(R, T) = \sum_{i=1}^K q_i \log \left(\frac{q_i}{p_i} \right)$$

$$p_i = \frac{T_i}{\sum_{i=1}^K T_i}, \quad q_i = \frac{R_i}{\sum_{i=1}^K R_i}$$

$D(T, R)$ is the relative entropy of target with respect to reference pixel while $D(R, T)$ is the relative entropy of R with respect to T . Also p_i is the desired probability vector resulting from target vector T while q_i denotes the probability distribution of reference pixel.

9.4.3 Matched Filter (MF)

MF generates from binary hypothesis test, it can also be described from the perspective of filter output energy. MF detector can be considered as an optimal solution for the detection of target, when the data origin is positioned at the mean vector [187] [188] [189]. The normalized expression of MF detector can be written

as,

$$w_{MF} = c_{MF} \Gamma^{-1}(d - m) = \frac{\Gamma^{-1}(d - m)}{(d - m)^T \Gamma^{-1}(d - m)} \quad (9.5)$$

Where, $m = \frac{\sum_{i=1}^K r_i}{K}$ is the mean vector with K number of bands,

$\Gamma = \left[\frac{\sum_{i=1}^K (r_i - m)(r_i - m)^T}{K} \right]$ is the covariance matrix and

$c_{MF} = \left[\frac{1}{(d - m)^T \Gamma^{-1}(d - m)} \right]$ is a scalar quantity.

9.4.4 Support Vector Machine (SVM)

The SVM classification is based on finding an optimal separation hyperplane performing the minimum distance. The optimal hyperplan is defined by a subset of feature vectors from the learning database named support vectors. The classification problem is equivalent to a quadratic optimization with different constraints. The optimization problem is parameterized by a penalty parameter that describes the separation complexity and the classification error [99] [100]. When the separability is nonlinear, nonlinear transform from the feature space to new space with greater dimension allows a linear separability. There is no requirement to find the transformation function, only a kernel function K is required. The kernel choice is determinative for the separability and depends on the classification application. Normally used kernel functions in SVM are radial basis function (RBF) and sigmoid function [190] [191] [192] [193], which are given by,

$$K(m, n) = \exp\left(\frac{\|m-n\|^2}{2\sigma^2}\right) \quad (9.6)$$

$$K(m, n) = \tanh(\gamma m^T n + r) \quad (9.7)$$

In Equation 9.6, σ is the adjustment parameter, which plays a main role in the development of a kernel. Further, in Equation 9.7, γ and r are the slope and intercept constant, respectively, which are used as adjustment parameters in sigmoid function. In this study the extraction has been carried out using RBF and sigmoid function both but the best training accuracy has been achieved in case of RBF, therefore this study only utilizes RBF as kernel for extraction of roads and roofs. The accuracy assessment is carried out using overall accuracy i.e. combination of training and testing accuracy.

9.5 Implementation

The whole analysis has been carried out in ENVI 5.3, MATLAB 2018B and ArcGIS 10.4 software environment. Implementation has been performed in four parallel data processing stages for Sentinel-2B, Landsat-8, AVIRIS-NG imagery and field data, respectively. After implementation of all the stages, performance evaluation and comparative assessment between different sensor imageries and simultaneously between various algorithms have been carried out. Different stages of implementation are represented by a flowchart, as shown in Figure 9.3.

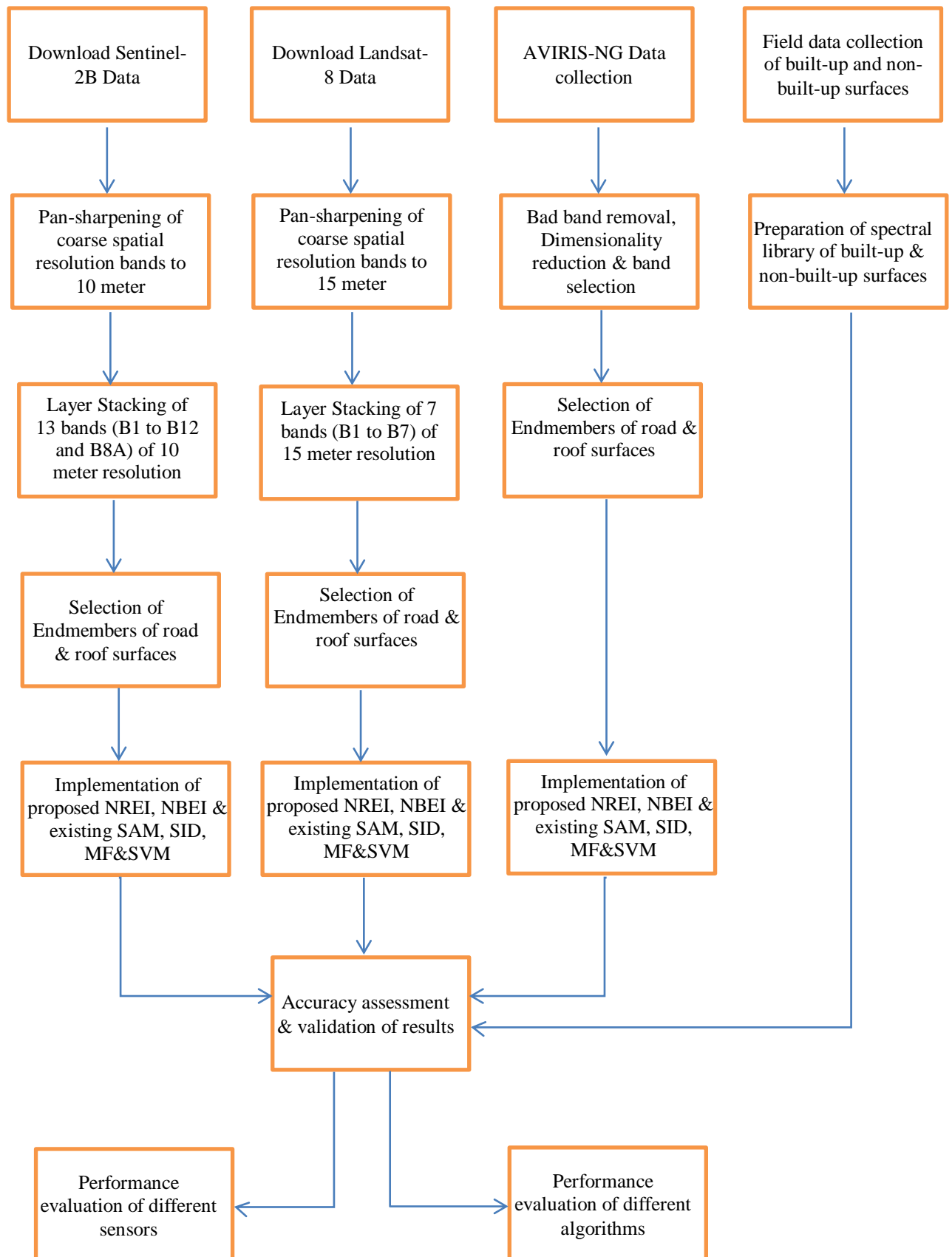


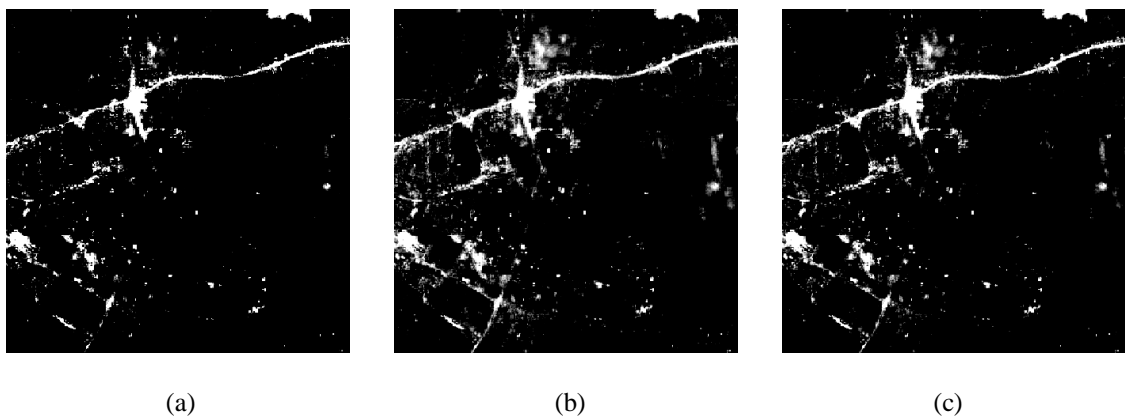
Figure 9.3 Flowchart describing implementation steps of the study

9.6 Results and Discussion

9.6.1 Road Extraction in different sensor imageries

9.6.1.1 Sentinel-2B

Road extraction results in Sentinel-2B satellite imagery using various approaches are shown in Figure 9.4 (a) to (e). These results are compared with high resolution imagery along with shape files of different land cover classes shown in Figure 9.1 (d). It is observed from the result shown in Figure 9.4 (a) that, NREI is capable of extracting major and minor road surfaces with few false alarms in the form of soil, as spectral characteristics of soil and roads show almost similar behavior. Further, it appears from the extraction result of SAM that, fewer pixels of road surfaces are highlighted with less false alarms, as shown in Figure 9.4 (b). SID and NREI appear to be superior in terms of probability of detection of road surfaces while slightly more false alarms in the form of roofs and soil are observed in SID. MF is having some better detection rate with more false alarms in the form of roofs and soil. In case of SVM, most of the soil and roof surfaces are detected as roads due to similar spectral behavior of these surfaces. The outcomes of MF and SVM appear to be similar.



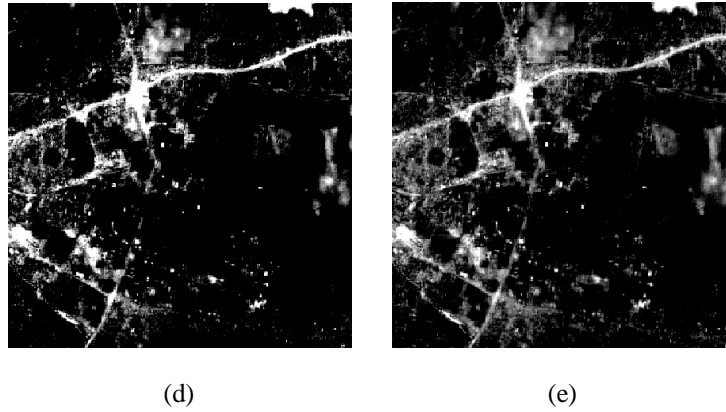


Figure 9.4 Road extraction in Sentinel-2B imagery using various algorithms, in which bright pixels are related to roads while dark pixels to non-road (a) NREI (b) SAM (c) SID (d) MF (e) SVM

9.6.1.2 Landsat-8

Road extraction results in Landsat-8 imagery using various approaches are shown in Figure 9.5 (a) to (e). It appears from Figure 9.5 (a) that, NREI is able to detect most of the road surfaces appropriately but a large number of soil and roof pixels are included in the category of roads. Further, SAM and SID extract road surfaces with some better detection rate while most of the roads are confused with soil and roof surfaces. This confusion seems to be more in case of SID in comparison to SAM. The similarity in the materials composition utilized for construction of road and roof surfaces may be a reason for mixing between these surfaces [135]. Further, MF seems to be better in terms of false alarms in Landsat-8 but there appears less probability of detection. The false alarms in MF come out in the form of soil and roof surfaces. Finally, a worst performance is observed in SVM for detection of road surfaces, as maximum part of non-road surfaces are included in the category of roads, as shown in Figure 9.5 (e).

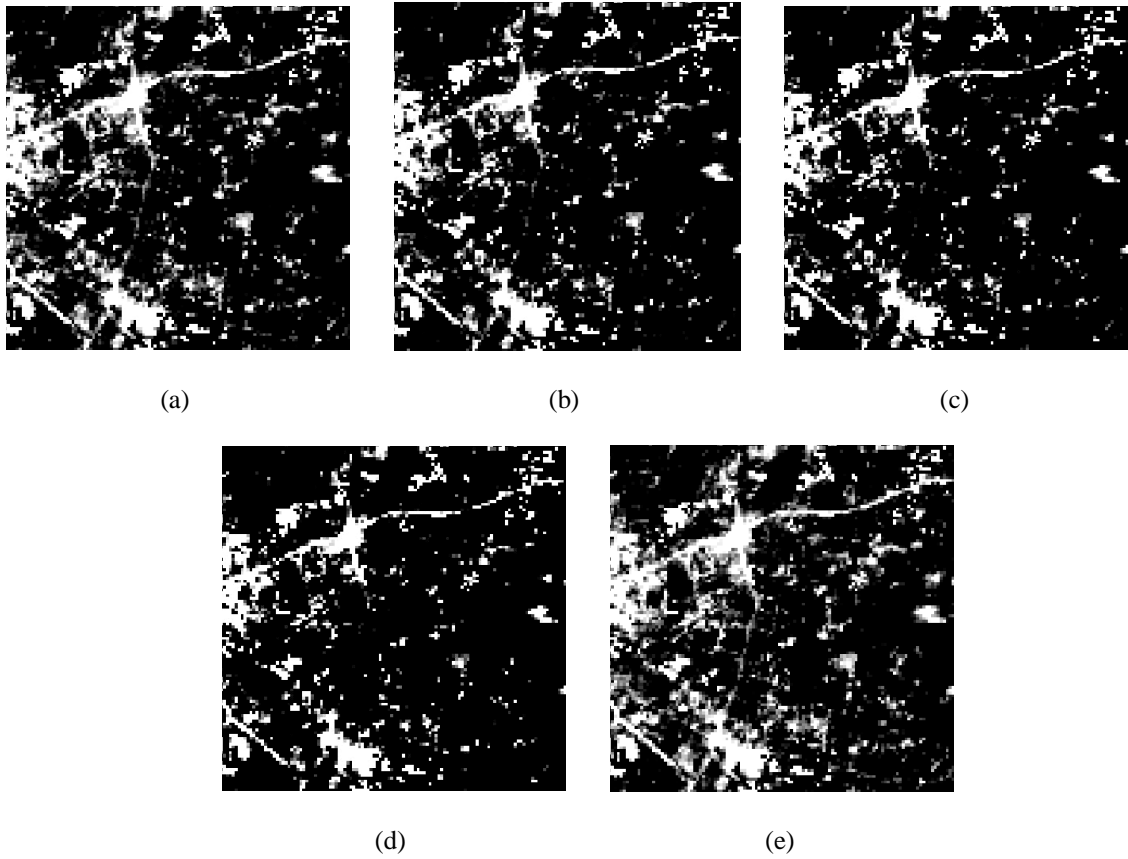


Figure 9.5 Road extraction in Landsat-8 imagery using various algorithms, in which bright pixels are related to roads while dark pixels to non-road (a) NREI (b) SAM (c) SID (d) MF (e) SVM

9.6.1.3 AVIRIS-NG

Extraction results of road surfaces using different algorithms in AVIRIS-NG hyperspectral imagery are shown in Figure 9.6 (a) to (e). Visually, it is observed from Figure 9.6 (a) that, NREI is capable of detecting all the major and minor road surfaces with very less false alarms. The road extraction results of SAM and SID appear to be same while more false alarms in the form of roofs are observed in case of SAM. Further, there appears fewer false alarms with better probability of detection in case of SID. MF is observed to be a better algorithm for extraction of road surfaces, as major and minor road surfaces are clearly highlighted with less false detection. Finally, SVM emerges as a better classifier for extraction of roads in

AVIRIS-NG imagery. The extraction results of NREI and SVM may be comparable in terms of probability of detection and false alarms.

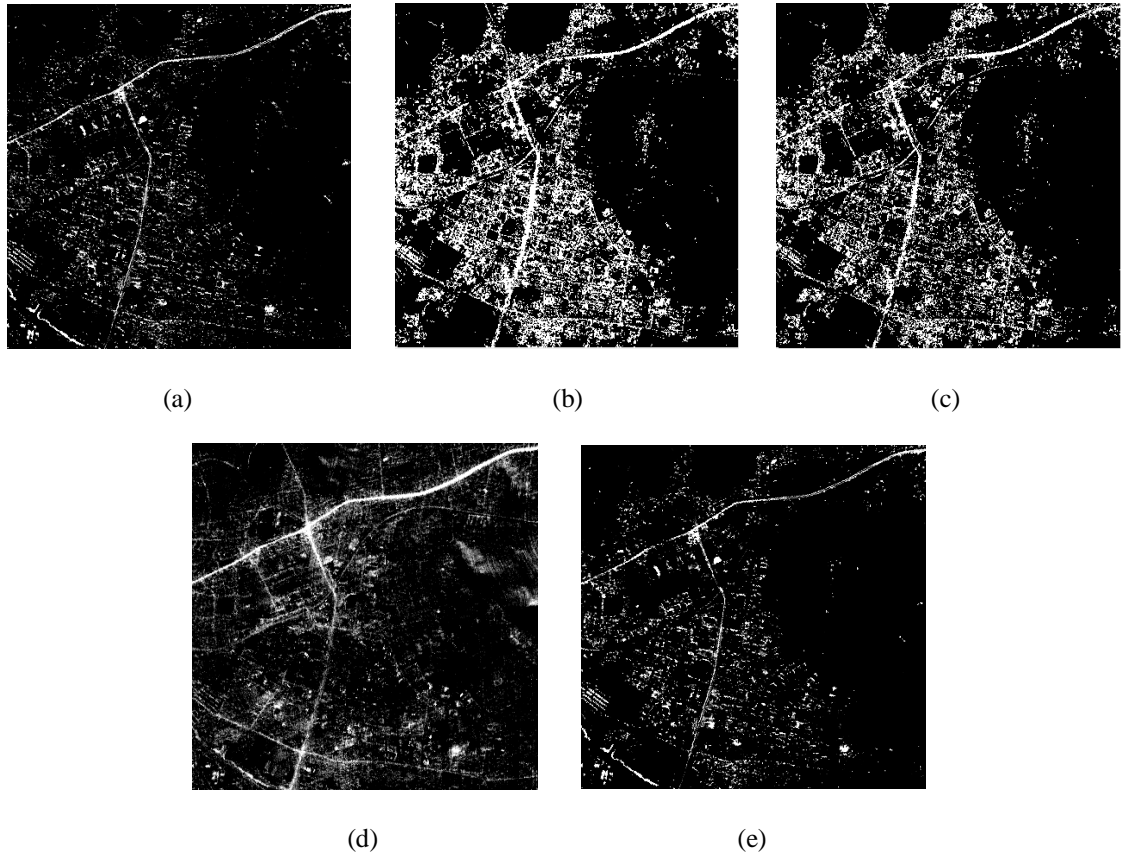


Figure 9.6 Road extraction in AVIRIS-NG imagery using different algorithms, in which bright pixels are related to roads while dark pixels to non-road (a) NREI (b) SAM (c) SID (d) MF (e) SVM

The overall analysis of the road extraction results suggests that AVIRIS-NG is capable of extracting all the major and minor road surfaces in comparison to Sentinel-2B and Landsat-8 multispectral imageries. Further, Sentinel-2B imagery appears to be better in comparison to Landsat-8 for extraction of road surfaces. If we compare the extraction results of different algorithms, then NREI and SID are observed to be suitable for extraction of road surfaces in Sentinel-2B imagery, while moderate performance is observed in case of SAM, MF and SVM. In case of Landsat-8 imagery, NREI and MF can prove to be effective for extraction of road surfaces while average performance is observed in SAM, SID and SVM. Finally,

NREI and SVM appear to be the best approaches for extraction of road surfaces in AVIRIS-NG imagery while satisfactory performance is observed in case of SAM, SID and MF. It is also examined from the aforesaid analysis that due to narrower band width of hyperspectral imagery, a minute detail about any surface can be extracted while due to wider band width and discrete channels of multispectral imagery, it may not be possible to extract most of the sub-categories of built-up surfaces effectively. Therefore, AVIRIS-NG is performed better than Sentinel-2B and Sentinel-2B appears to be better in comparison to Landsat-8. It is also examined that the higher spatial resolution of imagery leads to better extraction of road surfaces as there exists a little scope of mixing of various classes inside the pixels. Hence, high spatial resolution hyperspectral imagery outperforms other multispectral imageries such as Sentinel-2B and Landsat-8. The similar conclusion can be drawn for Sentinel-2B, which is having moderate spatial resolution.

9.6.2 Roof Extraction in different sensor imageries

9.6.2.1 Sentinel-2B

Roof extraction results using various algorithms in Sentinel-2B satellite imagery are shown in Figure 9.7 (a) to (e). As in case of road extraction results, the roof extraction results are also compared with high resolution base map along with shape files of different land cover classes shown in Figure 9.1 (d). The roof extraction index NBEI appears to be better in terms of probability of detection with less false alarms, as shown in Figure 9.7 (a). The extraction results of SAM and SID are almost similar with an excellent probability of detection while slightly more false alarms are observed in case of SAM in comparison to SID. Further, it is observed from the roof extraction result of MF that, most of the roof surfaces are effectively extracted with

more overlapping with soil while less detection of roofs with fewer false alarms are observed in case of SVM, as shown in Figure 9.7 (d) and (e), respectively.

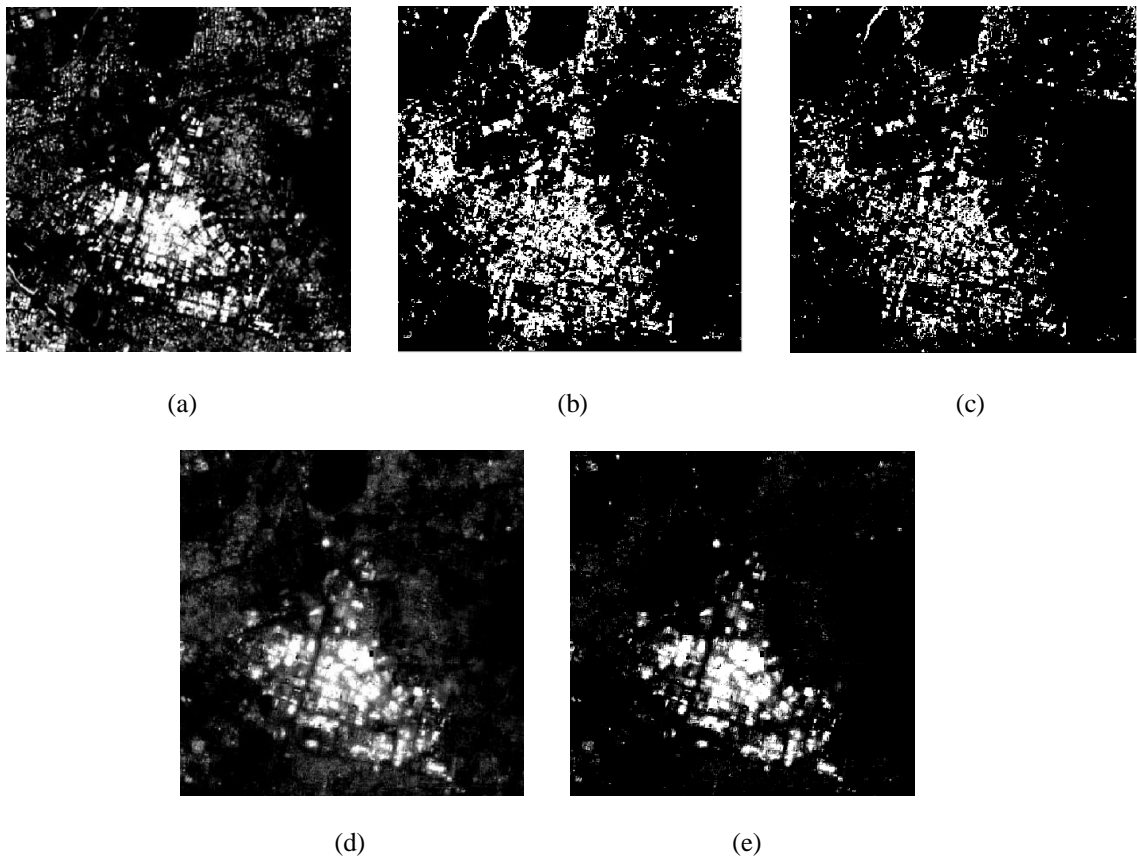


Figure 9.7 Roof extraction in Sentinel-2B imagery using various algorithms, in which bright pixels are related to roofs while dark pixels to non-roof (a) NBEI (b) SAM (c) SID (d) MF (e) SVM

9.6.2.2 Landsat-8

The roof extraction results using various approaches in Landsat-8 imagery are shown in Figure 9.8 (a) to (e). It is observed that, NBEI is efficiently extracting roof surfaces with better probability of detection and slight overlapping with soil. The results obtained from SAM and SID are almost similar while more false alarms appear in case of SID, as shown in Figure 9.8 (b) and (c). In both of these algorithms, majority of false alarms are observed due to spectrally similar bare soil. Further, the probability of detection of roof surfaces is less in case of MF with fewer false alarms. Finally, SVM can prove to be an effective algorithm for extraction of roof surfaces in

Landsat-8 imagery with better probability of detection and comparatively less false alarms. The performance of MF and SVM appears to be almost similar.

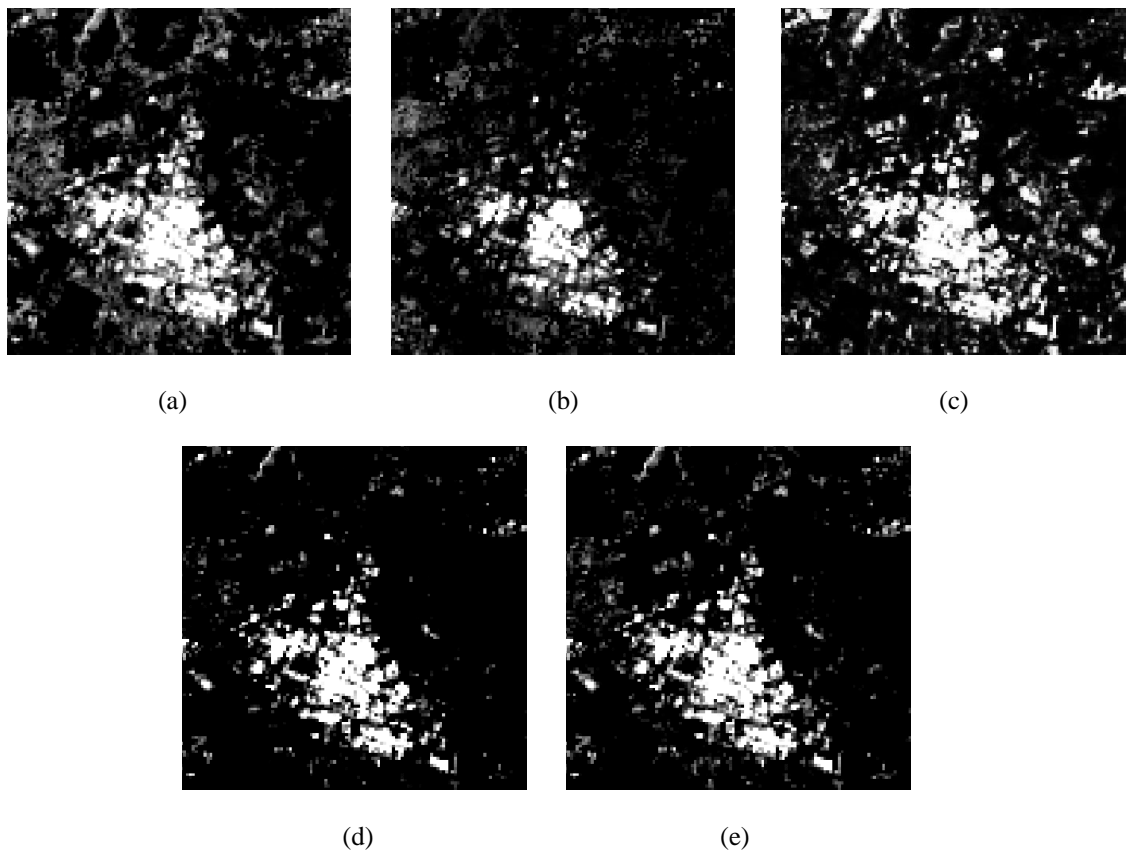


Figure 9.8 Roof extraction results in Landsat-8 imagery using different algorithms, in which bright pixels are related to roofs while dark pixels to non-roof (a) NBEI (b) SAM (c) SID (d) MF (e) SVM

9.6.2.3 AVIRIS-NG

The extraction results of roof surfaces using various algorithms in AVIRIS-NG hyperspectral imagery are shown in Figure 9.9 (a) to (e). In case of NBEI, the roof surfaces are perfectly extracted with very less false alarms. In roof extraction results of SAM and SID, there appear a high probability of detection with more false alarms. The most of the false alarms are observed due to road surfaces of similar construction materials as roof surfaces. Further, MF and SVM produce almost similar roof extraction results while more false alarms are observed in case of SVM in comparison to MF. The major advantage of NBEI and MF is that, the probability

of detection of these two algorithms is high with less false detection rate in comparison to other approaches.

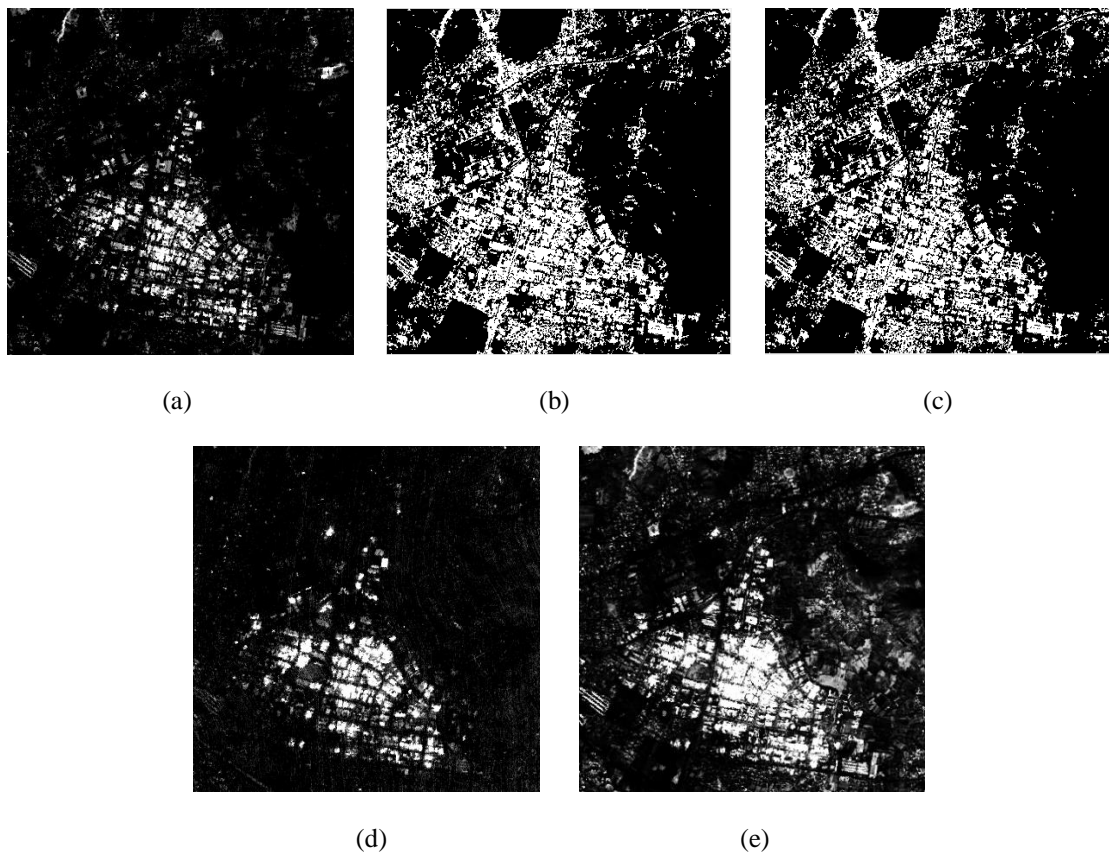


Figure 9.9 Roof extraction in AVIRIS-NG imagery using various algorithms, in which bright pixels are related to roofs while dark pixels to non-roof (a) NBEI (b) SAM (c) SID (d) MF (e) SVM

The overall observation of roof extraction results is that, due to brighter tone as well as maximum tonal variation of roof surfaces in comparison to other classes, these surfaces can easily be extracted from non-roof surfaces. So, if a comparison is carried out between the extraction of road and roof surfaces, then roofs can easily be separated from non-roof surfaces while road and non-road surfaces may not be easily separated. Further, if a comparison between different sensor's performances is carried out, then it is observed that, AVIRIS-NG is capable of extracting the minute details from the imagery due to narrower band width of hyperspectral data. In this study, some better roof extraction results are obtained in AVIRIS-NG hyperspectral

imagery in comparison to wider band Sentinel-2B and Landsat-8 multispectral imageries. Similarly, Sentinel-2B produces better roof extraction results in comparison to Landsat-8 sensor imagery due to slightly more number of bands. Moreover, it can also be concluded that higher spatial resolution results in better extraction of roof surfaces due to less mixing of roof and non-roof surfaces. If a comparison is performed between various algorithms used for extraction of roof surfaces in different multispectral and hyperspectral imageries, then it is observed that, NBEI and SID produce better roof extraction results while a moderate extraction is obtained in case of SAM, MF and SVM algorithms in Sentinel-2B imagery. Further, in Landsat-8, NBEI and SAM generate some better outcomes but rest of the algorithms such as SID, MF and SVM produce average roof extraction results. Finally, in case of AVIRIS-NG imagery, best results are obtained in case of NBEI and MF while better or satisfactory results are produced by SAM and SID followed by moderate in case of SVM.

9.6.3 Accuracy Assessment

Accuracy assessment of the extraction results of road surfaces has been carried out using in-situ information of 500 road and 1797 non-road pixels as target and background, respectively. In a similar manner, roof surfaces are validated using ground information of 532 roof and 1765 non-roof pixels. Further, along with ground information, a high resolution satellite imagery base map of ArcGIS 10.4 with shape files of respective target and background classes, as shown in Figure 9.1 (d), are also used to further validate the results of extraction of road and roof surfaces in different sensor imageries. The accuracy assessment of road extraction results in Sentinel-2B, Landsat-8 and AVIRIS-NG imagery using various algorithms is tabulated in Table

9.2 to 9.4, respectively. Similarly, accuracy assessment of roof extraction in same set of imageries and using similar approaches is shown in Table 9.5 to 9.7. The Overall Accuracy (OA) and Kappa Index (KI) have been divided into different categories on the basis of percentage range, as shown in Table 6.8 and 6.9, which may be helpful to identify the suitable approach for extraction of road and roof surfaces in different multispectral and hyperspectral imageries.

9.6.3.1 Road surfaces

It is observed from Table 9.2 that, NREI, SID and SAM are able to extract road surfaces with an OA of 84.54 %, 82.58 % and 80.54 %, while MF and SVM generate an OA of 78.75 % and 74.01 %, respectively. Therefore, NREI, SID and SAM may be suitable for extraction of road surfaces in Sentinel-2B imagery. Further, in case of Landsat-8 imagery, NREI and MF produce an OA of 83.32 % and 80.58 %, while rest of the approaches i.e. SAM, SID and SVM show an OA of 75.57 %, 72.92 % and 70.60 %, respectively, as shown in Table 9.3. Thus, NREI and MF may be the suitable approaches for extraction of road surfaces in Landsat-8 imagery. Finally, when the assessment of accuracy is carried out for AVIRIS-NG imagery, then it appears that NREI, SAM, SID, MF and SVM show an OA of 94.90 %, 90.55 %, 89.64 %, 92.51 % and 93.80 %, respectively, as shown in Table 9.4. Therefore, all the approaches are found to be suitable for extraction of road surfaces in hyperspectral imagery, while the best performance is achieved in case of NREI and SVM. When the assessment of accuracy is carried out using KI, then the similar results have been obtained as found in case of OA. Further, if we compare the performance of the sensor imagery on the basis of road extraction results, then it appears that, AVIRIS-NG sensor can prove to be effective for extraction of road

surfaces in comparison to Sentinel-2B and Landsat-8. Also, Sentinel-2B can prove be better for extraction of road surfaces in comparison to Landsat-8.

Table 9.2 Accuracy assessment of road extraction using various algorithms in Sentinel-2B imagery

Algorithm	Sentinel-2B					
	Class	Road	Non- road	Producer Accuracy (%)	OA (%)	Kappa Index (%)
NREI	Road	378	233	61.86	84.54	58.00
	Non-road	122	1564	92.76		
	User Accuracy (%)	75.60	87.03			
SAM	Road	339	286	54.24	80.54	47.60
	Non-road	161	1511	90.37		
	User Accuracy (%)	67.80	84.08			
SID	Road	405	305	57.04	82.58	55.60
	Non-road	95	1492	94.01		
	User Accuracy (%)	81	83.02			
MF	Road	417	405	50.73	78.75	49.40
	Non-road	83	1392	94.37		
	User Accuracy (%)	83.40	77.46			
SVM	Road	426	523	44.88	74.01	42.40
	Non-road	74	1274	94.51		
	User Accuracy (%)	85.20	70.89			

Table 9.3 Accuracy assessment of road extraction using various algorithms in Landsat-8 imagery

Algorithm	Landsat-8					
	Class	Road	Non-road	Producer Accuracy (%)	OA (%)	Kappa Index (%)
NREI	Road	402	285	58.51	83.32	56.90

SAM	Non-road	98	1512	93.91	75.57	41.50
	User Accuracy (%)	80.40	84.14			
	Road	376	437	46.24		
	Non-road	124	1360	91.64		
SID	User Accuracy (%)	75.20	75.68		72.92	35.10
	Road	345	467	42.48		
	Non-road	155	1330	89.56		
	User Accuracy (%)	69	74.01			
MF	Road	395	341	53.66	80.58	51.30
	Non-road	105	1456	93.27		
	User Accuracy (%)	79	81.02			
	Road	353	558	38.75		
SVM	Non-road	147	1239	89.39	70.60	30.50
	User Accuracy (%)	70.60	68.95			

Table 9.4 Accuracy assessment of road extraction using various algorithms in AVIRIS-NG imagery

Algorithm	AVIRIS-NG					
	Class	Road	Non-road	Producer Accuracy (%)	OA (%)	Kappa Index (%)
NREI	Road	485	102	82.62	94.90	85.90
	Non-road	15	1695	99.12		
	User Accuracy (%)	97	94.32			
SAM	Road	453	170	72.71	90.55	74.50
	Non-road	47	1627	97.19		
	User Accuracy (%)	90.60	90.54			
SID	Road	440	178	71.19	89.64	72.00
	Non-road	60	1619	96.42		
	User Accuracy (%)	88	90.09			
MF	Road	423	95	81.66	92.51	78.30

	Non-road	77	1702	95.67		
	User Accuracy (%)	84.60	94.71			
SVM	Road	469	148	76.01	93.80	78.90
	Non-road	31	1649	98.15		
	User Accuracy (%)	93.80	91.76			

Figure 9.10 depicts the comparison of various algorithms on the basis of sensor performance. Here, two measures are utilized for investigating the performance, which are OA and KI [22] [194]. It is observed from Figure 9.10 (a) and (b) that, AVIRIS-NG can prove to be effective for extraction of road surfaces in comparison to Sentinel-2B and Landsat-8 multispectral sensors. Further, Sentinel-2B appears to be better in comparison to Landsat-8.

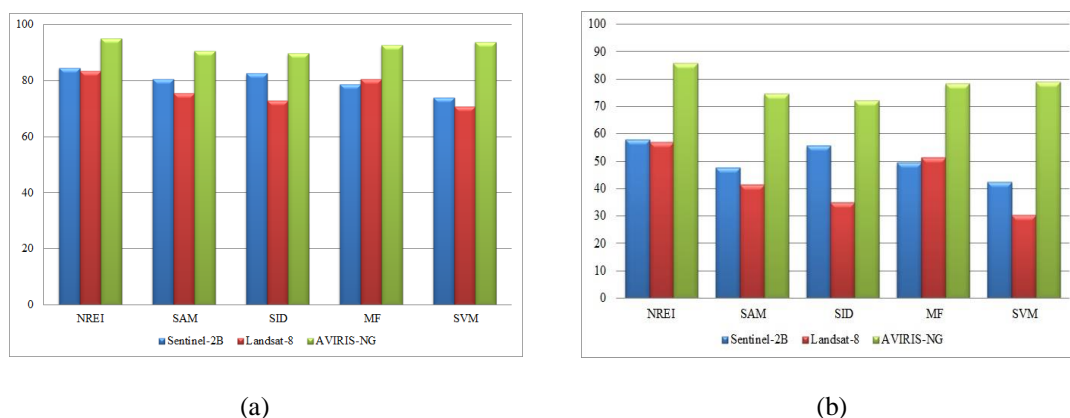


Figure 9.10 Comparison on the basis of sensor performance using (a) Overall Accuracy (b) Kappa Index

Figure 9.11 describes the performance of various algorithms in different sensor imageries using similar measures. It is observed from Figure 9.11 (a) that, proposed NREI can prove to be suitable for extraction of road surfaces in all the imageries while SID, MF and SVM show some better results in Sentinel-2B, Landsat-8 and AVIRIS-NG images, respectively, which are comparable with NREI. It is further investigated from Figure 9.11 (b) that, NREI produces better results for all the

imageries. As in previous case, here also, SID, MF and SVM show some better results in Sentinel-2B, Landsat-8 and AVIRIS-NG images, respectively. Further, the performance of all the algorithms is found to be satisfactory in case of AVIRIS-NG.

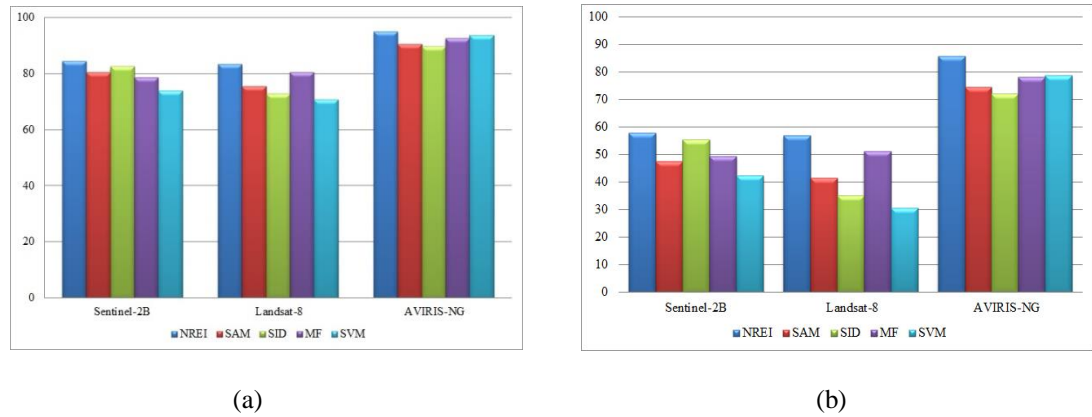


Figure 9.11 Comparison on the basis of different algorithms using (a) Overall Accuracy (b) Kappa Index

9.6.3.2 Roof surfaces

It is examined from Table 9.5 that, NBEI, SID and SAM produce an OA of 86.72 %, 84.59 % and 81.28 %, while OA of 79.23 % and 78.97 % are obtained in case of SVM and MF, respectively. Therefore, NBEI, SID and SAM are observed to be the effective approaches for extraction of roof surfaces in Sentinel-2B imagery. Further, in Landsat-8, NBEI and SAM extract roof surfaces with an OA of 82.45 % and 80.88 %, while OA of 77.10 %, 76.66 % and 75.53 % are obtained in case of SID, SVM and MF, respectively, as shown in Table 9.6. Thus, NBEI and SAM can prove to be the appropriate algorithms for extraction of roof surfaces in Landsat-8. Finally, in case of AVIRIS-NG imagery, NBEI, MF and SVM offer an OA of 95.43 %, 92.42 % and 90.33 %, while SAM and SID produce an OA of 88.59 % and 87.24 %, respectively, as shown in Table 9.7. Therefore, NBEI, MF and SVM are found to be the best suitable approaches for extraction of roof surfaces in AVIRIS-NG imagery,

while the performance of SAM and SID is also satisfactory. Further, the similar results have been obtained, when the analysis is carried out using KI as accuracy measure. Moreover, if a comparison is performed between different sensors, then it appears that AVIRIS-NG hyperspectral sensor can prove to be effective for extraction of roof surfaces in comparison to Sentinel-2B and Landsat-8 multispectral sensors. It may be due to narrower spectral bands of hyperspectral imagery in comparison to multispectral imageries. Also, Sentinel-2B imagery performed well in comparison to Landsat-8 for extraction of roof surfaces.

Table 9.5 Accuracy assessment of roof extraction using various algorithms in Sentinel-2B imagery

Algorithm	Sentinel-2B					
	Class	Roof	Non-roof	Producer Accuracy (%)	OA (%)	Kappa Index (%)
NBEI	Roof	453	226	66.17	86.72	66.00
	Non-roof	79	1539	95.11		
	User Accuracy (%)	85.15	87.12			
SAM	Roof	414	312	57.02	81.28	53.30
	Non-roof	118	1453	92.48		
	User Accuracy (%)	77.82	82.32			
SID	Roof	490	312	61.10	84.59	63.20
	Non-roof	42	1453	97.19		
	User Accuracy (%)	92.10	82.32			
MF	Roof	410	361	53.17	78.97	48.90
	Non-roof	122	1404	92.00		
	User Accuracy (%)	77.06	79.54			
SVM	Roof	304	249	54.97	79.23	42.40
	Non-roof	228	1516	86.92		
	User Accuracy (%)	57.14	85.89			

Table 9.6 Accuracy assessment of roof extraction using various algorithms in Landsat-8 imagery

Algorithm	Landsat-8					
	Class	Roof	Non-roof	Producer Accuracy (%)	OA (%)	Kappa Index (%)
NBEI	Roof	316	187	62.82	82.45	49.80
	Non-roof	216	1578	87.96		
	User Accuracy (%)	59.39	89.40			
SAM	Roof	373	280	57.12	80.88	50.30
	Non-roof	159	1485	90.32		
	User Accuracy (%)	57.33	89.40			
SID	Roof	361	355	50.41	77.10	42.60
	Non-roof	171	1410	89.18		
	User Accuracy (%)	67.85	79.88			
MF	Roof	305	335	47.65	75.53	35.80
	Non-roof	227	1430	86.30		
	User Accuracy (%)	57.33	81.02			
SVM	Roof	317	321	49.68	76.66	38.70
	Non-roof	215	1444	87.04		
	User Accuracy (%)	59.58	81.81			

Table 9.7 Accuracy assessment of roof extraction using various algorithms in AVIRIS-NG imagery

Algorithm	AVIRIS-NG					
	Class	Roof	Non-roof	Producer Accuracy (%)	OA (%)	Kappa Index (%)
NBEI	Roof	512	85	85.76	95.43	87.70
	Non-roof	20	1680	98.82		
	User Accuracy (%)	96.24	95.18			
SAM	Roof	503	233	68.34	88.59	71.70
	Non-roof	29	1532	98.14		

	User Accuracy (%)	94.54	86.79			
	Roof	495	256	65.91		
SID	Non-roof	37	1509	97.60	87.24	68.70
	User Accuracy (%)	93.04	85.49			
	Roof	477	119	80.03		
MF	Non-roof	55	1646	96.76	92.42	79.60
	User Accuracy (%)	89.66	93.25			
	Roof	498	188	72.59		
SVM	Non-roof	34	1577	97.89	90.33	75.30
	User Accuracy (%)	93.60	89.34			

Figure 9.12 describes the comparison of various algorithms based on the sensor performance. It appears from Figure 9.12 (a) and (b) that all the algorithms have been performed well in AVIRIS-NG imagery for extraction of roof surfaces. Further, Sentinel-2B is investigated to be a better sensor in comparison to Landsat-8 for extraction of rooftops. It is also examined that OA is not perfectly able to differentiate between all the sensors but KI did the same very well.

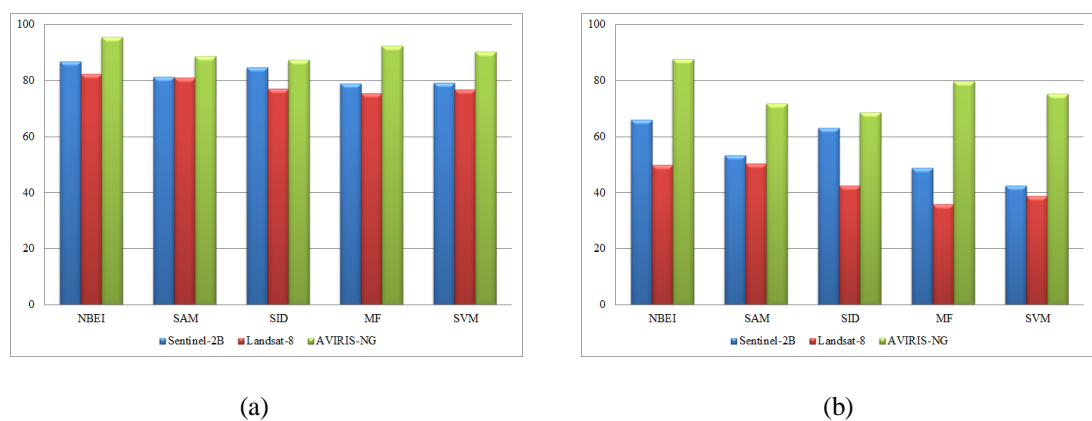


Figure 9.12 Comparison on the basis of sensor performance using (a) Overall Accuracy (b) Kappa Index

Figure 9.13 depicts the performance of various algorithms in different sensor imageries using similar measures. It is examined from Figure 9.13 (a) that, proposed NBEI can prove be an effective algorithm for extraction of roof surfaces in all the imageries, while SID, SAM and MF produce some better results in Sentinel-2B, Landsat-8 and AVIRIS-NG imageries, respectively, which are almost similar to NBEI. The performance of rest of the algorithms is satisfactory in AVIRIS-NG imagery, while better in Sentinel-2B and average in Landsat-8. Further, when the analysis is carried out using KI, the similar results are obtained as found using OA, but the differentiation between all the algorithms are clearly observed, as shown in Figure 9.13 (b).

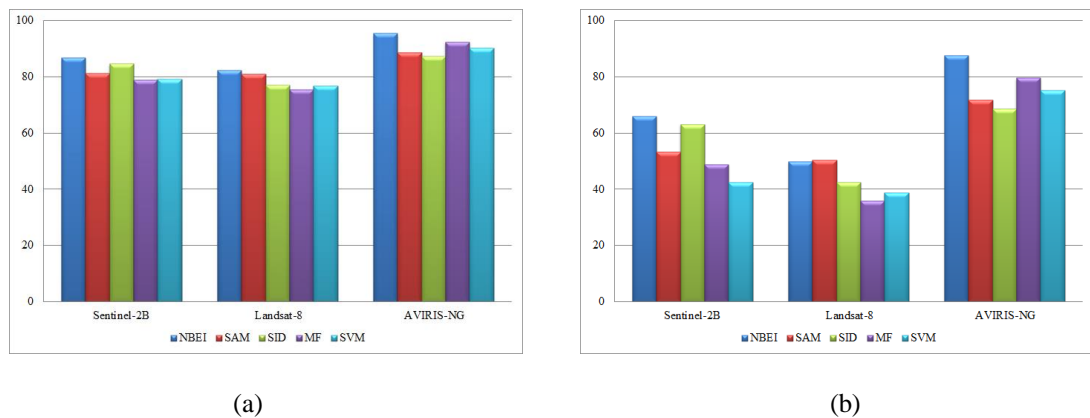


Figure 9.13 Comparison on the basis of different algorithms using (a) Overall Accuracy (b) Kappa Index

It can be deduced from the overall analysis that, in extraction of road and roof surfaces, as the number of spectral bands of remote sensing imagery increases, the separability between different classes can be increased by proper selection of dimensionality reduction and band selection algorithms. The increase in separability increases the target detection rate and decreases the false alarm rate and therefore enhances the accuracy. Moreover, due to coarse spatial resolution Landsat-8, there may be the maximum chances of overlapping with other background classes, while

in medium resolution Sentinel-2B, chances of mixing of target and background may be less. Similarly, in fine resolution AVIRIS-NG, the mixing may be the least. Therefore, AVIRIS-NG can prove to be effective for extraction of road and roof surfaces, while Sentinel-2B may be a better choice than Landsat-8. If we compare the extraction results of road and roof surfaces, then higher OA and KI are obtained in all the algorithms used for extraction of roof surfaces in comparison to approaches used for road extraction in all the imageries. It may be due to higher brightness and tonal variation of roof surfaces, while low tone road surfaces are generally confused with water, shadow and wet soil [195] [196]. Further, in case of roof surfaces, there may be the maximum chances of occupancy inside the spatially fine, medium and coarse resolution pixels due to their clustered behavior [197] [198] [199], while in case of road surfaces, chances of occupancy inside the pixels of aforesaid resolution may be less due to un-even dimensionality or non-clustered behavior, which results in high mixing of roads with non-road background [200] [201] [202].

Table 9.8 and 9.9 describe the overall performance of all the sensor imageries and algorithms using different categories. These are divided into three different groups, which are best ($OA > 90\%$ and $KI > 75\%$), better ($80\% < OA < 90\%$ and $55\% < KI < 75\%$) and moderate ($OA < 80\%$ and $KI < 55\%$). Table 9.8 describes the performance on the basis of OA while Table 9.9 depicts the same on the basis of KI. It can be observed from Table 9.8 and 9.9 that best roads and roofs extraction results are obtained only in case of AVIRIS-NG imagery. NREI, MF and SVM can prove to be the best approaches for extraction of road surfaces in AVIRIS-NG, while SAM and SID may produce better extraction results. Similarly, NBEI, MF and SVM are found to be the best algorithms for extraction of roofs in AVIRIS-NG imagery with some better performance in case of SAM and SID. Further, if a comparison is carried

out on the basis of OA and KI both, NREI can prove to be effective for extraction of roads in Landsat-8. Next, OA makes NBEI and SAM to be the better algorithms for extraction of roof surfaces in Landsat-8 imagery while KI put all the algorithms in the moderate category. Finally, NREI and SID can prove to be efficient for extraction of road surfaces followed by NBEI and SID for roofs in Sentinel-2B imagery.

Table 9.8 Performance of various algorithms in different sensor imageries on the basis of overall accuracy

	Sensor imagery	Best	Better	Moderate
		(>90 %)	(80-90 %)	(<80 %)
Road Extraction	Sentinel-2B		NREI, SAM, SID	MF, SVM
	Landsat-8		NREI, MF	SAM, SID, SVM
	AVIRIS-NG	NREI, SAM, MF, SVM	SID	
Roof Extraction	Sentinel-2B		NBEI, SAM, SID	MF, SVM
	Landsat-8		NBEI, SAM	SID, MF, SVM
	AVIRIS-NG	NBEI, MF, SVM	SAM, SID	

Table 9.9 Performance of various algorithms in different sensor imageries on the basis of kappa index

	Sensor imagery	Best	Better	Moderate
		(>75 %)	(55-75 %)	(<55%)
Road Extraction	Sentinel-2B		NREI, SID	SAM, MF, SVM
	Landsat-8		NREI	SAM, SID, MF, SVM
	AVIRIS-NG	NREI, MF, SVM	SAM, SID	
	Sentinel-2B		NBEI, SID	SAM, MF, SVM

Roof	Landsat-8	NBEI, SAM, SID,	
Extraction		MF, SVM	
	AVIRIS-NG	NBEI, MF,	SAM, SID
		SVM	

9.7 Summary

This study has been carried out with performance evaluation and a comparative assessment of various multispectral and hyperspectral sensors, used for extraction of road and roof surfaces in respective imageries using various algorithms. Sentinel-2B and Landsat-8 imageries have been used as multispectral with 13 and 7 bands, while AVIRIS-NG as hyperspectral with 380 narrow bands, respectively. Further, along with comparative assessment of different sensor's performance, a comparative analysis has also been performed between different algorithms used for extraction of road and roof surfaces in all the aforesaid imageries. In view, two spectral indices named as NREI and NBEI have been proposed for extraction of road and roof surfaces, respectively. Moreover, existing angle, information, filtering and machine learning based approaches i.e. SAM, SID, MF and SVM, have been used for extraction of road and roof surfaces both.

The results of the study suggested that, due to narrower spectral bands and fine spatial resolution of AVIRIS-NG sensor, it can be possible to extract the minute details from the imagery in terms of built-up surfaces and sub-surfaces at different levels. Therefore, best extraction results of road and roof surfaces have been produced in case of AVIRIS-NG in comparison to Sentinel-2B and Landsat-8 multispectral sensors. Further, the overall performance of Sentinel-2B has been found to be superior in comparison to Landsat-8 for extraction of road and roof surfaces. Next, when a comparison has been carried out between various approaches

used for extraction of road and roof surfaces in different imageries, then it was observed that NREI, MF and SVM generate excellent results for extraction of roads, while SAM and SID were found to be superior algorithms in AVIRIS-NG imagery. Moreover, for extraction of roofs in the same imagery, only NBEI replaced NREI. Further, NREI and MF were found to be suitable for extraction of roads followed by NBEI and SAM for extraction of roofs in Landsat-8. Finally, NREI, SAM and SID were investigated as better approaches for extraction of road surfaces, while NBEI, SAM and SID for roofs in Sentinel-2B imagery.

Chapter 10

Conclusions and Contributions

In this research, the detection and identification of engineered or built-up surfaces have been carried out under four different objectives using imaging spectrometry:

- i. The first objective deals with the creation of a spectral library of urban built-up surfaces and materials, and analysis of spectral signatures of these surfaces and materials.
- ii. The second objective of the research has been carried out under four different sub-objectives:
 - a. In first sub-objective, three new spectral indices i.e. NII, RDI, and NREI have been proposed for detection of built-up (Level-1), road and roof surfaces (Level-2), respectively.
 - b. In second sub-objective, two new spectral indices are introduced, in which CI-Road is utilized for condition analysis of road surfaces while DI-Roof is used for deterioration analysis of roof surfaces.
 - c. The third sub-objective utilizes existing built-up indices for detection of urban built-up surfaces in the first level followed by its subcategories in the second level.
 - d. Finally, extraction of impervious or engineered surfaces has been carried out using index based RGB and NIR band combinations in AVIRIS-NG imagery.
- iii. In the third objective, a new method is proposed, in which different combinations of feature bands have been created for extraction of built-up surfaces, sub-surfaces and materials in different levels (Level-1, 2 and 3).

- iv. The final objective of the research presented a performance evaluation of Sentinel-2B, Landsat-8 multispectral, and AVIRIS-NG hyperspectral imageries for extraction of road and roof surfaces using proposed spectral index based, and other conventional algorithms.

This chapter highlights the conclusion drawn from this research based on theoretical or experimental contributions made, research contribution and the limitations.

10.1 Conclusions

Several important conclusions appear to emerge from the research, which are:

- i. The spectral analysis of built-up surfaces and materials using hyperspectral data suggests that, these surfaces and materials can be extracted by identifying various significant wavelengths in different spectral regions of a particular built-up class. These wavelengths are identified based on the different major absorption features. The absorption features have been calculated using various statistical parameters such as relative depth, area of absorption, and asymmetry factor.
- ii. The proposed spectral indices NII, RDI, and NREI show an overall average accuracy of 96.12 %, 92.24 %, and 94.77 %, respectively, which is higher than all the other existing built-up indices. These indices have been found to be effective in extraction of built-up surfaces (Level-1 and 2) in comparison to existing indices. The quantification of built-up surfaces and its subclasses using aforesaid indices have also been carried out. The quantification results suggest that, the proposed indices can prove to be effective in estimation of built-up surfaces of different levels. Similarly, these indices have shown their effectiveness in

separating built-up surfaces from soil as well as roads and roofs, when compared with other existing indices.

iii. The comparison of proposed road condition index CI-Road and roof deterioration index DI-Roof results with MESMA unmixing suggests that indices results may outperform MESMA, which may be due to more geographical variability of endmembers and model complexity of MESMA algorithm.

iv. The existing BSI, NBI, and BAEI can prove to be effective in extraction of built-up surfaces with an overall accuracy (OA) of 93.89 %, 90.11 %, and 85.15 %, respectively. Further, REI with OA of 94.40 % appears to be suitable for extraction of road surfaces while NBAI with 95 % OA appears to be effective in extraction of rooftops in AVIRIS-NG imagery. It is also concluded that, for aforesaid indices, built-up surfaces (Level-1 and 2) can be effectively separated from the bare soil in hyperspectral imagery with slight confusion between road and roof surfaces.

v. It is observed that, index based Green-NIR band combination generates better inter-class separability with an OA of 95.20 %, Blue-NIR produces moderate OA as 90.20 % while least OA as 80.20 % is obtained for Red-NIR.

vi. It is observed that, the combined form of thematic spectral index, fractional abundance and major principal component based features generate better extraction results of built-up surfaces, sub-surfaces and materials. It has also been examined that, in case of combined form of all the features, detection rate is high with less false alarm for most of the built-up classes. Further, combination of spectral index and fractional abundance can prove to be effective when compare with combined form of spectral index and major principal component.

vii. The performance of imageries obtained from AVIRIS-NG sensor is found to be the best in comparison to Sentinel-2B and Landsat-8 multispectral sensors while Sentinel-2B performed better in comparison to Landsat-8 in extraction of road and roof surfaces. The comparison of various algorithms suggests that, proposed NREI, NBEI, and existing MF, and SVM produce best results for extraction of road and roof surfaces, while SAM and SID are superior algorithms for extraction of both the surfaces in AVIRIS-NG imagery. Further, NREI and MF are performed well for extraction of roads followed by NBEI and SAM for roofs in Landsat-8. Finally, NREI, SAM, and SID are found to be efficient for extraction of roads subsequently NBEI, SAM, and SID for roofs in Sentinel-2B imagery.

10.2 Research contributions

The outcome of this research by way of several experiments discussed in this thesis lead to the following major contributions:

- i. This research deals with the creation of a spectral library of urban built-up surfaces and materials for Indian Regions and reveals its applications in the analysis of urban surfaces. Field measurement has been carried out by using Spectroradiometer over the wavelength range of 350 to 2500 nm. Further, this research investigates the unique spectral characteristics and complexity of heterogeneous urban environments using spectral signatures of major urban built-up surfaces and materials in Indian regions.
- ii. In this research, three new spectral indices i.e. NII, RDI, and NREI have been developed for detection of built-up (Level-1), road and roof surfaces (Level-2), respectively, followed by a separability analysis between spectrally confused

urban land cover classes. Further, this research explores the most significant spectral bands in AVIRIS-NG hyperspectral imagery for detection of built-up surfaces and its subclasses i.e. roads and roofs.

iii. In this research, condition analysis of road surfaces and deterioration analysis of roof surfaces have been carried out using AVIRIS-NG image and field hyperspectral data. Various significant bands are identified using spectral characteristics of roads and roofs of different condition and deterioration, respectively. Accordingly, two new spectral indices are introduced, in which CI-Road is utilized for condition analysis of road surfaces while DI-Roof is used for deterioration analysis of roof surfaces.

iv. In this research, existing multispectral built-up indices have been applied on AVIRIS-NG imagery for detection of urban built-up surfaces in the first level followed by its subcategories in the second level. Finally, a separability analysis between spectrally mixed urban land cover classes using various measures is also addressed.

v. In this research, a new method is proposed, in which different combinations of knowledge based features have been utilized for extraction of built-up surfaces, sub-surfaces and materials in different levels (Level-1, 2 and 3) using AVIRIS-NG hyperspectral imagery. Features identified in this study are based on spectral indices, major principal components and fractional abundances, in which first combination is developed using spectral indices and fractional abundances while second is made using spectral indices and major principal components and finally third using combination of all the aforesaid features.

vi. Finally, this research presented a performance evaluation of Sentinel-2B, Landsat-8 multispectral, and AVIRIS-NG hyperspectral imageries for extraction

of road and roof surfaces using proposed spectral index based, and other conventional algorithms. The NREI and NBEI are developed for extraction of road and roof surfaces, respectively. Moreover, existing SAM, SID, MF, and SVM are utilized as angle, information, filtering, and machine learning based algorithms, respectively, for detection of both the surfaces.

10.3 Limitations

The limitation of this research is that it has not considered the effect of water in the urban environment, as water has already been masked in the preprocessing stage. The seasonal sensitivity has also not been considered for the extraction of built-up surfaces and its subcategories.

Chapter 11

Future Scope

This chapter explains the future scope of this research, which may be carried out to further extend the work of this research.

11.1 Future scope of the research

In this research, the extraction of built-up surfaces has been performed in first level, roads and roofs in the second level followed by sub-categories of roads such as bitumen road and concrete pavement as well as sub-classes of roofs such as concrete and metallic roofs, in third level of detection. Further research may be carried out to develop the built-up spectral indices for the detection of sub-classes of built-up surfaces in the fourth level with their condition and deterioration analysis using narrower bands AVIRIS-NG hyperspectral imagery. In future, the development of spectral indices may also be carried by considering the effect of water, and seasonal sensitivity in the image and field data.

Overall, the findings of this research would also raise awareness about the differences between Sentinel-2B, Landsat-8 multispectral sensors as well as AVIRIS-NG hyperspectral sensor. This study may be further carried out by utilizing sensors with similar spectral and spatial characteristics, such as SPOT, ETM+, ASTER and Hyperion. It would be supportive to the seamless integration of historical remote sensing images, and to build long term time series for dynamic monitoring in a synergistic scientific application based on more than one remote sensor.

References

- [1]. Weng, Q., 2001. Modeling urban growth effects on surface runoff with the integration of remote sensing and GIS. *Environmental management*, 28(6), pp.737-748.
- [2]. Conway, T.M., 2007. Built-up surface as an indicator of pH and specific conductance in the urbanizing coastal zone of New Jersey, USA. *Journal of environmental management*, 85(2), pp.308-316.
- [3]. Xu, H., 2008. A new index for delineating built-up land features in satellite imagery. *International Journal of Remote Sensing*, 29(14), pp.4269-4276.
- [4]. Weng, Q., Hu, X. and Lu, D., 2008. Extracting impervious surfaces from medium spatial resolution multispectral and hyperspectral imagery: a comparison. *International Journal of Remote Sensing*, 29(11), pp.3209-3232.
- [5]. Weng, Q., 2012. Remote sensing of impervious surfaces in the urban areas: Requirements, methods, and trends. *Remote Sensing of Environment*, 117, pp.34-49.
- [6]. Heiden, U., Segl, K., Roessner, S. and Kaufmann, H., 2007. Determination of robust spectral features for identification of urban surface materials in hyperspectral remote sensing data. *Remote Sensing of Environment*, 111(4), pp.537-552.
- [7]. Kavzoglu, T., Sen, Y.E. and Cetin, M., 2009. Mapping urban road infrastructure using remotely sensed images. *International Journal of Remote Sensing*, 30(7), pp.1759-1769.
- [8]. Manolakis, D. and Shaw, G., 2002. Detection algorithms for hyperspectral imaging applications. *IEEE signal processing magazine*, 19(1), pp.29-43.
- [9]. Mohapatra, R.P. and Wu, C., 2010. High resolution Built-up surface estimation. *Photogrammetric Engineering & Remote Sensing*, 76(12), pp.1329-1341.
- [10]. Goetz, A.F., Vane, G., Solomon, J.E. and Rock, B.N., 1985. Imaging spectrometry for earth remote sensing. *Science*, 228(4704), pp.1147-1153.
- [11]. Curran, P.J., 1994. Imaging spectrometry. *Progress in physical Geography*, 18(2), pp.247-266.
- [12]. Kumar, L., Schmidt, K., Dury, S. and Skidmore, A., 2002. Imaging spectrometry and vegetation science. In *Imaging spectrometry* (pp. 111-155). Springer, Dordrecht.

- [13]. Dozier, J., Green, R.O., Nolin, A.W. and Painter, T.H., 2009. Interpretation of snow properties from imaging spectrometry. *Remote Sensing of Environment*, 113, pp.S25-S37.
- [14]. Yan, R., Peng, J., Ma, D. and Wen, D., 2019. Spectral Tensor Synthesis Analysis for Hyperspectral Image Spectral–Spatial Feature Extraction. *Journal of the Indian Society of Remote Sensing*, 47(1), pp.91-100.
- [15]. Slonecker, E.T., Jennings, D.B. and Garofalo, D., 2001. Remote sensing of impervious surfaces: A review. *Remote Sensing Reviews*, 20(3), pp.227-255.
- [16]. Arnold Jr, C.L. and Gibbons, C.J., 1996. Impervious surface coverage: the emergence of a key environmental indicator. *Journal of the American planning Association*, 62(2), pp.243-258.
- [17]. Schueler, T.R., Fraley-McNeal, L. and Cappiella, K., 2009. Is impervious cover still important? Review of recent research. *Journal of Hydrologic Engineering*, 14(4), pp.309-315.
- [18]. Brun, S.E. and Band, L.E., 2000. Simulating runoff behavior in an urbanizing watershed. *Computers, Environment and Urban Systems*, 24(1), pp.5-22.
- [19]. Hurd, J.D. and Civco, D.L., 2004, May. Temporal characterization of impervious surfaces for the State of Connecticut. In *ASPRS Annual Conference Proceedings*, Denver, Colorado.
- [20]. Gillies, R.R., Box, J.B., Symanzik, J. and Rodemaker, E.J., 2003. Effects of urbanization on the aquatic fauna of the Line Creek watershed, Atlanta—a satellite perspective. *Remote sensing of environment*, 86(3), pp.411-422.
- [21]. Yang, L., Xian, G., Klaver, J.M. and Deal, B., 2003. Urban land-cover change detection through sub-pixel built-upness mapping using remotely sensed data. *Photogrammetric Engineering & Remote Sensing*, 69(9), pp.1003-1010.
- [22]. Lu, D. and Weng, Q., 2007. A survey of image classification methods and techniques for improving classification performance. *International journal of Remote sensing*, 28(5), pp.823-870.
- [23]. Weng, Q. and Quattrochi, D.A. eds., 2018. *Urban remote sensing*. CRC press.
- [24]. Praskievicz, S. and Chang, H., 2009. A review of hydrological modelling of basin-scale climate change and urban development impacts. *Progress in Physical Geography*, 33(5), pp.650-671.
- [25]. Xu, H., 2010. Analysis of impervious surface and its impact on urban heat environment using the normalized difference impervious surface index (NDISI). *Photogrammetric Engineering & Remote Sensing*, 76(5), pp.557-565.

- [26]. Kerekes, J.P., Ludgate, K., Giannandrea, A., Raqueno, N.G. and Goldberg, D.S., 2013, May. SHARE 2012: subpixel detection and unmixing experiments. In Algorithms and Technologies for Multispectral, Hyperspectral, and Ultraspectral Imagery XIX (Vol. 8743, p. 87430H). International Society for Optics and Photonics.
- [27]. Giannandrea, A., Raqueno, N., Messinger, D.W., Faulring, J., Kerekes, J.P., van Aardt, J., Canham, K., Hagstrom, S., Ontiveros, E., Gerace, A. and Kaufman, J., 2013, May. The SHARE 2012 data campaign. In Algorithms and Technologies for Multispectral, Hyperspectral, and Ultraspectral Imagery XIX (Vol. 8743, p. 87430F). International Society for Optics and Photonics.
- [28]. Roberts, D.A. and Herold, M., 2004. Imaging spectrometry of urban materials. *Infrared Spectroscopy in Geochemistry, Exploration and Remote Sensing*, Mineral Association of Canada, Short Course Series, 33, pp.155-181.
- [29]. Herold, M., Gardner, M.E. and Roberts, D.A., 2003. Spectral resolution requirements for mapping urban areas. *IEEE Transactions on Geoscience and remote sensing*, 41(9), pp.1907-1919.
- [30]. Herold, M., Roberts, D.A., Gardner, M.E. and Dennison, P.E., 2004. Spectrometry for urban area remote sensing—Development and analysis of a spectral library from 350 to 2400 nm. *Remote Sensing of Environment*, 91(3-4), pp.304-319.
- [31]. Roessner, S., Segl, K., Heiden, U. and Kaufmann, H., 2001. Automated differentiation of urban surfaces based on airborne hyperspectral imagery. *IEEE Transactions on Geoscience and Remote sensing*, 39(7), pp.1525-1532.
- [32]. Andreou, C., Karathanassi, V. and Kolokoussis, P., 2011. Investigation of hyperspectral remote sensing for mapping asphalt road conditions. *International journal of remote sensing*, 32(21), pp.6315-6333.
- [33]. Ben-Dor, E., Levin, N. and Saaroni, H., 2001. A spectral based recognition of the urban environment using the visible and near-infrared spectral region (0.4-1.1 μm). A case study over Tel-Aviv, Israel. *International Journal of Remote Sensing*, 22(11), pp.2193-2218.
- [34]. Mueller, M., Segl, K., Heiden, U. and Kaufmann, H., 2006. Potential of high-resolution satellite data in the context of vulnerability of buildings. *Natural hazards*, 38(1-2), pp.247-258.
- [35]. Milton, E.J., Schaepman, M.E., Anderson, K., Kneubühler, M. and Fox, N., 2009. Progress in field spectroscopy. *Remote Sensing of Environment*, 113, pp.S92-S109.

- [36]. Herold, M. and Roberts, D.A., 2010. The spectral dimension in urban remote sensing. In *Remote sensing of urban and suburban areas* (pp. 47-65). Springer, Dordrecht.
- [37]. Abebe, G.A., 2013. Quantifying urban growth pattern in developing countries using remote sensing and spatial metrics: A case study in Kampala, Uganda (p. 108). University of Twente Faculty of Geo-Information and Earth Observation (ITC).
- [38]. Wan, Z., Ng, D. and Dozier, J., 1994. Spectral emissivity measurements of land-surface materials and related radiative transfer simulations. *Advances in Space Research*, 14(3), pp.91-94.
- [39]. Heiden, U., Roessner, S., Segl, K. and Kaufmann, H., 2001, November. Analysis of spectral signatures of urban surfaces for their identification using hyperspectral HyMap data. In *IEEE/ISPRS Joint Workshop on Remote Sensing and Data Fusion over Urban Areas* (Cat. No. 01EX482) (pp. 173-177). IEEE.
- [40]. Nasarudin, N.E.M. and Shafri, H.Z.M., 2011. Development and utilization of urban spectral library for remote sensing of urban environment. *Journal of Urban and Environmental Engineering*, 5(1), pp.44-56.
- [41]. Kotthaus, S., Smith, T.E., Wooster, M.J. and Grimmond, C.S.B., 2014. Derivation of an urban materials spectral library through emittance and reflectance spectroscopy. *ISPRS Journal of Photogrammetry and Remote Sensing*, 94, pp.194-212.
- [42]. Baldridge, A.M., Hook, S.J., Grove, C.I. and Rivera, G., 2009. The ASTER spectral library version 2.0. *Remote Sensing of Environment*, 113(4), pp.711-715.
- [43]. Kokaly, R.F., Clark, R.N., Swayze, G.A., Livo, K.E., Hoefen, T.M., Pearson, N.C., Wise, R.A., Benzel, W.M., Lowers, H.A., Driscoll, R.L. and Klein, A.J., 2017. *Usgs spectral library version 7 data: Us geological survey data release*. United States Geological Survey (USGS): Reston, VA, USA.
- [44]. Sobrino, J.A., Oltra-Carrió, R., Jiménez-Muñoz, J.C., Julien, Y., Soria, G., Franch, B. and Mattar, C., 2012. Emissivity mapping over urban areas using a classification-based approach: Application to the Dual-use European Security IR Experiment (DESIREX). *International Journal of Applied Earth Observation and Geoinformation*, 18, pp.141-147.
- [45]. Ilebag, R., Schenk, A., Huang, Y. and Hinz, S., 2019. KLUM: An Urban VNIR and SWIR Spectral Library Consisting of Building Materials. *Remote Sensing*, 11(18), p.2149.

- [46]. Swayze, G., Clark, R.N., Kruse, F., Sutley, S. and Gallagher, A., 1992. Ground-truthing AVIRIS mineral mapping at Cuprite, Nevada.
- [47]. Van Der Meer, F., 2004. Analysis of spectral absorption features in hyperspectral imagery. *International journal of applied earth observation and geoinformation*, 5(1), pp.55-68.
- [48]. Mulder, V.L., De Bruin, S., Schaepman, M.E. and Mayr, T.R., 2011. The use of remote sensing in soil and terrain mapping—A review. *Geoderma*, 162(1-2), pp.1-19.
- [49]. Hu, X. and Weng, Q., 2009. Estimating Built-up surfaces from medium spatial resolution imagery using the self-organizing map and multi-layer perceptron neural networks. *Remote Sensing of Environment*, 113(10), pp.2089-2102.
- [50]. Du, Z., Li, W., Zhou, D., Tian, L., Ling, F., Wang, H., Gui, Y. and Sun, B., 2014. Analysis of Landsat-8 OLI imagery for land surface water mapping. *Remote sensing letters*, 5(7), pp.672-681.
- [51]. Gong, C. and Wu, W., 2014. Comparisons of regression tree models for sub-pixel built-upness estimation in a Gulf Coast city of Mississippi, USA. *International journal of remote sensing*, 35(10), pp.3722-3740.
- [52]. Dennison, P.E. and Roberts, D.A., 2003. Endmember selection for multiple endmember spectral mixture analysis using endmember average RMSE. *Remote sensing of environment*, 87(2-3), pp.123-135.
- [53]. Lu, D. and Weng, Q., 2006. Spectral mixture analysis of ASTER images for examining the relationship between urban thermal features and biophysical descriptors in Indianapolis, Indiana, USA. *Remote Sensing of Environment*, 104(2), pp.157-167.
- [54]. Powell, R.L., Roberts, D.A., Dennison, P.E. and Hess, L.L., 2007. Sub-pixel mapping of urban land cover using multiple endmember spectral mixture analysis: Manaus, Brazil. *Remote sensing of environment*, 106(2), pp.253-267.
- [55]. Somers, B., Asner, G.P., Tits, L. and Coppin, P., 2011. Endmember variability in spectral mixture analysis: A review. *Remote Sensing of Environment*, 115(7), pp.1603-1616.
- [56]. Zare, A. and Ho, K.C., 2013. Endmember variability in hyperspectral analysis: Addressing spectral variability during spectral unmixing. *IEEE Signal Processing Magazine*, 31(1), pp.95-104.
- [57]. Deng, C. and Wu, C., 2012. BCI: A biophysical composition index for remote sensing of urban environments. *Remote Sensing of Environment*, 127, pp.247-259.

- [58]. Kawamura, M., Jayamana, S., Tsujiko, Y., 1996. Relation between social and environmental conditions in Colombo Sri Lanka and the urban index estimated by satellite remote sensing data. *Int. Arch. Photogramm. Remote Sens.*, 31, pp. 321–326.
- [59]. Zha, Y., Gao, J. and Ni, S., 2003. Use of normalized difference built-up index in automatically mapping urban areas from TM imagery. *International journal of remote sensing*, 24(3), pp.583-594.
- [60]. He, C., Shi, P., Xie, D. and Zhao, Y., 2010. Improving the normalized difference built-up index to map urban built-up areas using a semiautomatic segmentation approach. *Remote Sensing Letters*, 1(4), pp.213-221.
- [61]. Jieli, C., Manchun, L.I., Yongxue, L.I.U., Chenglei, S. and Wei, H.U., 2010, June. Extract residential areas automatically by new built-up index. In 2010 18th International Conference on Geoinformatics (pp. 1-5). IEEE.
- [62]. Waqar, M.M., Mirza, J.F., Mumtaz, R. and Hussain, E., 2012. Development of new indices for extraction of built-up area & bare soil from landsat data. *Open Access Scientific Reports*, 1(1), pp.01-04.
- [63]. Stathakis, D., Perakis, K. and Savin, I., 2012. Efficient segmentation of urban areas by the VIBI. *International journal of remote sensing*, 33(20), pp.6361-6377.
- [64]. Bhatti, S.S. and Tripathi, N.K., 2014. Built-up area extraction using Landsat 8 OLI imagery. *GIScience & remote sensing*, 51(4), pp.445-467.
- [65]. Liu, Y., Chen, J., Cheng, W., Sun, C., Zhao, S. and Pu, Y., 2014. Spatiotemporal dynamics of the urban sprawl in a typical urban agglomeration: a case study on Southern Jiangsu, China (1983–2007). *Frontiers of earth science*, 8(4), pp.490-504.
- [66]. Bouzekri, S., Lasbet, A.A. and Lachehab, A., 2015. A new spectral index for extraction of built-up area using Landsat-8 data. *Journal of the Indian Society of Remote Sensing*, 43(4), pp.867-873.
- [67]. Shahi, K., Shafri, H.Z., Taherzadeh, E., Mansor, S. and Muniandy, R., 2015. A novel spectral index to automatically extract road networks from WorldView-2 satellite imagery. *The Egyptian Journal of Remote Sensing and Space Science*, 18(1), pp.27-33.

- [68]. Sinha, P., Verma, N.K. and Ayele, E., 2016. Urban built-up area extraction and change detection of Adama municipal area using time-series Landsat images. *Int. J. Adv. Remote Sens. GIS*, 5(8), pp.1886-1895.
- [69]. Sameen, M.I. and Pradhan, B., 2016, June. A novel built-up spectral index developed by using multiobjective particle-swarm-optimization technique. In *IOP Conference Series: Earth and Environmental Science* (Vol. 37, No. 1, p. 012006). IOP Publishing.
- [70]. Sun, G., Chen, X., Jia, X., Yao, Y. and Wang, Z., 2016. Combinational build-up index (CBI) for effective Built-up surface mapping in urban areas. *IEEE Journal of Selected Topics in Applied Earth Observations and Remote Sensing*, 9(5), pp.2081-2092.
- [71]. Gu, L., Cao, Q. and Ren, R., 2018. Building extraction method based on the spectral index for high-resolution remote sensing images over urban areas. *Journal of Applied Remote Sensing*, 12(4), p.045501.
- [72]. Bouhennache, R., Bouden, T., Taleb-Ahmed, A. and Cheddad, A., 2019. A new spectral index for the extraction of built-up land features from Landsat 8 satellite imagery. *Geocarto International*, 34(14), pp.1531-1551.
- [73]. Firozjaei, M.K., Sedighi, A., Kiavarz, M., Qureshi, S., Haase, D. and Alavipanah, S.K., 2019. Automated Built-Up Extraction Index: A New Technique for Mapping Surface Built-Up Areas Using LANDSAT 8 OLI Imagery. *Remote Sensing*, 11(17), p.1966.
- [74]. Mhangara, P., Odindi, J., Kleyn, L. and Remas, H., 2011. Road extraction using object oriented classification. *Visualisation Technical*, pp.45-50.
- [75]. Estoque, R.C. and Murayama, Y., 2015. Classification and change detection of built-up lands from Landsat-7 ETM+ and Landsat-8 OLI/TIRS imageries: A comparative assessment of various spectral indices. *Ecological Indicators*, 56, pp.205-217.
- [76]. Huete, A., 1988. Huete, AR A soil-adjusted vegetation index (SAVI). *Remote Sensing of Environment. Remote sensing of environment*, 25, pp.295-309.
- [77]. Han-Qiu, X.U., 2005. A study on information extraction of water body with the modified normalized difference water index (MNDWI). *Journal of remote sensing*, 5, pp.589-595.
- [78]. Xu, H., Ding, F. and Wen, X., 2009. Urban expansion and heat island dynamics in the Quanzhou region, China. *IEEE Journal of selected topics in applied earth observations and remote sensing*, 2(2), pp.74-79.

- [79]. Zhang, S., Yang, K., Li, M., Ma, Y. and Sun, M., 2018. Combinational biophysical composition index (CBCI) for effective mapping biophysical composition in urban areas. *IEEE Access*, 6, pp.41224-41237.
- [80]. Ridd, M.K., 1995. Exploring a VIS (vegetation-impervious surface-soil) model for urban ecosystem analysis through remote sensing: comparative anatomy for cities. *International journal of remote sensing*, 16(12), pp.2165-2185.
- [81]. Fan, F., Fan, W. and Weng, Q., 2015. Improving urban impervious surface mapping by linear spectral mixture analysis and using spectral indices. *Canadian Journal of Remote Sensing*, 41(6), pp.577-586.
- [82]. Zhuo, L., Zheng, J., Li, X., Wang, F., Ai, B. and Qian, J., 2008, November. A genetic algorithm based wrapper feature selection method for classification of hyperspectral images using support vector machine. In *Geoinformatics 2008 and Joint Conference on GIS and Built Environment: Classification of Remote Sensing Images* (Vol. 7147, p. 71471J). International Society for Optics and Photonics.
- [83]. Wieland, M. and Pittore, M., 2014. Performance evaluation of machine learning algorithms for urban pattern recognition from multi-spectral satellite images. *Remote Sensing*, 6(4), pp.2912-2939.
- [84]. Sun, G., Chen, X., Jia, X., Yao, Y. and Wang, Z., 2015. Combinational build-up index (CBI) for effective impervious surface mapping in urban areas. *IEEE Journal of selected topics in applied earth observations and remote sensing*, 9(5), pp.2081-2092.
- [85]. Hazaymeh, K., Mosleh, M.K. and Al-Rawabdeh, A.M., 2019. A Combined PCA-SIs Classification Approach for Delineating Built-up Area from Remote Sensing Data. *PFG–Journal of Photogrammetry, Remote Sensing and Geoinformation Science*, 87(3), pp.91-102.
- [86]. Xu, H., 2007. Extraction of urban built-up land features from Landsat imagery using a thematic oriented index combination technique. *Photogrammetric Engineering & Remote Sensing*, 73(12), pp.1381-1391.
- [87]. As-syakur, A., Adnyana, I., Arthana, I.W. and Nuarsa, I.W., 2012. Enhanced built-up and bareness index (EBBI) for mapping built-up and bare land in an urban area. *Remote Sensing*, 4(10), pp.2957-2970.

- [88]. Azmi, R., Alami, O.B., Saadane, A.E., Kacimi, I. and Chafiq, T., 2016. A modified and enhanced normalized built-up index using multispectral and thermal bands. *Indian J. Sci. Technol*, 9(28), pp.1-11.
- [89]. Gadal, S. and Ouerghemmi, W., 2019. Multi-level morphometric characterization of built-up areas and change detection in Siberian sub-arctic urban area: Yakutsk. *ISPRS International Journal of Geo-Information*, 8(3), p.129.
- [90]. Braun, M. and Herold, M., 2004, February. Mapping imperviousness using NDVI and linear spectral unmixing of ASTER data in the Cologne-Bonn region (Germany). In *Remote Sensing for Environmental Monitoring, GIS Applications, and Geology III* (Vol. 5239, pp. 274-284). International Society for Optics and Photonics.
- [91]. Rasul, A., Balzter, H., Ibrahim, G.R.F., Hameed, H.M., Wheeler, J., Adamu, B., Ibrahim, S.A. and Najmaddin, P.M., 2018. Applying built-up and bare-soil indices from landsat 8 to cities in dry climates. *Land*, 7(3), p.81.
- [92]. Xu, R., Liu, J. and Xu, J., 2018. Extraction of high-precision urban impervious surfaces from sentinel-2 multispectral imagery via modified linear spectral mixture analysis. *Sensors*, 18(9), p.2873.
- [93]. Holobacă, I.H., Ivan, K. and Alexe, M., 2019. Extracting built-up areas from Sentinel-1 imagery using land-cover classification and texture analysis. *International Journal of Remote Sensing*, 40(20), pp.8054-8069.
- [94]. Ferrato, L.J. and Forsythe, K.W., 2013. Comparing hyperspectral and multispectral imagery for land classification of the Lower Don River, Toronto. *Journal of Geography and Geology*, 5(1), pp.92-107.
- [95]. Poursanidis, D., Chrysoulakis, N. and Mitraka, Z., 2015. Landsat 8 vs. Landsat 5: A comparison based on urban and peri-urban land cover mapping. *International Journal of Applied Earth Observation and Geoinformation*, 35, pp.259-269.
- [96]. Petropoulos, G.P., Vadrevu, K.P. and Kalaitzidis, C., 2013. Spectral angle mapper and object-based classification combined with hyperspectral remote sensing imagery for obtaining land use/cover mapping in a Mediterranean region. *Geocarto international*, 28(2), pp.114-129.
- [97]. Zhang, E., Zhang, X., Yang, S. and Wang, S., 2013. Improving hyperspectral image classification using spectral information divergence. *IEEE Geoscience and Remote Sensing Letters*, 11(1), pp.249-253.

- [98]. Manolakis, D., Marden, D. and Shaw, G.A., 2003. Hyperspectral image processing for automatic target detection applications. *Lincoln laboratory journal*, 14(1), pp.79-116.
- [99]. Pal, M. and Mather, P.M., 2005. Support vector machines for classification in remote sensing. *International journal of remote sensing*, 26(5), pp.1007-1011.
- [100]. Waske, B., Benediktsson, J.A. and Sveinsson, J.R., 2009, June. Classifying remote sensing data with support vector machines and imbalanced training data. In *International Workshop on Multiple Classifier Systems* (pp. 375-384). Springer, Berlin, Heidelberg.
- [101]. Puttinaovaratt, S. and Horkaew, P., 2018. Multi-spectral and Topographic Fusion for Automated Road Extraction. *Open Geosciences*, 10(1), pp.461-473.
- [102]. Valdiviezo-N, J.C., Téllez-Quinones, A., Salazar-Garibay, A. and López-Caloca, A.A., 2018. Built-up index methods and their applications for urban extraction from Sentinel 2A satellite data: discussion. *JOSA A*, 35(1), pp.35-44.
- [103]. Memarsadeghi, N., Mount, D.M., Netanyahu, N.S. and Le Moigne, J., 2007. A fast implementation of the ISODATA clustering algorithm. *International Journal of Computational Geometry & Applications*, 17(01), pp.71-103.
- [104]. Wu, C. and Murray, A.T., 2003. Estimating impervious surface distribution by spectral mixture analysis. *Remote sensing of Environment*, 84(4), pp.493-505.
- [105]. Yue, W., Xu, J., Tan, W. and Xu, L., 2007. The relationship between land surface temperature and NDVI with remote sensing: application to Shanghai Landsat 7 ETM+ data. *International Journal of Remote Sensing*, 28(15), pp.3205-3226.
- [106]. Huang, J., Lu, X.X. and Sellers, J.M., 2007. A global comparative analysis of urban form: Applying spatial metrics and remote sensing. *Landscape and urban planning*, 82(4), pp.184-197.
- [107]. Wang, J. and Chang, C.I., 2006. Independent component analysis-based dimensionality reduction with applications in hyperspectral image analysis. *IEEE transactions on geoscience and remote sensing*, 44(6), pp.1586-1600.
- [108]. Prasad, S. and Bruce, L.M., 2008. Limitations of principal components analysis for hyperspectral target recognition. *IEEE Geoscience and Remote Sensing Letters*, 5(4), pp.625-629.
- [109]. Luo, G., Chen, G., Tian, L., Qin, K. and Qian, S.E., 2016. Minimum noise fraction versus principal component analysis as a preprocessing step for hyperspectral imagery denoising. *Canadian Journal of Remote Sensing*, 42(2), pp.106-116.

- [110]. Martel, E., Lazcano, R., López, J., Madroñal, D., Salvador, R., López, S., Juarez, E., Guerra, R., Sanz, C. and Sarmiento, R., 2018. Implementation of the principal component analysis onto high-performance computer facilities for hyperspectral dimensionality reduction: Results and comparisons. *Remote Sensing*, 10(6), p.864.
- [111]. Martínez-Usó Martínez-Uso, A., Pla, F., Sotoca, J.M. and García-Sevilla, P., 2007. Clustering-based hyperspectral band selection using information measures. *IEEE Transactions on Geoscience and Remote Sensing*, 45(12), pp.4158-4171.
- [112]. Qian, Y., Yao, F. and Jia, S., 2009. Band selection for hyperspectral imagery using affinity propagation. *IET Computer Vision*, 3(4), pp.213-222.
- [113]. Wang, Q., Lin, J. and Yuan, Y., 2016. Salient band selection for hyperspectral image classification via manifold ranking. *IEEE transactions on neural networks and learning systems*, 27(6), pp.1279-1289.
- [114]. Liu, X.Y., Lin, H., Xiong, J.L., Xiong, Y.J., Sun, H. and Mo, D.K., 2005. Band Selection from Hyperspectral Data of Forestry Species. *Remote Sensing Information*, 4, pp.41-44.
- [115]. Zhou, S., Cheng, J.L., Huang, M.X. and Lian-Qing, Z.H.O.U., 2006. Assessing reclamation levels of coastal saline lands with integrated stepwise discriminant analysis and laboratory hyperspectral data. *Pedosphere*, 16(2), pp.154-160.
- [116]. Tang, F. and Xu, H., 2017. Impervious surface information extraction based on hyperspectral remote sensing imagery. *Remote Sensing*, 9(6), p.550.
- [117]. Otsu, N., 1979. A threshold selection method from gray-level histograms. *IEEE transactions on systems, man, and cybernetics*, 9(1), pp.62-66.
- [118]. Liu, B., Chen, X., Ma, C., Zhang, D., Zhou, X. and He, Y., 2010, May. Research on threshold segmentation in tracking technology of moving objects. In *2010 The 2nd International Conference on Industrial Mechatronics and Automation (Vol. 1)*, pp. 398-400). IEEE.
- [119]. Xu, R., Liu, J. and Xu, J., 2018. Extraction of high-precision urban impervious surfaces from sentinel-2 multispectral imagery via modified linear spectral mixture analysis. *Sensors*, 18(9), p.2873.
- [120]. Yadav, P., Agrawal, S., 2018. Road network identification and extraction in satellite imagery using Otsu's method and connected component analysis. *International Archives of the Photogrammetry, Remote Sensing & Spatial Information Sciences*.

- [121]. He, Z.Y., Sun, L.N. and Chen, L.G., 2013. Fast computation of threshold based on Otsu criterion. *Dianzi Xuebao (Acta Electronica Sinica)*, 41(2), pp.267-272.
- [122]. Pereira, J.M., 1999. A comparative evaluation of NOAA/AVHRR vegetation indexes for burned surface detection and mapping. *IEEE Transactions on Geoscience and Remote Sensing*, 37(1), pp.217-226.
- [123]. Kaufman, Y.J., Remer, L.A., 1994. Detection of forests using mid-IR reflectance: an application for aerosol studies. *IEEE Transactions on Geoscience and Remote Sensing*, 32(3), pp.672-683.
- [124]. Swain, P.H., Davis, S.M., 1981. Remote sensing: the quantitative approach. *IEEE Transactions on Pattern Analysis & Machine Intelligence*, 6, pp.713-714.
- [125]. Mausel, P.W., 1990. Optimum band selection for supervised classification of multispectral data. *Photogrammetric Engineering & Remote Sensing*, 56(1), pp.55-60.
- [126]. Roberts, D.A., Gardner, M., Church, R., Ustin, S., Scheer, G. and Green, R.O., 1998. Mapping chaparral in the Santa Monica Mountains using multiple endmember spectral mixture models. *Remote sensing of environment*, 65(3), pp.267-279.
- [127]. Rouse Jr, J., Haas, R.H., Schell, J.A. and Deering, D.W., 1974. Monitoring vegetation systems in the Great Plains with ERTS.
- [128]. Tarabalka, Y., Benediktsson, J.A. and Chanussot, J., 2009. Spectral-spatial classification of hyperspectral imagery based on partitional clustering techniques. *IEEE Transactions on Geoscience and Remote Sensing*, 47(8), pp.2973-2987.
- [129]. Qian, Y., Yao, F. and Jia, S., 2009. Band selection for hyperspectral imagery using affinity propagation. *IET Computer Vision*, 3(4), pp.213-222.
- [130]. Wang, Q., Lin, J. and Yuan, Y., 2016. Salient band selection for hyperspectral image classification via manifold ranking. *IEEE transactions on neural networks and learning systems*, 27(6), pp.1279-1289.
- [131]. Alonzo, M., Roth, K. and Roberts, D., 2013. Identifying Santa Barbara's urban tree species from AVIRIS imagery using canonical discriminant analysis. *Remote Sensing Letters*, 4(5), pp.513-521.
- [132]. Robert, P., Bertrand, D., Devaux, M.F. and Sire, A., 1992. Identification of chemical constituents by multivariate near-infrared spectral imaging. *Analytical chemistry*, 64(6), pp.664-667.

- [133]. Patel, N. and Mukherjee, R., 2015. Extraction of Built-up features from spectral indices using artificial neural network. *Arabian Journal of Geosciences*, 8(6), pp.3729-3741.
- [134]. McFeeters, S.K., 1996. The use of the Normalized Difference Water Index (NDWI) in the delineation of open water features. *International journal of remote sensing*, 17(7), pp.1425-1432.
- [135]. Herold, M. and Roberts, D., 2005. Spectral characteristics of asphalt road aging and deterioration: implications for remote-sensing applications. *Applied optics*, 44(20), pp.4327-4334.
- [136]. Casselgren, J., Sjö Dahl, M. and LeBlanc, J., 2007. Angular spectral response from covered asphalt. *Applied optics*, 46(20), pp.4277-4288.
- [137]. Franke, J., Roberts, D.A., Halligan, K. and Menz, G., 2009. Hierarchical multiple endmember spectral mixture analysis (MESMA) of hyperspectral imagery for urban environments. *Remote Sensing of Environment*, 113(8), pp.1712-1723.
- [138]. Liu, T. and Yang, X., 2015. Monitoring land changes in an urban area using satellite imagery, GIS and landscape metrics. *Applied Geography*, 56, pp.42-54.
- [139]. Michishita, R., Jiang, Z. and Xu, B., 2012. Monitoring two decades of urbanization in the Poyang Lake area, China through spectral unmixing. *Remote Sensing of Environment*, 117, pp.3-18.
- [140]. Gao, B.C., 1996. NDWI—A normalized difference water index for remote sensing of vegetation liquid water from space. *Remote sensing of environment*, 58(3), pp.257-66.
- [141]. Cablk, M.E. and Minor, T.B., 2003. Detecting and discriminating impervious cover with high-resolution IKONOS data using principal component analysis and morphological operators. *International Journal of Remote Sensing*, 24(23), pp.4627-4645.
- [142]. Vaddi, R. and Prabukumar, M., 2017, June. Comparative study of feature extraction techniques for hyper spectral remote sensing image classification: a survey. In 2017 International Conference on Intelligent Computing and Control Systems (ICICCS) (pp. 543-548). IEEE.
- [143]. Ye, M., Ji, C., Chen, H., Lei, L., Lu, H. and Qian, Y., 2019. Residual deep PCA-based feature extraction for hyperspectral image classification. *Neural Computing and Applications*, pp.1-14.
- [144]. Uddin, M.P., Mamun, M.A. and Hossain, M.A., 2020. PCA-based Feature Reduction for Hyperspectral Remote Sensing Image Classification. *IETE Technical Review*, pp.1-21.
- [145]. Zhang, J., Li, P. and Wang, J., 2014. Urban built-up area extraction from Landsat TM/ETM+ images using spectral information and multivariate texture. *Remote Sensing*, 6(8), pp.7339-7359.

- [146]. Ettehadi Osgouei, P., Kaya, S., Sertel, E. and Alganci, U., 2019. Separating built-up areas from bare land in mediterranean cities using sentinel-2a imagery. *Remote Sensing*, 11(3), p.345.
- [147]. Pesaresi, M. and Ehrlich, D., 2009. A methodology to quantify built-up structures from optical VHR imagery. In *Global mapping of human settlement* (pp. 55-86). CRC Press.
- [148]. Wu, C., 2004. Normalized spectral mixture analysis for monitoring urban composition using ETM+ imagery. *Remote Sensing of Environment*, 93(4), pp.480-492.
- [149]. Momeni, R., Aplin, P. and Boyd, D.S., 2016. Mapping complex urban land cover from spaceborne imagery: the influence of spatial resolution, spectral band set and classification approach. *Remote Sensing*, 8(2), p.88.
- [150]. Wu, C., 2009. Quantifying high-resolution impervious surfaces using spectral mixture analysis. *International Journal of Remote Sensing*, 30(11), pp.2915-2932.
- [151]. Deng, C. and Wu, C., 2013. A spatially adaptive spectral mixture analysis for mapping subpixel urban impervious surface distribution. *Remote Sensing of Environment*, 133, pp.62-70.
- [152]. Heinz, D.C., 2001. Fully constrained least squares linear spectral mixture analysis method for material quantification in hyperspectral imagery. *IEEE transactions on geoscience and remote sensing*, 39(3), pp.529-545.
- [153]. Bateson, C.A., Asner, G.P. and Wessman, C.A., 2000. Endmember bundles: A new approach to incorporating endmember variability into spectral mixture analysis. *IEEE transactions on geoscience and remote sensing*, 38(2), pp.1083-1094.
- [154]. Karathanassi, V., Iossifidis, C.H. and Rokos, D., 2000. A texture-based classification method for classifying built areas according to their density. *International Journal of Remote Sensing*, 21(9), pp.1807-1823.
- [155]. Segl, K., Roessner, S., Heiden, U. and Kaufmann, H., 2003. Fusion of spectral and shape features for identification of urban surface cover types using reflective and thermal hyperspectral data. *ISPRS Journal of Photogrammetry and Remote Sensing*, 58(1-2), pp.99-112.
- [156]. Ouma, Y.O., Tateishi, R. and Sri-Sumantyo, J.T., 2010. Urban features recognition and extraction from very-high resolution multi-spectral satellite imagery: a micro–macro texture determination and integration framework. *IET image processing*, 4(4), pp.235-254.

- [157]. Amarsaikhan, D., Saandar, M., Ganzorig, M., Blotevogel, H.H., Egshiglen, E., Gantuyal, R., Nergui, B. and Enkhjargal, D., 2012. Comparison of multisource image fusion methods and land cover classification. *International Journal of Remote Sensing*, 33(8), pp.2532-2550.
- [158]. Zhang, J., Li, P. and Xu, H., 2013, July. Urban built-up area extraction using combined spectral information and multivariate texture. In *2013 IEEE International Geoscience and Remote Sensing Symposium-IGARSS* (pp. 4249-4252). IEEE.
- [159]. Liu, S. and Gu, G., 2017. Improving the impervious surface estimation from hyperspectral images using a spectral-spatial feature sparse representation and post-processing approach. *Remote Sensing*, 9(5), p.456.
- [160]. Yu, Y., Li, J., Zhu, C. and Plaza, A., 2018. Urban impervious surface estimation from remote sensing and social data. *Photogrammetric Engineering & Remote Sensing*, 84(12), pp.771-780.
- [161]. Lynch, P. and Blesius, L., 2019. *Urban Remote Sensing: Feature Extraction*.
- [162]. Nong, D.H., Fox, J., Miura, T. and Saksena, S., 2015. Built-up area change analysis in hanoi using support vector machine classification of landsat multi-temporal image stacks and population data. *Land*, 4(4), pp.1213-1231.
- [163]. Ma, X., Tong, X., Liu, S., Luo, X., Xie, H. and Li, C., 2017. Optimized sample selection in SVM classification by combining with DMSP-OLS, Landsat NDVI and GlobeLand30 products for extracting urban built-up areas. *Remote Sensing*, 9(3), p.236.
- [164]. Melgani, F. and Bruzzone, L., 2004. Classification of hyperspectral remote sensing images with support vector machines. *IEEE Transactions on geoscience and remote sensing*, 42(8), pp.1778-1790.
- [165]. Li, S., Wu, H., Wan, D. and Zhu, J., 2011. An effective feature selection method for hyperspectral image classification based on genetic algorithm and support vector machine. *Knowledge-Based Systems*, 24(1), pp.40-48.
- [166]. Mountrakis, G., Im, J. and Ogole, C., 2011. Support vector machines in remote sensing: A review. *ISPRS Journal of Photogrammetry and Remote Sensing*, 66(3), pp.247-259.
- [167]. Muñoz-Marí, J., Bovolo, F., Gómez-Chova, L., Bruzzone, L. and Camp-Valls, G., 2010. Semisupervised one-class support vector machines for classification of remote sensing data. *IEEE transactions on geoscience and remote sensing*, 48(8), pp.3188-3197.

- [168]. Gehler, P.V., Schölkopf, B., Camps-Valls, G. and Bruzzone, L., 2009. An introduction to kernel learning algorithms. *Kernel methods for remote sensing data analysis*, pp.25-45.
- [169]. Maulik, U. and Chakraborty, D., 2017. Remote Sensing Image Classification: A survey of support-vector-machine-based advanced techniques. *IEEE Geoscience and Remote Sensing Magazine*, 5(1), pp.33-52.
- [170]. Camps-Valls, G. and Bruzzone, L., 2005. Kernel-based methods for hyperspectral image classification. *IEEE Transactions on Geoscience and Remote Sensing*, 43(6), pp.1351-1362.
- [171]. Camps-Valls, G., Shervashidze, N. and Borgwardt, K.M., 2010. Spatio-spectral remote sensing image classification with graph kernels. *IEEE Geoscience and Remote Sensing Letters*, 7(4), pp.741-745.
- [172]. Van der Linden, S., Janz, A., Waske, B., Eiden, M. and Hostert, P., 2007. Classifying segmented hyperspectral data from a heterogeneous urban environment using support vector machines. *Journal of Applied Remote Sensing*, 1(1), p.013543.
- [173]. Cao, X., Chen, J., Imura, H. and Higashi, O., 2009. A SVM-based method to extract urban areas from DMSP-OLS and SPOT VGT data. *Remote Sensing of Environment*, 113(10), pp.2205-2209.
- [174]. Pal, M., Maxwell, A.E. and Warner, T.A., 2013. Kernel-based extreme learning machine for remote-sensing image classification. *Remote Sensing Letters*, 4(9), pp.853-862.
- [175]. Shang, R., Sun, Z., Xu, J. and Shen, G., 2017, July. Comparisons of impervious surface mapping using multiple indices from TM, ETM+ and OLI-TIRS. In *2017 IEEE International Geoscience and Remote Sensing Symposium (IGARSS)* (pp. 5870-5873). IEEE.
- [176]. Manjunath, K.R., Ray, S.S. and Panigrahy, S., 2011. Discrimination of spectrally-close crops using ground-based hyperspectral data. *Journal of the Indian Society of Remote Sensing*, 39(4), pp.599-602.
- [177]. Cheng, Q., Varshney, P.K. and Arora, M.K., 2006. Logistic regression for feature selection and soft classification of remote sensing data. *IEEE Geoscience and Remote Sensing Letters*, 3(4), pp.491-494.
- [178]. Nimbalkar, P., Jarocinska, A. and Zagajewski, B., 2018. Optimal Band Configuration for the Roof Surface Characterization Using Hyperspectral and LiDAR Imaging. *Journal of Spectroscopy*, 2018.

- [179]. Ahmad, M., Lee, S., Haq, I.U. and Mushtaq, Q., 2012. Hyperspectral remote sensing: Dimensional reduction and end member extraction. *International journal of soft computing and engineering*, 2(2), pp.170-175.
- [180]. Bajcsy, P. and Groves, P., 2004. Methodology for hyperspectral band selection. *Photogrammetric Engineering & Remote Sensing*, 70(7), pp.793-802.
- [181]. Girouard, G., Bannari, A., El Harti, A. and Desrochers, A., 2004, July. Validated spectral angle mapper algorithm for geological mapping: comparative study between QuickBird and Landsat-TM. In XXth ISPRS congress, geo-imagery bridging continents, Istanbul, Turkey (pp. 12-23).
- [182]. Liu, X. and Yang, C., 2013, December. A kernel spectral angle mapper algorithm for remote sensing image classification. In 2013 6th International Congress on Image and Signal Processing (CISP) (Vol. 2, pp. 814-818). IEEE.
- [183]. Petropoulos, G.P., Vadrevu, K.P. and Kalaitzidis, C., 2013. Spectral angle mapper and object-based classification combined with hyperspectral remote sensing imagery for obtaining land use/cover mapping in a Mediterranean region. *Geocarto international*, 28(2), pp.114-129.
- [184]. Chang, C.I., 1999, June. Spectral information divergence for hyperspectral image analysis. In IEEE 1999 International Geoscience and Remote Sensing Symposium. IGARSS'99 (Cat. No. 99CH36293) (Vol. 1, pp. 509-511). IEEE.
- [185]. Zhang, E., Zhang, X., Yang, S. and Wang, S., 2013. Improving hyperspectral image classification using spectral information divergence. *IEEE Geoscience and Remote Sensing Letters*, 11(1), pp.249-253.
- [186]. Robila, S.A. and Gershman, A., 2005, July. Spectral matching accuracy in processing hyperspectral data. In International Symposium on Signals, Circuits and Systems, 2005. ISSCS 2005. (Vol. 1, pp. 163-166). IEEE.
- [187]. Truslow, E., Manolakis, D., Pieper, M., Cooley, T. and Brueggeman, M., 2013. Performance prediction of matched filter and adaptive cosine estimator hyperspectral target detectors. *IEEE Journal of Selected Topics in Applied Earth Observations and Remote Sensing*, 7(6), pp.2337-2350.
- [188]. DiPietro, R.S., Manolakis, D., Lockwood, R.B., Cooley, T. and Jacobson, J., 2012. Hyperspectral matched filter with false-alarm mitigation. *Optical Engineering*, 51(1), p.016202.
- [189]. Manolakis, D., Marden, D. and Shaw, G.A., 2003. Hyperspectral image processing for automatic target detection applications. *Lincoln laboratory journal*, 14(1), pp.79-116.

- [190]. Sharma, V., Baruah, D., Chutia, D., Raju, P.L.N. and Bhattacharya, D.K., 2016, May. An assessment of support vector machine kernel parameters using remotely sensed satellite data. In 2016 IEEE International Conference on Recent Trends in Electronics, Information & Communication Technology (RTEICT) (pp. 1567-1570). IEEE.
- [191]. Soliman, O.S. and Mahmoud, A.S., 2012, May. A classification system for remote sensing satellite images using support vector machine with non-linear kernel functions. In 2012 8th International Conference on Informatics and Systems (INFOS) (pp. BIO-181). IEEE.
- [192]. Tbarki, K., Said, S.B., Ksantini, R. and Lachiri, Z., 2016, November. RBF kernel based SVM classification for landmine detection and discrimination. In 2016 International Image Processing, Applications and Systems (IPAS) (pp. 1-6). IEEE.
- [193]. Yang, X., 2011. Parameterizing support vector machines for land cover classification. *Photogrammetric Engineering & Remote Sensing*, 77(1), pp.27-37.
- [194]. Adefioye, S.A., 2014. Quantitative Image Classification Accuracy Assessment Program for Sustainable Geospatial Technology Applications. In XXV FIG Congress (p. 17).
- [195]. Feyisa, G.L., Meilby, H., Jenerette, G.D. and Pauliet, S., 2016. Locally optimized separability enhancement indices for urban land cover mapping: Exploring thermal environmental consequences of rapid urbanization in Addis Ababa, Ethiopia. *Remote Sensing of Environment*, 175, pp.14-31.
- [196]. Lu, D., Hetrick, S. and Moran, E., 2010. Land cover classification in a complex urban-rural landscape with QuickBird imagery. *Photogrammetric Engineering & Remote Sensing*, 76(10), pp.1159-1168.
- [197]. Lu, T., Ming, D., Lin, X., Hong, Z., Bai, X. and Fang, J., 2018. Detecting building edges from high spatial resolution remote sensing imagery using richer convolution features network. *Remote Sensing*, 10(9), p.1496.
- [198]. Bo, D., Liangpei, Z., Pingxiang, L. and Yanfei, Z., 2009, May. A target detection algorithm for urban areas using HSRH imagery. In 2009 Joint Urban Remote Sensing Event (pp. 1-5). IEEE.
- [199]. Segl, K. and Kaufmann, H., 2001. Detection of small objects from high-resolution panchromatic satellite imagery based on supervised image segmentation. *IEEE Transactions on geoscience and remote sensing*, 39(9), pp.2080-2083.

- [200]. Singh, P.P. and Garg, R.D., 2014. Road detection from remote sensing images using impervious surface characteristics: Review and implication. *The International Archives of Photogrammetry, Remote Sensing and Spatial Information Sciences*, 40(8), p.955.
- [201]. Ma, H., Cheng, X., Wang, X. and Yuan, J., 2013, December. Road information extraction from high resolution remote sensing images based on threshold segmentation and mathematical morphology. In *2013 6th International Congress on Image and Signal Processing (CISP)* (Vol. 2, pp. 626-630). IEEE.
- [202]. Song, M. and Civco, D., 2004. Road extraction using SVM and image segmentation. *Photogrammetric Engineering & Remote Sensing*, 70(12), pp.1365-1371.

Author's Biography



Dwijendra Pandey

2K17/PhD/EC/09

Department of Electronics and Communication

Engineering, Delhi Technological University, Delhi,

India- 110042

Email: dwijpandey068@gmail.com

Dwijendra Pandey received the Bachelor of Technology (B.Tech.) from Meerut Institute of Engineering and Technology (Affiliated to Uttar Pradesh Technical University), Meerut, Uttar Pradesh, India in the year 2009 and the Master of Technology (M.Tech.) from Motilal Nehru National Institute of Technology, Allahabad, India in the year 2016. Presently, he is pursuing his PhD in the Department of Electronics and Communication Engineering, Delhi Technological University, Delhi, India. He has also worked as a Junior/Senior Research Fellow (JRF/SRF) in a Clustered based Networked Project on Imaging Spectrometer and its Applications (NISA) funded by Department of Science and Technology (DST), Government of India, and as a Research Associate (RA) in Announcement of opportunity (hyper AO) airborne hyperspectral mission- science & applications project funded by Space Application Centre (SAC), Indian Space Research Organisation (ISRO), Government of India. His research interests include Remote Sensing of Engineered / Built-up / Impervious Surfaces, Hyperspectral Remote Sensing, Image Processing, Spectral Index based target detection and classification, and Machine Learning.